

Dissertation

Ultranonlocality in Density Functional Theory

Thilo Aschebrock



UNIVERSITÄT
BAYREUTH

Ultranonlocality in Density Functional Theory

Von der Universität Bayreuth
zur Erlangung des Grades eines
Doktors der Naturwissenschaften (Dr. rer. nat.)
genehmigte Abhandlung

von

Thilo Aschebrock

aus Reutlingen

1. Gutachter: Prof. Dr. Stephan Kümmel
2. Gutachter: Prof. Dr. Walter Zimmermann
3. Gutachter: Prof. Dr. Leeor Kronik

Tag der Einreichung: 30. Juli 2019

Tag des Kolloquiums: 11. Dezember 2019

Abstract

The decisive advantage of density functional theory in comparison with other electronic structure methods is its favorable ratio of accuracy to computational cost. In its standard Kohn-Sham formulation, both of these aspects are determined by the density functional that is selected to approximate the exchange-correlation energy. While the computational cost plays a minor role for systems of small to moderate size, its significance rises quickly when one considers extended systems of increasing size as it is common, e.g., in the realms of biology, nano-science, or supramolecular science. These real-world systems, which are areas of great scientific interest, are, thus, typically only accessible with computationally feasible density functional approximations. However, this so-called class of semilocal functionals is known to have hallmark deficits that are closely interconnected by the absence of ultranonlocality. This absence manifests itself, e.g., in the inability to properly describe band gaps or charge transfer. The latter deficit is, for instance, detrimental when one tries to understand light-harvesting systems. Therefore, long-standing effort was and is invested to address this problem and develop semilocal density functional approximations that possess or mimic ultranonlocality.

The first part of this thesis focuses on two promising candidates for this task, the Becke-Johnson potential and the Armiento-Kümmel generalized gradient approximation (GGA). Both functionals share a signature asymptotically nonvanishing potential and, as is shown here, also anomalous features that constitute a formidable challenge for their application and the future development of functionals based on their construction concept. Most notably, the corresponding potentials are demonstrated to diverge exponentially in the vicinity of orbital nodal surfaces. These topological challenges of orbital nodal surfaces are also shown to affect many other frequently used density functional approximations. Consequently, exact constraints to avoid such divergences are formulated.

In the second part of this thesis, a new construction strategy for meta-GGAs that focuses on the derivative discontinuity is developed and employed. The resulting computationally feasible semilocal functionals are demonstrated to achieve substantial ultranonlocality due to their use of the kinetic energy density. Thereby, considerably more realistic band gaps are obtained in comparison to other semilocal exchange-correlation energy functionals. The meta-GGAs of this thesis are, therefore, promising future candidates for the study of large-scale systems that is presently limited by the above-mentioned deficits of traditional semilocal functionals.

Furthermore, the concept of a local range-separation parameter is revisited. It promises formal and practical improvements for the class of range-separated hybrid functionals, which currently spearhead the description of charge transfer in systems of small to moderate size. In particular, a local range-separation parameter is constructed that satisfies additional exact constraints, such as one-electron self-interaction freedom, and exhibits a non-trivial spin-dependence. Lastly, the hyper-GGA approximation, which is based on semilocal exchange hole models and computationally essential to the local range-separation approach, is assessed.

Kurzdarstellung

Der entscheidende Vorteil der Dichtefunktionaltheorie im Vergleich mit anderen Methoden zur Berechnung der elektronischen Struktur ist ihr vorteilhaftes Verhältnis von Genauigkeit zu Rechenkosten. In ihrer typischen Kohn-Sham-Formulierung werden diese beiden Aspekte durch das Dichtefunktional bestimmt, das als Näherung an die Austauschkorrelationsenergie ausgewählt wird. Während für kleine und mittelgroße Systeme die Rechenkosten eine untergeordnete Rolle spielen, nimmt deren Bedeutung signifikant zu, sobald zunehmend ausgedehntere Systeme betrachtet werden, wie es etwa in den Bereichen der Biologie, Nanowissenschaften, oder Supramolekularforschung üblich ist. Die dort betrachteten Systeme, die aus der realen Welt stammen und von hohem wissenschaftlichen Interesse sind, sind somit typischerweise nur mit Dichtefunktionalen zugänglich, die niedrige Rechenkosten aufweisen. Diese Klasse an sogenannten semilokalen Funktionalen ist jedoch für ihre schwerwiegenden Defizite bekannt, die mit dem Fehlen an Ultranichtlokalität verknüpft sind. Dieser Mangel manifestiert sich in einer fehlerhaften Beschreibung von Bandlücken oder Ladungstransfer. Letzteres Defizit ist beispielweise sehr beeinträchtigend, wenn man in der Natur vorkommende Lichtsammelsysteme verstehen möchte. Entsprechend werden seit längerem intensive Anstrengungen unternommen, semilokale Dichtefunktionalnäherungen zu entwickeln, die Ultranichtlokalität besitzen oder nachahmen.

Der erste Teil dieser Dissertation beschäftigt sich mit zwei vielversprechenden Kandidaten für dieses Ziel: dem Becke-Johnson Potential und der Armiento-Kümmel *generalized gradient approximation* (GGA). Beide Funktionale teilen sich ein charakteristisches, asymptotisch nicht verschwindendes Potential und, wie hier gezeigt wird, ebenso anomale Eigenschaften, die eine ernsthafte Herausforderung für ihre Anwendung sowie für die zukünftige Funktionalentwicklung auf Basis ihrer Konstruktionsprinzipien darstellen. Insbesondere wird aufgezeigt, dass die zugehörigen Potentiale in der Nähe von Knotenflächen der Orbitale exponentiell divergieren. Ebenso zeigt sich, dass diese topologischen Herausforderungen viele weitere Dichtefunktionalnäherungen betreffen, die häufig Verwendung finden. Entsprechend werden exakte Bedingungen formuliert, um diese Art von Divergenzen zu vermeiden.

Im zweiten Teil dieser Arbeit wird eine neue Konstruktionsstrategie für meta-GGAs, welche sich auf die sogenannte *derivative discontinuity* fokussiert, entwickelt und angewendet. Es wird gezeigt, dass die resultierenden semilokalen und entsprechend kostengünstigen Funktionale substantielle Ultranichtlokalität aufgrund ihrer Abhängigkeit von der kinetischen Energiedichte aufweisen. Entsprechend sind diese meta-GGAs vielversprechende zukünftige Kandidaten für die Anwendung in ausgedehnten Systemen, die momentan aufgrund der obengenannten Defizite herkömmlicher semilokaler Funktionale nur eingeschränkt möglich ist.

Zusätzlich wird das Konzept eines lokalen Parameters für die Reichweitentrennung untersucht. Dieses Konzept verspricht formale und praktische Verbesserungen für die Klasse der reichweitenseparierten Hybridfunktionale, welche momentan die Beschreibung von Ladungs-

transfer in Systemen kleiner und mittlerer Größe anführen. Insbesondere wird ein lokaler Parameter für die Reichweitentrennung konstruiert, der zusätzlichen exakten Bedingungen wie etwa der Freiheit von Einelektronenselbstwechselwirkung genügt und eine nicht triviale Spinabhängigkeit aufweist. Abschließend wird die hyper-GGA-Näherung detailliert untersucht, welche auf semilokalen Austauschlochmodellen beruht und essenziell für den Ansatz einer lokalen Reichweitentrennung ist.

Contents

| | |
|--|------------|
| Abstract | v |
| Kurzdarstellung | vii |
| I Overview and Perspective | 1 |
| 1 Introduction | 3 |
| 2 Fundamentals of Density Functional Theory | 5 |
| 3 Ultranonlocality in Density Functional Theory | 7 |
| 3.1 Fractional Particle Numbers and Derivative Discontinuity | 8 |
| 3.2 Band Gap Problem | 11 |
| 3.3 Shell and Step Structures | 12 |
| 3.4 Polarizabilities and Charge Transfer | 13 |
| 3.5 Delocalization, Density-Driven, and Self-Interaction Errors | 15 |
| 4 Constraint-Guided Construction of Density Functional Approximations | 17 |
| 4.1 Size Consistency | 17 |
| 4.2 Unitary Invariance | 18 |
| 4.3 Spin Scaling | 18 |
| 4.4 Asymptotic Behavior | 19 |
| 4.5 Density Scaling | 20 |
| 4.6 Homogeneous Electron Gas Limit and Gradient Expansion | 23 |
| 4.7 Lieb-Oxford and Strongly Tightened Bound | 25 |
| 4.8 Density-Path Integrals and Virial Theorem | 26 |
| 4.9 Exchange-Correlation Hole | 26 |
| 5 Orbital-Dependent Density Functionals | 29 |
| 5.1 Exact Exchange and Beyond | 29 |
| 5.2 Optimized Effective Potential Theory | 30 |
| 5.3 Generalized Kohn-Sham Scheme | 32 |
| 6 Developments and Results | 35 |
| 6.1 Limitations of Semilocal Approximations | 36 |

| | | |
|-----------|--|------------|
| 6.2 | Capturing Ultranonlocality via a Kinetic Energy Density Dependence | 38 |
| 6.3 | Nonlocality from the Range-Separated Coulomb Interaction | 40 |
| A | Complementary Work | 45 |
| A.1 | Functional Derivatives of the Developed Meta-GGAs | 45 |
| A.2 | Slater-Type Basis Set Code for Closed-Shell Atoms | 50 |
| | List of Abbreviations | 58 |
| | Bibliography | 59 |
| | List of Publications | 81 |
| II | Publications | 83 |
| | Publication 1 | |
| | Orbital nodal surfaces: Topological challenges for density functionals | 85 |
| | Publication 2 | |
| | Challenges for semilocal density functionals with asymptotically nonvanishing potentials | 101 |
| | Publication 3 | |
| | Ultranonlocality and accurate band gap from a meta-generalized gradient approximation | 115 |
| | Publication 4 | |
| | Exploring local range separation: The role of spin scaling and one-electron self-interaction | 131 |
| | Acknowledgments | 151 |
| | Eidesstattliche Versicherung | 153 |

Part I

Overview and Perspective

CHAPTER 1

Introduction

Nearly a century past the modern formulation of quantum theory, we have achieved a remarkable accuracy in the description of the microscopic world of atoms and molecules around us. We likewise have well-established models to describe physical phenomena at the macroscopic length scale at our disposal. The intermediate region between the microscopic description based on quantum theory and the macroscopic description based on classical physics is, however, still difficult to access. These difficulties arise in this mesoscopic region because the length scale is typically still small enough that a quantum-mechanical description is required, as, e.g., quantum interference is of significant relevance, but at the same time large enough that such a description is close to or beyond today's computational capabilities. Yet, the mesoscopic length scale is of increasing importance: First, from an epistemological point of view, as a proper mesoscopic description would provide us with a direct link from fundamental physics to macroscopic phenomena and thus a fundamental understanding. Second, from a practical point of view, as the scientific interest and progress are increasingly heading into mesoscopic length scales. Prime examples for the latter can be found in biophysics, nano-science, or supramolecular science.

Density functional theory [HK64, KS65] has proven to be a predestined electronic structure theory for this purpose [Koh99]. Since it relies on the electron density distribution in place of the many-body wave function, density functional theory grants computationally inexpensive access to large-scale systems and provides transparent insight into their nature. The low computational cost, however, is closely tied to the approximation to the exchange-correlation energy, which is in practice necessary for every density functional theory calculation. The low-cost approximations to the exchange-correlation energy, which are required to access the mesoscopic length scale, unfortunately miss important features that may be characterized as "ultranonlocal".

This ultranonlocality, which illustratively depicts that small changes in the density of the system can influence the associated exchange-correlation potential over arbitrary distances, is, e.g., pivotal to the proper description of electronic charge transfer. The absence of ultranonlocality in the description can, therefore, have severe consequences and effectively limits the usefulness of density functional theory for many systems of high practical relevance. Many such systems can be found in biology or biochemistry, where processes are frequently driven by electrochemical gradients and thus involve charge transfer or related physics. To gain deeper scientific understanding of such mesoscopic processes, it is, hence, essential to develop low-cost approximations to the exchange-correlation energy that incorporate ultranonlocality. This thesis is dedicated to this aspiration and part of the long-standing scientific effort in this direction.

To this end, the fundamentals of density functional theory are briefly summarized in Chapter 2 and followed by Chapter 3, which outlines how and where ultranonlocality manifests itself in this theory. An overview of the constraint-guided construction of density functional approximations is given in Chapter 4. Thereupon, Chapter 5 completes the presentation of the fundamentals of this thesis by portraying the power of orbital dependence to model ultranonlocality in density functional theory. Building upon this, the final Chapter 6 summarizes the developments and results of the four publications, which make for Part II of this thesis, and puts them into perspective: While [Pubs. 1](#) and [2](#) analyze already proposed exchange-correlation functionals critically, new low-cost functionals that capture ultranonlocality are constructed and presented in [Pub. 3](#). This thesis concludes with [Pub. 4](#), which advances a rather unexplored concept to improve certain exchange-correlation functionals that are currently used primarily to describe ultranonlocality at smaller length scales.

CHAPTER 2

Fundamentals of Density Functional Theory

Density functional theory (DFT) is an in principle exact reformulation of many-body quantum theory to predict quantum physical properties without requiring the calculation or actual knowledge of the corresponding many-body wave function. While DFT is not limited to the description of electrons in condensed matter, this is unquestionable its main application and biggest success story since DFT has become the most popular electronic structure method in computational physics, chemistry and materials science [Bur12, Bec14, Jon15]. For a comprehensive introduction to and overview of DFT see, e.g., Refs. [PY89, PK03, ED11].

The foundation of DFT is the Hohenberg-Kohn theorem [HK64], which ensures that stationary many-particle systems can be fully characterized by their ground-state density $n(\mathbf{r})$. This allows to express DFT entirely in terms of the density and hereby surpass the “exponential wall” [Koh99] that wave function methods encounter and are ultimately stopped by – the sheer exponential growth of the wave functions dimensionality with respect to the particle number. Moreover, the Hohenberg-Kohn theorem states that the ground-state density can be determined by minimizing the energy functional $E[n]$ [Lev82, Lie83] and is thus given by the variational equation

$$\frac{\delta}{\delta n(\mathbf{r})} \left\{ E[n] - \mu \left(\int n(\mathbf{r}) d^3r - N \right) \right\} = 0, \quad (2.1)$$

where the Lagrange multiplier μ of the subsidiary condition to enforce the correct particle number N defines the chemical potential. In the standard formulation of DFT [KS65] within the Born-Oppenheimer approximation [BO27], the electronic energy functional is partitioned as

$$E[n] = T_s[n] + E_H[n] + E_{\text{ext}}[n] + E_{\text{xc}}[n] \quad (2.2)$$

in terms of the kinetic energy functional

$$T_s[n] = T_s[\{\varphi_{i\sigma}[n]\}] = -\frac{\hbar^2}{2m_e} \sum_{\sigma=\uparrow,\downarrow} \sum_{i=1}^{N_\sigma} \int \varphi_{i\sigma}^*(\mathbf{r}) \nabla^2 \varphi_{i\sigma}(\mathbf{r}) d^3r \quad (2.3)$$

of non-interacting fermionic particles, the classical (Hartree) interaction energy

$$E_H[n] = \frac{e^2}{2} \iint \frac{n(\mathbf{r})n(\mathbf{r}')}{|\mathbf{r} - \mathbf{r}'|} d^3r' d^3r, \quad (2.4)$$

the external energy

$$E_{\text{ext}}[n] = \int v_{\text{ext}}(\mathbf{r})n(\mathbf{r})d^3r, \quad (2.5)$$

and in terms of the exchange-correlation (xc) energy $E_{\text{xc}}[n]$ that absorbs all remaining energy contributions. This partitioning allows to minimize the energy and thus to obtain both the ground-state density and energy by solving an effective non-interacting system, the Kohn-Sham (KS) system. In the spin-polarized formulation of DFT [vBH72] the corresponding single-particle equations are given by

$$\left\{ -\frac{\hbar^2}{2m_e}\nabla^2 + v_{\text{KS}\sigma}([n_{\uparrow}, n_{\downarrow}]; \mathbf{r}) \right\} \varphi_{i\sigma}(\mathbf{r}) = \varepsilon_{i\sigma} \varphi_{i\sigma}(\mathbf{r}), \quad (2.6)$$

where the effective multiplicative potential, the KS potential, is a functional of the density itself,

$$v_{\text{KS}\sigma}([n_{\uparrow}, n_{\downarrow}]; \mathbf{r}) = e^2 \int \frac{n(\mathbf{r}')}{|\mathbf{r} - \mathbf{r}'|} d^3r' + v_{\text{ext}}(\mathbf{r}) + \frac{\delta E_{\text{xc}}[n_{\uparrow}, n_{\downarrow}]}{\delta n_{\sigma}(\mathbf{r})}. \quad (2.7)$$

As the KS orbitals $\varphi_{i\sigma}(\mathbf{r})$ in turn sum up to the true electron density,

$$n(\mathbf{r}) = \sum_{\sigma=\uparrow, \downarrow} n_{\sigma}(\mathbf{r}) = \sum_{\sigma=\uparrow, \downarrow} \sum_{i=1}^{N_{\sigma}} |\varphi_{i\sigma}(\mathbf{r})|^2, \quad (2.8)$$

the KS scheme of Eq. (2.7) requires a self-consistent solution that is typically obtained in an iterative procedure.

The central quantity of DFT and also this thesis is the xc energy $E_{\text{xc}}[n]$ and its functional derivative, $v_{\text{xc}\sigma}([n_{\uparrow}, n_{\downarrow}]; \mathbf{r}) = \delta E_{\text{xc}}[n_{\uparrow}, n_{\downarrow}]/\delta n_{\sigma}(\mathbf{r})$, the xc potential. In principle the exact xc functional is known [LP77, Lev79, GL94] and can even be constructed, see, e.g., Ref. [MSC18]. However, obtaining the ground-state energy after constructing the exact functional is significantly more difficult than directly solving the many-body Schrödinger equation. Therefore, in practice virtually every DFT calculation requires an explicit density functional approximation (DFA) to $E_{\text{xc}}[n]$. The choice of this approximation to $E_{\text{xc}}[n]$ does not only dictate the accuracy with which specific properties can be calculated but also determines the associated computational cost.

Despite representing a rather small energy contribution, $E_{\text{xc}}[n]$ is crucial for obtaining a qualitatively correct description of condensed matter and is conventionally split further into the exchange $E_{\text{x}}[n]$ and the correlation energy $E_{\text{c}}[n]$ [PK03]. The recurring theme of this thesis is to capture ultranonlocal properties of the xc potential within DFAs. As the exchange energy makes for the substantial contribution to $E_{\text{xc}}[n]$ and also typically captures the significant portion of its ultranonlocality, this thesis is primarily focused on $E_{\text{x}}[n]$ and $v_{\text{x}}(\mathbf{r})$. The following Chapter 3 is dedicated to ultranonlocality, while other exact properties of $E_{\text{xc}}[n]$ and $v_{\text{xc}}(\mathbf{r})$ that are typically used to guide the construction of DFAs are presented in Chapter 4.

CHAPTER 3

Ultranonlocality in Density Functional Theory

Despite the fact that in KS formulation of DFT the xc potential is merely a multiplicative potential, the exact $v_{xc}(\mathbf{r})$ has to mediate the entire correlated two-particle interaction – aside from the Fermi repulsion in $T_s[n]$ and the classical repulsion in $E_H[n]$. As a consequence, the xc potential has remarkable but at the same time unconventional properties. Some of these properties can be characterized as “ultranonlocal” and will be discussed in detail in this chapter.

As the term “ultranonlocality” [GGG95, GvGSB00, vFdBvL⁺02, AKK08, NV11] has been used in the literature in different contexts, is sometimes interchanged with nonlocality, and has thus been assigned different meanings, it is necessary to define what ultranonlocality should mean throughout this thesis. Here “ultranonlocality” comes down to the functional dependence of the xc potential with respect to the density, $v_{xc}([n]; \mathbf{r})$:

An xc potential is said to be “local” if at each point of space \mathbf{r} , it is an ordinary function of the density at the same point, $n(\mathbf{r})$. The most prominent example of a local xc potential is the one of the local density approximation (LDA) [HK64], cf. Sec. 4.6. In terms of the xc kernel

$$f_{xc}([n]; \mathbf{r}, \mathbf{r}') = \frac{\delta v_{xc}([n]; \mathbf{r})}{\delta n(\mathbf{r}')} \quad (3.1)$$

that mathematically describes how the xc potentials changes at \mathbf{r} if the density is changed at \mathbf{r}' ,

$$\delta v_{xc}([n]; \mathbf{r}) = \int f_{xc}([n]; \mathbf{r}, \mathbf{r}') \delta n(\mathbf{r}') d^3 r', \quad (3.2)$$

a local potential is associated with a kernel of the form

$$f_{xc}^{\text{local}}([n]; \mathbf{r}, \mathbf{r}') = f_0([n]; \mathbf{r}) \delta(\mathbf{r} - \mathbf{r}'). \quad (3.3)$$

The next tier is labeled “semilocal” and describes the situation that the potential at \mathbf{r} depends not only on the value of the density at this point, but also on density in a neighborhood around \mathbf{r} , i.e., on spatial derivatives of the density at \mathbf{r} like $\nabla n(\mathbf{r})$ or $\nabla^2 n(\mathbf{r})$. The kernel of a semilocal potential, thus, takes the form

$$f_{xc}^{\text{sl}}([n]; \mathbf{r}, \mathbf{r}') = f_0([n]; \mathbf{r}) \delta(\mathbf{r} - \mathbf{r}') + \mathbf{f}_1([n]; \mathbf{r}) \cdot \nabla \delta(\mathbf{r} - \mathbf{r}') + f_2([n]; \mathbf{r}) \nabla^2 \delta(\mathbf{r} - \mathbf{r}') + \dots \quad (3.4)$$

and is historically sometimes already termed “nonlocal” in the sense of “not local” [PBE96].

Going by this definition, generalized gradient approximations (GGAs) [PW86], for instance, yield an entirely semilocal potential. However, meta generalized gradient approximations (meta-GGAs), which are termed “semilocal functionals” in the literature as well as in this thesis since their energy density depends on semilocal quantities only, do not have a purely semilocal potential due to their kinetic energy dependence [NV11] as will be discussed in detail in Chapter 5.

Next comes a “nonlocal” potential, which is the most ambiguously used term in the literature, e.g., used to describe a “non-multiplicative” potential [SGV⁺96]. Throughout this thesis, however, a “nonlocal” potential – in contrast to an ultranonlocal potential – shall mean that $v_{xc}([n]; \mathbf{r})$ depends continuously on the density in the long-ranged neighborhood of the corresponding point in space. A kernel in the form

$$f_{xc}^{nl}([n]; \mathbf{r}, \mathbf{r}') \propto 1/|\mathbf{r} - \mathbf{r}'| \quad (3.5)$$

and the corresponding potential as, e.g., realized by the Hartree potential, $v_h([n]; \mathbf{r})$, are considered nonlocal by this definition. A nonlocal xc potential is, therefore, here associated with long-rangedness of the Coulomb interaction.

Ultranonlocality shall be defined as the nonlocality in the xc potential that goes beyond the common long-rangedness associated with the Coulomb interaction. An xc potential is therefore considered ultranonlocal if either $v_{xc}([n]; \mathbf{r})$ at \mathbf{r} depends on the density at a distant point \mathbf{r}' that may in principle be infinitely far apart or if an infinitesimally small change of the density leads to a finite change of the corresponding xc potential. Consequently, ultranonlocality is typically associated with divergences in the xc kernel [GGG97a, DHG04].

Understandably, these ultranonlocal properties are notoriously hard to capture within a DFA and are cause to hallmark deficiencies, reaching from the early days of DFT to the present [CMSY08, KK08, CMSY12]. Moreover, they are not only vital to ground-state DFT but also [LK05, MK05, EFRM12, MT06] to time-dependent DFT [RG84]. To this end, the central question of this thesis is how to capture these ultranonlocal properties on a feasible computational level. The following sections will outline how and where ultranonlocality manifests itself in ground-state DFT.

3.1 Fractional Particle Numbers and Derivative Discontinuity

A vital point of view to gain understanding of ultranonlocality in DFT are fractional particle numbers. Within the ensemble extension of DFT by Perdew *et al.* [PPLB82] a fractional particle number $N = N_0 + \eta$, where N_0 is an integer and $0 < \eta < 1$, is associated to an open system described by a statistical mixture of the pure N_0 and $N_0 + 1$ ground states. Consequently, the exact ground-state energy as a function of the fractional particle number consists of straight line segments between the values at integer points [PPLB82, YZA00],

$$E(N) = (1 - \eta)E(N_0) + \eta E(N_0 + 1). \quad (3.6)$$

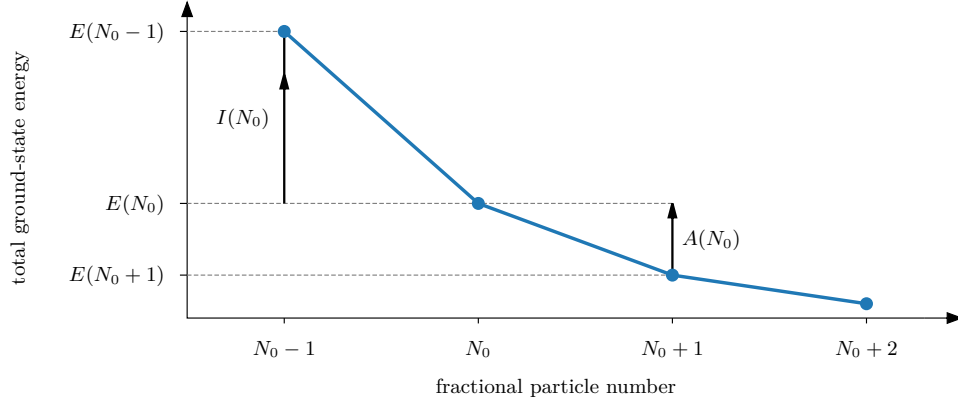


Figure 3.1: Illustration of the straight-line condition: Particle number dependence of the exact total ground-state energy $E(N)$ for fractional particle number N .

Thus, when crossing an integer the exact chemical potential $\mu(N) = \partial E(N)/\partial N$ jumps discontinuously [PPLB82],

$$\mu(N) = \begin{cases} -I(N_0), & N_0 - 1 < N \leq N_0 \\ -A(N_0), & N_0 < N \leq N_0 + 1 \end{cases}, \quad (3.7)$$

from the negative ionization potential $-I(N_0) = E(N_0) - E(N_0 - 1)$ to the negative electron affinity $-A(N_0) = E(N_0 + 1) - E(N_0)$. The discontinuity of the total energy derivative is therefore given by the fundamental gap Δ_g ,

$$\lim_{\eta \rightarrow 0^+} \left(\left. \frac{\partial E}{\partial N} \right|_{N_0 + \eta} - \left. \frac{\partial E}{\partial N} \right|_{N_0 - \eta} \right) = I(N_0) - A(N_0) =: \Delta_g, \quad (3.8)$$

and implies that the underlying total energy functional $E[n]$ of Eq. (2.2) must have derivative discontinuities with respect $n(\mathbf{r})$. The exact $E(N)$ curve with its straight line segments is illustrated in Fig. 3.1.

Within KS DFT the total ensemble density is calculated from a single KS system,

$$n(\mathbf{r}) = (1 - \eta)n_{N_0}(\mathbf{r}) + \eta n_{N_0+1}(\mathbf{r}) = \sum_{i=1}^{N_0} |\varphi_i(\mathbf{r})|^2 + \eta |\varphi_{N_0+1}(\mathbf{r})|^2, \quad (3.9)$$

using the corresponding ensemble xc potential¹, i.e., $v_{xc}([n]; \mathbf{r}) = \delta E_{xc}[n]/\delta n(\mathbf{r})$ where $n(\mathbf{r})$ can integrate to a non-integer particle number. Following the variational Eq. (2.1) and KS partitioning of energy according to Eq. (2.2), the discontinuity splits into two contributions

¹Note that other non-standard generalizations of $E_{xc}[n]$ to fractional particle numbers have been put forward in, e.g., Refs. [KK13, Gö15].

[PL83, SS83],

$$\Delta_g = \lim_{\eta \rightarrow 0^+} \underbrace{\left\{ \frac{\delta T_s[n]}{\delta n(\mathbf{r})} \Big|_{N_0+\eta} - \frac{\delta T_s[n]}{\delta n(\mathbf{r})} \Big|_{N_0-\eta} \right\}}_{=:\Delta_{\text{KS}}} + \lim_{\eta \rightarrow 0^+} \underbrace{\left\{ \frac{\delta E_{\text{xc}}[n]}{\delta n(\mathbf{r})} \Big|_{N_0+\eta} - \frac{\delta E_{\text{xc}}[n]}{\delta n(\mathbf{r})} \Big|_{N_0-\eta} \right\}}_{=:\Delta_{\text{xc}}}. \quad (3.10)$$

The first contribution is due to the non-interacting kinetic energy $T_s[n]$ and reduces to the KS gap, i.e., the energy difference between the lowest unoccupied (lu) and the highest occupied (ho) KS eigenvalue at integer electron number,

$$\Delta_{\text{KS}} = \varepsilon_{N_0+1}(N_0) - \varepsilon_{N_0}(N_0) = \varepsilon_{\text{lu}} - \varepsilon_{\text{ho}}. \quad (3.11)$$

As the Hartree and external energy are continuous functionals of the density by definition, the second contribution to Δ_g emerges from $E_{\text{xc}}[n]$,

$$\Delta_{\text{xc}} = \lim_{\eta \rightarrow 0^+} \left\{ \frac{\delta E_{\text{xc}}[n]}{\delta n(\mathbf{r})} \Big|_{N_0+\eta} - \frac{\delta E_{\text{xc}}[n]}{\delta n(\mathbf{r})} \Big|_{N_0-\eta} \right\} = v_{\text{xc}}^+([n]; \mathbf{r}) - v_{\text{xc}}^-([n]; \mathbf{r}), \quad (3.12)$$

and is attributed to a spatially uniform jump of the xc potential. This global discontinuous shift of the exact xc potential by a finite constant, Δ_{xc} , upon an infinitesimal small change of the density is the prime example for ultranonlocality in DFT. Naturally, other aspects of ultranonlocality in the potential are closely related to the derivative discontinuity Δ_{xc} . Again, Δ_{xc} can be split into an exchange Δ_x and correlation Δ_c contribution. All experience and arguments to the present date point at a positive Δ_x and Δ_{xc} , while Δ_c is known to partially compensate Δ_x in many cases [PL83, Cha99, SP08]. Note that the extension to fractional particle numbers uniquely defines

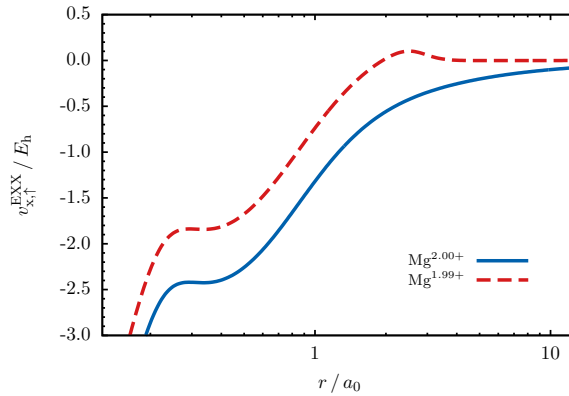


Figure 3.2: Visualization of the derivative discontinuity in $v_{\text{xc}}(\mathbf{r})$ as shown in Fig. 5 of Pub. 2: The exact-exchange potential (EXX) jumps in a finite domain upon addition of a fraction of an electron to double-ionized atomic magnesium. When the fraction is further decreased the step wanders outwards to infinity. Thereby the plateau in $v_{\text{xc}}(\mathbf{r})$ and thus the domain of the jump stretch out to all of space until a spatially uniform jump of $v_{\text{xc}}(\mathbf{r})$ by Δ_{xc} is reached in the limit of an infinitesimally small fraction.

the xc potential for a given energy functional and associates the potential at integer particle number with the limit from below, $v_{xc}([n]; \mathbf{r}) = v_{xc}^-([n]; \mathbf{r})$, whereas it is only defined up to a spatial constant for integer number of particles.

When one considers a DFA to $E_{xc}[n]$ and not the exact functional, the corresponding $E(N)$ curve is not given by perfectly straight line segments. The deviation from the straight-line condition is typically convex because the local or semilocal potentials of common DFAs lack a derivative discontinuity completely and thus average over it [PL83, Toz03]. The corresponding $E(N)$ curve, however, still displays kinks due to the KS gap Δ_{KS} but of underestimated magnitude. Moreover, Janak's theorem [Jan78],

$$\mu(N) = \frac{\partial E(N)}{\partial N} = \varepsilon_{ho}(N), \quad (3.13)$$

ensures that even for DFAs to $E_{xc}[n]$ the chemical potential equals the highest occupied KS eigenvalue. However, $\varepsilon_{ho}(N)$ and thus $\mu(N)$ vary unphysically as function of fractional N between integer points. Janak's theorem is employed in Pub. 2 to prove that the potential of a specific DFA is not discontinuous, even though it mimics features that are typically associated with a xc derivative discontinuity.

One might be tempted to dismiss the significance of the (missing) derivative discontinuity and its associated physics, as every extended system will correspond to a integer number of electrons. The fact, however, is that the missing derivative discontinuity of traditional DFA has detrimental consequences for the prediction of band gaps [PL83, GSS86, MSCY08], polarizabilities [vGSG⁺99, KKP04], charge transfer [Toz03], charge localization or charge distribution between subsystems [MSCY08, HKSG17] as will be outlined in the following sections.

3.2 Band Gap Problem

In solid-state physics it is common to use ground-state DFT to calculate the electronic band structures directly from KS eigenvalues, e.g., as these can be viewed as the leading order contribution to the quasiparticle energies [CGB02]. While the band shapes are typically well reproduced by the KS eigenvalues and in good agreement with experiment, the band gap of insulators and semiconductors, i.e., the energetic difference between the conduction and valence band, is systematically and significantly underestimated [GSS86, PL83]. This is especially concerning in cases where semiconductors are predicted to be metallic. The underlying reasons for this band gap problem are twofold and summarized briefly below – for a detailed discussion see, e.g., Ref. [KK08].

First, from a conceptual point of view, KS ground-state DFT is not supposed to yield the complete (fundamental) band gap directly from the KS eigenvalue gap Δ_{KS} . The latter energy difference is exactly short of the xc derivative discontinuity Δ_{xc} because the KS potential and thus the KS eigenvalues would jump by Δ_{xc} upon occupying the conduction band. However, if the exact $E_{xc}[n]$ or a DFA with a sizable derivative discontinuity thereof is used to calculate the

KS band structure, Δ_{xc} can be evaluated and added to Δ_{KS} to obtain an accurate fundamental band gap. Another frequently taken option is to resort to generalized Kohn-Sham [SGV⁺96], cf. Sec. 5.3, where the restriction of a multiplicative KS potential is lifted and thereby the derivative discontinuity is readily and directly incorporated into the then generalized KS gap [SGV⁺96, PYB⁺17, YPSP16, PR18], $\Delta_g = \Delta_{gKS} \approx \Delta_{KS} + \Delta_{xc}$.

Second, while the band gap problem is thus solved conceptually, the problem still persists from a practical point of view: Given that Δ_{xc} makes for the pivotal missing contribution to the band gap and that common semilocal DFAs completely lack a Δ_{xc} , the band gap problem of (semilocal) DFT is apparent and an intrinsic limitation of explicit density-dependent semilocal functionals. Upto now, the options to surpass the band gap problem in practice are either to employ nonlocal DFA [KK08] such as range-separated hybrids [HSE03], which increase the computational cost, or to use semi-empirical methods like DFT+ U [AZA91, LAZ95] or model potentials [GvLvLB95, BJ06, TB09, KOER10, KTB12]. Both of the latter come with formal and practical limitations [AKJS06, MKvLR07, GS09, KAK09, KAK13], which are also partially discussed in Pubs. 1 and 2 in case of the model potentials. While meta-GGAs have been recently shown [YPSP16] to improve on the band gap problem, Pub. 3 demonstrates that a meta-GGA with a novel construction strategy with focus on the derivative discontinuity is able to overcome the band gap problem of semilocal DFT. Thereby, a new computationally feasible avenue without the formal and practical limitations of the methods mentioned above opens.

3.3 Shell and Step Structures

When adding a small, but finite fractional charge to a system, the ultrasnonlocal discontinuous shift of $v_{xc}(\mathbf{r})$ that is associated with the derivative discontinuity reduces to a plateau of finite width that lifts the KS system energetically and thus increases the energy to add an electron, cf. Fig. 3.2. When the added fractional charge is continuously decreased the steps of the plateau wander outwards to infinity [PL83, KLI92a]. In the opposite limit, i.e., when the fractional charge approaches a full electron, the step is absorbed into the $v_{xc}(\mathbf{r})$ and is, e.g., associated with a pronounced shell structure [HS89, vLGB95, BJ06] that can be found in the exchange potential of atoms.

A plateau in $v_{xc}(\mathbf{r})$ and thus step structures are also observed in a different but related physical situation [Per90, GB96, MKK11, KAK09, HKSG17], which is schematically depicted in Fig. 3.3: In case of a combined system composed of two different subsystems, e.g., two atoms of different species, separated by a large distance a plateau in the exact $v_{xc}(\mathbf{r})$ forms around one of the subsystems to ensure the physically correct distribution of charge, i.e., the correct integer number of electrons at each subsystem. The link to the derivative discontinuity is apparent when considering the physically equivalent description of the two isolated subsystems. Upon moving an infinitesimal test charge between the systems in a thought experiment in order to minimize the energy, the acceptor system would prevent this charge transfer by virtue of a discontinuous upshift of its xc potential. In the combined system this shift has to be present as a plateau in

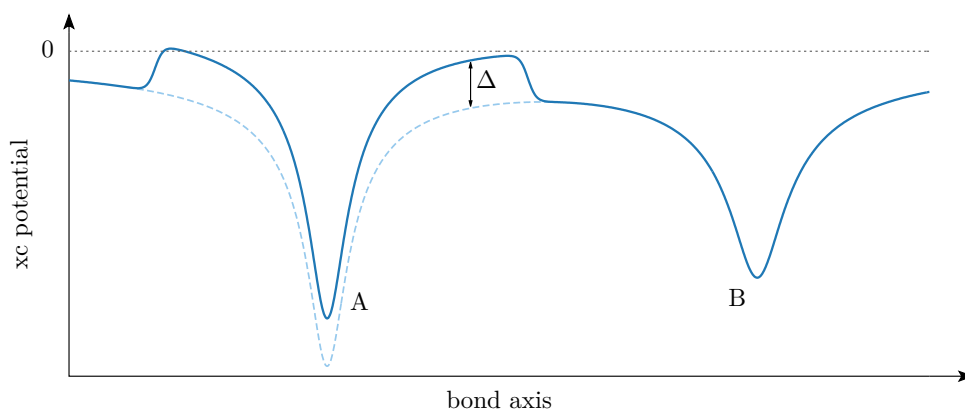


Figure 3.3: Schematic depiction of the exact xc potential for a combined system comprised of two well-separated subsystems (A and B) along their bond axis (without the interbond peak): the xc potential (solid blue line) forms a ultranlocal plateau that uplifts system A by a constant Δ relative to the potential that corresponds to the individual system A (dashed light blue line). Thereby, an integer number of electrons at both A and B is enforced in the combined KS system.

$v_{xc}(\mathbf{r})$ even at integer distribution of charge.

Common local and semilocal DFAs that do not possess the required ultranlocal properties, i.e., a derivative discontinuity, violate the integer preference principle [Per90] in these situations. The consequence is an unphysical dissociation limit with fractional numbers of electrons in both subsystems [RPC⁺06].

3.4 Polarizabilities and Charge Transfer

The basically same physics of the derivative discontinuity and thus ultranlocality present themselves in the case of charge transfer [Toz03, DWHG03, Mai05, TFSB05, KBY07, Kü17], especially long-range charge transfer. Here, the energies of the subsystems are shifted relative to each other by an additional external electric field. When the distance between the subsystems is sufficiently large, no charge should be transferred until the potential difference of the external electric field surpasses the difference between the electron affinity of the acceptor and the ionization potential of the donor. At this point, precisely one electron should be transferred and the transfer should stop until the next threshold field strength is reached and the next integer electron transfer occurs. In addition to the plateau discussed in the previous section, which is already present without an external electric field when different donor and acceptor molecules are used, $v_{xc}(\mathbf{r})$ has to build a plateau around the acceptor to prevent a fractional transfer of charge induced by the external field until the external field threshold is reached. Consequently, this plateau counteracts the external electric field and thus increases with the field strength. Once an integer electron transfer occurred a step in the opposite direction, i.e., a plateau around the donor system, can be observed in the xc potential in order to stabilize the transferred charge [HK12]. The initial plateau and the field-counteracting terms in the xc potential are thus vital

to the proper description of charge transfer within DFT. An absence of these ultranonlocal properties in common DFAs results in a significant underestimation of charge transfer energies [Toz03] and in the prediction of a fractional transfer of charge [KBY07].

Moreover, these field-counteracting properties of $v_{xc}(\mathbf{r})$ are also present [CPvG⁺98, KKP04, KK18] when the distance between the subsystems approaches zero, i.e., within molecules. This is especially relevant for extended molecular systems such as conjugated polymers that are of particular interest because of their widespread optoelectronic applications [KRM94]. The absence of the derivative discontinuity and hence of the field-counteracting term manifests itself very prominently in the incorrect description of electric response properties such as the detrimental overestimation of the static electric (hyper)polarizabilities of extended molecular systems [CPvG⁺98, vGSG⁺99, KKP04, KK06, AKK08, KAK09]. This type of ultranonlocality can also be observed in solids and is of relevance when calculating their polarization dependence [GGG95, GGG97a, GGG97b].

Valuable model systems that are frequently used to investigate these field-counteracting physics and to benchmark DFAs are hydrogen chains, i.e., linear chains of hydrogen atoms. While they are most difficult to describe accurately within DFT, their electronic structure remains transparent and mimics features of polymers like polyacetylene [KKP04]. Hydrogen chains can either be used to study the field-counteracting term and its effects on the static electric response within a single chain [CMVA95, vGSG⁺99, GGB02, MSWY03, vFdBvL⁺02, KKP04, KK06, MvF07, KMK08, RPC⁺08, PSB08, AKK08] or to assess charge transfer properties and integer preference between two chains [KBY07, HK12, SK16]. Figure 3.4 showcases the field-counteracting term in the former model of a single linear chain consisting of twelve hydrogen atoms with alternating distances. The single chain model is also used briefly in Pub. 2, whereas both models play a central role in Pub. 3.

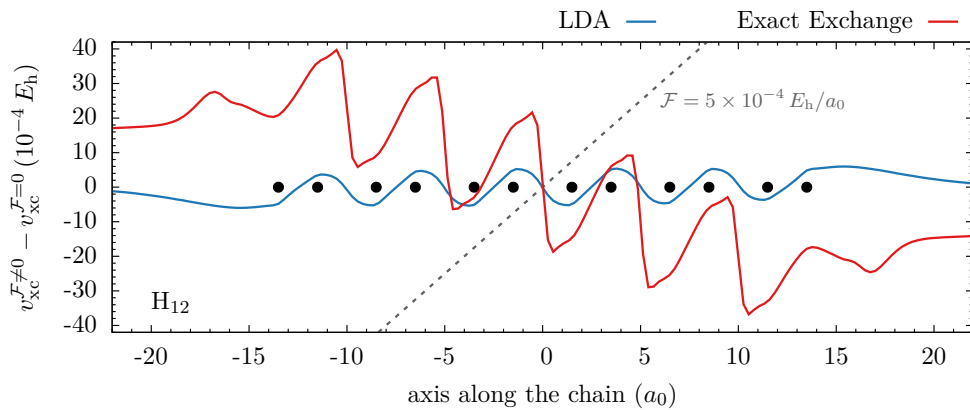


Figure 3.4: Visualization of the field-counteracting term in the xc potential as present in the hydrogen chain model: Difference between the xc potential of calculations with and without a small external linear electric field (dashed gray line) for a H_{12} chain (atom positions are indicated by circles). The solid red line shows the desired field-counteracting behavior of the exact-exchange potential, whereas the solid blue line shows the absence of this ultranonlocal term in the LDA xc potential.

3.5 Delocalization, Density-Driven, and Self-Interaction Errors

The error related to a missing derivative discontinuity in $E_{xc}[n]$ is also frequently referred to differently in the literature, connoting different perspectives on the same principle issue at the core, e.g., delocalization, density-driven, or self-interaction error. The related changes in perspective were and still remain useful to find, better understand and overcome the various manifestations of this tedious error, which appears to be ultimately solved by the exact functional only.

A powerful perspective is the delocalization error [MSCY08, JMICY08] which depicts the tendency of common semilocal DFAs to $E_{xc}[n]$ to unphysically favor delocalization of charge in the system. This delocalization error is directly related to the convex violation of the straight-line condition between integer points in the $E(N)$ curve and can instructively explain the various practical deficiencies reaching from the band gap problem to charge transfer and the prediction of fractional charge distributions. Overcoming the delocalization error is, however, a fine line because overcorrection leads to the reverse error, which is termed localization error.

Many of these deficits of common DFAs related to the missing derivative discontinuity may also be characterized as density-driven errors [Jan17, WNJ⁺17, SSB18]. A density-driven error is defined as the error of DFAs due to not being evaluated at the exact but on the self-consistently calculated density. While many DFAs yield surprisingly accurate energies when evaluated at the exact densities, they perform considerably worse at their self-consistent densities that can deviate from the exact one substantially [MBS⁺17]. This deviation in turn is attributed to their incorrect functional derivative, i.e., their potential that misses crucial features – for example ultranonlocal features like step structures in the potential. This underscores that DFAs to $E_{xc}[n]$ should ideally not only be constructed with the focus on the energy as it is very common but also with a focus on the corresponding potential.

A final perspective is given by the self-interaction error [Per79, PZ81, ZY98]. Due to the nature of DFT that is based on the density, there is no obvious way to distinguish between the legit Coulomb-interaction between two electrons and the artificial interaction of an electron with itself. The resulting self-interaction error is most transparent for one-electron systems, where the correlation energy should vanish and the exchange energy should cancel the Hartree energy completely, i.e., $E_H[n^{1e}] + E_{xc}[n^{1e}] = 0$ for any single-electron ground-state density $n^{1e}(\mathbf{r})$. For a many-electron system this definition of one-electron self-interaction freedom is commonly extended [Per79, PZ81] by identifying the fictional KS orbitals with electrons [KKM08] to

$$\sum_{\sigma=\uparrow,\downarrow} \sum_{i=1}^{N_\sigma} \{E_H[n_{i\sigma}] + E_{xc}[n_{i\sigma}, 0]\} = 0, \quad (3.14)$$

where $n_{i\sigma}(\mathbf{r}) = |\varphi_{i\sigma}(\mathbf{r})|^2$ are the KS orbital densities. A DFA is thus considered one-electron self-interaction free if $E_H[n^{1e}] + E_{xc}^{\text{DFA}}[n^{1e}] = 0$ for any single-electron density including non-ground-state densities. Explicit elimination of the one-electron self-interaction by subtracting Eq. (3.14) lead to self-interaction corrected DFAs [PZ81, KKM08], which can be shown

[Per90, TFSB05, KMK08, RPC⁺08, PSB08] to improve on the various longstanding problems outlined throughout this chapter. Other pathways to eliminate the one-electron self-interaction error involve semilocal iso-orbital indicators [Bec98, PKZB99, JSE03, KP03c, SKM⁺14, FS19] in combination with nonlocal functional expressions in order to cancel the nonlocal Hartree energy. This is demonstrated in Pub. 4 for local range-separated hybrids. While these single-orbital indicators are also frequently used in meta-GGAs, meta-GGAs cannot be formally one-electron self-interaction free. However, one-electron correlation freedom is achievable [Bec98, PKZB99]. Additionally, one-electron self-interaction freedom of the exchange part can be realized in a loose sense by typically requiring one-electron self-interaction freedom for the exact hydrogen ground state only [TPSS03] as it is done in Pub. 3. Eliminating the one-electron self-interaction error is, however, not sufficient to completely eliminate [RPC⁺07] – or in instances even reduce [SK16] – the many-electron self-interaction [MSCY06], which in turn is defined by satisfying the straight-line condition in the $E(N)$ curve, i.e., identical to the definition of the absence of the (de-)localization error.

CHAPTER 4

Constraint-Guided Construction of Density Functional Approximations

This chapter presents an overview of the formal properties of the exact xc energy and potential that are typically used as constraints on DFAs to $E_{xc}[n]$ and in particular as guidance on their construction. Depending on the given form of the DFA, however, some exact constraints are impossible to satisfy, incompatible with others, or may be inappropriate. Moreover, even a complete set of known appropriate constraints does not define a functional uniquely since there are still infinitely many ways to satisfy these constraints [SRP15]. Consequently, the selection and realization of exact constraints in the DFA construction are to some extent experience-driven and an active field of research. The advantage of constraint-guided DFAs [PBE96, TPSS03, SRP15, TM16] in contrast to DFAs that are optimized for a dedicated purpose, e.g., by fitting to molecule data, is that they are non-empirical and expected [PS01, PSTS08, RCFB09, SRP15] and found [KPB99, MBS⁺17] to be more reliable – or at least systematic in their error – over a wide range of situations and systems, e.g., atoms, molecules, solids, and surfaces. In particular, this includes situations that are different from those the DFA has been constructed, tested, and validated for. Therefore, these non-empirical DFAs are, e.g., valuable in material science and in their search for new materials. The DFAs developed as part of this thesis and presented in Pubs. 3 and 4 follow this constraint-guided construction concept.

4.1 Size Consistency

A fundamental principle of physics and thus of electronic structure theory including DFT is size consistency [PK03]. It states that the total energy of a system comprised of two subsystems (A and B) separated by a large distance must equal the sum of the energies of the separate parts,

$$E(A \cdots B) = E(A) + E(B). \quad (4.1)$$

Moreover, the density should also be additive,

$$n_{A \cdots B}(\mathbf{r}) = n_A(\mathbf{r}) + n_B(\mathbf{r}). \quad (4.2)$$

In absence of degeneracy most DFAs such as the LDA, GGAs, or meta-GGAs are size consistent [Sav09]. Functionals which are not size-consistent should in general be avoided in ground state DFT. An example of DFAs that violate size consistency are optimally tuned range-separated hybrid functionals [KKK13]. The concept of a local range separation, which is the topic of Pub. 4, is in part motivated by restoring size consistency for this class of functionals.

4.2 Unitary Invariance

The exact xc functional is ultimately by virtue of the Hohenberg-Kohn theorem [HK64] a functional of the density alone, $E_{xc}[n]$. DFAs that model this complex density dependence implicitly via other ingredients should consequently yield the same energy when evaluated at the same density. Therefore, DFAs to $E_{xc}[n]$ should be invariant under changes that do not alter the density. Such a change, which is highly relevant for explicitly orbital-dependent DFAs, is a unitary transformation of the orbitals. A prominent counterexample for a DFA that is unitary variant is the self-interaction correction to LDA [PZ81]. Following this line of arguments, orbital-dependent functionals should only use unitary invariant ingredients, such as the positive non-interacting kinetic energy density

$$\tau(\mathbf{r}) = \sum_{\sigma=\uparrow,\downarrow} \tau_{\sigma}(\mathbf{r}) = \sum_{\sigma=\uparrow,\downarrow} \frac{\hbar^2}{2m_e} \sum_{i=1}^{N_{\sigma}} |\nabla \phi_{i\sigma}(\mathbf{r})|^2. \quad (4.3)$$

4.3 Spin Scaling

Both the exchange energy $E_x[n]$ as well as the non-interacting kinetic energy $T_s[n]$ are by definition separable with respect to the two spin orientations. This implies [OP79] the exact spin-scaling relations

$$E_x[n_{\uparrow}, n_{\downarrow}] = \frac{1}{2} E_x[2n_{\uparrow}] + \frac{1}{2} E_x[2n_{\downarrow}] \quad (4.4)$$

and

$$T_s[n_{\uparrow}, n_{\downarrow}] = \frac{1}{2} T_s[2n_{\uparrow}] + \frac{1}{2} T_s[2n_{\downarrow}]. \quad (4.5)$$

The former is typically utilized to generate spin-density approximations of a DFA to $E_x[n_{\uparrow}, n_{\downarrow}]$ from the corresponding spin-unpolarized form $E_x[n]$ as demonstrated in Appendix A.1. For a meta-GGA in particular, the combination of both spin-scaling relations allows notating the kinetic energy dependence explicitly,

$$E_x[n_{\uparrow}, n_{\downarrow}, \tau_{\uparrow}, \tau_{\downarrow}] = \frac{1}{2} E_x[2n_{\uparrow}, 2\tau_{\uparrow}] + \frac{1}{2} E_x[2n_{\downarrow}, 2\tau_{\downarrow}]. \quad (4.6)$$

While in certain cases the spin dependence of the correlation energy $E_c[n]$ is similar to the one of the exchange energy [vBH72], there is, in general, no simple spin-scaling relation for $E_c[n]$ since two electrons of anti-parallel spin repel one another due to their Coulomb interaction.

To account for the spin dependence of $E_c[n]$, the (local fractional) spin-polarization

$$\zeta(\mathbf{r}) = \frac{n_{\uparrow}(\mathbf{r}) - n_{\downarrow}(\mathbf{r})}{n_{\uparrow}(\mathbf{r}) + n_{\downarrow}(\mathbf{r})} \quad (4.7)$$

is typically used as an additional variable. [Publication 4](#) exploits this fact to model a local range-separation parameter for exchange with explicit dependence on $\zeta(\mathbf{r})$ since range separation effectively models not only exchange but partly also correlation, cf. Sec. 6.3.

4.4 Asymptotic Behavior

In the asymptotic region of space, i.e., outside of the domain of substantial electronic density $n(\mathbf{r})$, the xc potential is governed [\[AvB85\]](#) by its exchange part and can be shown [\[GJL79, ECMV92\]](#) to decay as

$$v_{xc}(\mathbf{r}) \sim v_x(\mathbf{r}) \sim -\frac{e^2}{|\mathbf{r}|}. \quad (4.8)$$

The associated exchange(-correlation) energy density per unit volume in the conventional gauge¹ is proportional to the electron density in the asymptotic region and thus decays exponentially [\[GJL79, ECMV92\]](#),

$$e_{xc}(\mathbf{r}) \sim e_x(\mathbf{r}) \sim -\frac{e^2 n(\mathbf{r})}{2|\mathbf{r}|}. \quad (4.9)$$

This long-rangedness of $v_x(\mathbf{r})$ is reflective of the fact that exchange has to cancel the self-interaction that is induced by the Hartree potential also in the asymptotic region [\[SKKK14\]](#).

In the presence of a nodal surface of the highest occupied orbital that extends to infinity – a

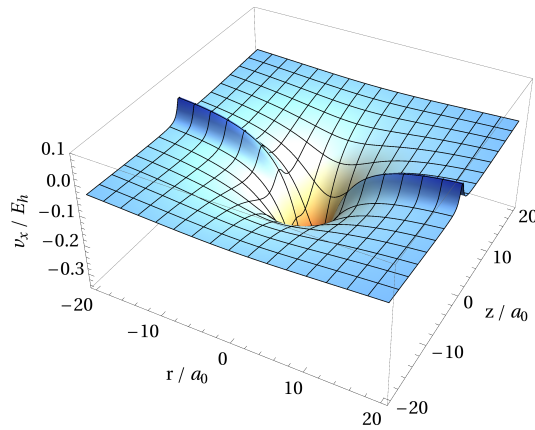


Figure 4.1: Exact-exchange potential evaluated in a minimal nodal plane model as shown in Fig. 3 of [Pub. 1](#). The characteristic pronounced ridge is visible in the potential along the nodal surface, here given by $z = 0$, at intermediate distances. For large distances, the ridge contracts exponentially.

¹Note that energy densities are not uniquely defined and can be subjected to a gauge transformation. The conventional gauge of the exchange energy density is given by Eq. (5.1). See Ref. [\[TSSP08\]](#) for further details.

situation that is rather the norm than the exception, especially in case of organic molecules – the exact-exchange potential does not decay isotropically to zero as Eq. (4.8) indicates. Instead, the exchange potential approaches a positive system-dependent constant along the nodal surfaces, as depicted in Fig. 4.1, leading to ridges in the KS potential that contract exponentially to a set of zero measure [DSG02a, DSG02b, KP03a]. The behavior of the exact $v_{xc}(\mathbf{r})$, including correlation, in the presence of orbital nodal surfaces is still an area of active research [WAY03, GGGB16, GGB18].

While the long-range behavior of $v_x(\mathbf{r})$ is pivotal to properly describe, e.g., Rydberg states [CJCS98], anions [LFB10], or the binding of excitons [RORO02], semilocal DFAs on the GGA or meta-GGA level are only capable to model long-range behavior within narrow conditions [Bec88, BR89, ECMV92, CEGVT15, DSFC15]. Additionally, these semilocal attempts to model long-rangedness are typically exclusive to certain aspects [ECMV92], e.g., either to the potential or to the energy density, numerically fragile, cf. Pub. 2, and are shown to result in divergences of the KS potential in presence of the above-mentioned orbital nodal surfaces in Pub. 1. Consequently, satisfying the exact asymptotic behavior within a semilocal approximation to $E_x[n]$ is uncommon and typically considered inappropriate.

4.5 Density Scaling

An important concept in DFT is density scaling, which describes how the different components of the energy, especially $E_x[n]$ and $E_c[n]$, change under certain well-defined transformations of the density. The resulting scaling relations define fundamental exact constraints on DFAs.

Uniform Density-Scaling

The most relevant density transformation is the uniform density-scaling [LP85] where the density is scaled as

$$n_\lambda(\mathbf{r}) = \lambda^3 n(\lambda\mathbf{r}) \quad (4.10)$$

with an inverse scaling length $\lambda > 0$. The uniform density-scaling is norm-conserving, i.e.,

$$\int n_\lambda(\mathbf{r}) d^3r = \int n(\mathbf{r}) d^3r = N, \quad (4.11)$$

and leads to higher, but compressed density for $\lambda > 1$, and to lower, but expanded density for $\lambda < 1$. Accordingly, $\lambda \rightarrow \infty$ is labeled as the high-density limit, whereas $\lambda \rightarrow 0$ is termed the low-density limit.

In the high-density limit the non-interacting kinetic energy dominates the Hartree and the exchange energy due to the Fermi repulsion. This is reflected in the scaling relations [LP85]

$$T_s[n_\lambda] = \lambda^2 T_s[n], \quad (4.12)$$

$$E_H[n_\lambda] = \lambda E_H[n], \quad (4.13)$$

and

$$E_x[n_\lambda] = \lambda E_x[n]. \quad (4.14)$$

The latter relation is used to fix the form of semilocal approximations to $E_x[n]$. To this end, it is easy to see that for an approximation to $E_x[n]$ where the exchange energy density is an ordinary function of semilocal ingredients, i.e.,

$$e_x(\mathbf{r}) = e_x(n(\mathbf{r}), |\nabla n(\mathbf{r})|, \tau(\mathbf{r}), \nabla^2 n(\mathbf{r}), \dots), \quad (4.15)$$

one can write the corresponding exchange energy in the form

$$E_x^{\text{sl}}[n] = A_x \int n^{4/3}(\mathbf{r}) F_x(s(\mathbf{r}), t(\mathbf{r}), q(\mathbf{r}), \dots) d^3r, \quad (4.16)$$

where the functional is solely defined by its exchange enhancement factor F_x : a function of dimensionless semilocal variables that are invariant under uniform density scaling. These dimensionless variables are, up to second order in ∇ , the reduced density gradient

$$s(\mathbf{r}) = \frac{|\nabla n(\mathbf{r})|}{2(3\pi^2)^{1/3} n^{4/3}(\mathbf{r})}, \quad (4.17)$$

the reduced Laplacian of the density

$$q(\mathbf{r}) = \frac{\nabla^2 n(\mathbf{r})}{4(3\pi^2)^{2/3} n^{5/3}(\mathbf{r})}, \quad (4.18)$$

and the reduced kinetic energy density

$$t(\mathbf{r}) = \frac{10m_e}{3\hbar^2} \frac{\tau(\mathbf{r})}{(3\pi^2)^{2/3} n^{5/3}(\mathbf{r})}. \quad (4.19)$$

The prefactor A_x is fixed by the homogeneous electron gas limit as discussed in the corresponding Section 4.6. If F_x is only a function of $s(\mathbf{r})$ this semilocal form defines a GGA for exchange [PW86]. Once F_x depends either on $t(\mathbf{r})$ or $q(\mathbf{r})$ – optionally alongside the other variables – it defines a meta-GGA [DSFC16] for exchange. However, the reduced Laplacian $q(\mathbf{r})$ is rarely used as an actual meta-GGA ingredient because it typically produces strong and unphysical oscillations in the xc potential [DSFC16, CWW12, Asc14].

While no straightforward uniform scaling relation for $E_c[n]$ exists, the high-density behavior of the correlation energy may be characterized by the inequality [LP85]

$$E_c[n_\lambda] < \lambda E_c[n] \quad \text{for } \lambda > 1, \quad (4.20)$$

which reflects that exchange dominates correlation in the high-density limit. This allows to define the exchange part of an arbitrary DFA to $E_{xc}[n]$ as [Lev91]

$$E_x[n] = \lim_{\lambda \rightarrow \infty} \frac{E_{xc}[n_\lambda]}{\lambda} \quad (4.21)$$

and thus also the correlation part [Lev91]

$$E_c[n] = E_{xc}[n] - \lim_{\lambda \rightarrow \infty} \frac{E_{xc}[n_\lambda]}{\lambda}. \quad (4.22)$$

In similar fashion, one can define [PSTS08] a DFA to $E_{xc}[n]$ to have “full” exact exchange by

$$\lim_{\lambda \rightarrow \infty} \frac{E_{xc}[n_\lambda]}{E_x^{\text{ex}}[n_\lambda]} = 1, \quad (4.23)$$

where $E_x^{\text{ex}}[n_\lambda]$ is the exact-exchange energy. This defines an exact constraint that is utilized in Pub. 4 for the construction of a local range-separation parameter.

Non-Uniform Density-Scaling

Starting from a density $n(x, y, z)$ and a corresponding finite $E_x[n]$, one can also define the one-dimensionally scaled density [Lev91]

$$n_\lambda^{(1)}(x, y, z) = \lambda n(\lambda x, y, z). \quad (4.24)$$

The result is a density with the same electron number that is compressed ($\lambda > 1$) or expanded ($\lambda < 1$) in x -direction. Of particular importance is again the high-density limit, $\lambda \rightarrow \infty$, where the density fully contracts in the x -direction and thus collapses from three to two dimensions. It has been proven [Lev91] that the exchange energy remains finite and negative in this true two-dimensional limit, i.e.,

$$-\infty < \lim_{\lambda \rightarrow \infty} E_x[n_\lambda^{(1)}] < 0. \quad (4.25)$$

Satisfying this exact constraint within a meta-GGA (or a GGA) for exchange implies [PRSB14] a condition for the large- s behavior,

$$\lim_{s \rightarrow \infty} F_x(s, \alpha = 0) \propto s^{-1/2} \quad (4.26)$$

with $\alpha = t - 5s^2/3$, cf. definitions of s in Eq. (4.17) and t in Eq. (4.19). While Pub. 1 shows that this particular large- s behavior can, in principle, lead to weak divergences in the presence of orbital nodal-surfaces, it is still employed as a constraint in the meta-GGA construction of Pub. 3.

Note that one can also define [Lev91] a non-uniform two-dimensional scaling in analogy to Eq. (4.24). This, however, yields no additional constraint as satisfying the uniform scaling relation of Eq. (4.14) and the one-dimensional scaling relation of Eq. (4.25) implies the correct two-dimensional scaling for exchange [Lev91, PRSB14].

4.6 Homogeneous Electron Gas Limit and Gradient Expansion

The simplest model of interacting electrons that has been studied since the early days of condensed matter physics [Tho27, Fer28] is the homogeneous electron gas. As it is characterized by a constant uniform density $n(\mathbf{r}) = n_{\text{unif}}$, it is ideally suited to be described exactly within DFT and has, thereby, led to the most influential DFA, the LDA [HK64].

While the exact exchange energy density of a homogeneous electron gas can be calculated analytically, obtaining [Dir30]

$$e_x^{\text{unif}} = A_x n_{\text{unif}}^{4/3} \quad \text{with} \quad A_x = -\frac{3e^2}{4\pi} (3\pi^2)^{1/3} \quad (4.27)$$

for the spin-saturated case, no closed expression for the correlation energy density of a homogeneous electron gas $e_c^{\text{unif}}(n_{\text{unif}}, \zeta_{\text{unif}})$ is known. In practice, however, this does not cause any restrictions as parametrizations [VWN80, PZ81, PW92a] of the latter based on highly accurate Quantum Monte Carlo data [CA80] are available.

Based on this exactly known homogeneous electron gas limit, the LDA is defined by approximating the xc energy density $e_{xc}(\mathbf{r})$ per unit volume of an inhomogeneous system locally at each point in space \mathbf{r} by the xc energy density of the homogeneous electron gas $e_{xc}^{\text{unif}}(n, \zeta)$ of density $n(\mathbf{r})$ [and spin-polarization $\zeta(\mathbf{r})$] corresponding to that point,

$$E_{xc}^{\text{LDA}}[n] = \int e_{xc}^{\text{unif}}(n(\mathbf{r}), \zeta(\mathbf{r})) d^3r. \quad (4.28)$$

While the condition under which the LDA should be valid are rarely satisfied in real electronic systems, it produces surprisingly good results and has become the (historic) workhorse of DFT. The reasons for this success are well understood and attributed to the fact that LDA satisfies many exact constraints inherited from its exact description of the homogeneous electron gas [GL76, PK03].

A DFA is said to respect the homogeneous electron gas limit if for a homogeneous density it reduces to the exact energy, i.e., to the one of LDA. For a semilocal exchange functional in the form of Eq. (4.16) this is equivalent with $F_x(s, t, q) = 1$ at $s = 0$, $q = 0$, and $t = 1$, i.e., for a vanishing density variation $[\nabla n(\mathbf{r}) \rightarrow 0, \nabla^2 n(\mathbf{r}) \rightarrow 0, \dots]$ and when the kinetic energy density reduces to its homogeneous electron gas limit,

$$\tau(\mathbf{r}) \rightarrow \tau_{\text{unif}}(\mathbf{r}) = \frac{3\hbar^2}{10m_e} (3\pi^2)^{2/3} n^{5/3}(\mathbf{r}). \quad (4.29)$$

For small density variations it is possible to expand the exact xc energy systematically around the homogeneous electron gas limit. The resulting gradient expansion (GE) is based on reciprocal space analysis [HK64, ED11]. The GE for exchange in its usual real space form is given by [SvB96]

$$E_x^{\text{GE}}[n] = A_x \int n^{4/3} [1 + \mu s^2 + C_x (q^2 + a_x s^2 q + b_x s^4) + \dots] d^3r, \quad (4.30)$$

where only the second-order coefficient $\mu = 10/81$ [AK85] as well as one of the fourth-order coefficients $C_x = 146/2025$ [EV90] are known exactly. The best numerical estimates for the two remaining fourth-order coefficients that are typically used in practice are $a_x = -5/2$ [SvB96] and $b_x = 0$ [TPSS03].

Note that this GE, as well as any xc energy density, is only determined up to some partial integration, whereas the corresponding total xc energy and potential are unambiguous quantities [ED11]. This, for instance, allows one to rewrite the second-order GE (GE2) contribution as a linear combination of s^2 and q ,

$$\Delta E_x^{\text{GE2}}[n] = A_x \int n^{4/3} \mu [cs^2 + 3(c-1)q] d^3r \quad \text{with} \quad c \in \mathbb{R}, \quad (4.31)$$

assuming vanishing surface contributions, and thus to change variables [ED11]. It is, however, impossible to reformulate the fourth-order terms solely in terms of s . Consequently, a GGA can by construction only satisfy the GE2 for exchange, whereas the meta-GGA form for exchange allows to reproduce the fourth-order GE (GE4) completely. Further note that modified GEs can be derived from the semiclassical theory of neutral atoms based on a large- Z asymptotic expansion of the exchange energy [ELCB08, CTDS⁺16].

As meta-GGAs are commonly based on the kinetic energy density τ and not the Laplacian of the density $\nabla^2 n$, reproduction of the GE4 requires to express q in terms of t . To this end, the GE of $\tau(\mathbf{r})$ [BJC76, PSHP86] in the limit of a slowly varying density,

$$t(\mathbf{r}) = \tau(\mathbf{r})/\tau_{\text{unif}}(\mathbf{r}) \sim 1 + \frac{5}{27}s^2(\mathbf{r}) + \frac{20}{9}q(\mathbf{r}) + \mathcal{O}(\nabla^4), \quad (4.32)$$

is employed [PKZB99]. However, this second-order expansion of the kinetic energy allows one either to use $t(\mathbf{r})$ for the exchange GE in second-order [SPR15] and thus to satisfy only the GE2 or to use it only in the fourth-order terms [PKZB99, TPSS03, SRP15] but then to satisfy the complete GE4. The usage of $t(\mathbf{r})$ in both second and fourth order while satisfying the GE4 for exchange would require the GE4 of $\tau(\mathbf{r})$. Although this expansion is known [BJC76, PSHP86], it is not being used for this purpose so far because its fourth-order terms cannot readily be expressed in terms of s and q . Publication 3 is forced to address this issue because the second-order contribution of $t(\mathbf{r})$ to the GE4 is pivotal to its meta-GGA construction strategy. To this end, a new generalized formulation of the GE4 for exchange in terms of the variables s and t – or more precisely s and $\alpha = t - 5s^2/3$ – is derived and employed in Pub. 3. The central idea of this reformulation is that, while the fourth-order terms in the GE of t (4.32) cannot be written in terms of s and q in general, they can very well be written this way under the exchange energy integral:

$$A_x \int n^{4/3} t d^3r = A_x \int n^{4/3} \left[1 + \frac{5}{27}s^2 + \frac{20}{9}q + \frac{2}{81}(2q^2 - 3s^2q + s^4) + \mathcal{O}(\nabla^6) \right] d^3r. \quad (4.33)$$

Hence, one can account for the fourth-order contributions to the GE for exchange that are induced by the corresponding second-order contributions written in terms of $t(\mathbf{r})$.

4.7 Lieb-Oxford and Strongly Tightened Bound

Helpful guidance on the construction of semilocal DFAs can further be found in bounds on the xc energy, or more importantly on the xc exchange energy density when they are interpreted locally. The most elementary such bound is the negativity of the exchange energy, $E_x[n] \leq 0$, which can be locally enforced by a positive exchange enhancement factor [DSFC16],

$$F_x \geq 0, \quad (4.34)$$

cf. the semilocal exchange form in terms of F_x as given by Eq. (4.16).

The Lieb-Oxford bound [LO81],

$$E_x[n_\uparrow, n_\downarrow] \geq E_{xc}[n_\uparrow, n_\downarrow] \geq 2.273 E_x^{\text{LDA}}[n], \quad (4.35)$$

is another important rigorous bound. Since it is based on a best estimation for the true bound value, it has been suggested [OC07, RPCP09] that it can be tightened further. While formally only the global condition is an exact constraint, it is typically enforced locally [PBE96]. Thereby, an upper bound on the exchange enhancement factor,

$$F_x \leq 1.804, \quad (4.36)$$

is implied. While this is a sufficient condition to satisfy the global bound, it has also been argued based on gedanken densities that this condition is also necessary in the semilocal form [PRSB14]. In contrast, the exact-exchange energy density in the conventional gauge [TSSP08] is known [MSGG12] to violate the local interpretation of the Lieb-Oxford bound, e.g., in the tail region of the density. This is not necessarily a contradiction, as semilocal DFAs are known to describe the exchange energy in a different gauge [TSSP08].

Recently, a strongly tightened bound compared to the Lieb-Oxford bound has been proved [PRSB14] for one- and two-electron densities, i.e.,

$$F_x(s, \alpha = 0) \leq 1.174, \quad (4.37)$$

as one- and two-electron systems are characterized by $\alpha = 0$ [SXF⁺13]. Furthermore, based on the conjecture [PRSB14, SPR15]

$$F_x(s, \alpha) \leq F_x(s, \alpha = 0), \quad (4.38)$$

this strongly tightened bound is suspected to hold for all values of α ,

$$F_x(s, \alpha) \leq F_x(s, \alpha = 0) \leq 1.174, \quad (4.39)$$

and thus generally [PRSB14]. As this strongly tightened bound is not considered compatible [SPR15] with the GE2 for exchange on the GGA level, it has so far only been applied on the

meta-GGA level [SPR15, SRP15]. Interestingly, the conjectured strongly tightened bound (4.39) is well in line with the novel meta-GGA construction principle put forward in Pub. 3.

4.8 Density-Path Integrals and Virial Theorem

A useful analytical tool to derive exact constraints or analyze DFAs are density-path integrals [vLB95]. A density path $n_\lambda(\mathbf{r})$ is defined by connecting two densities $n_0(\mathbf{r})$ and $n_1(\mathbf{r})$ smoothly by means of a continuous parameter $\lambda \in [0, 1]$. The energy difference for an arbitrary DFA to $E_{xc}[n]$ with its functional derivative $v_{xc}([n]; \mathbf{r}) = \delta E_{xc} / \delta n(\mathbf{r})$ can then be written as a density-path integral,

$$\begin{aligned} E_{xc}[n_1] - E_{xc}[n_0] &= \int_0^1 \frac{dE_{xc}[n_\lambda]}{d\lambda} d\lambda = \int_0^1 \int \frac{\delta E_{xc}[n_\lambda]}{\delta n_\lambda(\mathbf{r})} \frac{dn_\lambda}{d\lambda}(\mathbf{r}) d^3r d\lambda \\ &= \int_0^1 \int v_{xc}([n_\lambda]; \mathbf{r}) \frac{dn_\lambda}{d\lambda}(\mathbf{r}) d^3r d\lambda. \end{aligned} \quad (4.40)$$

If the density path is chosen such that $n_1(\mathbf{r}) = n(\mathbf{r})$ and $E_x[n_0] = 0$, e.g., as $n_0(\mathbf{r}) \equiv 0$, it allows to connect the energy with the corresponding potential,

$$E_{xc}[n] = \int_0^1 \int v_{xc}([n_\lambda]; \mathbf{r}) \frac{dn_\lambda}{d\lambda}(\mathbf{r}) d^3r d\lambda, \quad (4.41)$$

provided that $v_{xc}([n]; \mathbf{r})$ is the true functional derivative of $E_{xc}[n]$.

An important density-path is the uniform density path defined by Eq. (4.10). In Pub. 2 this particular density path is used as the central part of a proof. Additionally, it is closely connected to the virial theorem of DFT [GP85], which can be obtained by utilizing the uniform density-scaling relation of $E_x[n]$ (4.14) along the uniform density path and reads

$$E_x[n] = \int [3n(\mathbf{r}) + \mathbf{r} \cdot \nabla n(\mathbf{r})] v_x([n]; \mathbf{r}) d^3r = - \int n(\mathbf{r}) \mathbf{r} \cdot \nabla v_x([n]; \mathbf{r}) d^3r. \quad (4.42)$$

It is valid for any DFA for exchange provided that the DFA satisfies the correct uniform density-scaling and that the potential $v_x([n]; \mathbf{r})$ is the actual functional derivative of the DFA, i.e., $\delta E_x[n] / \delta n(\mathbf{r}) = v_x([n]; \mathbf{r})$. Therefore, this virial relation allows one to assess the numerical and, in the case of orbital-dependent functionals, also the analytical quality of a numerically implemented exchange potential corresponding to a DFA. The various implementations of, e.g., the meta-GGAs of Pub. 3 have been checked frequently on this basis.

4.9 Exchange-Correlation Hole

An alternative ansatz to formulate, understand, and model the xc energy is the xc hole $h_{xc}(\mathbf{r}, \mathbf{r}')$. It can be interpreted as a hole in the average density of electrons at \mathbf{r}' , given that there is an electron at \mathbf{r} . Consequently, the hole cannot be deeper than the density, $h_{xc}(\mathbf{r}, \mathbf{r}') \geq -n(\mathbf{r}')$. The xc energy can be written as [GL76] the electrostatic interaction between each electron and the

surrounding xc hole,

$$E_{xc}[n] = \frac{e^2}{2} \iint \frac{n(\mathbf{r})h_{xc}(\mathbf{r}, \mathbf{r}')}{|\mathbf{r} - \mathbf{r}'|} d^3 r' d^3 r, \quad (4.43)$$

and is thus fully determined by the xc hole and its properties. Hence, all exact constraints on $E_{xc}[n]$ can in principle be reformulated as constraints on the xc hole instead. Similar to the energy, the hole can also be decomposed in an exchange and a correlation component,

$$h_{xc}(\mathbf{r}, \mathbf{r}') = h_x(\mathbf{r}, \mathbf{r}') + h_c(\mathbf{r}, \mathbf{r}'), \quad (4.44)$$

where the exact exchange hole may be expressed in terms of the KS orbitals [Per85],

$$h_x(\mathbf{r}, \mathbf{r}') = - \sum_{\sigma=\uparrow, \downarrow} \sum_{i, j=1}^{N_\sigma} \frac{\varphi_{i\sigma}^*(\mathbf{r}) \varphi_{i\sigma}(\mathbf{r}') \varphi_{j\sigma}^*(\mathbf{r}') \varphi_{j\sigma}(\mathbf{r})}{n(\mathbf{r})}. \quad (4.45)$$

The symmetry of $n(\mathbf{r})h_x(\mathbf{r}, \mathbf{r}')$ with respect to interchange of coordinates ($\mathbf{r} \leftrightarrow \mathbf{r}'$) that is apparent from this definition of the exchange hole also holds for the exact correlation hole and thus for the complete hole. Further, the exchange hole, which is strictly non-positive, $h_x(\mathbf{r}, \mathbf{r}) \leq 0$, satisfies the sum rule [Per85]

$$\int h_x(\mathbf{r}, \mathbf{r}') d^3 r' = -1 \quad (4.46)$$

and the latter relation holds also for the complete hole, as the correlation hole integrates to zero. Moreover, the ‘‘on-top’’ value of the exchange hole is given by [Per85]

$$h_x(\mathbf{r}, \mathbf{r}) = -\frac{1}{2}n(\mathbf{r}) \quad (4.47)$$

for spin-unpolarized systems. The general case follows from the reformulation of the exchange spin-scaling relation (4.4) for the hole [PBW96],

$$h_x([n_\uparrow, n_\downarrow]; \mathbf{r}, \mathbf{r}') = \sum_{\sigma=\uparrow, \downarrow} \frac{n_\sigma(\mathbf{r})}{n(\mathbf{r})} h_x([2n_\sigma]; \mathbf{r}, \mathbf{r}'). \quad (4.48)$$

Since the Coulomb interaction in Eq. (4.43) only depends on the inter-electron separation $u = |\mathbf{u}| = |\mathbf{r}' - \mathbf{r}|$, it is sufficient to only consider the spherical-averaged hole [Bec83],

$$\bar{h}_{xc}(\mathbf{r}, u) = \frac{1}{4\pi} \oint h_{xc}(\mathbf{r}, \mathbf{r} + \mathbf{u}) d\Omega_{\mathbf{u}}, \quad (4.49)$$

without loss of generality. All of the exact properties listed above translate directly to the spherical-averaged hole as well. Moreover, it allows for a series expansion of its exchange component around the reference point [Bec83, BR89, WZE17],

$$\bar{h}_x(\mathbf{r}, u) \sim -\frac{1}{2}n(\mathbf{r}) - \frac{1}{12} \left\{ \nabla^2 n(\mathbf{r}) - 4 \left[\frac{m_e}{\hbar^2} \tau(\mathbf{r}) - \frac{|\nabla n(\mathbf{r})|^2}{8n(\mathbf{r})} \right] \right\} u^2 + \mathcal{O}(u^4). \quad (4.50)$$

Semilocal models for the spherical-averaged exchange (and correlation) hole [BR89, PW92b,

[PBW96](#), [CPT06](#), [HJS08](#), [TBS17](#)] are frequently constructed based on these exact constraints and are designed to describe the energy,

$$E_{\text{xc}}[n] = 2\pi N e^2 \int_0^\infty \langle \bar{h}_{\text{xc}} \rangle(u) u \, du, \quad (4.51)$$

rather in terms of the corresponding system- and spherical-averaged hole [[BP95](#)]

$$\langle \bar{h}_{\text{xc}} \rangle(u) = \frac{1}{N} \int n(\mathbf{r}) \bar{h}_{\text{xc}}(\mathbf{r}, u) \, d^3 r. \quad (4.52)$$

These semilocal hole models can be used to directly construct xc functionals [[PW86](#), [TM16](#)]. Moreover, they are built *a posteriori* to reproduce a DFA [[PW92b](#), [PBW96](#), [CPT06](#), [TBS17](#)] and serve as a starting point to construct more advanced DFAs, e.g., in the range-separation scheme [[HSE03](#)], cf. Sec. 6.3, in the xc factor approach [[AZE14](#), [PBKE14](#), [PPBKE15](#)], or to model non-dynamical correlation [[Bec03](#), [Bec13](#)]. In [Pub. 4](#) particularly semilocal exchange hole models are used to reduce the computational cost of local range-separated hybrids through a hyper-GGA approximation [[KSPS08](#)] where the exact exchange hole is mapped onto a semilocal hole model.

CHAPTER 5

Orbital-Dependent Density Functionals

The most widely used and successful way to incorporate ultranonlocality into DFT is given by orbital-dependent DFAs. Orbital-dependent functionals have a natural mechanism that allows for a particle number discontinuity as the addition of infinitesimal charge is realized by occupying previously unoccupied orbitals. The non-interacting kinetic energy $T_s[n]$ of Eq. (2.3) serves as a prime example. This pivotal functional to the KS formulation [KS65] and thus to the success story of DFT is written in terms of one-electron orbitals and thus is only an implicit functional of the density. While $T_s[n]$ is only semilocal in the orbitals, it yields a sizable derivative discontinuity in form of the KS gap, cf. Eq. (3.10). The associated ultranonlocality enters because each KS orbital $\varphi_{i\sigma}(\mathbf{r})$ at \mathbf{r} depends on the density $n(\mathbf{r}')$ at all points \mathbf{r}' as mediated by the KS potential. Consequently, $T_s[n]$ is (ultra)nonlocal in density while being semilocal in the orbitals. The following chapter will outline the aspects of orbital-dependent density functionals relevant for this thesis. For a comprehensive review see, e.g., Refs. [KK08, Eng03].

5.1 Exact Exchange and Beyond

Another functional that is naturally written in terms of the orbitals is the exact-exchange energy (EXX) as it is defined via

$$\begin{aligned} E_x^{\text{ex}}[\{\varphi_{i\sigma}[n]\}] &= \langle \Phi_{\text{KS}} | \hat{W} | \Phi_{\text{KS}} \rangle - E_{\text{H}}[n] \\ &= -\frac{e^2}{2} \sum_{\sigma=\uparrow,\downarrow} \sum_{i,j=1}^{N_\sigma} \iint \frac{\varphi_{i\sigma}^*(\mathbf{r}) \varphi_{i\sigma}(\mathbf{r}') \varphi_{j\sigma}^*(\mathbf{r}') \varphi_{j\sigma}(\mathbf{r})}{|\mathbf{r} - \mathbf{r}'|} d^3r' d^3r \end{aligned} \quad (5.1)$$

as the difference between the expectation value of the inter-electron interaction \hat{W} in the non-interacting KS system and the Hartree energy [PK03, ED11]. Therefore, the EXX functional coincides with the Fock exchange expression but evaluated with KS orbitals and satisfies by definition all exact exchange constraints. Furthermore, it possesses pronounced ultranonlocality including a derivative discontinuity Δ_x .

Despite of these formal merits, EXX has two severe practical limitations. First, the evaluation of EXX and its corresponding potential, is computationally expensive due to the Fock integrals and, as outlined below, due the orbital dependence. Second, EXX alone naturally lacks correlation and usually performs worse than LDA or even exchange-only LDA for thermochemical properties such as atomization energies [ED11]. This is an important point because due to

the (ultra)nonlocal nature of EXX finding a corresponding suitable correlation functional is a challenging task [KK08]. One avenue to do so is the modification of EXX and its (partial) combination with traditional semilocal expression for $E_{xc}[n]$ into hybrid functionals between EXX (or Hartree-Fock) and semilocal DFT. This hybrid class of DFAs includes global hybrids [Bec93, SDCF94, PEB96], local hybrids [PSTS08, JSE03, SKM⁺14] and range-separated hybrids [LSWS97, YTH04, SKB09]. By going beyond the hybrid concept via inclusion of unoccupied KS orbitals and eigenvalues yet higher accuracy can be reached to the impressive point that DFT starts to rival wave-function based methods in accuracy [EBG16].

The accuracy, however, comes at a steep increase in computational cost. Thus, instead of starting from EXX and climbing Jacob's ladder of DFAs [PS01] and thereby increasing computational cost, one has the option to descend one level and withdraw to explicit but semilocal orbital-dependent ingredients such as the kinetic energy density, i.e., to meta-GGAs. Publication 3 demonstrates that substantial ultranonlocality can be achieved even on this level.

5.2 Optimized Effective Potential Theory

Given an explicit orbital-dependent $E_{xc}[\{\varphi_{i\sigma}\}]$ and implicit dependence of the orbitals $\{\varphi_{i\sigma}\}$ on the density, the question arises of how to calculate the functional derivative with respect to the density, $v_{xc\sigma}(\mathbf{r}) = \delta E_{xc}[\{\varphi_{i\sigma}[n]\}]/\delta n_{\sigma}(\mathbf{r})$, i.e., the corresponding multiplicative xc potential. The answer is given by the optimized effective potential (OEP) scheme [SH53, TS76, SGP82, KK08], where by virtue of the chain rule the change of the energy is expressed in changes of the KS orbitals due to a change of density that is in turn mediated by the KS potential,

$$v_{xc\sigma}(\mathbf{r}) = \sum_{\alpha, \beta=\uparrow, \downarrow} \sum_{i=1}^{N_{\sigma}} \iint \frac{\delta E_{xc}[\{\varphi_{j\sigma}\}]}{\delta \varphi_{i\alpha}(\mathbf{r}')} \frac{\delta \varphi_{i\alpha}(\mathbf{r}')}{\delta v_{KS\beta}(\mathbf{r}'')} \frac{\delta v_{KS\beta}(\mathbf{r}'')}{\delta n_{\sigma}(\mathbf{r})} d^3 r' d^3 r'' + \text{c.c.} \quad (5.2)$$

This expression can eventually be recast into an integral equation for $v_{xc\sigma}(\mathbf{r})$,

$$v_{xc\sigma}(\mathbf{r}) = \frac{1}{2n_{\sigma}(\mathbf{r})} \sum_{i=1}^{N_{\sigma}} \left\{ |\varphi_{i\sigma}(\mathbf{r})|^2 \left[u_{xc i\sigma}(\mathbf{r}) + (\bar{v}_{xc i\sigma} - \bar{u}_{xc i\sigma}) \right] - \frac{\hbar^2}{m_e} \nabla \cdot \left[\psi_{i\sigma}^*(\mathbf{r}) \nabla \varphi_{i\sigma}(\mathbf{r}) \right] \right\} + \text{c.c.}, \quad (5.3)$$

where $\psi_{i\sigma}(\mathbf{r})$ denotes the orbital shift that represents the first-order change of the KS orbital $\varphi_{i\sigma}(\mathbf{r})$ upon replacing the KS potential with the orbital-specific potential

$$u_{xc i\sigma}(\mathbf{r}) = \frac{1}{\varphi_{i\sigma}^*(\mathbf{r})} \frac{\delta E_{xc}[\{\varphi_{j\sigma}\}]}{\delta \varphi_{i\sigma}(\mathbf{r})}. \quad (5.4)$$

Moreover, an overscore denotes the orbital expectation value of the potentials, i.e.,

$$\bar{v}_{xc i\sigma} = \int \varphi_{i\sigma}^*(\mathbf{r}) v_{xc\sigma}(\mathbf{r}) \varphi_{i\sigma}(\mathbf{r}) d^3 r \quad \text{and} \quad \bar{u}_{xc i\sigma} = \int \varphi_{i\sigma}^*(\mathbf{r}) u_{xc i\sigma}(\mathbf{r}) \varphi_{i\sigma}(\mathbf{r}) d^3 r. \quad (5.5)$$

The orbital shifts can be obtained either as solutions of partial differential equations [KP03b] or by their Green's functions representation,

$$\psi_{i\sigma}^*(\mathbf{r}) = - \sum_{\substack{j=1 \\ j \neq i}}^{\infty} \frac{\langle \varphi_{i\sigma} | u_{xc i\sigma} - v_{xc\sigma} | \varphi_{j\sigma} \rangle}{\epsilon_{i\sigma} - \epsilon_{j\sigma}} \varphi_{j\sigma}^*(\mathbf{r}), \quad (5.6)$$

in terms of occupied and unoccupied KS eigenvalues and orbitals. While a further reformulation [KLI92b] of the OEP equation (5.2),

$$S_{\sigma}(\mathbf{r}) = \sum_{i=1}^{N_{\sigma}} \psi_{i\sigma}^*(\mathbf{r}) \varphi_{i\sigma}(\mathbf{r}) + \text{c.c.} = 0, \quad (5.7)$$

allows for simple iterative construction of the OEP potential by S -iterations [KP03b, KP03a], solving the OEP integral equation remains numerically challenging and a computationally costly task. A thus vital approximation to the full OEP potential, as it drastically reduces the numerical effort, was first suggested by Krieger, Li, and Iafrate (KLI) [KLI92a, KLI92b],

$$v_{xc\sigma}^{\text{KLI}}(\mathbf{r}) = \frac{1}{2n_{\sigma}(\mathbf{r})} \sum_{i=1}^{N_{\sigma}} |\varphi_{i\sigma}(\mathbf{r})|^2 \left[u_{xc i\sigma}(\mathbf{r}) + (\bar{v}_{xc i\sigma} - \bar{u}_{xc i\sigma}) \right] + \text{c.c.} \quad (5.8)$$

Even though the KLI approximation remains an integral equation for $v_{xc\sigma}(\mathbf{r})$, it allows to be solved efficiently as system of linear equations. A similar approximation to the OEP potential is given by the common energy denominator approximation (CEDA) [GB01, DSG01]. While CEDA is superior to KLI on a formal level as it restores unitary invariance, cf. Sec. 4.2, the increase in computational cost is seldom justifiable from a practical perspective since the difference to KLI is modest and not necessarily a step closer to the full OEP [KK08].

The full OEP as well as the KLI or CEDA potential can be partitioned into two contributions. The first part is the local average of the orbital-specific potentials of all occupied orbitals,

$$v_{xc\sigma}^{\text{hole}}(\mathbf{r}) = \frac{1}{2n_{\sigma}(\mathbf{r})} \sum_{i=1}^{N_{\sigma}} |\varphi_{i\sigma}(\mathbf{r})|^2 u_{xc i\sigma}(\mathbf{r}) + \text{c.c.} \quad (5.9)$$

As it may be written as the smooth Coulomb potential of the associated xc hole, cf. Eq. (4.43), it is termed hole potential (or Slater potential). The exact hole potential makes for the substantial part of the full potential and is responsible for the $1/r$ -long-rangedness of $v_{xc\sigma}(\mathbf{r})$, but does not show any ultranonlocality [vLGB95]. All ultranonlocality including the derivative discontinuity [KLI92a], shell- and step structure [vLGB95], and the field-counteracting term [vGSG⁺99, KKP04] are contained in the second part of $v_{xc\sigma}(\mathbf{r})$, the response potential $v_{xc\sigma}^{\text{resp}}(\mathbf{r})$. In the KLI approximation the response potential takes the transparent form

$$v_{xc\sigma}^{\text{resp,KLI}}(\mathbf{r}) = \frac{1}{2n_{\sigma}(\mathbf{r})} \sum_{i=1}^{N_{\sigma}} |\varphi_{i\sigma}(\mathbf{r})|^2 (\bar{v}_{xc i\sigma} - \bar{u}_{xc i\sigma}) + \text{c.c.}, \quad (5.10)$$

where at each point in space a orbital-specific constant $C_{i\sigma} = \bar{v}_{xc i\sigma} - \bar{u}_{xc i\sigma} + \text{c.c.}$ is weighted by the local contribution of each orbital to the density. As the differences between the orbital-specific potentials $u_{xc i\sigma}(\mathbf{r})$ and the multiplicative potential $v_{xc\sigma}(\mathbf{r})$ lead to different constants $\{C_{i\sigma}\}$, an ultranlocal step structure emerges naturally in the response potential. Moreover, the ridges in asymptotic xc potential that arise in the presence of orbital nodal surfaces, as mentioned in Sec. 4.4, are also a direct consequence of $v_{xc\sigma}^{\text{resp}}(\mathbf{r})$ and the constants $\{C_{i\sigma}\}$ [DSG02a, DSG02b, KP03a].

Further note that the solution to the OEP problem is only determined up to a global shift of $v_{xc\sigma}(\mathbf{r})$. Fixing this global constant in the OEP potential such that it corresponds to the unique xc potential of an ensemble, cf. Sec. 3.1, corresponds to the choice $C_{N\sigma\sigma} = 0$ [KLI92a, EH14]. As this condition is tied to the highest occupied orbital, the condition changes discontinuously when an additional orbital is fractionally occupied. Thereby, this condition gives rise to a uniform jump of $v_{xc\sigma}(\mathbf{r})$, i.e., to the derivative discontinuity Δ_{xc} [KLI92a].

5.3 Generalized Kohn-Sham Scheme

A computationally feasible and frequently used alternative to the OEP scheme is given by the generalized Kohn-Sham (gKS) scheme [SGV⁺96]. Formally, the gKS scheme corresponds to a different partitioning of the energy and, thereby, an implicit redefinition of $E_{xc}[n]$. Therefore, employing the same orbital-dependent approximation to $E_{xc}[n]$ to the KS and gKS schemes defines different energy functionals on a formal level. Their performance is, however, expected to be qualitatively similar.

In the gKS scheme the interacting system of electrons is – in contrast to the standard KS framework – not mapped into a non-interacting but into a, e.g., partially interacting system. The type of the corresponding auxiliary system, which is still describable by a single Slater determinant, is, however, no longer universal but depends on the precise type of the employed functional [KK08, BK18]. Single-particle equations similar to the KS Eqs. (2.7) emerge, where the multiplicative xc potential for all orbitals is replaced by the orbital-specific potential $u_{xc i\sigma}(\mathbf{r})$, which is also representable by a nonlocal potential operator for all orbitals. Thus, the gKS scheme for EXX essentially reduces to Hartree-Fock and $v_x(\mathbf{r})$ becomes the usual Fock-integral operator, whereas the gKS potential operator of a meta-GGA becomes a spatial-dependent differential operator [NNH96, AK03].

In order to remain formally exact in the same sense that KS DFT is exact given the exact $E_{xc}[n]$, a remainder energy functional and potential enters the gKS equation but is typically neglected when not comprised by a conventional $E_{xc}[n]$ contribution. For meta-GGAs the gKS scheme has additional drawbacks in time-dependent DFT and requires further care and adjustments [BF12]. While the gKS scheme, hence, has formal deficits compared to the KS scheme, it is in practice the primary way to employ orbital-dependent functionals – especially so because operator potentials are readily implemented in basis set codes. But, since the ultranlocality in the gKS scheme is hidden in orbital-specific potentials, it is not employed

throughout this thesis with the single exception of the band gap calculations of [Pub. 3](#): because the gKS potential operator is continuous, the band gap readily approximates the fundamental gap in this case since it includes the derivative discontinuity due to the explicit orbital dependence [[SGV⁺96](#), [PYB⁺17](#), [YPSP16](#), [PR18](#)].

CHAPTER 6

Developments and Results

As discussed in Chapter 3, the inclusion of ultranonlocality in DFAs plays a decisive role to describe certain situations with DFT and its absence is responsible for hallmark deficits throughout the history of DFT. So far, the key to capture ultranonlocality, as outlined in Chapter 5, is primarily the use of orbital-dependent functionals that are based on or make explicit use of EXX. These functionals are, however, restricted to much smaller systems than common semilocal functionals since they are computationally much more demanding. This restriction can have serious consequences because often the interesting features of real-world systems, especially in the realm of nano- and supramolecular science, stem from an intrinsic complexity that requires the explicit treatment of a large number of particles. Understanding light-harvesting systems [CGK06, JSARM⁺15, CM17] is a paradigm example: It requires calculating energy- and charge transfer through arrays of dozens of chromophores, where each chromophore typically has hundreds of electrons. The chromophores in turn are typically embedded in a protein matrix, at least parts of which should also be taken into account explicitly [JSARM⁺15, CJC⁺16, ADH17, SFG⁺19]. However, semilocal functionals are currently at their limits for such systems due to their inability to properly describe charge transfer [Sun03, DHG04, SK18]. Therefore, there is a serious need for functionals that do not suffer from the large, qualitative errors that traditional semilocal functionals plague, yet come at a comparable computational price.

To this end, the following Sec. 6.1 outlines, as detailed in Pubs. 1 and 2, that previous semilocal attempts to mimic ultranlocal properties based on model potentials or on the GGA form for exchange cannot fully meet these expectations and have serious limitations. This is followed by Sec. 6.2 summarizing the results of Pub. 3 and showcasing that, contrary to long-standing past experience, meta-GGAs can show substantial ultranonlocality and therefore are likely to live up to this expectation. The final Sec. 6.3 then focuses on the computational more demanding class of range-separated hybrids that currently spearhead the description of charge transfer for systems of small to moderate size. After explaining the range-separation approach and outlining its formal and practical deficits the ansatz of Pub. 4 is presented, which tackles these deficits with a local range-separation parameter, and the corresponding results are summarized.

6.1 Limitations of Semilocal Approximations

More than a decade ago, two model potentials for the response part of the exchange potential $v_x^{\text{resp}}(\mathbf{r})$, cf. Eq. (5.10), have been put forward and shown to improve the atomic-shell structure. These exchange potentials by Gritsenko *et al.* (GLLB) [GvLvLB95] and by Becke and Johnson (BJ) [BJ06] are termed model potentials as they – in contrast to being given by a functional derivative of an associated energy functional $E_x[n]$ – directly model the potential. Over the past years, these model potentials and various modifications thereof [AKK08, TB09, KOER10, RPP10, KTB12], especially of the BJ potential, have sparked interest by delivering on other properties associated with ultranonlocality such as polarizabilities and band gaps [TBS07, AKK08, KAK09, TB09, KOER10, TEB18, NS18, TBLDH⁺19].

Yet, the usefulness of model potentials is seriously limited due to their lack of a corresponding energy functional [AKJS06, MKvLR07, GS09, KAK09, NV11, KAK13]: First, they cannot be used in applications that require energies. Second, they are incapable of being propagated in the time-dependent KS equations as being an actual functional derivative is pivotal for this purpose. Third, they cause formal problems since directly modeling the xc potential sidesteps the variational principle at the core of the KS DFT framework that leads to the KS equations.

These model potential limitations were meant to be resolved by the construction of the Armiento-Kümmel GGA (AK13) [AK13], which is an explicit semilocal energy functional. The AK13 energy functional is designed such that the corresponding AK13 potential shares the asymptotic behavior of the BJ potential that was previously [AKK08] made out for effectively mimicking the ultranonlocal features.

This signature asymptotic of the BJ potential,

$$v_x^{\text{BJ}}(\mathbf{r}) = v_x^{\text{Slater}}(\mathbf{r}) + \frac{e^2}{\pi} \sqrt{\frac{5m_e}{6\hbar^2} \frac{\tau(\mathbf{r})}{n(\mathbf{r})}} \quad (6.1)$$

with the kinetic energy density $\tau(\mathbf{r})$ as defined in Eq. (4.3), relies on the asymptotic decay of the density: Normally, the density decay is governed by the highest occupied KS orbital and under assumption of spherical symmetry given by [KKG98]

$$n(\mathbf{r}) \sim n_0 |\mathbf{r}|^q \exp(-\kappa |\mathbf{r}|) \quad \text{as } |\mathbf{r}| \rightarrow \infty, \quad (6.2)$$

with an explicit dependence on the highest occupied KS eigenvalue ϵ_{ho} via

$$\kappa = 2 \sqrt{\frac{2m_e}{\hbar^2} (v_x^\infty - \epsilon_{\text{ho}})}. \quad (6.3)$$

In this spherically symmetric case the BJ potential approaches,

$$v_x^\infty = \lim_{|\mathbf{r}| \rightarrow \infty} v_x^{\text{BJ}}(\mathbf{r}) \propto \kappa \propto \sqrt{v_x^\infty - \epsilon_{\text{ho}}}, \quad (6.4)$$

a positive, system-dependent constant far outside the system. Moreover, whenever the density is

dominated by the exponential decay of any single orbital, the potential approaches a different but corresponding constant. Thereby, this gives not only rise to a step structure in the potential, but also to a derivative discontinuity [AKK08]: Since the BJ potential is a model potential, it can be arbitrarily shifted by a constant. Therefore, if the BJ potential is, in accordance with the exact $v_x(\mathbf{r})$, thoroughly aligned to vanish asymptotically as $|\mathbf{r}| \rightarrow \infty$, it undergoes a discontinuous uniform shift upon fractionally occupying the next orbital.

In the AK13 construction it was demonstrated [AK13] that a very similar asymptotic behavior of a system-dependent asymptotic constant can also be realized within the restricted GGA form for exchange, cf. Eq. (4.16), and thus in conjunction with a corresponding energy functional. Since the exponential decay of the density (6.2) translates to an exponential growth of the dimensionless GGA variable $s(\mathbf{r})$, cf. Eq. (4.17), this characteristic asymptotic behavior of the potential is achieved by a precisely diverging enhancement factor,

$$F_x^{\text{AK13}}(s) = 1 + B_1 s \ln(1 + s) + B_2 s \ln[1 + \ln(1 + s)] \sim B_1 s \ln s \quad \text{as } s \rightarrow \infty, \quad (6.5)$$

where $B_1 = 2/27 + 8\pi/15$ and $B_2 = 4/81 - 8\pi/15$ were determined in non-empirical fashion. The resulting AK13 functional can also, to some degree, deliver on improving properties typically associated with ultranonlocality [AK13, COM14, TBS15, VSNL⁺15, LA16, TBBB16, TB17]. However, it also led to the discovery of anomalous features that are closely connected to the nonvanishing asymptotic potential. The findings, which are the topic of Pubs. 1 and 2 and thus of this thesis, constitute a formidable challenge for the future development of semilocal functionals based on the BJ and AK13 concept.

Publication 1 focuses on orbital nodal surfaces and demonstrates that they represent serious topological challenges for density functionals. In many finite systems, in particular organic systems, the highest occupied ground-state KS orbital has one or multiple nodal surfaces that extend to infinity. In these situations, as noted in Sec. 4.4, protruding ridges along such regions emerge in the asymptotic EXX potential, cf. Fig. 4.1. As the analytic origin of these ridges can be traced back to the response part of the exchange potential $v_x^{\text{resp}}(\mathbf{r})$, cf. Sec. 5.2, i.e., the origin of all ultranonlocal properties, it is not surprising that semilocal functionals which mimic ultranonlocality display anomalous features there as well.

However, **Pub. 1** shows that nodal surfaces can heavily affect the potential of semilocal DFAs in the sense that exponential divergences in the vicinity of nodal surfaces emerge. To this end, an analytic minimal nodal surface model is developed and utilized. These unphysical divergences present not only conceptual challenges but can also severely hinder self-consistent calculations. The AK13 and BJ functionals serve as a paradigm for the latter: The nonvanishing asymptotic potentials of AK13 and BJ rely crucially on the idealized spherically symmetric decay of the density in accordance with Eq. (6.2). As their nonvanishing constant is precariously realized by spatial derivatives, the asymptotic potential responds strongly to any deviation of the asymptotic density from the idealized decay. Such a deviation is, e.g., given in the presence of orbital nodal surfaces, which break the spherical symmetry of the asymptotic density and thus lead to an exponentially divergent potential along the nodes. The affected functionals are, however,

not limited to functionals with a nonvanishing asymptotic potential. Various frequently used DFAs, such as the van Leeuwen-Baerends (LB94) [vLB94] potential, the Armiento-Mattsson (AM05) GGA [AM05], or the Becke88 GGA [Bec88], are also implicated to a lesser extent. The Becke88 GGA makes for the semilocal exchange part of the hybrid functional B3LYP [Bec93, SDCF94], which is one of the most used density functionals [Bec14].

Based on the minimal nodal surface model, Pub. 1 further derives new formal constraints on the GGA exchange enhancement factor for a well-behaved potential: To avoid divergences in the presence of nodal surfaces the asymptotic enhancement factor,

$$F_x(s) \propto s^d \quad \text{as } s \rightarrow \infty, \quad (6.6)$$

has to satisfy $d \leq -2$ in general with the exception of a constant limiting value of $F_x(s)$, while for some systems $-2 < d < 2/5$ is also sufficient. For further details and a more rigorous formulation of the constraint see Pub. 1. A rather far-reaching implication thereof is that the following GGA design criteria are all incompatible with a regularly behaving potential in the vicinity of asymptotic nodal surfaces: a nonvanishing asymptotic constant in the potential and the correct asymptotic Coulombic long-range behavior of the potential or of the energy density.

Publication 2 continues along this line and uncovers further challenges for semilocal density functionals with asymptotically nonvanishing potentials. It is shown that in the context of ensemble DFT the AK13 potential does not include the actual ultranlocal shift associated with the derivative discontinuity. Based on a density-path integration it is further proven that no straightforward energy correction to the AK13 functional exists that yields the missing discontinuous shift. Additionally, the inaccurate energetics of AK13, numerical and therefore practical difficulties, as well as the nonphysical response to an external electric field are also a topic of Pub. 2. The latter is detrimental as it discloses the inability of AK13 to properly describe charge transfer via a field-counteracting term in the potential.

Further unfavorable findings [GHAK18] for AK13 in the context of time-dependent DFT complete the case that the semilocal construction strategies of AK13 and BJ have serious deficits on both a formal and a practical level. Consequently, different approaches are likely needed to properly incorporate ultranlocality in DFT at a computationally feasible level. A very promising approach in this respect is given by the meta-GGA form and outlined in the following section.

6.2 Capturing Ultranonlocality via a Kinetic Energy Density Dependence

The inclusion of the kinetic energy density $\tau(\mathbf{r})$, cf. Eq. (4.3), as an additional ingredient for semilocal DFAs to $E_{xc}[n]$ has by now been long-standing practice for over two decades. The resulting meta-GGAs have become an impressive success story [DSFC16, PKZB99, TPSS03, ZT06, SXF⁺13, SRP15, TM16], as they, e.g., produced and still produce the energetically most

accurate semilocal functionals [TPSS03, CPT06, SRP15, TM16]. Yet, even though the orbital dependence of the kinetic energy density makes meta-GGAs explicitly orbital-dependent by definition and thereby nonlocal in the density, experience so far seemed to show that, in practice, semilocality in the orbitals is similar to semilocality in the density [KK08]. From a historical perspective, this is not surprising given that the development of meta-GGAs emerged from and naturally stayed close to the firm ground that was paved by years of experience with GGAs. While, therefore, most traditional meta-GGAs do not incorporate a derivative discontinuity [EH14] and the associated ultranonlocality [NV11] in sufficient magnitude, more recent work, e.g., on band gaps [YPS16], indicate improvement in this area. So, while in principle, it is known that meta-GGAs can show ultranonlocality in the corresponding potential, the central question becomes how to capture ultranonlocality via a kinetic energy dependence.

An answer to this question is provided by Pub. 3. To this end, first a relation between the derivative discontinuity of a meta-GGA $\Delta_x^{\text{meta-GGA}}$ and the partial derivative of the corresponding exchange energy density $e_x(n(\mathbf{r}), |\nabla n(\mathbf{r})|, \tau(\mathbf{r}))$ with respect to $\tau(\mathbf{r})$ is established,

$$\begin{aligned} \Delta_x^{\text{meta-GGA}} &= \lim_{\eta \rightarrow 0^+} \left[v_x^{\text{meta-GGA}}(\mathbf{r})|_{N_0+\eta} - v_x^{\text{meta-GGA}}(\mathbf{r})|_{N_0-\eta} \right] \\ &= \lim_{\eta \rightarrow 0^+} \int \frac{\partial e_x}{\partial \tau}(\mathbf{r}') \left[\frac{\delta \tau(\mathbf{r}')}{\delta n(\mathbf{r})} \Big|_{N_0+\eta} - \frac{\delta \tau(\mathbf{r}')}{\delta n(\mathbf{r})} \Big|_{N_0-\eta} \right] d^3 r' \\ &\approx \frac{\partial e_x}{\partial \tau} \lim_{\eta \rightarrow 0^+} \left[\frac{\delta T_s[n]}{\delta n(\mathbf{r})} \Big|_{N_0+\eta} - \frac{\delta T_s[n]}{\delta n(\mathbf{r})} \Big|_{N_0-\eta} \right] = \frac{\partial e_x}{\partial \tau} \Delta_{\text{KS}}. \end{aligned} \quad (6.7)$$

As both the derivative discontinuity $\Delta_x^{\text{meta-GGA}}$ as well as the KS gap Δ_{KS} should be positive, cf. Sec. 3.1, this relation suggests a positive $(\partial e_x / \partial \tau)(\mathbf{r})$ with a large enough magnitude as a design criterium to obtain a sizable derivative discontinuity and thus ultranonlocality for a meta-GGA for exchange. Second, Pub. 3 demonstrates that the dimensionless variable [TPSS03, RSXC12, SXR12, SHX⁺13, SPR15, SXF⁺13, SRP15, DSFC15]

$$\alpha(\mathbf{r}) = t(\mathbf{r}) - \frac{5}{3} s^2(\mathbf{r}) = \frac{\tau(\mathbf{r}) - \tau^{\text{W}}(\mathbf{r})}{\tau^{\text{unif}}(\mathbf{r})} \geq 0, \quad (6.8)$$

cf. Eqs. (4.17) and (4.19) for the definition of $s(\mathbf{r})$ and $t(\mathbf{r})$, is well suited to introduce ultranonlocality. Here $\tau^{\text{unif}}(\mathbf{r})$ is the uniform-density limit, cf. Eq. (4.29), and the von-Weizsäcker kinetic energy density

$$\tau^{\text{W}}(\mathbf{r}) = \frac{\hbar^2}{8m_e} \frac{|\nabla n(\mathbf{r})|^2}{n(\mathbf{r})} \quad (6.9)$$

the single-orbital limit of $\tau(\mathbf{r})$.

For the meta-GGA exchange enhancement factor $F_x(s, \alpha)$ parametrized in $s(\mathbf{r})$ and $\alpha(\mathbf{r})$ the design criterium for ultranonlocality becomes

$$\frac{\partial F_x(s, \alpha)}{\partial \alpha} < 0 \quad (6.10)$$

and a larger negative slope is expected to correspond to a larger derivative discontinuity. Given that $\alpha(\mathbf{r})$ is a well established measure for electron localization [SJF⁺92, SS94, SNWF97] by virtue of the electron localization function [BE90],

$$\text{ELF}(\mathbf{r}) = \frac{1}{1 + \alpha^2(\mathbf{r})}, \quad (6.11)$$

Eq. (6.10) can be illustratively interpreted to energetically favor electron localization and thereby combat the delocalization error of common semilocal DFT, which is closely interconnected with the lack of ultranonlocality, as detailed in Sec. 3.5.

Based on this insight, two meta-GGAs for exchange are constructed and presented in Pub. 3. First, a proof of concept (PoC) meta-GGA is discussed. It impressively demonstrates that a simplistic meta-GGA solely parametrized in α can achieve ultranonlocality in the same magnitude as the nonlocal EXX functional. For this demonstration, the two hydrogen model systems as detailed in Sec. 3.4 are employed. In these model systems the PoC meta-GGA yields polarizabilities close to reference values of higher-order methods, possesses a similar field-counteracting term in $v_x(\mathbf{r})$ as EXX, and demonstrates integer preference in the charge-transfer model system due to a proper ultranonlocal step structure in the potential. In a second meta-GGA, named TASK for the initials of the developers, the construction strategy based on the derivative discontinuity is combined with the well-established constraint-guided construction concept of meta-GGAs, which was detailed in Chapter 4. The resulting TASK functional is a non-empirical, general purpose meta-GGA for exchange that shows substantial improvement for properties associated with ultranonlocality while giving reasonable energetics. To this end, it is demonstrated that the TASK meta-GGA yields significantly improved band gaps in close agreement with experimental values for systems ranging from traditional semiconductors to wide-gap insulators. Thereby, it showcases that the band gap problem of semilocal DFT, cf. Sec. 3.2, can be overcome within the meta-GGA form for $E_{xc}[n]$.

The analytic formulas for the functional derivatives of the PoC and TASK meta-GGAs of Pub. 3 as implemented in BAND [tVB91, WB91, FPV13, FPvLV14, SCM], BTDFDFT [SK18], DARSEC [MKK09], and PARSEC [KMT⁺06] are given in Appendix A.1.

6.3 Nonlocality from the Range-Separated Coulomb Interaction

The meta-GGAs of the previous section and Pub. 3 are ultimately aimed to describe particularly large systems due to their low computational cost. However, powerful approaches to capture ultranonlocality and, in particular, to describe charge transfer already exist for systems of small to moderate size in the form of range-separated hybrids (RSH) [KSRAB12, Kü17].

The underlying concept of this class of DFAs is to split [SF95, TCS04] the Coulomb

interaction formally,

$$\frac{1}{|\mathbf{r}-\mathbf{r}'|} = \underbrace{\frac{1-\operatorname{erf}(\omega|\mathbf{r}-\mathbf{r}'|)}{|\mathbf{r}-\mathbf{r}'|}}_{\text{short range}} + \underbrace{\frac{\operatorname{erf}(\omega|\mathbf{r}-\mathbf{r}'|)}{|\mathbf{r}-\mathbf{r}'|}}_{\text{long range}}, \quad (6.12)$$

into a short-range (SR) and a long-range (LR) component by means of a range-separation parameter ω . Subsequently, this splitting is applied to the exchange energy $E_x[n]$ in its representation via the exchange hole $h_x(\mathbf{r}, \mathbf{r}')$, cf. Eq. (4.43). By using the exact orbital-dependent exchange hole (4.45) for one component and a semilocal exchange hole model,

$$h_x^{\text{sl}}(\mathbf{r}, \mathbf{r}') = \bar{h}_x^{\text{sl}}(n(\mathbf{r}), |\nabla n(\mathbf{r})|, \tau(\mathbf{r}), \nabla^2 n(\mathbf{r}), |\mathbf{r}-\mathbf{r}'|), \quad (6.13)$$

for the other component, an effective model for exchange and correlation¹ is created. While in solids the exact exchange hole is typically screened and therefore used in the SR component [HSE03], the standard for finite systems [LSWS97] and subsequently for this thesis is to model SR semilocally,

$$E_x^{\text{sl,SR}}[n, \omega] = \frac{e^2}{2} \iint \frac{n(\mathbf{r}) h_x^{\text{sl}}(\mathbf{r}, \mathbf{r}')}{|\mathbf{r}-\mathbf{r}'|} [1 - \operatorname{erf}(\omega|\mathbf{r}-\mathbf{r}'|)] d^3 r' d^3 r, \quad (6.14)$$

and to treat the LR component exactly,

$$E_x^{\text{ex,LR}}[n, \omega] = -\frac{e^2}{2} \sum_{\sigma=\uparrow, \downarrow} \sum_{i,j=1}^{N_\sigma} \iint \frac{\varphi_{i\sigma}^*(\mathbf{r}) \varphi_{i\sigma}(\mathbf{r}') \varphi_{j\sigma}^*(\mathbf{r}') \varphi_{j\sigma}(\mathbf{r})}{|\mathbf{r}-\mathbf{r}'|} \operatorname{erf}(\omega|\mathbf{r}-\mathbf{r}'|) d^3 r' d^3 r. \quad (6.15)$$

The choice of the semilocal exchange hole model, which is usually based on a common semilocal DFA, defines different RSHs: the exchange hole [PBW96] of the PBE GGA [PBE96], for example, defines the RSH ω PBE [VS06]. In Pub. 4 the SR component is, however, modeled for transparency via the LDA exchange hole [GAP96, Sav96].

In addition to the SR component, the value of the range-separation parameter ω , which determines an inverse length for the separation between SR and LR, must also be chosen. Based on this choice, the performance of an RSH can vary considerably [VHKS06]. Moreover, a parameter dilemma is observed [RH08] as a universal range-separation parameter cannot simultaneously describe thermochemical and optical properties – for instance, binding energies and ionization potentials. And even when one considers only a single property, the optimal value of ω can be strongly system-dependent [KSSB11, SEKB10, RABK11].

For the description of charge transfer or optical spectra, in particular, the freedom to choose ω can be exploited further by determining an optimal ω in a self-consistent procedure for each system individually [SKB09, KSRAB12]. However, this tuning procedure, which determines ω by essentially optimizing for the straight-line condition of Eq. (3.6), is not only taxing,

¹As the range-separation approach models only a nonlocal part of the correlation energy, a common semilocal DFA to $E_c[n]$ (typically corresponding to the semilocal exchange component) is additionally employed.

computationally demanding, and requires special care [Kü17], it also violates the formal concept of size-consistency implying actual practical drawbacks [KKK13]. As the tuning procedure effectively makes the global range-separation parameter an implicit density-functional, $\omega = \omega[n]$, a naturally next step is to construct this density-functional explicitly. However, size-consistency, cf. Sec. 4.1, requires that the range-separation parameter cannot be a global parameter, but has to be, at least, a local function, $\omega = \omega([n]; \mathbf{r})$. If this approach is successful, it might be possible to solve the parameter dilemma of RSHs, supersede the taxing tuning procedure, and resolve additional formal restraints of the RSH class, e.g., the violation of size-consistency or the one-electron self-interaction error.

The ansatz of a local range-separation parameter was first and so far last investigated by Krukau *et al.* [KSPS08]. This work, which is central to Pub. 4, demonstrates that the local range-separation parameter

$$\omega^K([n]; \mathbf{r}) = 0.135 \frac{|\nabla n(\mathbf{r})|}{n(\mathbf{r})} \quad (6.16)$$

gives excellent thermochemical properties, superior to any spatially constant choice for ω . This ansatz for $\omega([n]; \mathbf{r})$ also later inspired a seminal modification of the BJ potential [TB09], cf. Sec. 6.1.

It was further pointed out by Krukau *et al.* [KSPS08] that, due to the spatial dependence of $\omega(\mathbf{r})$, the various techniques [Sav96, GAP96, DSG01] to numerically efficiently evaluate the computationally critical LR component can no longer be applied. Therefore, a hyper-GGA approximation to the LR component was proposed [KSPS08],

$$\begin{aligned} E_x^{\text{ex,LR}}[n, \omega] &\approx E_x^{\text{hyper-GGA,LR}}[n, \omega] \\ &= \frac{e^2}{2} \iint \frac{n(\mathbf{r}) \bar{h}_x^{\text{sl}}(n(\mathbf{r}), |\nabla n(\mathbf{r})|, \tau(\mathbf{r}), e_x^{\text{ex}}(\mathbf{r}), |\mathbf{r} - \mathbf{r}'|)}{|\mathbf{r} - \mathbf{r}'|} \text{erf}(\omega([n]; \mathbf{r}) |\mathbf{r} - \mathbf{r}'|) d^3 r' d^3 r. \end{aligned} \quad (6.17)$$

In this approximation the spherically averaged exact exchange hole $\bar{h}_x^{\text{ex}}(\mathbf{r}, |\mathbf{r} - \mathbf{r}'|)$ at each reference point \mathbf{r} is mapped onto a semilocal model $\bar{h}_x^{\text{sl}}(\mathbf{r}, |\mathbf{r} - \mathbf{r}'|)$ by virtue of the exact exchange energy density $e_x^{\text{ex}}(\mathbf{r})$ and exact constraints. As the \mathbf{r}' -integral can subsequently be carried out analytically, the computational cost is drastically reduced and the resulting DFA takes the usual hyper-GGA form [PS01], where $e_x^{\text{ex}}(\mathbf{r})$ is used as an additional ingredient alongside the common semilocal ingredients. The quality and reliability, which depends on the choice for \bar{h}_x^{sl} , is only mildly assessed by Krukau *et al.* because, e.g., only a single variant of the exchange hole model [CPT06] of the TPSS meta-GGA [TPSS03] adapted for this purpose was used.

Hence, Pub. 4 revisits the hyper-GGA approximation and investigates a newly revised TPSS exchange hole model [TBS17] as well as a generalized version [Bec03, PPBKE15] of the Becke-Roussel (BR) exchange hole model [BR89] in comparison with the initially used TPSS hole. Moreover, Pub. 4 showcases that for spherically symmetric systems, e.g., closed-shell atoms, a direct assessment of the hyper-GGA approximation including a real space analysis of the screened exchange holes is possible. To this end, a Slater-type [Sla30] basis set code for closed-shell atoms was written as part of this thesis and is employed in Pub. 4 – see Appendix

A.2 for further details. [Publication 4](#) concludes this assessment by advocating that the hyper-GGA approximation is substantial and therefore the resulting DFA should rather be seen as a definition of a hyper-GGA motivated by the range-separation approach than as an approximation to a (local) RSH.

In a second part of [Pub. 4](#), the local range-separation parameter construction is refined by applying additional exact constraints. Most notably, the correct high-density limit (4.23) under uniform density-scaling (4.10) as well as one-electron self-interaction freedom (3.14) are enforced. While the former constraint takes the form [[KSPS08](#)]

$$\omega([n_\lambda]; \mathbf{r}) \gg \lambda \omega([n]; \lambda \mathbf{r}) \quad \text{as } \lambda \rightarrow \infty, \quad (6.18)$$

the latter may be formulated as a pole of the range-separation parameter

$$\omega([n]; \mathbf{r}) \rightarrow \infty \quad (6.19)$$

whenever a chosen semilocal one-electron indicator detects a corresponding point in space to have single-electron character. For this task, a common single-orbital indicator [[PKZB99](#), [TPSS03](#), [DSFC16](#)]

$$z(\mathbf{r}) = \tau^W(\mathbf{r}) / \tau(\mathbf{r}), \quad (6.20)$$

which has already been used for the same purpose in local hybrids [[JSE03](#), [SKM⁺14](#), [SKKK14](#)], is employed. [Publication 4](#) demonstrates further that this one-electron self-interaction pole is best combined with a spin scaling for $\omega_\sigma([n_\uparrow, n_\downarrow]; \mathbf{r})$ that deviates from the straightforward spin scaling for exchange (4.4) by explicit use of the spin-polarization $\zeta(\mathbf{r})$ to detect one-electron instead of iso-orbital regions. The constructed local range-separation parameter of [Pub. 4](#), which satisfies the two additional exact constraint, is given by

$$\omega_\sigma([n_\uparrow, n_\downarrow]; \mathbf{r}) = \frac{0.68 \omega_\sigma^K(\mathbf{r}) \{1 + \ln[1 + 0.90 a_0 \omega_\sigma^K(\mathbf{r})]\}}{1 - z_\sigma(\mathbf{r}) \zeta^2(\mathbf{r})} \quad (6.21)$$

with

$$\omega_\sigma^K(\mathbf{r}) = \omega^K([2n_\sigma]; \mathbf{r}) = 0.135 \frac{|\nabla n_\sigma(\mathbf{r})|}{n_\sigma(\mathbf{r})}. \quad (6.22)$$

It is shown to significantly improve on the original local range-separation parameter (6.16) proposed by Krukau *et al.* [[KSPS08](#)] in the considered thermochemical test set. This improvement is closely tied to the modification of the spin scaling in conjunction with the self-interaction pole. Moreover, it demonstrates that local range separation is a promising avenue for the constraint-guided construction of DFAs in DFT to combine ultranonlocality with thermochemical accuracy.

APPENDIX A

Complementary Work

A.1 Functional Derivatives of the Developed Meta-GGAs

The meta-GGAs of [Pub. 3](#), i.e., PoC and TASK, may both be written in the general exchange energy form of

$$E_x^{\text{mGGA}}[n] = A_x \int n^{4/3} F_x(s, \alpha) d^3r \quad (\text{A.1})$$

with $A_x = -(3e^2/4\pi)(3\pi^2)^{1/3}$ for spin-saturated systems – the spin-polarized case will be considered hereafter. Thus, the associated exchange energy density per unit volume is given by

$$e_x(\mathbf{r}) = A_x n^{4/3}(\mathbf{r}) F_x(s(\mathbf{r}), \alpha(\mathbf{r})). \quad (\text{A.2})$$

The exchange enhancement factor $F_x(s, \alpha)$ is parametrized by the dimensionless variables

$$s(\mathbf{r}) = \frac{|\nabla n(\mathbf{r})|}{2\gamma n^{4/3}(\mathbf{r})} \quad (\text{A.3})$$

with $\gamma = (3\pi^2)^{1/3}$ and

$$\alpha(\mathbf{r}) = \frac{\tau(\mathbf{r}) - \tau^{\text{W}}(\mathbf{r})}{\tau_{\text{unif}}(\mathbf{r})}, \quad (\text{A.4})$$

where

$$\tau_{\text{unif}}(\mathbf{r}) = \frac{3\hbar^2}{10m_e} \gamma^2 n^{5/3}(\mathbf{r}) \quad (\text{A.5})$$

is the uniform-density limit of the (positive) non-interacting kinetic energy density

$$\tau(\mathbf{r}) = \frac{\hbar^2}{2m_e} \sum_i f_i |\nabla \phi_i(\mathbf{r})|^2 \quad (\text{A.6})$$

and the von-Weizsäcker kinetic energy density

$$\tau^{\text{W}}(\mathbf{r}) = \frac{\hbar^2}{8m_e} \frac{|\nabla n(\mathbf{r})|^2}{n(\mathbf{r})} \quad (\text{A.7})$$

its single-orbital limit. For completeness, the (fractional) occupation number f_i will be considered explicitly and hence the density is given by $n(\mathbf{r}) = \sum_i f_i |\phi_i(\mathbf{r})|^2$.

To separate the explicit density and kinetic energy density dependence, $n(\mathbf{r})$ and $\tau(\mathbf{r})$ are

considered to be independent and therefore the chain rule of functional derivatives yields

$$\varphi_i^*(\mathbf{r})u_{xi}(\mathbf{r}) = \frac{1}{f_i} \frac{\delta E_x^{\text{mGGA}}[n]}{\delta \varphi_i(\mathbf{r})} = \int \frac{\delta E_x^{\text{mGGA}}}{\delta n(\mathbf{r}')} \frac{1}{f_i} \frac{\delta n(\mathbf{r}')}{\delta \varphi_i(\mathbf{r})} d^3 r' + \int \frac{\delta E_x^{\text{mGGA}}}{\delta \tau(\mathbf{r}')} \frac{1}{f_i} \frac{\delta \tau(\mathbf{r}')}{\delta \varphi_i(\mathbf{r})} d^3 r' \quad (\text{A.8})$$

in an initial step to calculate the meta-GGA functional derivative. From the definitions of $n(\mathbf{r})$ and $\tau(\mathbf{r})$ now follows

$$\frac{1}{f_i} \frac{\delta n(\mathbf{r}')}{\delta \varphi_i(\mathbf{r})} = \varphi_i^*(\mathbf{r}') \delta(\mathbf{r} - \mathbf{r}') \quad (\text{A.9})$$

as well as

$$\frac{1}{f_i} \frac{\delta \tau(\mathbf{r}')}{\delta \varphi_i(\mathbf{r})} = \frac{\hbar^2}{2m_e} \nabla' \varphi_i^*(\mathbf{r}') \cdot \nabla' \delta(\mathbf{r} - \mathbf{r}'). \quad (\text{A.10})$$

While $\delta E_x^{\text{mGGA}}/\delta \tau(\mathbf{r}) = (\partial e_x/\partial \tau)(\mathbf{r})$, the explicit dependence on the density-gradient $\nabla n(\mathbf{r})$ implies

$$\begin{aligned} \frac{\delta E_x^{\text{mGGA}}}{\delta n(\mathbf{r})} &= \frac{\partial e_x}{\partial n}(\mathbf{r}) + \int \frac{\delta E_x^{\text{mGGA}}}{\delta \nabla' n(\mathbf{r}')} \cdot \frac{\delta \nabla' n(\mathbf{r}')}{\delta n(\mathbf{r})} d^3 r' \\ &= \frac{\partial e_x}{\partial n}(\mathbf{r}) + \int \frac{\delta E_x^{\text{mGGA}}}{\delta \nabla' n(\mathbf{r}')} \cdot \nabla' \delta(\mathbf{r} - \mathbf{r}') d^3 r' = \frac{\partial e_x}{\partial n}(\mathbf{r}) - \nabla \cdot \left[\frac{\partial e_x}{\partial \nabla n}(\mathbf{r}) \right]. \end{aligned} \quad (\text{A.11})$$

Combination of these relations gives the meta-GGA functional derivative in its general form

$$\begin{aligned} \frac{1}{f_i} \frac{\delta E_x^{\text{mGGA}}}{\delta \varphi_i(\mathbf{r})} &= \varphi_i^*(\mathbf{r}) \left\{ \frac{\partial e_x}{\partial n}(\mathbf{r}) - \nabla \cdot \left[\frac{\partial e_x}{\partial \nabla n}(\mathbf{r}) \right] \right\} \\ &\quad - \frac{\hbar^2}{2m_e} \left\{ \frac{\partial e_x}{\partial \tau}(\mathbf{r}) \nabla^2 \varphi_i^*(\mathbf{r}) + \nabla \left[\frac{\partial e_x}{\partial \tau}(\mathbf{r}) \right] \cdot \nabla \varphi_i^*(\mathbf{r}) \right\}. \end{aligned} \quad (\text{A.12})$$

For further evaluation, a change of variables from $\{s, \alpha\}$ to $\{s, t\}$, where $t = \tau/\tau^{\text{unif}}$ and hence $\alpha = t - 5s^2/3$, is convenient. In connection with this and for numerical stability of the single-orbital limit, i.e., when $n(\mathbf{r}) \rightarrow |\varphi(\mathbf{r})|^2$ and thus $\tau(\mathbf{r}) \rightarrow \tau^W(\mathbf{r})$, it is important to treat $n(\mathbf{r})$ and $\varphi_i(\mathbf{r})$ identically on a numerical level, see, e.g., Ref. [SKM⁺14]. Consequently, henceforth $n(\mathbf{r})$ is written in terms of $\sqrt{n(\mathbf{r})}$ whenever appropriate, as for real-valued orbitals in the single-orbital limit $\varphi(\mathbf{r}) = \pm \sqrt{n(\mathbf{r})}$.

From the chain rule follows

$$\begin{aligned} \frac{\partial e_x}{\partial n} &= \frac{4}{3} A_x n^{1/3} F_x + A_x n^{4/3} \left. \frac{\partial F_x}{\partial s} \right|_t \frac{\partial s}{\partial n} + A_x n^{4/3} \left. \frac{\partial F_x}{\partial t} \right|_s \frac{\partial t}{\partial n} \\ &= A_x n^{1/3} \left[\frac{4}{3} F_x(s, t) - \frac{4}{3} s \left. \frac{\partial F_x}{\partial s} \right|_t - \frac{5}{3} t \left. \frac{\partial F_x}{\partial t} \right|_s \right] \end{aligned} \quad (\text{A.13})$$

as well as

$$-\nabla \cdot \left[\frac{\partial e_x}{\partial \nabla n}(\mathbf{r}) \right] = -\nabla \cdot \left(A_x \frac{1}{s} \left. \frac{\partial F_x}{\partial s} \right|_t \frac{\nabla n}{4\gamma^2 n^{4/3}} \right) =$$

$$\begin{aligned}
 &= -\frac{A_x}{2} \left[\frac{\nabla n}{n} \cdot \nabla \left(\frac{1}{2\gamma^2 n^{1/3}} \frac{1}{s} \frac{\partial F_x}{\partial s} \Big|_t \right) + \frac{1}{2\gamma^2 n^{1/3}} \frac{1}{s} \frac{\partial F_x}{\partial s} \Big|_t \frac{\nabla^2 n}{n} - \frac{1}{2\gamma^2 n^{1/3}} \frac{1}{s} \frac{\partial F_x}{\partial s} \Big|_t \frac{|\nabla n|^2}{n^2} \right] \\
 &= -A_x \left[\frac{\nabla \sqrt{n}}{\sqrt{n}} \cdot \nabla \left(\frac{1}{2\gamma^2 n^{1/3}} \frac{1}{s} \frac{\partial F_x}{\partial s} \Big|_t \right) + \frac{1}{2\gamma^2 n^{1/3}} \frac{1}{s} \frac{\partial F_x}{\partial s} \Big|_t \frac{\nabla^2 \sqrt{n}}{\sqrt{n}} - \frac{1}{2} n^{1/3} s \frac{\partial F_x}{\partial s} \Big|_t \right], \quad (\text{A.14})
 \end{aligned}$$

and therefore

$$\begin{aligned}
 \frac{\partial e_x}{\partial n}(\mathbf{r}) - \nabla \cdot \left[\frac{\partial e_x}{\partial \nabla n}(\mathbf{r}) \right] &= A_x n^{1/3} \left(\frac{4}{3} F_x - \frac{5}{6} s \frac{\partial F_x}{\partial s} \Big|_t - \frac{5}{3} t \frac{\partial F_x}{\partial t} \Big|_s \right) \\
 &\quad - A_x \left[\frac{\nabla^2 \sqrt{n}}{\sqrt{n}} \frac{1}{2\gamma^2 n^{1/3}} \frac{1}{s} \frac{\partial F_x}{\partial s} \Big|_t + \frac{\nabla \sqrt{n}}{\sqrt{n}} \cdot \nabla \left(\frac{1}{2\gamma^2 n^{1/3}} \frac{1}{s} \frac{\partial F_x}{\partial s} \Big|_t \right) \right]. \quad (\text{A.15})
 \end{aligned}$$

Similarly

$$\frac{\partial e_x}{\partial \tau} = A_x n^{4/3} \frac{\partial F_x}{\partial t} \Big|_s \frac{\partial t}{\partial \tau} = A_x n^{-1/3} \frac{10m_e}{3\hbar^2} \frac{1}{\gamma^2} \frac{\partial F_x}{\partial t} \Big|_s \quad (\text{A.16})$$

and thus

$$\begin{aligned}
 -\frac{\hbar^2}{2m_e} \left[\frac{\partial e_x}{\partial \tau} \nabla^2 \varphi_i^* + \nabla \varphi_i^* \cdot \nabla \left(\frac{\partial e_x}{\partial \tau} \right) \right] \\
 = -\frac{5}{3} A_x \left[\frac{\nabla^2 \varphi_i^*}{\gamma^2 n^{1/3}} \frac{\partial F_x}{\partial t} \Big|_s + \nabla \varphi_i^* \cdot \nabla \left(\frac{1}{\gamma^2 n^{1/3}} \frac{\partial F_x}{\partial t} \Big|_s \right) \right]. \quad (\text{A.17})
 \end{aligned}$$

With the help of the auxiliary functions

$$h_s(n, s, t) = \frac{1}{2\gamma^2 n^{1/3}} \frac{1}{s} \frac{\partial F_x}{\partial s} \Big|_t \quad (\text{A.18})$$

and

$$h_t(n, s, t) = \frac{1}{A_x} \frac{\hbar^2}{2m_e} \frac{\partial e_x}{\partial \tau} = \frac{5}{3} \frac{1}{\gamma^2 n^{1/3}} \frac{\partial F_x}{\partial t} \Big|_s, \quad (\text{A.19})$$

one obtains

$$\begin{aligned}
 \varphi_i^*(\mathbf{r}) u_{xi}(\mathbf{r}) &= \frac{1}{f_i} \frac{\delta E_x^{\text{mGGA}}}{\delta \varphi_i(\mathbf{r})} = \varphi_i^* A_x n^{1/3} \left(\frac{4}{3} F_x - \frac{5}{6} s \frac{\partial F_x}{\partial s} \Big|_t - \frac{5}{3} t \frac{\partial F_x}{\partial t} \Big|_s \right) \\
 &\quad - \varphi_i^* A_x \left(h_s \frac{\nabla^2 \sqrt{n}}{\sqrt{n}} + \nabla h_s \cdot \frac{\nabla \sqrt{n}}{\sqrt{n}} \right) - A_x (h_t \nabla^2 \varphi_i^* + \nabla h_t \cdot \nabla \varphi_i^*). \quad (\text{A.20})
 \end{aligned}$$

In a final step, the change of variables is reversed back to $\{s, \alpha\}$ or more precisely to $\{s^2, \alpha\}$ as it is implied that $F_x(s, \alpha)$ depends only on even powers of s (since $s \geq 0$, this is no loss of generality). To this end,

$$\frac{1}{2s} \frac{\partial F_x}{\partial s} \Big|_t = \frac{\partial F_x}{\partial s^2} \Big|_t = \frac{\partial F_x}{\partial s^2} \Big|_\alpha - \frac{5}{3} \frac{\partial F_x}{\partial \alpha} \Big|_{s^2} \quad \text{and} \quad \frac{\partial F_x}{\partial t} \Big|_s = \frac{\partial F_x}{\partial \alpha} \Big|_{s^2} \quad (\text{A.21})$$

is used to rewrite Eq. (A.20) as

$$\begin{aligned} \varphi_i^*(\mathbf{r})u_{xi}(\mathbf{r}) &= \frac{1}{f_i} \frac{\delta E_x^{\text{mGGA}}}{\delta \varphi_i(\mathbf{r})} = \varphi_i^* A_x n^{1/3} \left(\frac{4}{3} F_x - \frac{5}{3} s^2 \frac{\partial F_x}{\partial s^2} \Big|_{\alpha} - \frac{5}{3} \alpha \frac{\partial F_x}{\partial \alpha} \Big|_{s^2} \right) \\ &\quad - \varphi_i^* A_x \left(h_s \frac{\nabla^2 \sqrt{n}}{\sqrt{n}} + \nabla h_s \cdot \frac{\nabla \sqrt{n}}{\sqrt{n}} \right) - A_x (h_t \nabla^2 \varphi_i^* + \nabla h_t \cdot \nabla \varphi_i^*) \end{aligned} \quad (\text{A.22})$$

with

$$h_s(n, s, \alpha) = \frac{1}{\gamma^2 n^{1/3}} \left(\frac{\partial F_x}{\partial s^2} \Big|_{\alpha} - \frac{5}{3} \frac{\partial F_x}{\partial \alpha} \Big|_{s^2} \right) \quad (\text{A.23})$$

and

$$h_t(n, s, \alpha) = \frac{5}{3} \frac{1}{\gamma^2 n^{1/3}} \frac{\partial F_x}{\partial \alpha} \Big|_{s^2}. \quad (\text{A.24})$$

Equation (A.22) reflects the grid-based meta-GGA implementation that is used in BTDFE, DARSEC, and PARSEC. Other implementations, such as in BAND or in LIBXC [LSOM18], explicitly need

$$\begin{aligned} \frac{\partial e_x}{\partial n} &= A_x n^{1/3} \left[\frac{4}{3} F_x - \frac{8}{3} s^2 \frac{\partial F_x}{\partial s^2} \Big|_t - \frac{5}{3} t \frac{\partial F_x}{\partial t} \Big|_{s^2} \right] \\ &= A_x n^{1/3} \left[\frac{4}{3} F_x - \frac{8}{3} s^2 \frac{\partial F_x}{\partial s^2} \Big|_{\alpha} + \frac{5}{3} (s^2 - \alpha) \frac{\partial F_x}{\partial \alpha} \Big|_{s^2} \right], \end{aligned} \quad (\text{A.25})$$

as well as

$$\begin{aligned} \frac{\partial e_x}{\partial |\nabla n|^2} &= A_x n^{4/3} \frac{\partial F_x}{\partial s^2} \Big|_t \frac{\partial s^2}{\partial |\nabla n|^2} = \frac{A_x}{4 \gamma^2 n^{4/3}} \frac{\partial F_x}{\partial s^2} \Big|_t \\ &= \frac{A_x}{4 \gamma^2 n^{4/3}} \left(\frac{\partial F_x}{\partial s^2} \Big|_{\alpha} - \frac{5}{3} \frac{\partial F_x}{\partial \alpha} \Big|_{s^2} \right) = \frac{A_x}{4} \frac{h_s}{n} \end{aligned} \quad (\text{A.26})$$

and

$$\frac{\partial e_x}{\partial \tau} = \frac{10 m_e}{3 \hbar^2} \frac{A_x}{\gamma^2 n^{1/3}} \frac{\partial F_x}{\partial t} \Big|_{s^2} = \frac{10 m_e}{3 \hbar^2} \frac{A_x}{\gamma^2 n^{1/3}} \frac{\partial F_x}{\partial \alpha} \Big|_{s^2} = \frac{2 m_e A_x}{\hbar^2} h_t. \quad (\text{A.27})$$

For a particular meta-GGA these implementations require the specification of the enhancement factor $F_x(s, \alpha)$ and its partial first-order derivatives, $\partial F_x / \partial s^2 |_{\alpha}$ and $\partial F_x / \partial \alpha |_{s^2}$, as given below for PoC and TASK. Additional details on and insight into the functional derivative of meta-GGAs and their implementation can be found in Refs. [AK03, ZLG13].

Spin-Polarization

The generalization for a spin-polarized system follows from the spin-scaling relationship for the exchange energy given by Eq. (4.6). It implies

$$e_x(n_{\uparrow}, n_{\downarrow}, |\nabla n_{\uparrow}|^2, |\nabla n_{\downarrow}|^2, \tau_{\uparrow}, \tau_{\downarrow}) = \frac{1}{2} e_x(2n_{\uparrow}, 4|\nabla n_{\uparrow}|^2, 2\tau_{\uparrow}) + \frac{1}{2} e_x(2n_{\downarrow}, 4|\nabla n_{\downarrow}|^2, 2\tau_{\downarrow}) \quad (\text{A.28})$$

for the exchange energy density, which leads to

$$\frac{\partial e_x}{\partial n_\sigma} = \frac{\partial e_x}{\partial n} \Big|_{n=2n_\sigma, \tau=2\tau_\sigma}, \quad \frac{\partial e_x}{\partial \nabla n_\sigma} = \frac{\partial e_x}{\partial \nabla n} \Big|_{n=2n_\sigma, \tau=2\tau_\sigma}, \quad (\text{A.29})$$

$$\frac{\partial e_x}{\partial |\nabla n_\sigma|^2} = 2 \frac{\partial e_x}{\partial |\nabla n|^2} \Big|_{n=2n_\sigma, \tau=2\tau_\sigma}, \quad \frac{\partial e_x}{\partial \tau_\sigma} = \frac{\partial e_x}{\partial \tau} \Big|_{n=2n_\sigma, \tau=2\tau_\sigma}. \quad (\text{A.30})$$

Therefore, the generalization of Eq. (A.22) is given by

$$\begin{aligned} \varphi_{i\sigma}^*(\mathbf{r}) u_{x i\sigma}(\mathbf{r}) &= \frac{1}{f_{i\sigma}} \frac{\delta E_x^{\text{mGGA}}}{\delta \varphi_{i\sigma}(\mathbf{r})} = \varphi_{i\sigma}^* A_x n^{1/3} \left(\frac{4}{3} F_x - \frac{5}{3} s^2 \frac{\partial F_x}{\partial s^2} \Big|_\alpha - \frac{5}{3} \alpha \frac{\partial F_x}{\partial \alpha} \Big|_{s^2} \right) \\ &\quad - \varphi_{i\sigma}^* A_x \left(h_s \frac{\nabla^2 \sqrt{n}}{\sqrt{n}} + \nabla h_s \cdot \frac{\nabla \sqrt{n}}{\sqrt{n}} \right) - A_x (h_t \nabla^2 \varphi_{i\sigma}^* + \nabla h_t \cdot \nabla \varphi_{i\sigma}^*) \end{aligned} \quad (\text{A.31})$$

but evaluated at $n = 2n_\sigma$ and $\tau = 2\tau_\sigma$, as is also evident when taking the functional derivative of Eq. (4.6) with respect to $n_\sigma(\mathbf{r})$,

$$v_{x\sigma}([n_\uparrow, n_\downarrow, \tau_\uparrow, \tau_\downarrow]; \mathbf{r}) = \frac{\delta E_x[n_\uparrow, n_\downarrow, \tau_\uparrow, \tau_\downarrow]}{\delta n_\sigma(\mathbf{r})} = \frac{1}{2} \frac{\delta E_x[2n_\sigma, 2\tau_\sigma]}{\delta n_\sigma(\mathbf{r})} = v_x([2n_\sigma, 2\tau_\sigma]; \mathbf{r}). \quad (\text{A.32})$$

PoC meta-GGA

The PoC meta-GGA enhancement factor is parametrized solely by α and given by [P3]

$$F_x^{\text{PoC}}(\alpha) = c_H - \frac{c_1 \alpha}{1 + c_2 \alpha} \quad (\text{A.33})$$

with $c_H = (40/81) (4\pi^2/3)^{1/3}$, $c_1 = 27/40$, and $c_2 = c_1/(3 + c_H)$. Thus, only

$$\frac{\partial F_x^{\text{PoC}}}{\partial \alpha} \Big|_{s^2} = -\frac{c_1}{(1 + c_2 \alpha)^2} \quad (\text{A.34})$$

is required, as $\partial F_x^{\text{PoC}}/\partial s^2 \Big|_\alpha = 0$, and therefore $h_s = -h_t$.

TASK meta-GGA

The TASK meta-GGA enhancement factor is given by [P3]

$$F_x^{\text{TASK}}(s, \alpha) = h_x^0 g_x(s) + [1 - f_x(\alpha)] [h_x^1(s) - h_x^0] [g_x(s)]^d \quad (\text{A.35})$$

with $h_x^0 = 1.174$, $d = 10$,

$$g_x(s) = 1 - \exp(-cs^{-1/2}), \quad (\text{A.36})$$

where $c = 4.9479$. Moreover,

$$h_x^1(s) = \sum_{v=0}^2 a_v R_v(s^2), \quad f_x(\alpha) = \sum_{v=0}^4 b_v R_v(\alpha), \quad (\text{A.37})$$

are written in terms of Chebyshev rational functions [Boy87, GSW02, PTVF92] $R_v(x)$ of degree v . In particular,

$$R_0(x) = 1, \quad (\text{A.38})$$

$$R_1(x) = \frac{x-1}{x+1}, \quad (\text{A.39})$$

$$R_2(x) = \frac{x^2 - 6x + 1}{(x+1)^2}, \quad (\text{A.40})$$

$$R_3(x) = \frac{x^3 - 15x^2 + 15x - 1}{(x+1)^3}, \quad (\text{A.41})$$

$$R_4(x) = \frac{x^4 - 28x^3 + 70x^2 - 28x + 1}{(x+1)^4}. \quad (\text{A.42})$$

The coefficients of the Chebyshev rational functions are $a_0 = 0.938719$, $a_1 = -0.076371$, $a_2 = -0.0150899$, $b_0 = -0.628591$, $b_1 = -2.10315$, $b_2 = -0.5$, $b_3 = 0.103153$, $b_4 = 0.128591$. Consequently, the required derivatives are given by

$$\begin{aligned} \left. \frac{\partial F_x^{\text{TASK}}}{\partial s^2} \right|_{\alpha} &= \left\{ h_x^0 + d [1 - f_x(\alpha)] [h_x^1(s) - h_x^0] [g_x(s)]^{d-1} \right\} \frac{\partial g_x}{\partial s^2} \\ &\quad + [1 - f_x(\alpha)] [g_x(s)]^d \frac{\partial h_x^1}{\partial s^2} \end{aligned} \quad (\text{A.43})$$

and

$$\left. \frac{\partial F_x^{\text{TASK}}}{\partial \alpha} \right|_{s^2} = [h_x^1(s) - h_x^0] [g_x(s)]^d \frac{\partial f_x}{\partial \alpha} \quad (\text{A.44})$$

with

$$\frac{\partial g_x}{\partial s^2} = -\frac{c}{4s^{5/2}} \exp(-cs^{-1/2}) \quad (\text{A.45})$$

and

$$\frac{\partial h_x^1}{\partial s^2} = \sum_{v=1}^2 a_v R'_v(s^2), \quad \frac{\partial f_x}{\partial \alpha} = \sum_{v=1}^4 b_v R'_v(\alpha). \quad (\text{A.46})$$

For numerical purpose, the functions $h_x^1(s)$ and $f_x(\alpha)$, which are represented by a series of Chebyshev rational functions, as well as their derivatives, $\partial h_x^1 / \partial s^2$ and $\partial f_x / \partial \alpha$, can be evaluated efficiently via a recursion relation [PTVF92].

A.2 Slater-Type Basis Set Code for Closed-Shell Atoms

Publication 4 employs a Slater-type basis set code for closed-shell atoms written as part of this thesis. This section outlines the analytic formulas the code is based on. Even though the use of Slater-type basis sets [Sla30] is rather uncommon, most of these formulas should also be available in the literature. However, since only the special case of a closed-shell atom is considered and the formulas were derived directly from the definition of the basis set, no explicit references are given. Hartree atomic units are used throughout this section, as these are also

utilized in the code.

As only spin-saturated atoms with closed shells are considered, the density and therefore the KS potential maintains spherical symmetry. Consequently, the KS orbitals can be written as a product of a real-valued radial function and a spherical harmonic,

$$\varphi_i(\mathbf{r}) = R_n^l(r)Y_{lm}(\theta, \phi), \quad (\text{A.47})$$

where $i = (n, l, m)$ serves as a multi-index. For each principle quantum number n , i.e., for each shell, all orbitals with the same angular momentum $l = 0, 1, \dots$ – enumerated by the magnetic quantum number $m = 0, \pm 1, \dots, \pm l$ – are degenerated and either completely double-occupied (spin-up and -down) or completely unoccupied. Thus, the sum over all occupied orbitals of either spin-channel can be written as

$$\sum_{i=1}^N \varphi_i(\mathbf{r}) = \sum_{l=0}^{l_{\max}} \sum_{n=1}^{N_l} R_n^l(r) \sum_{m=-l}^l Y_{lm}(\theta, \phi), \quad (\text{A.48})$$

where N is the number of occupied orbitals per spin channel, i.e., half of the number of electrons, l_{\max} is the highest occupied angular quantum number, and N_l is the number of occupied states with angular quantum number l . For later purposes, note the spherical harmonic addition theorem

$$\sum_{m=-l}^l Y_{lm}^*(\theta', \phi') Y_{lm}(\theta, \phi) = \frac{2l+1}{4\pi} P_l(\cos \delta), \quad (\text{A.49})$$

where $P_l(x)$ is the Legendre polynomial of degree l [AS72] and δ is the intermediate angle between \mathbf{r} and \mathbf{r}' . For $\delta = 0$, in particular,

$$\sum_{m=-l}^l |Y_{lm}(\theta, \phi)|^2 = \frac{2l+1}{4\pi} \quad (\text{A.50})$$

follows from the spherical harmonic addition theorem.

The radial function for each n and l is expanded with real coefficients $c_{\mathbf{v}}^{nl}$ in terms of a Slater-type basis set $\{\mathbf{v}\}_l$ that in turn is unique with respect to l , i.e.,

$$R_n^l(r) = \sum_{\{\mathbf{v}\}_l} c_{\mathbf{v}}^{nl} \chi_{\mathbf{v}}(r). \quad (\text{A.51})$$

However, the notation of the implicit l -dependence of the basis set $\{\mathbf{v}\}_l$ will be suppressed hereinafter. Each Slater-type basis function [Sla30],

$$\chi_{\mathbf{v}}(r) = \chi_a^{\zeta}(r) = r^{a-1} e^{-\zeta r}, \quad (\text{A.52})$$

is specified by a double-index $\mathbf{v} = (a, \zeta)$ – a pair of a positive integer $a \geq 1$ and a positive parameter $\zeta > 0$. As the radial basis functions are neither normalized nor orthogonal, an overlap

matrix of basis functions with the same angular momentum l

$$S_{\nu\mu} := \frac{1}{4\pi} \int \chi_\nu(r) \chi_\mu(r) d^3r = \int_0^\infty \chi_\nu(r) \chi_\mu(r) r^2 dr = \frac{(a+b)!}{(\zeta + \xi)^{a+b+1}} \quad (\text{A.53})$$

is defined with $\nu = (a, \zeta)$ and $\mu = (b, \xi)$ here and hereon. The overlap matrix allows to formulate the orbital normalization as

$$1 \stackrel{!}{=} \int |\varphi_i(\mathbf{r})|^2 d^3r = \sum_{\nu, \mu} \int c_\nu^{nl} c_\mu^{nl} \chi_\nu(r) \chi_\mu(r) |Y_{lm}(\theta, \phi)|^2 d^3r = \sum_{\nu, \mu} c_\nu^{nl} S_{\nu\mu} c_\mu^{nl}. \quad (\text{A.54})$$

Similarly, one can define the kinetic energy matrix

$$\begin{aligned} T_{\nu\mu}^l &:= -\frac{1}{2} \int \chi_\nu(r) Y_{lm}^*(\theta, \phi) \nabla^2 [\chi_\mu(r) Y_{lm}(\theta, \phi)] d^3r \\ &= -\frac{1}{2} \frac{a(a-1)\zeta^2 + b(b-1)\xi^2 - 2ab\zeta\xi - l(l+1)(\zeta + \xi)^2}{(a+b)(a+b-1)} S_{\nu\mu}, \end{aligned} \quad (\text{A.55})$$

and the Coulomb matrix

$$V_{\nu\mu} := -\frac{1}{4\pi} \int \chi_\nu(r) \frac{1}{r} \chi_\mu(r) d^3r = -\int_0^\infty \chi_\nu(r) \chi_\mu(r) r dr = -\frac{\zeta + \xi}{a+b} S_{\nu\mu}. \quad (\text{A.56})$$

For a KS calculation the evaluation of the Hartree and xc potential, $v_{\text{hxc}}(r) = v_{\text{h}}(r) + v_{\text{xc}}(r)$, is required additionally. While $v_{\text{xc}}(r)$ depends on the DFA employed, the Hartree potential can be calculated as

$$\begin{aligned} v_{\text{h}}(r) &= \int \frac{n(\mathbf{r}')}{|\mathbf{r} - \mathbf{r}'|} d^3r' = \sum_{i=1}^N \int \frac{2|\varphi_i(\mathbf{r}')|^2}{|\mathbf{r} - \mathbf{r}'|} d^3r' = 2 \sum_{l=0}^{l_{\max}} \sum_{n=1}^{N_l} \int \frac{|R_n^l(r')|^2}{|\mathbf{r} - \mathbf{r}'|} \sum_{m=-l}^l |Y_{lm}(\theta', \phi')|^2 d^3r' \\ &= \sum_{l=0}^{l_{\max}} 2(2l+1) \sum_{n=1}^{N_l} \sum_{\nu, \mu} c_\nu^{nl} c_\mu^{nl} \frac{1}{4\pi} \int \frac{\chi_\nu(r') \chi_\mu(r')}{|\mathbf{r} - \mathbf{r}'|} d^3r' \\ &= \sum_{l=0}^{l_{\max}} 2(2l+1) \sum_{n=1}^{N_l} \sum_{\nu, \mu} c_\nu^{nl} v_{\text{h}}^{\nu\mu}(r) c_\mu^{nl} \end{aligned} \quad (\text{A.57})$$

with

$$\begin{aligned} v_{\text{h}}^{\nu\mu}(r) &= \frac{1}{4\pi} \int \frac{\chi_\nu(r') \chi_\mu(r')}{|\mathbf{r} - \mathbf{r}'|} d^3r' = \frac{1}{r} \int_0^r \chi_\nu(r') \chi_\mu(r') r'^2 dr' + \int_r^\infty \chi_\nu(r') \chi_\mu(r') r' dr' \\ &= \left[\frac{P(a+b+1, (\zeta + \xi)r)}{r} + (\zeta + \xi) \frac{Q(a+b, (\zeta + \xi)r)}{a+b} \right] S_{\nu\mu}, \end{aligned} \quad (\text{A.58})$$

where $P(s, x)$ and $Q(s, x)$ are the regularized lower- and upper incomplete gamma functions [AS72, PTVF92]. Let then

$$U_{\nu\mu}^{\text{hxc}} = \frac{1}{4\pi} \int \chi_\nu(r) v_{\text{hxc}}(r) \chi_\mu(r) d^3r = \int_0^\infty \chi_\nu(r) v_{\text{hxc}}(r) \chi_\mu(r) r^2 dr \quad (\text{A.59})$$

be the hxc matrix to be evaluated numerically on a radial grid.

Finally, based on the KS Hamiltonian

$$\hat{H} = -\frac{\nabla^2}{2} - \frac{Z}{r} + v_{\text{hxc}}(r) \quad (\text{A.60})$$

with the nuclear charge Z , the KS equation can be recast into independent generalized eigenvalue problems for each angular momentum l ,

$$\sum_{\nu} \left(H_{\mu\nu}^l - \varepsilon^{nl} S_{\mu\nu} \right) c_{\nu}^{nl} = 0, \quad (\text{A.61})$$

where

$$H_{\nu\mu}^l = \int \chi_{\nu}(r) Y_{lm}^*(\theta, \phi) \hat{H} \chi_{\mu}(r) Y_{lm}(\theta, \phi) d^3r = T_{\nu\mu}^l + ZV_{\nu\mu} + U_{\nu\mu}^{\text{hxc}} \quad (\text{A.62})$$

and ε^{nl} is the eigenvalue of the orbital corresponding to the n -th shell and angular momentum l . These real generalized symmetric-definite eigenproblems can be solved conveniently with a standard linear algebra library. The closed-shell code outlined here uses the LAPACK DSYGV routine [ABB⁺99] for this purpose.

The KS iterations as well as the evaluation of the local range-separation parameters and of the hyper-GGA approximation, cf. Sec. 6.3 and Pub. 4, require the semilocal quantities $n(r)$, $\nabla n(r)$, $\nabla^2 n(r)$, $\tau(r)$, and $e_x^{\text{ex}}(r)$. These quantities can be calculated from the Slater-type basis as follows:

$$\begin{aligned} n(r) &= 2 \sum_{i=1}^N |\varphi_i(\mathbf{r})|^2 = 2 \sum_{l=0}^{l_{\max}} \sum_{n=1}^{N_l} |R_n^l(r)|^2 \sum_{m=-l}^l |Y_{lm}(\theta, \phi)|^2 \\ &= \sum_{l=0}^{l_{\max}} \frac{2l+1}{2\pi} \sum_{n=1}^{N_l} \left[\sum_{\nu} c_{\nu}^{nl} \chi_{\nu}(r) \right]^2, \end{aligned} \quad (\text{A.63})$$

$$\begin{aligned} \nabla n(r) &= \frac{\partial n}{\partial r}(r) \hat{e}_r = \sum_{l=0}^{l_{\max}} \frac{2l+1}{\pi} \sum_{n=1}^{N_l} \left[\sum_{\nu} c_{\nu}^{nl} \chi_{\nu}(r) \right] \left[\sum_{\mu} c_{\mu}^{nl} \frac{\partial \chi_{\mu}}{\partial r}(r) \right] \hat{e}_r \\ &= \sum_{l=0}^{l_{\max}} \frac{2l+1}{\pi} \sum_{n=1}^{N_l} \sum_{\nu, \mu} c_{\nu}^{nl} c_{\mu}^{nl} \chi_{\nu}(r) \left(\frac{b-1}{r} - \xi \right) \chi_{\mu}(r) \hat{e}_r, \end{aligned} \quad (\text{A.64})$$

$$\begin{aligned} \nabla^2 n(r) &= \sum_{l=0}^{l_{\max}} \frac{2l+1}{2\pi} \sum_{n=1}^{N_l} \sum_{\nu, \mu} c_{\nu}^{nl} c_{\mu}^{nl} \left(\frac{\partial^2}{\partial r^2} + \frac{2}{r} \frac{\partial}{\partial r} \right) \chi_{\nu}(r) \chi_{\mu}(r) \\ &= \sum_{l=0}^{l_{\max}} \frac{2l+1}{2\pi} \sum_{n=1}^{N_l} \sum_{\nu, \mu} c_{\nu}^{nl} c_{\mu}^{nl} \chi_{\nu}(r) \chi_{\mu}(r) \\ &\quad \times \left[\frac{(a+b-1)(a+b-2)}{r^2} - \frac{2(a+b-1)(\zeta+\xi)}{r} + (\zeta+\xi)^2 \right], \end{aligned} \quad (\text{A.65})$$

and

$$\begin{aligned}\tau(r) &= \sum_{i=1}^N |\nabla \varphi_i(\mathbf{r})|^2 = \sum_{l=0}^{l_{\max}} \sum_{n=1}^{N_l} \sum_{m=-l}^l \left[|\nabla R_n^l(r)|^2 |Y_{lm}(\theta, \phi)|^2 + |R_n^l(r)|^2 |\nabla Y_{lm}(\theta, \phi)|^2 \right] \\ &= \sum_{l=0}^{l_{\max}} \sum_{n=1}^{N_l} \frac{2l+1}{4\pi} \sum_{\nu, \mu} c_\nu^{nl} c_\mu^{nl} \chi_\nu(r) \chi_\mu(r) \left[\left(\frac{a-1}{r} - \zeta \right) \left(\frac{b-1}{r} - \xi \right) + \frac{l(l+1)}{r^2} \right],\end{aligned}\quad (\text{A.66})$$

where

$$\begin{aligned}\sum_{m=-l}^l |\nabla Y_{lm}(\theta, \phi)|^2 &= \frac{1}{2} \nabla^2 \sum_{m=-l}^l |Y_{lm}(\theta, \phi)|^2 - \frac{1}{2} \sum_{m=-l}^l [Y_{lm}^*(\theta, \phi) \nabla^2 Y_{lm}(\theta, \phi) + \text{c.c.}] \\ &= \frac{1}{2} \nabla^2 \left(\frac{2l+1}{4\pi} \right) + \frac{1}{2} \sum_{m=-l}^l \left[\frac{l(l+1)}{r^2} |Y_{lm}(\theta, \phi)|^2 + \text{c.c.} \right] = \frac{2l+1}{4\pi} \frac{l(l+1)}{r^2}\end{aligned}\quad (\text{A.67})$$

was used in the final step. Lastly,

$$\begin{aligned}e_x^{\text{ex}}(r) &= -\frac{e^2}{2} \sum_{\sigma=\uparrow, \downarrow} \sum_{i,j=1}^{N_\sigma} \int \frac{\varphi_{i\sigma}^*(\mathbf{r}) \varphi_{i\sigma}(\mathbf{r}') \varphi_{j\sigma}^*(\mathbf{r}') \varphi_{j\sigma}(\mathbf{r})}{|\mathbf{r} - \mathbf{r}'|} d^3 r' \\ &= -e^2 \sum_{l_1, l_2=0}^{l_{\max}} \sum_{n_1=1}^{N_{l_1}} \sum_{n_2=1}^{N_{l_2}} R_{n_1}^{l_1}(r) R_{n_2}^{l_2}(r) \int d^3 r' \frac{R_{n_1}^{l_1}(r') R_{n_2}^{l_2}(r')}{|\mathbf{r} - \mathbf{r}'|} \\ &\quad \times \left[\sum_{m_1=-l_1}^{l_1} Y_{l_1 m_1}^*(\theta, \phi) Y_{l_1 m_1}(\theta', \phi') \right] \left[\sum_{m_2=-l_2}^{l_2} Y_{l_2 m_2}^*(\theta', \phi') Y_{l_2 m_2}(\theta, \phi) \right].\end{aligned}\quad (\text{A.68})$$

Using the addition theorem (A.49) twice as well as the Legendre expansion [ÁGM06]

$$\frac{1}{|\mathbf{r} - \mathbf{r}'|} = \sum_{l=0}^{\infty} \frac{r_{<}^l}{r_{>}^{l+1}} P_l(\cos \delta), \quad (\text{A.69})$$

where $r_{>} = \max(r, r')$, $r_{<} = \min(r, r')$, and δ is the intermediate angle, then yields

$$\begin{aligned}e_x^{\text{ex}}(r) &= -e^2 \sum_{l_1, l_2=0}^{l_{\max}} \frac{(2l_1+1)(2l_2+1)}{4\pi} \sum_{n_1=1}^{N_{l_1}} \sum_{n_2=1}^{N_{l_2}} R_{n_1}^{l_1}(r) R_{n_2}^{l_2}(r) \\ &\quad \times \sum_{l=0}^{\infty} \int_0^{\infty} R_{n_1}^{l_1}(r') R_{n_2}^{l_2}(r') \frac{r_{<}^l}{r_{>}^{l+1}} r'^2 dr' \int_{-1}^1 P_{l_1}(x) P_{l_2}(x) P_l(x) dx \\ &= \gamma_{0,0,0}(r) + \gamma_{1,0,1}(r) + \gamma_{0,1,1}(r) + 3\gamma_{1,1,0}(r) + \frac{6}{5}\gamma_{1,1,2}(r)\end{aligned}\quad (\text{A.70})$$

with

$$\gamma_{l_1, l_2, l}(r) = -e^2 \sum_{n_1=1}^{N_{l_1}} \sum_{n_2=1}^{N_{l_2}} R_{n_1}^{l_1}(r) R_{n_2}^{l_2}(r) \int_0^{\infty} R_{n_1}^{l_1}(r') R_{n_2}^{l_2}(r') \frac{r_{<}^l}{r_{>}^{l+1}} r'^2 dr', \quad (\text{A.71})$$

as only atoms up to the p -shell ($l = 1$) are considered, cf. a similar calculation in the supplementary material of Pub. 4.

Publication 4 compares the exact spherical-averaged exchange hole, cf. Eq. (4.49), with corresponding semilocal hole models. The former hole can be obtained as follows, starting from its definition (4.45),

$$\bar{h}_x^{\text{ex}}(\mathbf{r}, u) = - \sum_{\sigma=\uparrow,\downarrow} \sum_{i,j=1}^{N_\sigma} \frac{\varphi_{i\sigma}^*(\mathbf{r})\varphi_{j\sigma}(\mathbf{r})}{n(\mathbf{r})} \oint \varphi_{j\sigma}^*(\mathbf{r}+\mathbf{u})\varphi_{i\sigma}(\mathbf{r}+\mathbf{u}) d\Omega_u, \quad (\text{A.72})$$

where the solid angle integral is evaluated over a sphere of radius u : Let $\mathbf{r}' = \mathbf{r} + \mathbf{u}$, δ be the intermediate angle between \mathbf{r} and \mathbf{r}' , and δ_u be the intermediate angle between \mathbf{r} and \mathbf{u} . Then for each \mathbf{r} the zenith direction of the Ω_u integration can be chosen parallel to \mathbf{r} and therefore such that δ_u is the polar angle of the Ω_u integration, cf. Fig. A.1. Hence,

$$\begin{aligned} \bar{h}_x^{\text{ex}}(r, u) &= - \frac{2}{n(r)} \sum_{l_1, l_2=0}^{l_{\max}} \sum_{n_1=1}^{N_{l_1}} \sum_{n_2=1}^{N_{l_2}} R_{n_1}^{l_1}(r) R_{n_2}^{l_2}(r) \\ &\times \oint R_{n_1}^{l_1}(r') R_{n_2}^{l_2}(r') \left[\sum_{m_1=-l_1}^{l_1} Y_{l_1 m_1}^*(\theta, \phi) Y_{l_1 m_1}(\theta', \phi') \right] \left[\sum_{m_2=-l_2}^{l_2} Y_{l_2 m_2}^*(\theta', \phi') Y_{l_2 m_2}(\theta, \phi) \right] d\Omega_u \\ &= - \frac{1}{n(r)} \sum_{l_1, l_2=0}^{l_{\max}} \frac{(2l_1+1)(2l_2+1)}{8\pi^2} \sum_{n_1=1}^{N_{l_1}} \sum_{n_2=1}^{N_{l_2}} R_{n_1}^{l_1}(r) R_{n_2}^{l_2}(r) \\ &\times \oint R_{n_1}^{l_1}(r') R_{n_2}^{l_2}(r') P_{l_1}(\cos \delta) P_{l_2}(\cos \delta) d\Omega_u \\ &= - \frac{1}{n(r)} \sum_{l_1, l_2=0}^{l_{\max}} \frac{(2l_1+1)(2l_2+1)}{4\pi} \sum_{n_1=1}^{N_{l_1}} \sum_{n_2=1}^{N_{l_2}} R_{n_1}^{l_1}(r) R_{n_2}^{l_2}(r) \sum_{\nu, \mu} c_\mu^{n_1 l_1} c_\nu^{n_2 l_2} \Lambda_{\zeta+\xi, a+b-1}^{l_1, l_2}(r, u) \quad (\text{A.73}) \end{aligned}$$

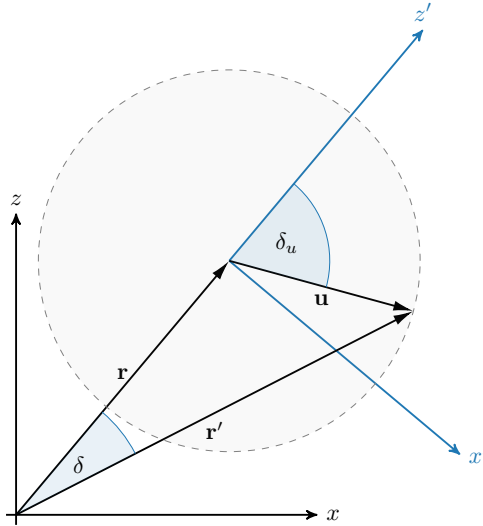


Figure A.1: Illustration of the solid angle integration Ω_u (blue coordinate system) of the exact exchange hole $h_x^{\text{ex}}(\mathbf{r}, \mathbf{r}')$ with $\mathbf{r}' = \mathbf{r} + \mathbf{u}$ and the intermediate angles δ (between \mathbf{r} and \mathbf{r}') and δ_u (between \mathbf{r} and \mathbf{u}). The latter is chosen as the polar angle of the Ω_u integration.

with

$$\Lambda_{\zeta+\xi, a+b-1}^{l_1, l_2}(r, u) = \int_0^\pi \chi_{a+b-1}^{\zeta+\xi}(r') P_{l_1}(\cos \delta) P_{l_2}(\cos \delta) \sin \delta_u d\delta_u. \quad (\text{A.74})$$

To derive an explicit formula for this remaining set of integrals, $\Lambda_{\zeta+\xi, a+b-1}^{l_1, l_2}(r, u)$,

$$r' = \sqrt{r^2 + u^2 + 2ru \cos \delta_u} \quad (\text{A.75})$$

and

$$\cos \delta = \frac{r + u \cos \delta_u}{\sqrt{r^2 + 2ru \cos \delta_u + u^2}} \quad (\text{A.76})$$

are used, cf. Fig. A.1, to write

$$\begin{aligned} \Lambda_{\zeta, n}^{l_1, l_2}(r, u) &= \frac{1}{2} \int_{-1}^1 \chi_n^\zeta(\sqrt{r^2 + u^2 + 2rux}) \\ &\quad \times P_{l_1}\left(\frac{r + ux}{\sqrt{r^2 + 2rux + u^2}}\right) P_{l_2}\left(\frac{r + ux}{\sqrt{r^2 + 2rux + u^2}}\right) dx. \end{aligned} \quad (\text{A.77})$$

As atoms up to the p -shell are considered, only the following three of these integrals are needed explicitly:

$$\Lambda_{\zeta, n}^{0,0}(r, u) = \frac{\Gamma(n, \zeta|r-u) - \Gamma(n, \zeta|r+u)}{2\zeta^n ru}, \quad (\text{A.78})$$

$$\begin{aligned} \Lambda_{\zeta, n}^{0,1}(r, u) = \Lambda_{\zeta, n}^{1,0}(r, u) &= \frac{\Gamma(n+1, \zeta|r-u) - \Gamma(n+1, \zeta|r+u)}{4\zeta^{n+1} r^2 u} \\ &\quad + \frac{(r^2 - u^2) [\Gamma(n-1, \zeta|r-u) - \Gamma(n-1, \zeta|r+u)]}{4\zeta^{n-1} r^2 u}, \end{aligned} \quad (\text{A.79})$$

and

$$\begin{aligned} \Lambda_{\zeta, n}^{1,1}(r, u) &= \frac{\Gamma(n+2, \zeta|r-u) - \Gamma(n+2, \zeta|r+u)}{2\zeta^{n+2} ru} \\ &\quad + \frac{(r^2 - u^2) [\Gamma(n, \zeta|r-u) - \Gamma(n, \zeta|r+u)]}{\zeta^n ru} \\ &\quad + \frac{(r^2 - u^2)^2 [\Gamma(n-2, \zeta|r-u) - \Gamma(n-2, \zeta|r+u)]}{8\zeta^{n-2} r^3 u}. \end{aligned} \quad (\text{A.80})$$

Here

$$\Gamma(s, x) = \int_x^\infty t^{s-1} e^{-t} dt \quad (\text{A.81})$$

is the upper incomplete gamma function [AS72].

List of Abbreviations

| | | |
|------------------|---|----|
| AK13 | Armiento-Kümmel GGA [AK13] | 36 |
| BAND | periodic all-electron code of the Amsterdam Modeling Suite [tVB91, WB91, FPV13, FPvLV14, SCM] in a locally modified version | 40 |
| BJ | Becke-Johnson potential [BJ06] | 36 |
| BR | Becke-Roussel exchange hole model [BR89] | 42 |
| BTDF | pseudopotential and real space grid based DFT code [SK18] | 40 |
| DARSEC | real space grid based electronic structure code for diatomic molecules [MKK09] in a locally modified version | 40 |
| DFA | density functional approximation, typically to $E_{xc}[n]$ | 6 |
| DFT | density functional theory | 5 |
| EXX | exact-exchange functional as defined in Eq. (5.1) | 29 |
| GE | gradient expansion, here typically of $E_x[n]$ | 23 |
| GGA | class of semilocal xc functionals that is based on a generalized-gradient approximation [PW86] | 8 |
| gKS | generalized Kohn-Sham scheme [SGV ⁺ 96] | 32 |
| ho | energetically highest occupied KS orbital or eigenvalue | 10 |
| hyper-GGA | class of xc functionals that go beyond the GGA and meta-GGA by inclusion of the exact exchange energy density [PS01] | 28 |
| KLI | approximation to the optimized effective potential equation proposed by Krieger, Li, and Iafrate [KLI92a, KLI92b] | 31 |
| KS | Kohn-Sham, usually referring to the KS scheme, orbitals, eigenvalues, potential, or equation [KS65] | 6 |
| LDA | local-density approximation xc functional | 7 |

| | | |
|-----------------|---|----|
| LIBXC | library of functionals for density functional theory [LSOM18]..... | 48 |
| LR | long-range part in the range-separation approach | 41 |
| lu | energetically lowest unoccupied KS orbital or eigenvalue | 10 |
| meta-GGA | meta generalized gradient approximation, a class of xc functionals that go beyond the GGA by inclusion of the kinetic energy density (or the Laplacian of the density) [DSFC16] | 8 |
| OEP | optimized effective potential [SH53 , TS76 , SGP82 , KK08] | 30 |
| PARSEC | pseudopotential and real space grid based electronic structure program [KMT+06] in a locally modified version | 40 |
| PBE | Perdew-Burke-Ernzerhof xc GGA [PBE96]..... | 41 |
| PoC | “proof of concept” meta-GGA for exchange as defined in Pub. 3 | 40 |
| RSH | range-separated hybrids | 40 |
| SR | short-range part in the range-separation approach | 41 |
| TASK | TASK meta-GGA for exchange as defined in Pub. 3 | 40 |
| TPSS | Tao-Perdew-Staroverov-Scuseria xc meta-GGA [TPSS03] | 42 |
| xc | exchange-correlation | 6 |

Bibliography

- [ABB⁺99] E. Anderson, Z. Bai, C. Bischof, S. Blackford, J. Demmel, J. Dongarra, J. Du Croz, A. Greenbaum, S. Hammarling, A. McKenney and D. Sorensen, *LAPACK Users' Guide*, Society for Industrial and Applied Mathematics, Philadelphia, PA, third edition, 1999.
- [ADH17] A. Anda, L. De Vico and T. Hansen, *Intermolecular Modes between LH2 Bacteriochlorophylls and Protein Residues: The Effect on the Excitation Energies*, *J. Phys. Chem. B* **121**, 5499 (2017).
- [ÁGM06] J. G. Ángyán, I. Gerber and M. Marsman, *Spherical harmonic expansion of short-range screened Coulomb interactions*, *J. Phys. A* **39**, 8613 (2006).
- [AK85] P. R. Antoniewicz and L. Kleinman, *Kohn-Sham exchange potential exact to first order in $\rho(\mathbf{K})/\rho_0$* , *Phys. Rev. B* **31**, 6779 (1985).
- [AK03] A. V. Arbuznikov and M. Kaupp, *The self-consistent implementation of exchange-correlation functionals depending on the local kinetic energy density*, *Chem. Phys. Lett.* **381**, 495 (2003).
- [AK13] R. Armiento and S. Kümmel, *Orbital Localization, Charge Transfer, and Band Gaps in Semilocal Density-Functional Theory*, *Phys. Rev. Lett.* **111**, 036402 (2013).
- [AKJS06] F. Aryasetiawan, K. Karlsson, O. Jepsen and U. Schönberger, *Calculations of Hubbard U from first-principles*, *Phys. Rev. B* **74**, 125106 (2006).
- [AKK08] R. Armiento, S. Kümmel and T. Körzdörfer, *Electrical response of molecular chains in density functional theory: Ultranonlocal response from a semilocal functional*, *Phys. Rev. B* **77**, 165106 (2008).
- [AM05] R. Armiento and A. E. Mattsson, *Functional designed to include surface effects in self-consistent density functional theory*, *Phys. Rev. B* **72**, 085108 (2005).
- [AS72] M. Abramowitz and I. A. Stegun, editors, *Handbook of Mathematical Functions with Formulas, Graphs, and Mathematical Tables*, U.S. Government Printing Office, Washington, DC, USA, tenth printing edition, 1972.
- [Asc14] T. Aschebrock, *Entwicklung von Gradientennäherungen für die Austauschenergie mit neuartiger Asymptotik*, Master's thesis, University Bayreuth, 2014.

- [AvB85] C.-O. Almbladh and U. von Barth, *Exact results for the charge and spin densities, exchange-correlation potentials, and density-functional eigenvalues*, *Phys. Rev. B* **31**, 3231 (1985).
- [AZA91] V. I. Anisimov, J. Zaanen and O. K. Andersen, *Band theory and Mott insulators: Hubbard U instead of Stoner I* , *Phys. Rev. B* **44**, 943 (1991).
- [AZE14] H. Antaya, Y. Zhou and M. Ernzerhof, *Approximating the exchange energy through the nonempirical exchange-factor approach*, *Phys. Rev. A* **90**, 032513 (2014).
- [BE90] A. D. Becke and K. E. Edgecombe, *A simple measure of electron localization in atomic and molecular systems*, *J. Chem. Phys.* **92**, 5397 (1990).
- [Bec83] A. D. Becke, *Hartree-Fock exchange energy of an inhomogeneous electron gas*, *Int. J. Quantum Chem.* **23**, 1915 (1983).
- [Bec88] A. D. Becke, *Density-functional exchange-energy approximation with correct asymptotic behavior*, *Phys. Rev. A* **38**, 3098 (1988).
- [Bec93] A. D. Becke, *Density-functional thermochemistry. III. The role of exact exchange*, *J. Chem. Phys.* **98**, 5648 (1993).
- [Bec98] A. D. Becke, *A new inhomogeneity parameter in density-functional theory*, *J. Chem. Phys.* **109**, 2092 (1998).
- [Bec03] A. D. Becke, *A real-space model of nondynamical correlation*, *J. Chem. Phys.* **119**, 2972 (2003).
- [Bec13] A. D. Becke, *Density functionals for static, dynamical, and strong correlation*, *J. Chem. Phys.* **138**, 074109 (2013).
- [Bec14] A. D. Becke, *Perspective: Fifty years of density-functional theory in chemical physics*, *J. Chem. Phys.* **140**, 18A301 (2014).
- [BF12] J. E. Bates and F. Furche, *Harnessing the meta-generalized gradient approximation for time-dependent density functional theory*, *J. Chem. Phys.* **137**, 164105 (2012).
- [BJ06] A. D. Becke and E. R. Johnson, *A simple effective potential for exchange*, *J. Chem. Phys.* **124**, 221101 (2006).
- [BJC76] M. Brack, B. Jennings and Y. Chu, *On the extended Thomas-Fermi approximation to the kinetic energy density*, *Phys. Lett. B* **65**, 1 (1976).
- [BK18] R. Baer and L. Kronik, *Time-dependent generalized Kohn-Sham theory*, *Eur. Phys. J. B* **91**, 170 (2018).

- [BO27] M. Born and R. Oppenheimer, *Zur Quantentheorie der Molekeln*, *Ann. Phys.* **389**, 457 (1927).
- [Boy87] J. P. Boyd, *Orthogonal rational functions on a semi-infinite interval*, *J. Comput. Phys.* **70**, 63 (1987).
- [BP95] K. Burke and J. P. Perdew, *Real-space analysis of the exchange-correlation energy*, *Int. J. Quantum Chem.* **56**, 199 (1995).
- [BR89] A. D. Becke and M. R. Roussel, *Exchange holes in inhomogeneous systems: A coordinate-space model*, *Phys. Rev. A* **39**, 3761 (1989).
- [Bur12] K. Burke, *Perspective on density functional theory*, *J. Chem. Phys.* **136**, 150901 (2012).
- [CA80] D. M. Ceperley and B. J. Alder, *Ground State of the Electron Gas by a Stochastic Method*, *Phys. Rev. Lett.* **45**, 566 (1980).
- [CEGVT15] J. Carmona-Espíndola, J. L. Gázquez, A. Vela and S. B. Trickey, *Generalized gradient approximation exchange energy functional with correct asymptotic behavior of the corresponding potential*, *J. Chem. Phys.* **142**, 054105 (2015).
- [CGB02] D. P. Chong, O. V. Gritsenko and E. J. Baerends, *Interpretation of the Kohn–Sham orbital energies as approximate vertical ionization potentials*, *J. Chem. Phys.* **116**, 1760 (2002).
- [CGK06] R. J. Cogdell, A. Gall and J. Köhler, *The architecture and function of the light-harvesting apparatus of purple bacteria: from single molecules to in vivo membranes*, *Q. Rev. Biophys.* **39**, 227 (2006).
- [Cha99] G. K.-L. Chan, *A fresh look at ensembles: Derivative discontinuities in density functional theory*, *J. Chem. Phys.* **110**, 4710 (1999).
- [CJC⁺16] L. Cupellini, S. Jurinovich, M. Campetella, S. Caprasecca, C. A. Guido, S. M. Kelly, A. T. Gardiner, R. Cogdell and B. Mennucci, *An Ab Initio Description of the Excitonic Properties of LH2 and Their Temperature Dependence*, *J. Phys. Chem. B* **120**, 11348 (2016).
- [CJCS98] M. E. Casida, C. Jamorski, K. C. Casida and D. R. Salahub, *Molecular excitation energies to high-lying bound states from time-dependent density-functional response theory: Characterization and correction of the time-dependent local density approximation ionization threshold*, *J. Chem. Phys.* **108**, 4439 (1998).
- [CM17] C. Curutchet and B. Mennucci, *Quantum Chemical Studies of Light Harvesting*, *Chem. Rev.* **117**, 294 (2017).

- [CMSY08] A. J. Cohen, P. Mori-Sánchez and W. Yang, *Insights into Current Limitations of Density Functional Theory*, *Science* **321**, 792 (2008).
- [CMSY12] A. J. Cohen, P. Mori-Sánchez and W. Yang, *Challenges for Density Functional Theory*, *Chem. Rev.* **112**, 289 (2012).
- [CMVA95] B. Champagne, D. H. Mosley, M. Vračko and J.-M. André, *Electron-correlation effects on the static longitudinal polarizability of polymeric chains*, *Phys. Rev. A* **52**, 178 (1995).
- [COM14] T. F. T. Cerqueira, M. J. T. Oliveira and M. A. L. Marques, *Benchmarking the AK13 Exchange Functional: Ionization Potentials and Electron Affinities*, *J. Chem. Theory Comput.* **10**, 5625 (2014).
- [CPT06] L. A. Constantin, J. P. Perdew and J. Tao, *Meta-generalized gradient approximation for the exchange-correlation hole with an application to the jellium surface energy*, *Phys. Rev. B* **73**, 205104 (2006).
- [CPvG⁺98] B. Champagne, E. A. Perpète, S. J. A. van Gisbergen, E.-J. Baerends, J. G. Snijders, C. Soubra-Ghaoui, K. A. Robins and B. Kirtman, *Assessment of conventional density functional schemes for computing the polarizabilities and hyperpolarizabilities of conjugated oligomers: An ab initio investigation of polyacetylene chains*, *J. Chem. Phys.* **109**, 10489 (1998).
- [CTDS⁺16] L. A. Constantin, A. Terentjevs, F. Della Sala, P. Cortona and E. Fabiano, *Semiclassical atom theory applied to solid-state physics*, *Phys. Rev. B* **93**, 045126 (2016).
- [CWW12] A. C. Cancio, C. E. Wagner and S. A. Wood, *Laplacian-based models for the exchange energy*, *Int. J. Quantum Chem.* **112**, 3796 (2012).
- [DHG04] A. Dreuw and M. Head-Gordon, *Failure of Time-Dependent Density Functional Theory for Long-Range Charge-Transfer Excited States: The Zinobacteriochlorin-Bacteriochlorin and Bacteriochlorophyll-Spheroidene Complexes*, *J. Am. Chem. Soc.* **126**, 4007 (2004).
- [Dir30] P. A. M. Dirac, *Note on Exchange Phenomena in the Thomas Atom*, *Math. Proc. Camb. Philos. Soc.* **26**, 376 (1930).
- [DSFC15] F. Della Sala, E. Fabiano and L. A. Constantin, *Kohn-Sham kinetic energy density in the nuclear and asymptotic regions: Deviations from the von Weizsäcker behavior and applications to density functionals*, *Phys. Rev. B* **91**, 035126 (2015).

- [DSFC16] F. Della Sala, E. Fabiano and L. A. Constantin, *Kinetic-energy-density dependent semilocal exchange-correlation functionals*, *Int. J. Quant. Chem.* **116**, 1641 (2016).
- [DSG01] F. Della Sala and A. Görling, *Efficient localized Hartree–Fock methods as effective exact-exchange Kohn–Sham methods for molecules*, *J. Chem. Phys.* **115**, 5718 (2001).
- [DSG02a] F. Della Sala and A. Görling, *Asymptotic Behavior of the Kohn–Sham Exchange Potential*, *Phys. Rev. Lett.* **89**, 033003 (2002).
- [DSG02b] F. Della Sala and A. Görling, *The asymptotic region of the Kohn–Sham exchange potential in molecules*, *J. Chem. Phys.* **116**, 5374 (2002).
- [DWHG03] A. Dreuw, J. L. Weisman and M. Head-Gordon, *Long-range charge-transfer excited states in time-dependent density functional theory require non-local exchange*, *J. Chem. Phys.* **119**, 2943 (2003).
- [EBG16] J. Erhard, P. Bleiziffer and A. Görling, *Power Series Approximation for the Correlation Kernel Leading to Kohn–Sham Methods Combining Accuracy, Computational Efficiency, and General Applicability*, *Phys. Rev. Lett.* **117**, 143002 (2016).
- [ECMV92] E. Engel, J. A. Chevary, L. D. Macdonald and S. H. Vosko, *Asymptotic properties of the exchange energy density and the exchange potential of finite systems: relevance for generalized gradient approximations*, *Z. Phys. D* **23** (1992).
- [ED11] E. Engel and R. M. Dreizler, *Density Functional Theory: An Advanced Course*, Springer, 2011.
- [EFRM12] P. Elliott, J. I. Fuks, A. Rubio and N. T. Maitra, *Universal Dynamical Steps in the Exact Time-Dependent Exchange–Correlation Potential*, *Phys. Rev. Lett.* **109**, 266404 (2012).
- [EH14] F. G. Eich and M. Hellgren, *Derivative discontinuity and exchange–correlation potential of meta-GGAs in density-functional theory*, *J. Chem. Phys.* **141**, 224107 (2014).
- [ELCB08] P. Elliott, D. Lee, A. Cangi and K. Burke, *Semiclassical Origins of Density Functionals*, *Phys. Rev. Lett.* **100**, 256406 (2008).
- [Eng03] E. Engel, *Orbital-Dependent Functionals for the Exchange–Correlation Energy: A Third Generation of Density Functionals*, in *A Primer in Density Functional Theory*, edited by C. Fiolhais, F. Nogueira and M. A. Marques, pp. 56–122, Springer-Verlag, Berlin Heidelberg, 2003.

- [EV90] E. Engel and S. H. Vosko, *Wave-vector dependence of the exchange contribution to the electron-gas response functions: An analytic derivation*, *Phys. Rev. B* **42**, 4940 (1990).
- [Fer28] E. Fermi, *Eine statistische Methode zur Bestimmung einiger Eigenschaften des Atoms und ihre Anwendung auf die Theorie des periodischen Systems der Elemente*, *Z. Phys.* **48**, 73 (1928).
- [FPV13] M. Franchini, P. H. T. Philipsen and L. Visscher, *The Becke Fuzzy Cells Integration Scheme in the Amsterdam Density Functional Program Suite*, *J. Comput. Chem.* **34**, 1819 (2013).
- [FPvLV14] M. Franchini, P. H. T. Philipsen, E. van Lenthe and L. Visscher, *Accurate Coulomb Potentials for Periodic and Molecular Systems through Density Fitting*, *J. Chem. Theory Comput.* **10**, 1994 (2014).
- [FS19] J. W. Furness and J. Sun, *Enhancing the efficiency of density functionals with an improved iso-orbital indicator*, *Phys. Rev. B* **99**, 041119 (2019).
- [GAP96] P. M. W. Gill, R. D. Adamson and J. A. Pople, *Coulomb-attenuated exchange energy density functionals*, *Mol. Phys.* **88**, 1005 (1996).
- [GB96] O. V. Gritsenko and E. J. Baerends, *Effect of molecular dissociation on the exchange-correlation Kohn-Sham potential*, *Phys. Rev. A* **54**, 1957 (1996).
- [GB01] O. V. Gritsenko and E. J. Baerends, *Orbital structure of the Kohn-Sham exchange potential and exchange kernel and the field-counteracting potential for molecules in an electric field*, *Phys. Rev. A* **64**, 042506 (2001).
- [GGB02] M. Grüning, O. V. Gritsenko and E. J. Baerends, *Exchange potential from the common energy denominator approximation for the Kohn-Sham Green's function: Application to (hyper)polarizabilities of molecular chains*, *J. Chem. Phys.* **116**, 6435 (2002).
- [GGB18] P. Gori-Giorgi and E. J. Baerends, *Asymptotic nodal planes in the electron density and the potential in the effective equation for the square root of the density*, *Eur. Phys. J. B* **91**, 160 (2018).
- [GGG95] X. Gonze, P. Ghosez and R. W. Godby, *Density-Polarization Functional Theory of the Response of a Periodic Insulating Solid to an Electric Field*, *Phys. Rev. Lett.* **74**, 4035 (1995).
- [GGG97a] P. Ghosez, X. Gonze and R. W. Godby, *Long-wavelength behavior of the exchange-correlation kernel in the Kohn-Sham theory of periodic systems*, *Phys. Rev. B* **56**, 12811 (1997).

- [GGG97b] X. Gonze, P. Ghosez and R. W. Godby, *Density-Functional Theory of Polar Insulators*, *Phys. Rev. Lett.* **78**, 294 (1997).
- [GGGB16] P. Gori-Giorgi, T. Gál and E. J. Baerends, *Asymptotic behaviour of the electron density and the Kohn–Sham potential in case of a Kohn–Sham HOMO nodal plane*, *Mol. Phys.* **114**, 1086 (2016).
- [GHAK18] J. Garhammer, F. Hofmann, R. Armiento and S. Kümmel, *On the challenge to improve the density response with unusual gradient approximations*, *Eur. Phys. J. B* **91**, 159 (2018).
- [GJL79] O. Gunnarsson, M. Jonson and B. I. Lundqvist, *Descriptions of exchange and correlation effects in inhomogeneous electron systems*, *Phys. Rev. B* **20**, 3136 (1979).
- [GL76] O. Gunnarsson and B. I. Lundqvist, *Exchange and correlation in atoms, molecules, and solids by the spin-density-functional formalism*, *Phys. Rev. B* **13**, 4274 (1976).
- [GL94] A. Görling and M. Levy, *Exact Kohn-Sham scheme based on perturbation theory*, *Phys. Rev. A* **50**, 196 (1994).
- [GP85] S. K. Ghosh and R. G. Parr, *Density-determined orthonormal orbital approach to atomic energy functionals*, *J. Chem. Phys.* **82**, 3307 (1985).
- [GS09] A. P. Gaiduk and V. N. Staroverov, *How to tell when a model Kohn–Sham potential is not a functional derivative*, *J. Chem. Phys.* **131**, 044107 (2009).
- [GSS86] R. W. Godby, M. Schlüter and L. J. Sham, *Accurate Exchange-Correlation Potential for Silicon and Its Discontinuity on Addition of an Electron*, *Phys. Rev. Lett.* **56**, 2415 (1986).
- [GSW02] B. Guo, J. Shen and Z. Wang, *Chebyshev rational spectral and pseudospectral methods on a semi-infinite interval*, *Int. J. Numer. Meth. Eng.* **53**, 65 (2002).
- [GvGSB00] O. V. Gritsenko, S. J. A. van Gisbergen, P. R. T. Schipper and E. J. Baerends, *Origin of the field-counteracting term of the Kohn-Sham exchange-correlation potential of molecular chains in an electric field*, *Phys. Rev. A* **62**, 012507 (2000).
- [GvLvLB95] O. Gritsenko, R. van Leeuwen, E. van Lenthe and E. J. Baerends, *Self-consistent approximation to the Kohn-Sham exchange potential*, *Phys. Rev. A* **51**, 1944 (1995).
- [Gö15] A. Görling, *Exchange-correlation potentials with proper discontinuities for physically meaningful Kohn-Sham eigenvalues and band structures*, *Phys. Rev. B* **91**, 245120 (2015).

- [HJS08] T. M. Henderson, B. G. Janesko and G. E. Scuseria, *Generalized gradient approximation model exchange holes for range-separated hybrids*, *J. Chem. Phys.* **128**, 194105 (2008).
- [HK64] P. Hohenberg and W. Kohn, *Inhomogeneous Electron Gas*, *Phys. Rev.* **136**, B864 (1964).
- [HK12] D. Hofmann and S. Kümmel, *Integer particle preference during charge transfer in Kohn-Sham theory*, *Phys. Rev. B* **86**, 201109 (2012).
- [HKSG17] M. J. P. Hodgson, E. Kraisler, A. Schild and E. K. U. Gross, *How Interatomic Steps in the Exact Kohn–Sham Potential Relate to Derivative Discontinuities of the Energy*, *J. Phys. Chem. Lett.* **8**, 5974 (2017).
- [HS89] M. K. Harbola and V. Sahni, *Quantum-Mechanical Interpretation of the Exchange-Correlation Potential of Kohn-Sham Density-Functional Theory*, *Phys. Rev. Lett.* **62**, 489 (1989).
- [HSE03] J. Heyd, G. E. Scuseria and M. Ernzerhof, *Hybrid functionals based on a screened Coulomb potential*, *J. Chem. Phys.* **118**, 8207 (2003).
- [Jan78] J. F. Janak, *Proof that $\partial E/\partial n_i = \varepsilon$ in density-functional theory*, *Phys. Rev. B* **18**, 7165 (1978).
- [Jan17] B. G. Janesko, *Reducing density-driven error without exact exchange*, *Phys. Chem. Chem. Phys.* **19**, 4793 (2017).
- [JMSCY08] E. R. Johnson, P. Mori-Sánchez, A. J. Cohen and W. Yang, *Delocalization errors in density functionals and implications for main-group thermochemistry*, *J. Chem. Phys.* **129**, 204112 (2008).
- [Jon15] R. O. Jones, *Density functional theory: Its origins, rise to prominence, and future*, *Rev. Mod. Phys.* **87**, 897 (2015).
- [JSARM⁺15] J. Jornet-Somoza, J. Alberdi-Rodríguez, B. F. Milne, X. Andrade, M. A. L. Marques, F. Nogueira, M. J. T. Oliveira, J. J. P. Stewart and A. Rubio, *Insights into colour-tuning of chlorophyll optical response in green plants*, *Phys. Chem. Chem. Phys.* **17**, 26599 (2015).
- [JSE03] J. Jaramillo, G. E. Scuseria and M. Ernzerhof, *Local hybrid functionals*, *J. Chem. Phys.* **118**, 1068 (2003).
- [KAK09] A. Karolewski, R. Armiento and S. Kümmel, *Polarizabilities of Polyacetylene from a Field-Counteracting Semilocal Functional*, *J. Chem. Theory Comput.* **5**, 712 (2009).

- [KAK13] A. Karolewski, R. Armiento and S. Kümmel, *Electronic excitations and the Becke-Johnson potential: The need for and the problem of transforming model potentials to functional derivatives*, *Phys. Rev. A* **88**, 052519 (2013).
- [KBY07] S.-H. Ke, H. U. Baranger and W. Yang, *Role of the exchange-correlation potential in ab initio electron transport calculations*, *J. Chem. Phys.* **126**, 201102 (2007).
- [KK06] S. Kümmel and L. Kronik, *Hyperpolarizabilities of molecular chains: A real-space approach*, *Comput. Mat. Sci.* **35**, 321 (2006).
- [KK08] S. Kümmel and L. Kronik, *Orbital-dependent density functionals: Theory and applications*, *Rev. Mod. Phys.* **80**, 3 (2008).
- [KK13] E. Kraisler and L. Kronik, *Piecewise Linearity of Approximate Density Functionals Revisited: Implications for Frontier Orbital Energies*, *Phys. Rev. Lett.* **110**, 126403 (2013).
- [KK18] A. Kaiser and S. Kümmel, *Revealing the field-counteracting term in the exact Kohn-Sham correlation potential*, *Phys. Rev. A* **98**, 052505 (2018).
- [KKG98] T. Kreibich, S. Kurth, T. Grabo and E. Gross, *Asymptotic Properties of the Optimized Effective Potential*, *Adv. Quantum Chem.* **33**, 31 (1998).
- [KKK13] A. Karolewski, L. Kronik and S. Kümmel, *Using optimally tuned range separated hybrid functionals in ground-state calculations: Consequences and caveats*, *J. Chem. Phys.* **138**, 204115 (2013).
- [KKM08] T. Körzdörfer, S. Kümmel and M. Mundt, *Self-interaction correction and the optimized effective potential*, *J. Chem. Phys.* **129**, 014110 (2008).
- [KKP04] S. Kümmel, L. Kronik and J. P. Perdew, *Electrical Response of Molecular Chains from Density Functional Theory*, *Phys. Rev. Lett.* **93**, 213002 (2004).
- [KLI92a] J. B. Krieger, Y. Li and G. J. Iafrate, *Construction and application of an accurate local spin-polarized Kohn-Sham potential with integer discontinuity: Exchange-only theory*, *Phys. Rev. A* **45**, 101 (1992).
- [KLI92b] J. B. Krieger, Y. Li and G. J. Iafrate, *Systematic approximations to the optimized effective potential: Application to orbital-density-functional theory*, *Phys. Rev. A* **46**, 5453 (1992).
- [KMK08] T. Körzdörfer, M. Mundt and S. Kümmel, *Electrical Response of Molecular Systems: The Power of Self-Interaction Corrected Kohn-Sham Theory*, *Phys. Rev. Lett.* **100**, 133004 (2008).

- [KMT⁺06] L. Kronik, A. Makmal, M. L. Tiago, M. M. G. Alemany, M. Jain, X. Huang, Y. Saad and J. R. Chelikowsky, *PARSEC – the pseudopotential algorithm for real-space electronic structure calculations: recent advances and novel applications to nano-structures*, *Phys. Status Solidi B* **243**, 1063 (2006).
- [KOER10] M. Kuisma, J. Ojanen, J. Enkovaara and T. T. Rantala, *Kohn-Sham potential with discontinuity for band gap materials*, *Phys. Rev. B* **82**, 115106 (2010).
- [Koh99] W. Kohn, *Nobel Lecture: Electronic structure of matter—wave functions and density functionals*, *Rev. Mod. Phys.* **71**, 1253 (1999).
- [KP03a] S. Kümmel and J. P. Perdew, *Optimized effective potential made simple: Orbital functionals, orbital shifts, and the exact Kohn-Sham exchange potential*, *Phys. Rev. B* **68**, 035103 (2003).
- [KP03b] S. Kümmel and J. P. Perdew, *Simple Iterative Construction of the Optimized Effective Potential for Orbital Functionals, Including Exact Exchange*, *Phys. Rev. Lett.* **90**, 043004 (2003).
- [KP03c] S. Kümmel and J. P. Perdew, *Two avenues to self-interaction correction within Kohn—Sham theory: unitary invariance is the shortcut*, *Mol. Phys.* **101**, 1363 (2003).
- [KPB99] S. Kurth, J. P. Perdew and P. Blaha, *Molecular and solid-state tests of density functional approximations: LSD, GGAs, and meta-GGAs*, *Int. J. Quantum Chem.* **75**, 889 (1999).
- [KRM94] D. R. Kanis, M. A. Ratner and T. J. Marks, *Design and construction of molecular assemblies with large second-order optical nonlinearities. Quantum chemical aspects*, *Chem. Rev.* **94**, 195 (1994).
- [KS65] W. Kohn and L. J. Sham, *Self-Consistent Equations Including Exchange and Correlation Effects*, *Phys. Rev.* **140**, A1133 (1965).
- [KSPS08] A. V. Krukau, G. E. Scuseria, J. P. Perdew and A. Savin, *Hybrid functionals with local range separation*, *J. Chem. Phys.* **129**, 124103 (2008).
- [KSRAB12] L. Kronik, T. Stein, S. Refaely-Abramson and R. Baer, *Excitation Gaps of Finite-Sized Systems from Optimally Tuned Range-Separated Hybrid Functionals*, *J. Chem. Theory Comput.* **8**, 1515 (2012).
- [KSSB11] T. Körzdörfer, J. S. Sears, C. Sutton and J.-L. Brédas, *Long-range corrected hybrid functionals for π -conjugated systems: Dependence of the range-separation parameter on conjugation length*, *J. Chem. Phys.* **135**, 204107 (2011).
- [KTB12] D. Koller, F. Tran and P. Blaha, *Improving the modified Becke-Johnson exchange potential*, *Phys. Rev. B* **85**, 155109 (2012).

- [Kü17] S. Kümmel, *Charge-Transfer Excitations: A Challenge for Time-Dependent Density Functional Theory That Has Been Met*, *Adv. Energy Mater.* **7**, 1700440 (2017).
- [LA16] A. Lindmaa and R. Armiento, *Energetics of the AK13 semilocal Kohn-Sham exchange energy functional*, *Phys. Rev. B* **94**, 155143 (2016).
- [LAZ95] A. I. Liechtenstein, V. I. Anisimov and J. Zaanen, *Density-functional theory and strong interactions: Orbital ordering in Mott-Hubbard insulators*, *Phys. Rev. B* **52**, R5467 (1995).
- [Lev79] M. Levy, *Universal variational functionals of electron densities, first-order density matrices, and natural spin-orbitals and solution of the v-representability problem*, *Proc. Natl. Acad. Sci. USA* **76**, 6062 (1979).
- [Lev82] M. Levy, *Electron densities in search of Hamiltonians*, *Phys. Rev. A* **26**, 1200 (1982).
- [Lev91] M. Levy, *Density-functional exchange correlation through coordinate scaling in adiabatic connection and correlation hole*, *Phys. Rev. A* **43**, 4637 (1991).
- [LFB10] D. Lee, F. Furche and K. Burke, *Accuracy of Electron Affinities of Atoms in Approximate Density Functional Theory*, *J. Phys. Chem. Lett.* **1**, 2124 (2010).
- [Lie83] E. H. Lieb, *Density functionals for coulomb systems*, *Int. J. Quantum Chem.* **24**, 243 (1983).
- [LK05] M. Lein and S. Kümmel, *Exact Time-Dependent Exchange-Correlation Potentials for Strong-Field Electron Dynamics*, *Phys. Rev. Lett.* **94**, 143003 (2005).
- [LO81] E. H. Lieb and S. Oxford, *Improved lower bound on the indirect Coulomb energy*, *Int. J. Quantum Chem.* **19**, 427 (1981).
- [LP77] D. C. Langreth and J. P. Perdew, *Exchange-correlation energy of a metallic surface: Wave-vector analysis*, *Phys. Rev. B* **15**, 2884 (1977).
- [LP85] M. Levy and J. P. Perdew, *Hellmann-Feynman, virial, and scaling requisites for the exact universal density functionals. Shape of the correlation potential and diamagnetic susceptibility for atoms*, *Phys. Rev. A* **32**, 2010 (1985).
- [LSOM18] S. Lehtola, C. Steigemann, M. J. Oliveira and M. A. Marques, *Recent developments in libxc — A comprehensive library of functionals for density functional theory*, *SoftwareX* **7**, 1 (2018).
- [LSWS97] T. Leininger, H. Stoll, H.-J. Werner and A. Savin, *Combining long-range configuration interaction with short-range density functionals*, *Chem. Phys. Lett.* **275**, 151 (1997).

- [Mai05] N. T. Maitra, *Undoing static correlation: Long-range charge transfer in time-dependent density-functional theory*, *J. Chem. Phys.* **122**, 234104 (2005).
- [MBS⁺17] M. G. Medvedev, I. S. Bushmarinov, J. Sun, J. P. Perdew and K. A. Lyssenko, *Density functional theory is straying from the path toward the exact functional*, *Science* **355**, 49 (2017).
- [MK05] M. Mundt and S. Kümmel, *Derivative Discontinuities in Time-Dependent Density-Functional Theory*, *Phys. Rev. Lett.* **95**, 203004 (2005).
- [MKK09] A. Makmal, S. Kümmel and L. Kronik, *Fully Numerical All-Electron Solutions of the Optimized Effective Potential Equation for Diatomic Molecules*, *J. Chem. Theory Comput.* **5**, 1731 (2009).
- [MKK11] A. Makmal, S. Kümmel and L. Kronik, *Dissociation of diatomic molecules and the exact-exchange Kohn-Sham potential: The case of LiF*, *Phys. Rev. A* **83**, 062512 (2011).
- [MKvLR07] M. Mundt, S. Kümmel, R. van Leeuwen and P.-G. Reinhard, *Violation of the zero-force theorem in the time-dependent Krieger-Li-Iafrate approximation*, *Phys. Rev. A* **75**, 050501 (2007).
- [MSC18] P. Mori-Sánchez and A. J. Cohen, *Exact Density Functional Obtained via the Levy Constrained Search*, *J. Phys. Chem. Lett.* **9**, 4910 (2018).
- [MSCY06] P. Mori-Sánchez, A. J. Cohen and W. Yang, *Many-electron self-interaction error in approximate density functionals*, *J. Chem. Phys.* **125**, 201102 (2006).
- [MSCY08] P. Mori-Sánchez, A. J. Cohen and W. Yang, *Localization and Delocalization Errors in Density Functional Theory and Implications for Band-Gap Prediction*, *Phys. Rev. Lett.* **100**, 146401 (2008).
- [MSGG12] A. Mirschink, M. Seidl and P. Gori-Giorgi, *Energy Densities in the Strong-Interaction Limit of Density Functional Theory*, *J. Chem. Theory Comput.* **8**, 3097 (2012).
- [MSWY03] P. Mori-Sánchez, Q. Wu and W. Yang, *Accurate polymer polarizabilities with exact exchange density-functional theory*, *J. Chem. Phys.* **119**, 11001 (2003).
- [MT06] N. T. Maitra and D. G. Tempel, *Long-range excitations in time-dependent density functional theory*, *J. Chem. Phys.* **125**, 184111 (2006).
- [MvF07] N. T. Maitra and M. van Faassen, *Improved exchange-correlation potential for polarizability and dissociation in density functional theory*, *J. Chem. Phys.* **126**, 191106 (2007).

- [NNH96] R. Neumann, R. H. Nobes and N. C. Handy, *Exchange functionals and potentials*, *Mol. Phys.* **87**, 1 (1996).
- [NS18] K. Nakano and T. Sakai, *Assessing the performance of the Tran–Blaha modified Becke–Johnson exchange potential for optical constants of semiconductors in the ultraviolet–visible light region*, *J. Appl. Phys.* **123**, 015104 (2018).
- [NV11] V. U. Nazarov and G. Vignale, *Optics of Semiconductors from Meta-Generalized-Gradient-Approximation-Based Time-Dependent Density-Functional Theory*, *Phys. Rev. Lett.* **107**, 216402 (2011).
- [OC07] M. M. Odashima and K. Capelle, *How tight is the Lieb-Oxford bound?*, *J. Chem. Phys.* **127**, 054106 (2007).
- [OP79] G. L. Oliver and J. P. Perdew, *Spin-density gradient expansion for the kinetic energy*, *Phys. Rev. A* **20**, 397 (1979).
- [PBE96] J. P. Perdew, K. Burke and M. Ernzerhof, *Generalized Gradient Approximation Made Simple*, *Phys. Rev. Lett.* **77**, 3865 (1996).
- [PBKE14] J. Přecechtělová, H. Bahmann, M. Kaupp and M. Ernzerhof, *Communication: A non-empirical correlation factor model for the exchange-correlation energy*, *J. Chem. Phys.* **141**, 111102 (2014).
- [PBW96] J. P. Perdew, K. Burke and Y. Wang, *Generalized gradient approximation for the exchange-correlation hole of a many-electron system*, *Phys. Rev. B* **54**, 16533 (1996).
- [PEB96] J. P. Perdew, M. Ernzerhof and K. Burke, *Rationale for mixing exact exchange with density functional approximations*, *J. Chem. Phys.* **105**, 9982 (1996).
- [Per79] J. Perdew, *Orbital functional for exchange and correlation: self-interaction correction to the local density approximation*, *Chem. Phys. Lett.* **64**, 127 (1979).
- [Per85] J. P. Perdew, *Accurate Density Functional for the Energy: Real-Space Cutoff of the Gradient Expansion for the Exchange Hole*, *Phys. Rev. Lett.* **55**, 1665 (1985).
- [Per90] J. P. Perdew, *Size-Consistency, Self-Interaction Correction, and Derivative Discontinuity in Density Functional Theory*, in *Density Functional Theory of Many-Fermion Systems*, edited by P.-O. Löwdin, volume 21 of *Advances in Quantum Chemistry*, pp. 113 – 134, Academic Press, 1990.
- [PK03] J. P. Perdew and S. Kurth, *Density Functionals for Non-relativistic Coulomb Systems in the New Century*, in *A Primer in Density Functional Theory*, edited by C. Fiolhais, F. Nogueira and M. A. Marques, pp. 1–55, Springer-Verlag, Berlin Heidelberg, 2003.

- [PKZB99] J. P. Perdew, S. Kurth, A. c. v. Zupan and P. Blaha, *Accurate Density Functional with Correct Formal Properties: A Step Beyond the Generalized Gradient Approximation*, [Phys. Rev. Lett.](#) **82**, 2544 (1999).
- [PL83] J. P. Perdew and M. Levy, *Physical Content of the Exact Kohn-Sham Orbital Energies: Band Gaps and Derivative Discontinuities*, [Phys. Rev. Lett.](#) **51**, 1884 (1983).
- [PPBKE15] J. Pavlíková Přecechtělová, H. Bahmann, M. Kaupp and M. Ernzerhof, *Design of exchange-correlation functionals through the correlation factor approach*, [J. Chem. Phys.](#) **143**, 144102 (2015).
- [PPLB82] J. P. Perdew, R. G. Parr, M. Levy and J. L. Balduz, *Density-Functional Theory for Fractional Particle Number: Derivative Discontinuities of the Energy*, [Phys. Rev. Lett.](#) **49**, 1691 (1982).
- [PR18] J. P. Perdew and A. Ruzsinszky, *Density-functional energy gaps of solids demystified*, [Eur. Phys. J. B](#) **91**, 108 (2018).
- [PRSB14] J. P. Perdew, A. Ruzsinszky, J. Sun and K. Burke, *Gedanken densities and exact constraints in density functional theory*, [J. Chem. Phys.](#) **140**, 18A533 (2014).
- [PS01] J. P. Perdew and K. Schmidt, *Jacob's ladder of density functional approximations for the exchange-correlation energy*, [AIP Conf. Proc.](#) **577**, 1 (2001).
- [PSB08] C. D. Pemmaraju, S. Sanvito and K. Burke, *Polarizability of molecular chains: A self-interaction correction approach*, [Phys. Rev. B](#) **77**, 121204 (2008).
- [PSHP86] J. P. Perdew, V. Sahni, M. K. Harbola and R. K. Pathak, *Fourth-order gradient expansion of the fermion kinetic energy: Extra terms for nonanalytic densities*, [Phys. Rev. B](#) **34**, 686 (1986).
- [PSTS08] J. P. Perdew, V. N. Staroverov, J. Tao and G. E. Scuseria, *Density functional with full exact exchange, balanced nonlocality of correlation, and constraint satisfaction*, [Phys. Rev. A](#) **78**, 052513 (2008).
- [PTVF92] W. H. Press, S. A. Teukolsky, W. T. Vetterling and B. P. Flannery, *Numerical Recipes*, Cambridge University Press, Cambridge, New York, 1992.
- [PW86] J. P. Perdew and Y. Wang, *Accurate and simple density functional for the electronic exchange energy: Generalized gradient approximation*, [Phys. Rev. B](#) **33**, 8800 (1986).
- [PW92a] J. P. Perdew and Y. Wang, *Accurate and simple analytic representation of the electron-gas correlation energy*, [Phys. Rev. B](#) **45**, 13244 (1992).

- [PW92b] J. P. Perdew and Y. Wang, *Pair-distribution function and its coupling-constant average for the spin-polarized electron gas*, *Phys. Rev. B* **46**, 12947 (1992).
- [PY89] R. G. Parr and W. Yang, *Density-Functional Theory of Atoms and Molecules*, International Series of Monographs on Chemistry, Vol. 16, Oxford University Press, New York, 1 edition, 1989.
- [PYB⁺17] J. P. Perdew, W. Yang, K. Burke, Z. Yang, E. K. U. Gross, M. Scheffler, G. E. Scuseria, T. M. Henderson, I. Y. Zhang, A. Ruzsinszky, H. Peng, J. Sun, E. Trushin and A. Görling, *Understanding band gaps of solids in generalized Kohn–Sham theory*, *Proc. Natl. Acad. Sci. USA* **114**, 2801 (2017).
- [PZ81] J. P. Perdew and A. Zunger, *Self-interaction correction to density-functional approximations for many-electron systems*, *Phys. Rev. B* **23**, 5048 (1981).
- [RABK11] S. Refaely-Abramson, R. Baer and L. Kronik, *Fundamental and excitation gaps in molecules of relevance for organic photovoltaics from an optimally tuned range-separated hybrid functional*, *Phys. Rev. B* **84**, 075144 (2011).
- [RCFB09] D. Rappoport, N. R. M. Crawford, F. Furche and K. Burke, *Approximate Density Functionals: Which Should I Choose?*, in *Encyclopedia of Inorganic Chemistry*, pp. 1–11, Wiley, 2009.
- [RG84] E. Runge and E. K. U. Gross, *Density-Functional Theory for Time-Dependent Systems*, *Phys. Rev. Lett.* **52**, 997 (1984).
- [RH08] M. A. Rohrdanz and J. M. Herbert, *Simultaneous benchmarking of ground- and excited-state properties with long-range-corrected density functional theory*, *J. Chem. Phys.* **129**, 034107 (2008).
- [RORO02] L. Reining, V. Olevano, A. Rubio and G. Onida, *Excitonic Effects in Solids Described by Time-Dependent Density-Functional Theory*, *Phys. Rev. Lett.* **88**, 066404 (2002).
- [RPC⁺06] A. Ruzsinszky, J. P. Perdew, G. I. Csonka, O. A. Vydrov and G. E. Scuseria, *Spurious fractional charge on dissociated atoms: Pervasive and resilient self-interaction error of common density functionals*, *J. Chem. Phys.* **125**, 194112 (2006).
- [RPC⁺07] A. Ruzsinszky, J. P. Perdew, G. I. Csonka, O. A. Vydrov and G. E. Scuseria, *Density functionals that are one- and two- are not always many-electron self-interaction-free, as shown for H₂⁺, He₂⁺, LiH⁺, and Ne₂⁺*, *J. Chem. Phys.* **126**, 104102 (2007).

- [RPC⁺08] A. Ruzsinszky, J. P. Perdew, G. I. Csonka, G. E. Scuseria and O. A. Vydrov, *Understanding and correcting the self-interaction error in the electrical response of hydrogen chains*, *Phys. Rev. A* **77**, 060502 (2008).
- [RPCP09] E. Räsänen, S. Pittalis, K. Capelle and C. R. Proetto, *Lower Bounds on the Exchange-Correlation Energy in Reduced Dimensions*, *Phys. Rev. Lett.* **102**, 206406 (2009).
- [RPP10] E. Räsänen, S. Pittalis and C. R. Proetto, *Universal correction for the Becke–Johnson exchange potential*, *J. Chem. Phys.* **132**, 044112 (2010).
- [RSXC12] A. Ruzsinszky, J. Sun, B. Xiao and G. I. Csonka, *A meta-GGA Made Free of the Order of Limits Anomaly*, *J. Chem. Theory Comput.* **8**, 2078 (2012).
- [Sav96] A. Savin, On degeneracy, near-degeneracy and density functional theory, in *Recent Developments and Applications of Modern Density Functional Theory*, edited by J. Seminario, volume 4 of *Theoretical and Computational Chemistry*, pp. 327–357, Elsevier, 1996.
- [Sav09] A. Savin, *Is size-consistency possible with density functional approximations?*, *Chem. Phys.* **356**, 91 (2009).
- [SCM] SCM, Theoretical Chemistry, Vrije Universiteit, Amsterdam, The Netherlands, BAND 2017.
- [SDCF94] P. J. Stephens, F. J. Devlin, C. F. Chabalowski and M. J. Frisch, *Ab Initio Calculation of Vibrational Absorption and Circular Dichroism Spectra Using Density Functional Force Fields*, *J. Chem. Phys.* **98**, 11623 (1994).
- [SEKB10] T. Stein, H. Eisenberg, L. Kronik and R. Baer, *Fundamental Gaps in Finite Systems from Eigenvalues of a Generalized Kohn-Sham Method*, *Phys. Rev. Lett.* **105**, 266802 (2010).
- [SF95] A. Savin and H.-J. Flad, *Density functionals for the Yukawa electron-electron interaction*, *Int. J. Quantum Chem.* **56**, 327 (1995).
- [SFG⁺19] I. Schelter, J. M. Foerster, A. T. Gardiner, A. W. Roszak, R. J. Cogdell, G. M. Ullmann, T. B. de Queiroz and S. Kümmel, *Assessing density functional theory in real-time and real-space as a tool for studying bacteriochlorophylls and the light-harvesting complex 2*, *J. Chem. Phys.* **151**, 134114 (2019).
- [SGP82] V. Sahni, J. Gruenebaum and J. P. Perdew, *Study of the density-gradient expansion for the exchange energy*, *Phys. Rev. B* **26**, 4371 (1982).
- [SGV⁺96] A. Seidl, A. Görling, P. Vogl, J. A. Majewski and M. Levy, *Generalized Kohn-Sham schemes and the band-gap problem*, *Phys. Rev. B* **53**, 3764 (1996).

- [SH53] R. T. Sharp and G. K. Horton, *A Variational Approach to the Unipotential Many-Electron Problem*, *Phys. Rev.* **90**, 317 (1953).
- [SHX⁺13] J. Sun, R. Haunschild, B. Xiao, I. W. Bulik, G. E. Scuseria and J. P. Perdew, *Semilocal and hybrid meta-generalized gradient approximations based on the understanding of the kinetic-energy-density dependence*, *J. Chem. Phys.* **138**, 044113 (2013).
- [SJF⁺92] A. Savin, O. Jepsen, J. Flad, O. K. Andersen, H. Preuss and H. G. von Schnering, *Electron Localization in Solid-State Structures of the Elements: the Diamond Structure*, *Angew. Chem., Int. Ed. Engl.* **31**, 187 (1992).
- [SK16] T. Schmidt and S. Kümmel, *One- and many-electron self-interaction error in local and global hybrid functionals*, *Phys. Rev. B* **93**, 165120 (2016).
- [SK18] I. Schelter and S. Kümmel, *Accurate Evaluation of Real-Time Density Functional Theory Providing Access to Challenging Electron Dynamics*, *J. Chem. Theory Comput.* **14**, 1910 (2018).
- [SKB09] T. Stein, L. Kronik and R. Baer, *Reliable Prediction of Charge Transfer Excitations in Molecular Complexes Using Time-Dependent Density Functional Theory*, *J. Am. Chem. Soc.* **131**, 2818 (2009).
- [SKKK14] T. Schmidt, E. Kraisler, L. Kronik and S. Kümmel, *One-electron self-interaction and the asymptotics of the Kohn–Sham potential: an impaired relation*, *Phys. Chem. Chem. Phys.* **16**, 14357 (2014).
- [SKM⁺14] T. Schmidt, E. Kraisler, A. Makmal, L. Kronik and S. Kümmel, *A self-interaction-free local hybrid functional: Accurate binding energies vis-à-vis accurate ionization potentials from Kohn-Sham eigenvalues*, *J. Chem. Phys.* **140**, 18A510 (2014).
- [Sla30] J. C. Slater, *Atomic Shielding Constants*, *Phys. Rev.* **36**, 57 (1930).
- [SNWF97] A. Savin, R. Nesper, S. Wengert and T. F. Fässler, *ELF: The Electron Localization Function*, *Angew. Chem., Int. Ed. Engl.* **36**, 1808 (1997).
- [SP08] E. Sagvolden and J. P. Perdew, *Discontinuity of the exchange-correlation potential: Support for assumptions used to find it*, *Phys. Rev. A* **77**, 012517 (2008).
- [SPR15] J. Sun, J. P. Perdew and A. Ruzsinszky, *Semilocal density functional obeying a strongly tightened bound for exchange*, *Proc. Natl. Acad. Sci. USA* **112**, 685 (2015).
- [SRP15] J. Sun, A. Ruzsinszky and J. P. Perdew, *Strongly Constrained and Appropriately Normed Semilocal Density Functional*, *Phys. Rev. Lett.* **115**, 036402 (2015).

- [SS83] L. J. Sham and M. Schlüter, *Density-Functional Theory of the Energy Gap*, *Phys. Rev. Lett.* **51**, 1888 (1983).
- [SS94] B. Silvi and A. Savin, *Classification of chemical bonds based on topological*, *Nature* **371**, 683 (1994).
- [SSB18] E. Sim, S. Song and K. Burke, *Quantifying Density Errors in DFT*, *J. Phys. Chem. Lett.* **9**, 6385 (2018).
- [Sun03] D. Sundholm, *A density-functional-theory study of bacteriochlorophyll b*, *Phys. Chem. Chem. Phys.* **5**, 4265 (2003).
- [SvB96] P. S. Svendsen and U. von Barth, *Gradient expansion of the exchange energy from second-order density response theory*, *Phys. Rev. B* **54**, 17402 (1996).
- [SXF⁺13] J. Sun, B. Xiao, Y. Fang, R. Haunschild, P. Hao, A. Ruzsinszky, G. I. Csonka, G. E. Scuseria and J. P. Perdew, *Density Functionals that Recognize Covalent, Metallic, and Weak Bonds*, *Phys. Rev. Lett.* **111**, 106401 (2013).
- [SXR12] J. Sun, B. Xiao and A. Ruzsinszky, *Communication: Effect of the orbital-overlap dependence in the meta generalized gradient approximation*, *J. Chem. Phys.* **137**, 051101 (2012).
- [TB09] F. Tran and P. Blaha, *Accurate Band Gaps of Semiconductors and Insulators with a Semilocal Exchange-Correlation Potential*, *Phys. Rev. Lett.* **102**, 226401 (2009).
- [TB17] F. Tran and P. Blaha, *Importance of the Kinetic Energy Density for Band Gap Calculations in Solids with Density Functional Theory*, *J. Phys. Chem. A* **121**, 3318 (2017).
- [TBBB16] F. Tran, P. Blaha, M. Betzinger and S. Blügel, *Approximations to the exact exchange potential: KLI versus semilocal*, *Phys. Rev. B* **94**, 165149 (2016).
- [TBLDH⁺19] B. Traoré, G. Boudier, W. Lafargue-Dit-Hauret, X. Rocquefelte, C. Katan, F. Tran and M. Kepenekian, *Efficient and accurate calculation of band gaps of halide perovskites with the Tran-Blaha modified Becke-Johnson potential*, *Phys. Rev. B* **99**, 035139 (2019).
- [TBS07] F. Tran, P. Blaha and K. Schwarz, *Band gap calculations with Becke-Johnson exchange potential*, *J. Phys. Condens. Matter* **19**, 196208 (2007).
- [TBS15] F. Tran, P. Blaha and K. Schwarz, *How Close Are the Slater and Becke-Roussel Potentials in Solids?*, *J. Chem. Theory Comput.* **11**, 4717 (2015).

- [TBS17] J. Tao, I. W. Bulik and G. E. Scuseria, *Semilocal exchange hole with an application to range-separated density functionals*, *Phys. Rev. B* **95**, 125115 (2017).
- [TCS04] J. Toulouse, F. Colonna and A. Savin, *Long-range–short-range separation of the electron-electron interaction in density-functional theory*, *Phys. Rev. A* **70**, 062505 (2004).
- [TEB18] F. Tran, S. Ehsan and P. Blaha, *Assessment of the GLLB-SC potential for solid-state properties and attempts for improvement*, *Phys. Rev. Materials* **2**, 023802 (2018).
- [TFBS05] C. Toher, A. Filippetti, S. Sanvito and K. Burke, *Self-Interaction Errors in Density-Functional Calculations of Electronic Transport*, *Phys. Rev. Lett.* **95**, 146402 (2005).
- [Tho27] L. H. Thomas, *The calculation of atomic fields*, *Math. Proc. Cam. Phil. Soc.* **23**, 542 (1927).
- [TM16] J. Tao and Y. Mo, *Accurate Semilocal Density Functional for Condensed-Matter Physics and Quantum Chemistry*, *Phys. Rev. Lett.* **117**, 073001 (2016).
- [Toz03] D. J. Tozer, *Relationship between long-range charge-transfer excitation energy error and integer discontinuity in Kohn–Sham theory*, *J. Chem. Phys.* **119**, 12697 (2003).
- [TPSS03] J. Tao, J. P. Perdew, V. N. Staroverov and G. E. Scuseria, *Climbing the Density Functional Ladder: Nonempirical Meta–Generalized Gradient Approximation Designed for Molecules and Solids*, *Phys. Rev. Lett.* **91**, 146401 (2003).
- [TS76] J. D. Talman and W. F. Shadwick, *Optimized effective atomic central potential*, *Phys. Rev. A* **14**, 36 (1976).
- [TSSP08] J. Tao, V. N. Staroverov, G. E. Scuseria and J. P. Perdew, *Exact-exchange energy density in the gauge of a semilocal density-functional approximation*, *Phys. Rev. A* **77**, 012509 (2008).
- [tVB91] G. te Velde and E. J. Baerends, *Precise density-functional method for periodic structures*, *Phys. Rev. B* **44**, 7888 (1991).
- [vBH72] U. von Barth and L. Hedin, *A local exchange-correlation potential for the spin polarized case. i*, *J. Phys. C: Solid State Phys.* **5**, 1629 (1972).
- [vFdBvL⁺02] M. van Faassen, P. L. de Boeij, R. van Leeuwen, J. A. Berger and J. G. Snijders, *Ultranonlocality in Time-Dependent Current-Density-Functional Theory: Application to Conjugated Polymers*, *Phys. Rev. Lett.* **88**, 186401 (2002).

- [vGSG⁺99] S. J. A. van Gisbergen, P. R. T. Schipper, O. V. Gritsenko, E. J. Baerends, J. G. Snijders, B. Champagne and B. Kirtman, *Electric Field Dependence of the Exchange-Correlation Potential in Molecular Chains*, *Phys. Rev. Lett.* **83**, 694 (1999).
- [VHKS06] O. A. Vydrov, J. Heyd, A. V. Krukau and G. E. Scuseria, *Importance of short-range versus long-range Hartree-Fock exchange for the performance of hybrid density functionals*, *J. Chem. Phys.* **125**, 074106 (2006).
- [vLB94] R. van Leeuwen and E. J. Baerends, *Exchange-correlation potential with correct asymptotic behavior*, *Phys. Rev. A* **49**, 2421 (1994).
- [vLB95] R. van Leeuwen and E. J. Baerends, *Energy expressions in density-functional theory using line integrals*, *Phys. Rev. A* **51**, 170 (1995).
- [vLGB95] R. van Leeuwen, O. Gritsenko and E. J. Baerends, *Step structure in the atomic Kohn-Sham potential*, *Z. Phys. D* **33**, 229 (1995).
- [VS06] O. A. Vydrov and G. E. Scuseria, *Assessment of a long-range corrected hybrid functional*, *J. Chem. Phys.* **125**, 234109 (2006).
- [VSNL⁺15] V. Vlček, G. Steinle-Neumann, L. Leppert, R. Armiento and S. Kümmel, *Improved ground-state electronic structure and optical dielectric constants with a semilocal exchange functional*, *Phys. Rev. B* **91**, 035107 (2015).
- [VWN80] S. H. Vosko, L. Wilk and M. Nusair, *Accurate spin-dependent electron liquid correlation energies for local spin density calculations: a critical analysis*, *Can. J. Phys.* **58**, 1200 (1980).
- [WAY03] Q. Wu, P. W. Ayers and W. Yang, *Density-functional theory calculations with correct long-range potentials*, *J. Chem. Phys.* **119**, 2978 (2003).
- [WB91] G. Wiesenekker and E. J. Baerends, *Quadratic integration over the three-dimensional Brillouin zone*, *J. Phys. Condens. Matter* **3**, 6721 (1991).
- [WNJ⁺17] A. Wasserman, J. Nafziger, K. Jiang, M.-C. Kim, E. Sim and K. Burke, *The Importance of Being Inconsistent*, *Annu. Rev. Phys. Chem.* **68**, 555 (2017).
- [WZE17] R. Wang, Y. Zhou and M. Ernzerhof, *Fourth-order series expansion of the exchange hole*, *Phys. Rev. A* **96**, 022502 (2017).
- [YPSP16] Z.-h. Yang, H. Peng, J. Sun and J. P. Perdew, *More realistic band gaps from meta-generalized gradient approximations: Only in a generalized Kohn-Sham scheme*, *Phys. Rev. B* **93**, 205205 (2016).

- [YTH04] T. Yanai, D. P. Tew and N. C. Handy, *A new hybrid exchange–correlation functional using the Coulomb-attenuating method (CAM-B3LYP)*, *Chem. Phys. Lett.* **393**, 51 (2004).
- [YZA00] W. Yang, Y. Zhang and P. W. Ayers, *Degenerate Ground States and a Fractional Number of Electrons in Density and Reduced Density Matrix Functional Theory*, *Phys. Rev. Lett.* **84**, 5172 (2000).
- [ZLG13] F. Zahariev, S. S. Leang and M. S. Gordon, *Functional derivatives of meta-generalized gradient approximation (meta-GGA) type exchange-correlation density functionals*, *J. Chem. Phys.* **138**, 244108 (2013).
- [ZT06] Y. Zhao and D. G. Truhlar, *A new local density functional for main-group thermochemistry, transition metal bonding, thermochemical kinetics, and noncovalent interactions*, *J. Chem. Phys.* **125**, 194101 (2006).
- [ZY98] Y. Zhang and W. Yang, *A challenge for density functionals: Self-interaction error increases for systems with a noninteger number of electrons*, *J. Chem. Phys.* **109**, 2604 (1998).

List of Publications

- Pub. 1** *Orbital nodal surfaces: Topological challenges for density functionals,*
Thilo Aschebrock, Rickard Armiento, Stephan Kümmel,
[Physical Review B **95**, 245118 \(2017\)](#)
- Pub. 2** *Challenges for semilocal density functionals with asymptotically
nonvanishing potentials,*
Thilo Aschebrock, Rickard Armiento, Stephan Kümmel,
[Physical Review B **96**, 075140 \(2017\)](#).
- Pub. 3** *Ultranonlocality and accurate band gaps from a meta-generalized gradient
approximation,*
Thilo Aschebrock and Stephan Kümmel,
[Physical Review Research **1**, 033082 \(2019\)](#).
- Pub. 4** *Exploring local range separation: The role of spin scaling and one-electron
self-interaction,*
Thilo Aschebrock and Stephan Kümmel,
[Journal of Chemical Physics **151**, 154108 \(2019\)](#).

Part II

Publications

Publication 1

Publ. 1

Orbital nodal surfaces: Topological challenges for density functionals

Physical Review B **95**, 245118 (2017)

Thilo Aschebrock,¹ Rickard Armineto,² Stephan Kümmel¹

¹Theoretical Physics IV, University of Bayreuth, 95440 Bayreuth, Germany

²Department of Physics, Chemistry and Biology (IFM), Linköping University, 58183 Linköping, Sweden

My contribution

I discovered the divergences in the vicinity of orbital nodal surfaces, developed the model system and math to quantify the divergences as presented in the paper. I began to gather these insights during my master's thesis [[Asc14](#)]. I implemented the relevant routines in PARSEC, performed all calculations, prepared all figures, and wrote the first draft of the manuscript.

Publ.1

Orbital nodal surfaces: Topological challenges for density functionalsThilo Aschebrock,¹ Rickard Armiento,² and Stephan Kümmel¹¹*Theoretical Physics IV, University of Bayreuth, D-95440 Bayreuth, Germany*²*Department of Physics, Chemistry and Biology (IFM), Linköping University, SE-58183 Linköping, Sweden*

(Received 22 December 2016; published 15 June 2017)

Nodal surfaces of orbitals, in particular of the highest occupied one, play a special role in Kohn-Sham density-functional theory. The exact Kohn-Sham exchange potential, for example, shows a protruding ridge along such nodal surfaces, leading to the counterintuitive feature of a potential that goes to different asymptotic limits in different directions. We show here that nodal surfaces can heavily affect the potential of semilocal density-functional approximations. For the functional derivatives of the Armiento-Kümmel (AK13) [Phys. Rev. Lett. **111**, 036402 (2013)] and Becke88 [Phys. Rev. A **38**, 3098 (1988)] energy functionals, i.e., the corresponding semilocal exchange potentials, as well as the Becke-Johnson [J. Chem. Phys. **124**, 221101 (2006)] and van Leeuwen-Baerends (LB94) [Phys. Rev. A **49**, 2421 (1994)] model potentials, we explicitly demonstrate exponential divergences in the vicinity of nodal surfaces. We further point out that many other semilocal potentials have similar features. Such divergences pose a challenge for the convergence of numerical solutions of the Kohn-Sham equations. We prove that for exchange functionals of the generalized gradient approximation (GGA) form, enforcing correct asymptotic behavior of the potential or energy density necessarily leads to irregular behavior on or near orbital nodal surfaces. We formulate constraints on the GGA exchange enhancement factor for avoiding such divergences.

DOI: [10.1103/PhysRevB.95.245118](https://doi.org/10.1103/PhysRevB.95.245118)**I. INTRODUCTION**

Kohn-Sham (KS) density-functional theory (DFT) [1,2] has become the method of choice for calculating the electronic structure of physical, chemical, and biological systems. This success is based on the favorable ratio of accuracy to computational cost that DFT offers, especially with semilocal approximations for the exchange-correlation (xc) energy $E_{xc}[n(\mathbf{r})]$. However, while the low computational cost of semilocal functionals has very much contributed to the success of DFT because it enables access to large systems of practical relevance, the functional derivatives of typical semilocal functionals, i.e., their corresponding xc potentials, miss important features of the exact xc potential, in particular discontinuities [3,4] and step structures [5–9] that are relevant, e.g., in charge-transfer situations [10–12] and ionization processes [5,13–16]. Many attempts have been made to incorporate some of the missing features into semilocal DFT [17–27]. In recent years, it was the Becke-Johnson (BJ) model potential [28] in particular that sparked interest in this respect [22,29–35]. Its key characteristic is to effectively mimic nonlocal exchange features in the asymptotic behavior of the potential by means of having a nonzero limiting value far away from a finite system. This key characteristic was later adopted for the Armiento-Kümmel 2013 energy functional (AK13) by two of the present authors [36]. While this asymptotic behavior of the xc potential has a variety of implications [37], one particularly striking consequence becomes most apparent in systems with nodal surfaces of the highest occupied (homo) KS orbital.

Such orbital nodal surfaces have emerged as a topic of particular interest in DFT in recent years. To be precise, by the term “nodal surface” we refer here to the situation in which the highest occupied KS orbital in the ground state of a finite system has a nodal surface that extends to infinity. The first observation that such nodal surfaces of the homo play a special role in KS theory came from studying the exact KS

exchange potential. It has been shown—first in the localized Hartree-Fock approximation [38,39] and then exactly via optimized effective potential (OEP) calculations [40,41]—that a pronounced “ridge” appears in the bare exchange potential along a nodal surface at intermediate distances. At large distances, it contracts exponentially to a set of zero measure. As visualization of this counterintuitive feature might be helpful for further discussion, we refer to Fig. 3 of Ref. [41] and to Fig. 3 of this article. It has been argued that such ridges are of practical relevance as they can significantly affect unoccupied KS orbitals and eigenvalues [38,39], i.e., quantities that are important in particular for time-dependent DFT calculations or perturbation theory methods.

However, the ridge feature has also sparked interest from a fundamental perspective. Along a ridge, the exact KS exchange potential asymptotically goes to a nonzero constant. In all other directions of space, it asymptotically falls off to zero. One may argue that no physical potential may go to different asymptotic limits in different directions of space, because this would allow us to build some sort of perpetual mobile: Consider an electron from the center of the system out to infinity along some direction that does not coincide with the nodal surface, i.e., does not coincide with the ridge. Common sense tells us that independent of the shape of the potential, there cannot be any interaction between the electron and the system when the electron is at infinity, so at infinity the electron can be moved at zero energy cost to any point, e.g., a point on the nodal surface and thus to the top of the ridge. Then bring the electron back into the center of the system right along the ridge. When the full cycle has been completed, the electron will have gained an amount of energy that is proportional to the height of the ridge “out of nothing.” Obviously this cannot be, so how can the KS exact exchange potential show such an “unphysical” feature? The gist of the matter is that the KS potential is not a physical potential, but a mathematical object defined as a functional derivative [46].

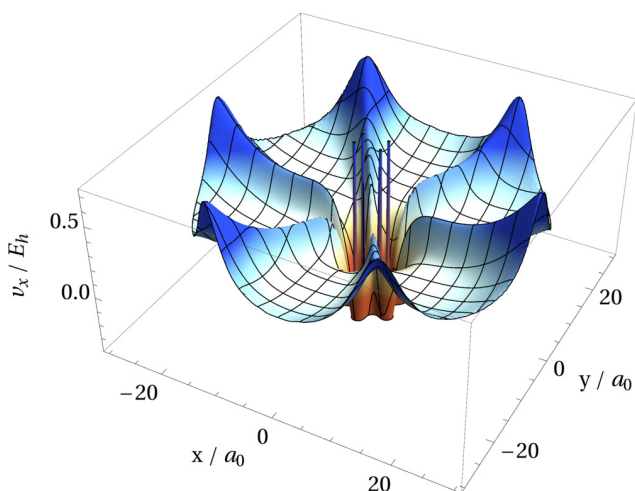


FIG. 1. Contour plot of the AK13 potential landscape of benzene in the plane of the molecule. The semilocal AK13 potential diverges exponentially along the three nodal planes. Due to serious numerical difficulties, which are intensified by the nodal surfaces issues, the AK13 potential could not be calculated self-consistently. For this plot, the AK13 potential was evaluated on a tightly converged self-consistent LDA valence density obtained from the Bayreuth version [42] of the PARSEC real-space code [43] with a sphere radius of $30a_0$ and a grid spacing of $0.3a_0$.

Therefore, one cannot move electrons (KS particles are not electrons) around in the KS potential and obviously cannot build an “exact exchange perpetual mobile.” Nevertheless, the question of whether the nonvanishing asymptotic constants and associated ridge structures are only a feature of bare exchange, or whether these signatures of nodal surfaces would prevail also in the total exchange-correlation potential, has been debated [47,48]. The discussion of nodal surfaces has gained further momentum through the recent discovery [49] that nodal surfaces can also lessen the significance of so-called “iso-orbital indicator” functionals that have been frequently

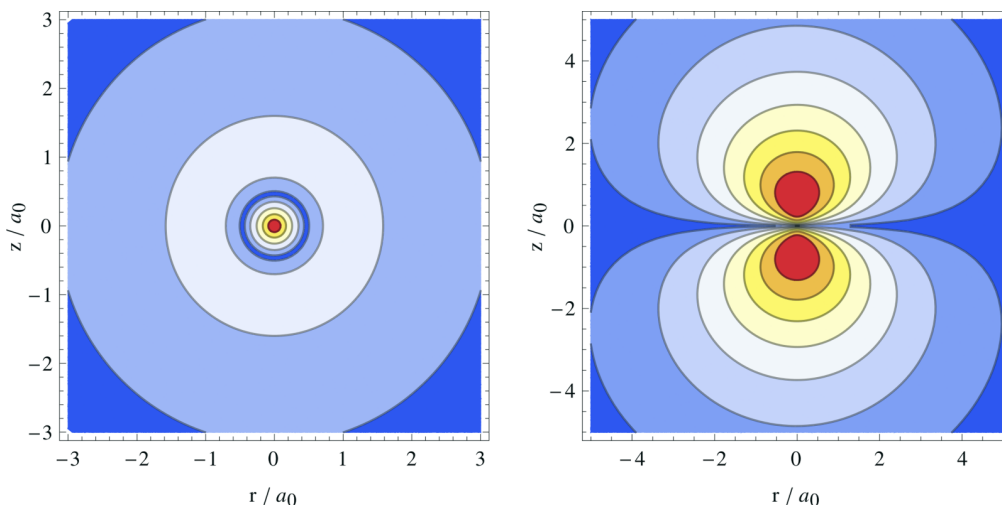


FIG. 2. Contour plots of the highest (right) and of the second highest occupied spin-up orbital densities (left) for the boron atom based on self-consistent LSDA all-electron calculations with the real-space grid program DARSEC [44,45]. While the homo-1 is of perfect spherical symmetry and exhibits a single radial node, the homo is a paradigm of a p_z orbital with its nodal plane at $z = 0$.

used, e.g., for the purpose of eliminating self-correlation errors.

One may wonder why nodal surfaces of an orbital can play such a special role in DFT, although a ground-state density itself does not have nodes [50]. The answer is that although the ground-state density is nodeless, it is nevertheless strongly affected by homo nodal surfaces. While the asymptotic density is governed by the homo in almost all of space, we discuss in this work that not all asymptotic properties of the density (such as certain partial derivatives) are determined solely by the homo in the vicinity of nodal surfaces. As a consequence, semilocal functionals that use derivative information can show unexpected and quite violent features in the vicinity of nodal surfaces. This is exemplified by Fig. 1, which shows the AK13 potential for benzene: The potential diverges exponentially in the vicinity of a nodal surface. We show in this paper that such an anomalous behavior is also found for the BJ exchange potential and even—though in somewhat weaker form—also for generalized gradient approximations (GGAs) with less strongly diverging enhancement factors than that of AK13. The most prominent example of such an affected GGA is the Becke 1988 exchange functional (B88) [51], which is the semilocal ingredient of the hybrid functional B3LYP [52,53]. As the latter is one of the most used density functionals for molecular systems, the relevance of the nodal surface features that we discuss here is apparent.

In addition to conceptual questions that a diverging potential raises, divergences at nodal surfaces can also severely hinder self-consistent calculations. This has far reaching consequences, because many systems of practical relevance, in particular organic molecules from a chemical and biological context, exhibit at least one and often even multiple nodal planes. Furthermore, simple systems can also show nodal planes. As a prime example, Fig. 2 visualizes the orbital structure of the boron atom with its noded p_z orbital. Similar features are seen in the density of many open-shell atoms. In first-principles electronic structure theory for finite systems, the occurrence of nodal surfaces is therefore the rule rather than the exception.

In this paper, we take a close look at the density in the vicinity of nodal surfaces, and we show how nodal surfaces can affect density functionals. Toward that end, we first introduce a minimal model of auxiliary orbitals that serves as a paradigm system with nodal planes. The model is then utilized to investigate the asymptotic behavior of the density, reduced density derivatives, and the kinetic energy density in the vicinity of nodal surfaces. Based on these findings, we study the exchange potentials of AK13 and B88, as well as the model potential of BJ and van Leeuwen and Baerends (LB94) [17], and we comment on several other functionals. We deliberately focus only on the exchange part in this analysis of approximate functionals, as the design criteria that led to irregular behavior in the vicinity of asymptotic nodal surfaces are specific to exchange. This is a consequence of the fact that the long-range part of the exact xc potential is dominated by exchange. Consequently, also approximate correlation potentials are typically constructed such that they vanish considerably faster than their exchange counterparts in the asymptotic region. Therefore, they are of little relevance in the present context. We conclude by discussing the implications of our findings. Hartree atomic units are used throughout.

II. MINIMAL NODAL SURFACE MODEL

In the following, we introduce a minimal model describing the simplest kind of nodal plane. The model is of general utility and inspired by the ground state of a neutral cluster of four sodium atoms [41]. It can be motivated equally well as a schematic variant of the boron-atom shown in Fig. 2. When the Na₄ cluster is described in the pseudopotential approximation [54,55], its two valence orbitals that are each occupied by two electrons are smooth and can be approximated by *s* and *p* orbitals, respectively. The energetically lower orbital is of *s* character, and for simplicity modeled by a 1*s* orbital. The highest occupied orbital is of *p* character and chosen to be described by a 2*p_z* orbital. Therefore, the nodal plane in our minimal model is given by the *x* – *y* plane and extends to infinity. Due to rotational symmetry with respect to the *z* axis, we chose cylindrical coordinates $\{r, z, \phi\}$. The density of the minimal model is thus given by

$$n(r, z) = 2n_s^0 \exp(-\alpha_s \sqrt{r^2 + z^2}) + 2n_p^0 z^2 \exp(-\alpha_p \sqrt{r^2 + z^2}), \quad (1)$$

where $n_s^0 = \alpha_s^3/8\pi$ and $n_p^0 = \alpha_p^5/32\pi$ for normalization. It is known that the exponential decay lengths α_s and α_p of the corresponding orbital contributions to the density are determined by their respective eigenvalues. All subsequent results are derived without explicit values for α_s and α_p , given that $\alpha_s > \alpha_p > 0$. Nonetheless, for the purpose of visualization we choose these free parameters inspired by the EXX eigenvalues of the cluster Na₄, given in Ref. [41], via $\alpha_s = 2\sqrt{-2\varepsilon_s} \approx 1.1873$ and $\alpha_p = 2\sqrt{-2\varepsilon_p} \approx 1.0587$, and thus we conclude our model.

The density is asymptotically dominated by the *p_z* orbital except in the neighborhood of the nodal plane (*z* = 0). In fact, for every distance to the nodal plane, *z* > 0, there exists a finite distance from the center of the molecule *r* such that $n(r, z)$ is

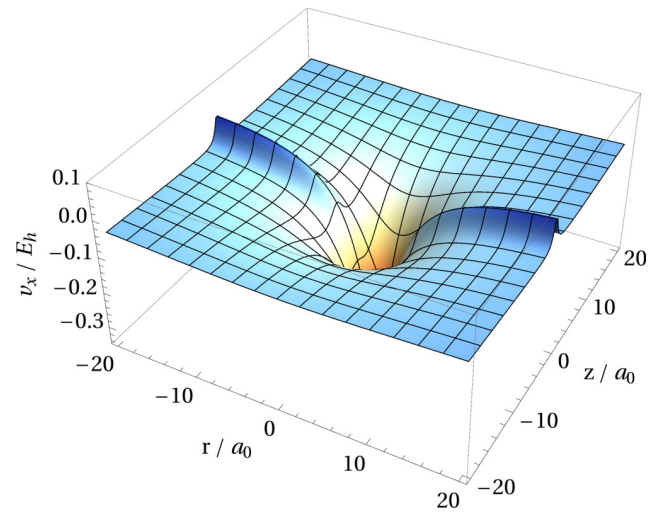


FIG. 3. EXX potential (shown in the KLI approximation [56]) evaluated in the minimal model of a nodal plane located at $z = 0$ using MATHEMATICA [57]. The characteristic pronounced “ridge” is visible in the potential along the nodal surface at intermediate distances. For large distances, the ridge contracts exponentially to the nodal plane—a set of zero measure.

arbitrarily accurately described by only its *p* component,

$$n_p(r, z) = 2n_p^0 z^2 \exp(-\alpha_p \sqrt{r^2 + z^2}). \quad (2)$$

This non-ground-state density, $n_p(r, z)$, will be referred to as the pure model of the nodal plane, as it features an actual node. In the limit $r \rightarrow \infty$ and except for a set of zero measure, given by the nodal plane itself, semilocal potentials are completely determined by this density of the pure model.

However, when considering a given finite value of *r*, the *s*-density part of the minimal model contributes noticeably in a small region of space that encloses the nodal plane. We will refer to this region as the transition region, as semilocal quantities in this region are typically determined by the interplay of contributions from both orbitals. In the limit $r \rightarrow \infty$, it contracts exponentially to a set of zero measure. Closely connected to this region is the behavior exactly on the nodal plane. While the *p* contribution to the density itself vanishes by construction on or along this plane, the *p* contribution to the Laplacian of the density, $\nabla^2 n$, remains finite and even dominates in the large-*r* limit, essentially explaining why some semilocal potentials with critical asymptotics diverge along nodal surfaces, as we will show below.

To showcase the capabilities of this minimal model of a nodal plane, we have plotted the EXX potential evaluated within this model in Fig. 3. For this purpose, the EXX potential is approximated by solving the KLI equation [56] for the fixed auxiliary orbitals of the minimal model. The clearly visible pronounced potential ridge along the nodal plane serves as verification of the model. The behavior of the EXX potential in this figure will be utilized as a reference to the subsequent study of the exchange potentials of AK13, BJ, B88, and LB94.

III. RESULTS FOR THE ASYMPTOTICS OF SEMILOCAL FUNCTIONAL EXPRESSIONS

Before examining the full expressions of semilocal potentials, we will use the minimal model to study the asymptotics of a few semilocal ingredients appearing in such potentials. We begin from the common definitions of reduced spatial derivatives of the density,

$$s = \frac{|\nabla n|}{2\gamma n^{4/3}}, \quad t = \frac{\nabla^2 n}{4\gamma^2 n^{5/3}}, \quad u = \frac{\nabla n \cdot \nabla |\nabla n|}{8\gamma^3 n^3}, \quad (3)$$

where $\gamma = (3\pi^2)^{1/3}$, and the positive-defined kinetic energy density is

$$\tau = \frac{1}{2} \sum_i f_i |\nabla \phi_i|^2 \quad (4)$$

with f_i the occupation number of KS orbital i .

For an electron density $n(\mathbf{r})$ that decays regularly, i.e., governed by the highest occupied orbital in a spherical symmetric manner, one finds [58]

$$n(\mathbf{r}) \sim n_0 |\mathbf{r}|^q \exp(-\alpha |\mathbf{r}|) \quad \text{as } |\mathbf{r}| \rightarrow \infty, \quad (5)$$

where n_0 and q are system-dependent constants, and the decay parameter

$$\alpha = 2\sqrt{-2(\varepsilon_{\text{ho}} - v_{\text{xc}}^\infty)} \quad (6)$$

is determined by the homo eigenvalue ε_{ho} relative to the limiting value of the potential $v_{\text{xc}}^\infty = \lim_{|\mathbf{r}| \rightarrow \infty} v_{\text{xc}}(\mathbf{r})$.

For a density that decays isotropically according to Eq. (5), one finds that the following characteristic combinations of semilocal components approach nonzero limiting values:

$$\begin{aligned} \frac{u}{s^3} &\sim 1, & \frac{t}{s^2} &\sim 1 - \frac{2}{3} \frac{1}{\ln(s)}, \\ 2\gamma n^{1/3} s &\sim \alpha, & \frac{\tau}{n} &\sim \frac{\alpha^2}{8} \end{aligned} \quad (7)$$

as $|\mathbf{r}| \rightarrow \infty$.

However, when the density does not decay regularly, e.g., due to a nodal plane of the homo, the asymptotic behaviors of the quantities in Eq. (7) are different. Figures 4–7 show these quantities evaluated in the minimal model via cross sections perpendicular to the nodal plane for several distances from the molecular center r .

The behavior of $t/s^2 = n \nabla^2 n / |\nabla n|^2$ is shown in Fig. 4: Well outside of the nodal plane (for large z values) the semilocal ratio approximately approaches its spherical asymptotic limit, $t/s^2 \sim 1$. Exactly on the plane, t/s^2 fails to balance the exponential decay of the density, due to the finite p contribution to $\nabla^2 n$, and it diverges exponentially as $r \rightarrow \infty$. However, the transition region surrounding this divergence contracts to a set of zero measure in the same limit, leaving the behavior of the quantity t/s^2 given by the pure model of the nodal plane [cf. Eq. (2)], which can be summarized by the asymptotic relation

$$\frac{t}{s^2} \sim \frac{1}{2} + \left(\frac{1}{8} - \frac{1}{\alpha_p r} \right) \alpha_p^2 z^2 \quad (8)$$

as $z \rightarrow 0^+$. In summary, the quantity t/s^2 diverges exponentially along a nodal plane, but the region affected by the

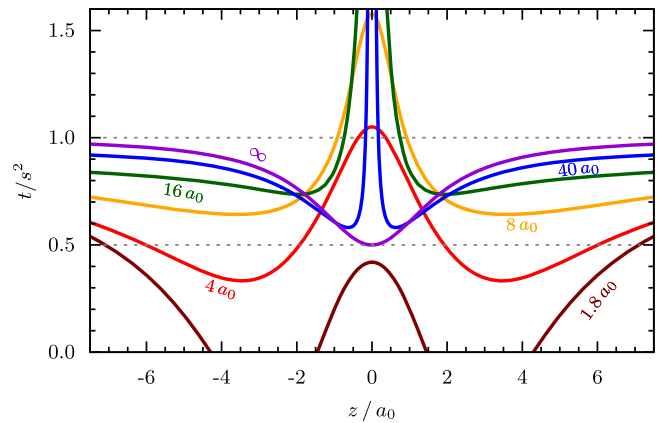


FIG. 4. Cross section of t/s^2 evaluated in the minimal model of a nodal plane ($z = 0$), cf. Eq. (1). Different lines correspond to different values of r as indicated by the subscripts.

divergence contracts to a set of zero measure leaving an almost everywhere finite limiting value. This value, however, differs considerably from its spherical symmetric limit in the vicinity of the nodal plane.

The ratio $u/s^3 = n \nabla n \cdot \nabla |\nabla n| / |\nabla n|^3$, shown in Fig. 5, behaves similar to t/s^2 : In the pure model, which is approached as $r \rightarrow \infty$ nearly everywhere, one obtains

$$\frac{u}{s^3} \sim \frac{1}{2} + \left(\frac{1}{4} - \frac{3}{4\alpha_p r} \right) \alpha_p^2 z^2 \quad (9)$$

as $z \rightarrow 0^+$, and likewise far outside the nodal plane u/s^3 approaches its ordinary spherical asymptotic limit, $u/s^3 \sim 1$. However, exactly on the nodal plane this ratio is given solely by the s contribution, thus u/s^3 converges to the spherical asymptotic limit instead of diverging. This limit is surrounded by a transition region, which features exponentially diverging elements but contracts to the nodal plane as $r \rightarrow \infty$.

So far all diverging contributions to semilocal potentials that we have examined contract to a set of zero measure in the limit $r \rightarrow \infty$, i.e., when evaluated in the pure model of the nodal plane. The quantity $2\gamma n^{1/3} s = |\nabla n|/n$, which is key to the construction of AK13, is different in this respect, as Fig. 6

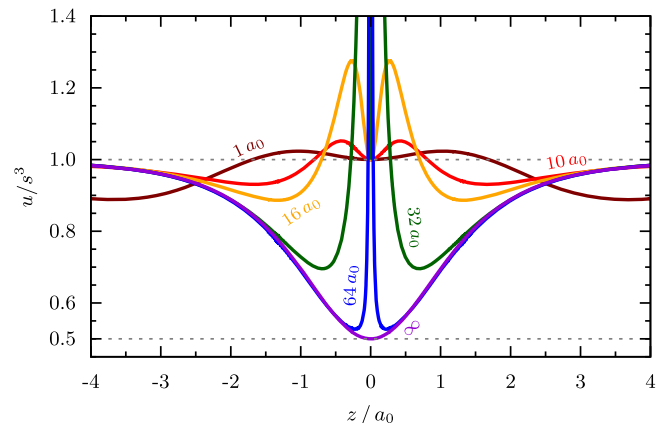


FIG. 5. Cross section of u/s^3 evaluated in the minimal model of a nodal plane.

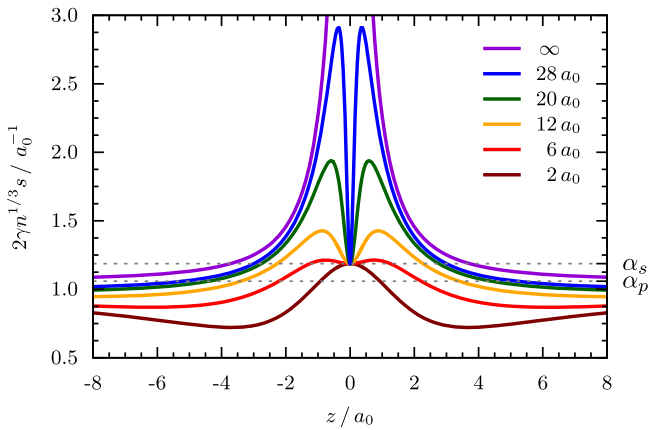


FIG. 6. Cross section of $2\gamma n^{1/3}s$ evaluated in the minimal model of a nodal plane.

demonstrates. Far from the nodal plane, i.e., for $|z| \rightarrow \infty$, $2\gamma n^{1/3}s$ approaches the system-dependent constant α_p , which is given by the homo as expected by Eq. (7). Once more, exactly on the nodal plane the quantity is solely determined by the s contribution and therefore approaches α_s , the analogous constant of the underlying s orbital. As the neighborhood affected by this limit contracts to the nodal plane as $r \rightarrow \infty$, the semilocal ratio approaches its behavior on the pure nodal plane, which is given by

$$2\gamma n^{1/3}s \sim \frac{2}{z} + \left(\frac{1}{4} - \frac{1}{\alpha_p r}\right) \alpha_p^2 z^2 \quad (10)$$

as $z \rightarrow 0^+$. Hence, unlike t/s^2 or u/s^3 , $2\gamma n^{1/3}s$ is not almost everywhere smooth as $r \rightarrow \infty$, but it develops a pole of first order: its denominator n has a double root on the pure nodal plane, while its numerator $|\nabla n|$ exhibits only a single root. Therefore, even infinitely far outside of the molecule the region affected by the nodal plane maintains a finite width for this quantity.

Finally, the semilocal quantity $2\sqrt{2\tau/n}$, which is key to the BJ potential, is examined. It is shown in Fig. 7. The kinetic energy density, τ , is constructed in analogy to the density of

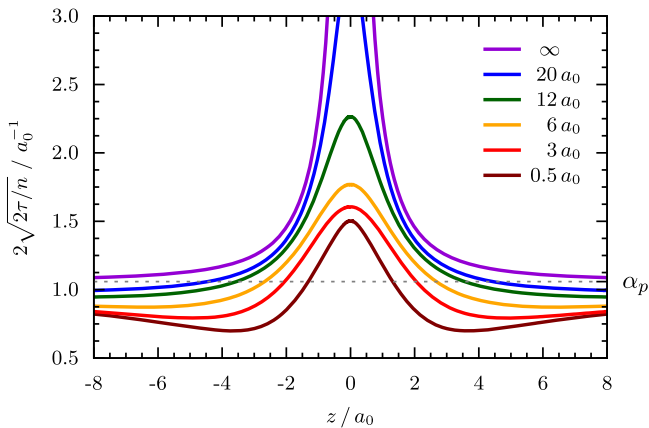


FIG. 7. Cross section of $2\sqrt{2\tau/n}$ evaluated in the minimal model of a nodal plane.

Eq. (1) by evaluating Eq. (4) with the orbitals of the minimal model. Since the prefactor is chosen such that the quantity approaches the same spherical symmetric limit as $2\gamma n^{1/3}s$, the behavior of $2\sqrt{2\tau/n}$ is similar to this quantity for $|z| \rightarrow \infty$ and the system-dependent constant α_p is likewise approached far outside the nodal surface. Exactly on the nodal plane, however, $2\sqrt{2\tau/n}$ does not approach the constant α_s , but it diverges exponentially along the plane, as the p contribution to τ does not vanish. Because the pure model, which is approached as $r \rightarrow \infty$ almost everywhere, is determined by a single orbital only, $2\sqrt{2\tau/n}$ equals $2\gamma n^{1/3}s$ strictly in this limit, as $\tau^W = |\nabla n|^2/8n$ is the single orbital limit of τ . Hence, on the pure nodal plane

$$2\sqrt{\frac{2\tau}{n}} \sim \frac{2}{z} + \left(\frac{1}{4} - \frac{1}{\alpha_p r}\right) \alpha_p^2 z^2 \quad (11)$$

as $z \rightarrow 0^+$, which features a pole of first order, implying once more a region of finite width affected by the nodal plane as $r \rightarrow \infty$. Further insight into the consequences that nodal surfaces have when τ is used as a part of an iso-orbital indicator, e.g., in the context of local hybrid functionals [59], is discussed in Ref. [49].

IV. RESULTS FOR THE ASYMPTOTICS OF SEMILOCAL POTENTIALS

We now evaluate the behavior of semilocal potentials in the vicinity of a nodal surface based on the minimal model. We focus on two aspects: First, we examine the behavior exactly along the nodal plane, which is described by the complete minimal model. While this gives insight into whether and how rapidly the potential diverges along the nodal plane, the affected region might be arbitrarily small and might contract with increasing distance from the center of the system r . Therefore, secondly, the pure model is used to classify the impact of the nodal surface on its neighborhood as $r \rightarrow \infty$.

A. The BJ potential functional in the vicinity of nodal surfaces

Various modifications of the BJ exchange potential functional are used quite frequently in the literature [29–35]. Therefore, we begin our application of the minimal model with the BJ expression. The BJ functional directly models the exchange potential as a sum of the Slater exchange potential [60] and a term expressed in the kinetic energy density,

$$v_x^{\text{BJ}} = v_x^{\text{Slater}} + C_{\Delta v} \sqrt{\frac{2\tau}{n}}, \quad (12)$$

where $C_{\Delta v} = \sqrt{5/12}/\pi$. As it is a potential functional, it has the major drawback that no corresponding exchange functional exists [24,61–63]. For a regular decaying density in the sense of Eq. (5), the correction term to the Slater potential approaches its characteristic positive asymptotic constant,

$$v_x^{\text{BJ}} \sim \frac{C_{\Delta v}}{2} \alpha, \quad (13)$$

as $|\mathbf{r}| \rightarrow \infty$.

Since the Slater potential vanishes $\propto -1/|\mathbf{r}|$ isotropically even in the presence of nodal surfaces, we can restrict the investigation to the correction term, which is proportional

to the semilocal quantity $2\sqrt{2\tau/n}$ of the last paragraph. Therefore, we can conclude that the BJ potential diverges exponentially along the nodal plane; insertion of the model density yields

$$v_x^{\text{BJ}}(r, z = 0) \sim C_{\Delta v} \sqrt{\frac{n_p^0}{n_s^0}} \exp[(\alpha_s - \alpha_p)r/2]. \quad (14)$$

Hence, the rate of the exponential divergence is given by the difference of the decay parameters of the homo, α_p , and that of the underlying orbital, α_s , which in turn are closely connected to the corresponding eigenvalues. A combination of Eq. (11) with the asymptotics of the Slater potential gives the behavior of the BJ potential in the vicinity of the pure nodal plane,

$$v_x^{\text{BJ}} \sim \frac{C_{\Delta v}}{z} - \frac{1}{r} + O(z^2) \quad (15)$$

as $z \rightarrow 0^+$. Therefore, the divergence of the BJ potential affects a finite region enclosing the nodal plane and does not contract to a set of zero measure as $r \rightarrow \infty$. A visualization of the asymptotic BJ potential in the vicinity of a nodal plane was essentially given in Fig. 7.

While it has already been noted in the original work that the BJ potentials diverges at orbital nodes, and should consequently be used with ground-state configurations only [28], our analysis aggravates these observations, as it shows them to be relevant for ground-state configurations as well.

B. AK13 in the vicinity of nodal surfaces

We now turn to the AK13 functional, which is based on the usual GGA form of the exchange energy,

$$E_x^{\text{GGA}} = A_x \int n^{4/3} F(s) d^3r. \quad (16)$$

In the case of AK13, the enhancement factor $F(s)$ is given by

$$F^{\text{AK13}}(s) = 1 + B_1 s \ln(1 + s) + B_2 s \ln[1 + \ln(1 + s)], \quad (17)$$

where the constants $B_1 = 2/27 + 8\pi/15$ and $B_2 = 4/81 - 8\pi/15$ have been determined in a nonempirical fashion. Its key feature is that its corresponding potential, i.e., the functional derivative of Eq. (16),

$$v_x^{\text{GGA}} = A_x \frac{4}{3} n^{1/3} \left[F(s) - s \partial_s F(s) + \frac{3}{4} \left(\frac{u}{s^3} - \frac{t}{s^2} \right) s \partial_s F(s) + \left(1 - \frac{3u}{4s^3} \right) s^2 \partial_s^2 F(s) \right], \quad (18)$$

typically approaches a positive system-dependent constant outside of a finite system. This novel GGA feature was inspired by the BJ exchange potential that we investigated in Sec. IV A. The asymptotic constant of the AK13 potential,

$$v_x^{\text{AK13}} \sim -\frac{A_x B_1}{6\gamma} \alpha \quad (19)$$

as $|\mathbf{r}| \rightarrow \infty$, follows formally from inserting the asymptotic relations for a regular decaying density, Eq. (7), together with the asymptotic enhancement factor of AK13 as $s \rightarrow \infty$ in

leading order,

$$F^{\text{AK13}}(s) \sim B_1 s \ln(s) + B_2 s \ln[\ln(s)]. \quad (20)$$

Hence, the asymptotic constant is related to the precise leading term in the divergent enhancement factor $F(s) \propto s \ln(s)$ as $s \rightarrow \infty$, which we will refer to as ‘‘critical asymptotic.’’ It is the threshold between asymptotic GGA potentials that are, for a regularly decaying density, vanishing and diverging in the limit $|\mathbf{r}| \rightarrow \infty$.

To discuss the behavior of a GGA potential in the vicinity of a nodal plane, Eq. (18) has to be examined in the limit $s \rightarrow \infty$ as well. The key difference is that one has to consider the altered relations of n , s , t , and u due to the presence of the nodal surface, which we have discussed in Sec. III. In particular, it was shown that the Laplacian contribution to the GGA potential is dominant exactly along the nodal plane. Therefore, the asymptotic of the GGA potential along the plane is given by

$$v_x^{\text{GGA}}(r, z = 0) \sim -A_x n^{1/3} \frac{t}{s} \partial_s F(s). \quad (21)$$

Inserting the asymptotic enhancement factor of AK13 as $s \rightarrow \infty$ in leading order given by Eq. (20), i.e., $\partial_s F^{\text{AK13}}(s) \sim B_1 \ln(s)$, and using the density of the minimal model, we find

$$v_x^{\text{AK13}}(r, z = 0) \sim -\frac{A_x B_1 r}{3\gamma} \left(\frac{n_p^0}{n_s^0} \right) \exp[(\alpha_s - \alpha_p)r]. \quad (22)$$

Thus, the AK13 potential diverges exponentially along nodal surfaces at twice the rate of the BJ potential; cf. Eq. (14).

To evaluate the behavior of the AK13 potential in the neighborhood of the nodal plane as $r \rightarrow \infty$, we use the pure minimal model: Inserting relations (8)–(10) into the asymptotic GGA potential, deduced from Eq. (18), yields

$$v_x^{\text{AK}} \sim -\frac{A_x B_1}{2} n^{1/3} s \sim -\frac{A_x B_1}{2\gamma} \frac{1}{z} \quad (23)$$

as $z \rightarrow 0^+$. Hence, far from the center of the molecule, the AK13 potential behaves similar to the BJ potential, i.e., as if it had a pole of first order on the nodal plane; even the amplitude of the pole is approximately of the same strength. Consequently, the region affected by the nodal plane has a fixed width and does not contract to a set of zero measure in the case of the AK13 potential, either. Figure 8 visualizes the AK13 potential in the vicinity of the nodal plane via cross sections.

In addition to the features that we just discussed, Fig. 8 demonstrates that local minima surrounding the nodal surface show up in the AK13 potential. To explain the mechanism behind them, we have to revisit the asymptotic GGA potential and note that the AK13 construction relies on the cancellation of the first-order terms, i.e., contribution to the potential $\propto s \ln(s)$. To achieve the cancellation, the asymptotic limits of t/s^2 and u/s^3 have to be equal, as they are in the spherical symmetric case and exactly on a pure nodal surface. However, for a fixed distance to the nodal surface $z > 0$ the limits of these semilocal ratios differ slightly as $r \rightarrow \infty$, as a comparison of the second-order terms in the asymptotic relations (8) and (9) readily demonstrates. Consequently, the leading-order terms

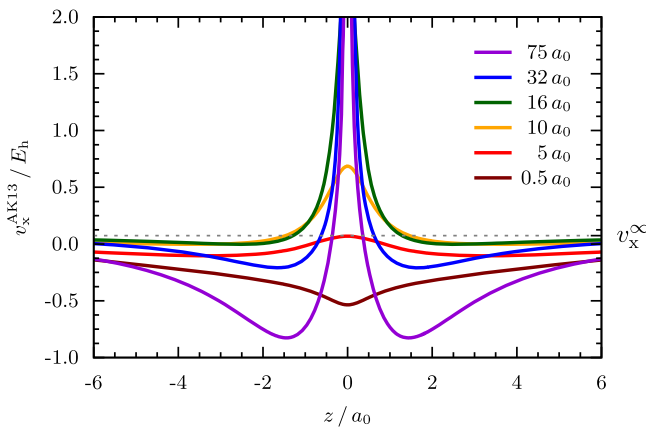


FIG. 8. Cross sections of the AK13 potential at different r values evaluated in the neighborhood of the nodal surface in the minimal model. Exactly at the nodal plane ($z=0$) the potential diverges exponentially as $r \rightarrow \infty$, being surrounded by an area where the potential behaves $\propto 1/z$. Given a finite r value, the potential approaches the constant v_x^∞ for $z \rightarrow \infty$. Additionally, with an increasing r value, local minima surrounding the nodal surface show up, as the potential diverges linearly in r toward negative infinity for every finite $z \neq 0$.

remain, i.e.,

$$v_x^{\text{AK13}} \sim \left[\lim_{r \rightarrow \infty} \left(\frac{u}{s^3} - \frac{t}{s^2} \right) \right] \frac{A_x B_1}{6\gamma} \alpha_p^2 r \quad (24)$$

as $r \rightarrow \infty$ for $z > 0$ fixed. This implies a linearly diverging potential. Hence, except for right on the nodal surface (a set of zero measure where the potential diverges exponentially to positive infinity), the AK13 potential approaches negative infinity linearly in r with a z -dependent slope. This results in a further amplification of the divergence. A nodal behavior very similar to the AK13 potential is to be expected of the potentials of exchange-enhanced GGAs [64] due to their usage of the same $s \ln(s)$ asymptotics.

C. B88 in the vicinity of nodal surfaces

Next, we turn to GGAs with enhancement factors $F(s) \ll s \ln(s)$ as $s \rightarrow \infty$, i.e., identified above as subcritical asymptotics. The potential of these GGAs will vanish with increasing distance from a finite spherically symmetric system. However, we will demonstrate that this condition is not sufficient to avoid the divergence of the corresponding potential along nodal surfaces. We discuss this issue with the widely used B88-GGA serving as an example. To reproduce the correct asymptotic behavior of the exact exchange-energy density, the B88 enhancement factor diverges slightly slower than that of AK13,

$$F^{\text{B88}}(s) \sim -\frac{\gamma}{3A_x} \frac{s}{\ln(s)} \quad (25)$$

as $s \rightarrow \infty$, causing the corresponding potential to vanish $\propto -1/|\mathbf{r}|^2$ [65] in the asymptotic region outside of nodal surfaces. Utilizing Eq. (21) and the minimal model gives the asymptotic

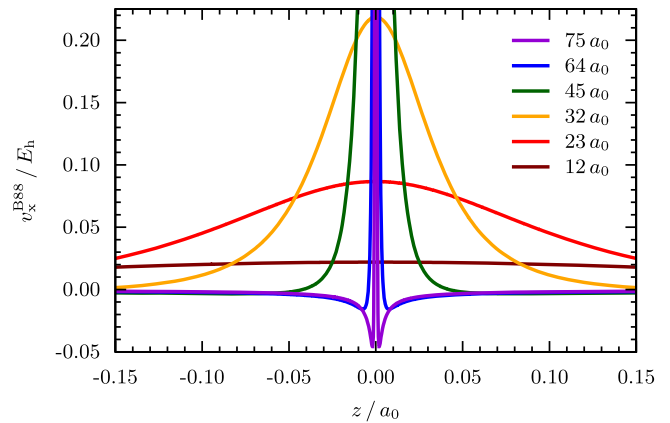


FIG. 9. Cross sections of the B88 potential at different r values evaluated in the immediate vicinity of the nodal surface in the minimal model. Exactly at the nodal plane ($z=0$) the potential diverges exponentially as $r \rightarrow \infty$, being surrounded by an area where the potential behaves $\propto -1/[z \ln^2(z)]$ (visible from $64a_0$ onward), which in turn contracts $\propto 1/r^2$ as $r \rightarrow \infty$.

behavior of the B88 potential along the nodal plane,

$$v_x^{\text{B88}}(r, z=0) \sim \frac{1}{\alpha_s^2 r} \left(\frac{n_p^0}{n_s^0} \right) \exp[(\alpha_s - \alpha_p)r] \quad (26)$$

as $r \rightarrow \infty$. Consequently, the B88 potential diverges slightly slower than the AK13 potential along nodal surfaces, while maintaining the same exponential rate, which is twice the rate of the BJ potential.

On the pure model and close to the nodal plane, the leading-order terms cancel and we find

$$v_x^{\text{B88}} \sim -\frac{\gamma}{6} \frac{n^{1/3} s}{\ln^2(s)} \quad (27)$$

as $s \rightarrow \infty$ and for $|z| \ll 1$. While the numerator $n^{1/3} s$ features a pole of first order in z [cf. Eq. (10)], the denominator is ambivalent, as, on the one hand,

$$\ln(s) \sim -\frac{5}{3} \ln(z) \quad (28)$$

as $z \rightarrow 0^+$ for fixed r , and, on the other hand,

$$\ln(s) \sim \alpha_p r / 3 \quad (29)$$

as $r \rightarrow \infty$ for fixed $z > 0$. Therefore, the B88 exchange potential exhibits a negative pole on the pure nodal surface,

$$v_x^{\text{B88}} \sim -\frac{3}{50} \frac{1}{z \ln^2(z)} \quad (30)$$

as $z \rightarrow 0^+$, but the region affected by the pole contracts, as for fixed $z > 0$ the quantity $n^{1/3} s$ approaches a constant as $r \rightarrow \infty$; cf. Fig. 6. Therefore, the potential vanishes,

$$v_x^{\text{B88}} \sim -\frac{3}{2} \gamma n^{1/3} s \frac{1}{\alpha_p^2 r^2} \quad (31)$$

as $r \rightarrow \infty$ for a fixed $z > 0$. All of these aspects are visualized in Fig. 9 by cross sections of the B88 potential in the immediate vicinity of the nodal plane.

The exchange parts of the AM05 functional [66] as well as QrevLB94 [67] are expected to be similar to B88 with respect to their nodal surface properties, because they share the asymptotic enhancement factor $\propto s / \ln(s)$ with B88.

D. LB94 potential functional in the vicinity of nodal surfaces

The final potential we wish to discuss in this context is the exchange model potential of van Leeuwen and Baerends (LB94) [17], as it also exhibits irregularities, but ones that are qualitative different from the ones of AK13, BJ, or B88. The LB94 model potential is designed as a semilocal correction to the exchange LDA potential based on n and s , with the aim to incorporate the correct $-1/|\mathbf{r}|$ asymptotic as well as an atomic-shell structure. In the asymptotic region, i.e., for $s \rightarrow \infty$, the LB94 model potential is generally described by the relation

$$v_x^{\text{LB94}} \sim -\frac{2\gamma}{3} \frac{n^{1/3}s}{\ln(s)} \quad (32)$$

even along or in the vicinity of nodal surfaces. Importantly, due to its model potential character, the LB94 potential does not depend on the Laplacian of the density, in contrast to GGA potentials that are functional derivatives. Consequently, the LB94 potential does not diverge exponentially exactly along a nodal plane, but vanishes there in Coulombic fashion $\propto -1/r$, and likewise in any other direction. Nevertheless, the LB94 potential features divergent behavior in a region enclosing the nodal plane. This can best be understood by using the pure minimal model, which gives the asymptotic relation

$$v_x^{\text{LB94}} \sim \frac{2}{5} \frac{1}{z \ln(z)} \quad (33)$$

as $z \rightarrow 0^+$, and it describes a negative pole of the LB94 potential on the pure nodal plane. In the full model, these poles translate into minima of the LB94 potential surrounding the nodal plane at intermediate distances. As $r \rightarrow \infty$, the depth of these minima grows without bounds as the position of the minima converges exponentially to the nodal plane. Yet, in the same limit the region affected by the minima contracts as the LB94 potential vanishes,

$$v_x^{\text{LB94}} \sim -2\gamma n^{1/3} s \frac{1}{\alpha_p r} \quad (34)$$

for a fixed $z > 0$. This follows from the same arguments as in the discussion of the B88 potential, i.e., for fixed $z > 0$ the quantity $n^{1/3}s$ approaches a constant while $\ln(s)$ shows a linear behavior in r . Figure 10 visualizes these findings for the LB94 potential, once more via cross sections in the vicinity of the nodal plane. We note that the nodal surface behavior of the model potentials of Lembarki *et al.* [68] can be expected to be similar to that of LB94.

E. Potential landscapes of semilocal potentials

For a final comparison of the behavior in response to nodal surfaces of all exchange potentials that were discussed in this article, we have plotted these potentials along the nodal plane of the minimal model in Fig. 11 and the landscapes of the potentials in Fig. 12. Figure 11 confirms the asymptotic relations of Eqs. (14), (22), and (26), while the EXX potential

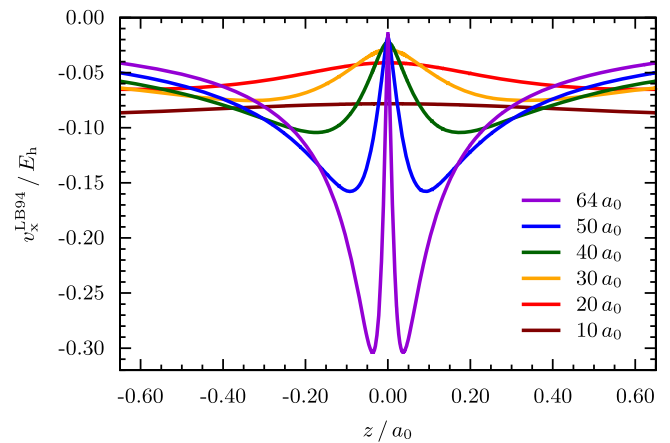


FIG. 10. Cross sections of the LB94 potential at different r values evaluated in the vicinity of the nodal surface in the minimal model. Exactly at the nodal plane ($z = 0$), the potential does not diverge but vanishes $\propto -1/r$, being surrounded by a divergent area where the potential behaves $\propto 1/[z \ln(z)]$, which in turn contracts $\propto 1/r$ as $r \rightarrow \infty$.

tends to a finite positive value in the same limit. Whereas the B88 potential diverges formally faster than the BJ potential, this is only relevant in the far asymptotic region, which is typically not part of numerical calculations.

Figure 12 displays the effect of the nodal plane on all four exchange potentials within the typical spatial range of a numerical calculation, and it should be compared to the EXX potential in Fig. 3. Aside from the (irregular) behavior exactly along the nodal plane, the landscapes demonstrate how the width of the affected region differs. In the case of EXX, the region affected by the nodal plane, i.e., the ridge, contracts exponentially with increasing distance from the center of the system. The closest to this ideal is the B88 potential, though the affected region contracts even faster. Therefore, the

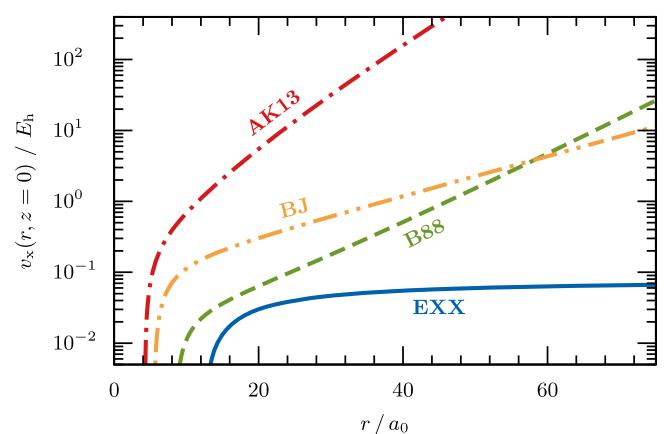


FIG. 11. Exchange potentials along the nodal surface of the homo ($z = 0$) in the minimal model. While the EXX potential [in the Krieger-Li-Iafrate (KLI) approximation [56]] reaches a positive constant, the AK13, B88, and the BJ potentials diverge exponentially as $r \rightarrow \infty$. The LB94 potential is not visible in this figure, as it behaves regularly exactly on the nodal plane and approaches zero from below.

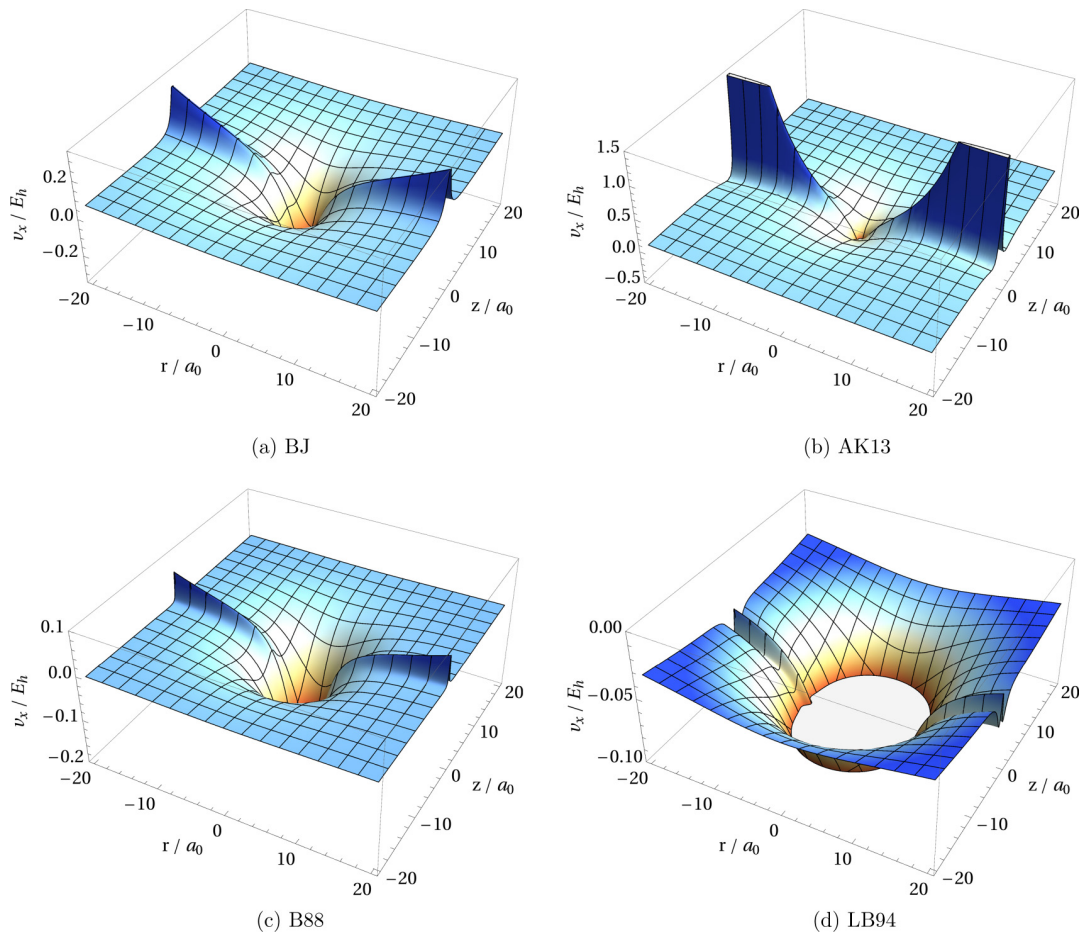


FIG. 12. Semilocal exchange potentials in the minimal model of a nodal plane located at $z = 0$. Note that the scale of the potential axis as well as the coloring visualizing the height of the potentials are not standardized. For a comparison to EXX, see Fig. 3. Except for LB94, all exchange potentials diverge exponentially along the nodal plane, though with different magnitude and width. All potentials were evaluated and plotted using MATHEMATICA [57].

numerical resolution of the B88 potential irregularity is highly questionable in practice, unless grid points exactly along the nodal plane are used. In the case of BJ, the region affected by the nodal plane is qualitatively different, as it does not contract but approaches a finite width as $r \rightarrow \infty$. The AK13 potential is similar in principle, though one could argue that in the case of AK13 the width is even expanding as minima surrounding the divergent region grow without limits. It is noteworthy that even though the GGA potentials of AK13 and B88 diverge along the nodal plane, their corresponding exchange energies per volume remain finite throughout.

V. FORMAL CONSTRAINTS FOR WELL-BEHAVED GGA POTENTIALS

The rate of divergence of a GGA potential for exchange along the nodal plane is determined by the leading power d of the asymptotic enhancement factor, $F(s) \propto s^d$ as $s \rightarrow \infty$ neglecting logarithmic contributions, i.e., $F(s) \sim C s^d \ln^c(s) \propto s^d$ regardless of the precise value of C and c ; consequently, in the case of AK13 and B88, $d = 1$. For more general enhancement factors, d may be defined via

$$d = \inf \{ b \in \mathbb{R} \mid \lim_{s \rightarrow \infty} F(s)/s^b = 0 \}. \quad (35)$$

Additionally, if $F(s)$ approaches a finite constant $F(\infty)$ as $s \rightarrow \infty$, one should replace $F(s)$ in the equations above by $[F(s) - F(\infty)]$, which then corresponds to a negative leading power $d < 0$.

One can show that in general

$$v_x^{\text{GGA}}(r, z = 0) \propto \exp \left[\left(\frac{2+d}{3} \alpha_s - \alpha_p \right) r \right] \quad (36)$$

based on Eq. (21) and the insight that $\nabla^2 n$ is in contrast to n and ∇n governed by the p orbital exactly along the nodal plane as $r \rightarrow \infty$ —a detailed derivation can be found in Appendix A. Thus, avoiding a divergence along a nodal surface requires

$$d \leq -2 + 3 \frac{\alpha_p}{\alpha_s} =: d_c, \quad (37)$$

or system-independently and therefore strictly formulated,

$$d \leq -2. \quad (38)$$

Consequently, $F(s) \sim C_1 + C_2/s^2$ as $s \rightarrow \infty$ is a sufficient condition to avoid a divergence along a nodal surface, while an asymptotic enhancement factor in the range $-2 < d < 1$ will diverge in some systems with a nodal surface, but not in all. Note that for exactly $d = 0$ without any logarithmic

contribution there is no divergence, because the proportionality constant in Eq. (36) vanishes trivially. The system-specific threshold value d_c depends on the difference between the highest and second highest occupied orbital eigenvalues. While a nearly degenerate situation corresponds to $d_c \approx 1$, the lower limit $d_c = -2$ is approached in the case of a weakly bound highest occupied orbital on top of a strongly bound second highest occupied orbital. The threshold of our minimal model is, for instance, $d_c \approx 0.775$ and thus describes a rather degenerate case.

Exchange GGAs that we therefore expect to show a system-dependent exponential divergence of the potential along the nodal planes are, e.g., PW86 [69] and B86b [70] with $d = 2/5$ as well as the Local Airy gas approximation (LAG) [71] with $d \approx 0.9$. Additionally, GGAs for exchange that are designed to satisfy the correct nonuniform coordinate scaling limit [72,73] via $F(s) \sim Cs^{-1/2}$ as suggested in Ref. [74] might in rare cases ($\alpha_s > 2\alpha_p$) lead to an exponential divergence of the corresponding potential along the nodal plane as well.

In addition to the exponential divergence along the nodal plane, irregular behavior in the neighborhood of the nodal plane has to be considered. To avoid this, i.e., a pole on the pure model of the nodal plane, the leading asymptotic power of the enhancement factor d , $F(s) \propto s^d$ as $s \rightarrow \infty$ neglecting logarithmic contributions, has to be in general less than or equal to $2/5$. This follows from Eq. (18), when using the asymptotic relations Eqs. (8) and (9) via

$$v_x^{\text{GGA}} \propto n^{1/3} s^d \propto z^{(2-5d)/3} \quad (39)$$

as $z \rightarrow 0^+$. As this requirement is naturally included in the constraint of Eq. (38), i.e., $d \leq -2$, the latter is sufficient to avoid any irregular behavior of a GGA potential in the vicinity of nodal surfaces. It follows from this argument that several widely used semilocal functionals for exchange are free of any irregular behavior in the vicinity of nodal surfaces, as they fulfill this sufficient condition. Among these are LDA, B86a [75], and PBE [76].

A rather far-reaching consequence of this analysis is that for the GGA exchange form, the design criteria of either a nonvanishing asymptotic constant in the potential or the correct asymptotic Coulombic behavior of the potential or of the energy density are all incompatible with the regular behavior of the potential in the vicinity of asymptotic nodal surfaces. The detailed line of arguments that leads to this conclusion is given in Appendix B.

VI. DISCUSSION

While many of the results of the previous sections were derived utilizing a model system, we expect them to be at least qualitatively transferable to true nodal surfaces of real molecules or atoms. Our reasoning is that the behavior of the density in the vicinity of an asymptotic nodal surface is universal in the sense that it essentially consists of two additive contributions. Both contributions vanish exponentially, but with different decay lengths. Whereas the slower decaying contribution is smooth and nodeless in the asymptotic region, the faster decaying contribution features a nodal surface, which is likely to be approximate harmonically in terms of the distance to the nodal surfaces. Since these conditions

are sufficient to derive all presented results to leading order and are satisfied by our minimal model, our results are of general relevance. For example, our arguments also apply to other nodal surfaces as, e.g., generated by higher spherical harmonics. In the latter case, all results will be maintained qualitatively, as well as quantitatively in leading order, when one measures the distance to a specific nodal surface by z , and the coordinate along the nodal surface by r . One may also specifically wonder how our arguments change if one replaces the p_z orbital in our model by the linear combination $p_x + ip_y$, changing the homo density into a torus. In this case, the nodal plane would reduce to a single line, the z axis. Yet, except for an interchange of r and z , the results and plots would look nearly indistinguishable to the ones that we present here. In addition to these arguments, the relevance of our findings is also evident from the divergences that are observed in real systems, as demonstrated, e.g., in Fig. 1 for the benzene molecule and the AK13 functional.

We observe that all functionals that we know of that incorporate in a semilocal fashion either a system-dependent asymptotic constant or the correct asymptotic Coulombic behavior of the potential or the energy density are affected by nodal surfaces issues—this list even includes Laplacian based meta-GGA constructions [19,77]. Additionally, we attempted to combine any of these asymptotic criteria with regular behavior on nodal surfaces in density functionals of rather general semilocal form—but without success so far. For the GGA exchange form in particular, such asymptotics are incompatible with a potential that behaves regularly in the vicinity of asymptotic nodal surfaces; cf. Appendix B. This is in line with the observation that commonly used semilocal functionals do not perform well when the exact xc hole is not localized around its electron. The hole-localization condition is radically violated in the asymptotic limit, where the electron is far out but its hole remains well inside the system. Therefore, the above-mentioned asymptotic features are very challenging design criteria for semilocal functionals.

The exponentially diverging semilocal exchange potentials of AK13, BJ, B88, and LB94 have several potentially unpleasant implications. Diverging potentials are suspicious from a conceptual perspective. Even though it was found that the EXX potential approaches a positive constant [38–41] in the direction of nodal surfaces, its implications and the behavior of the combined xc potential are still controversially discussed [47,48]. Adopting a positive perspective, one may interpret the divergences that we discuss here as a contribution to this discussion.

However, in terms of the practical application of these semilocal functionals, their irregular behavior is problematic. In particular, when the irregularities are confined to very narrow regions of space, such as, e.g., in the case of B88, a numerical representation in terms of some chosen basis set may not resolve the divergence. In this case, the numerical calculation may converge without problems. Strictly speaking, however, such a calculation has concealed a feature that is part of the proper functional derivative. On the other hand, choosing the numerical resolution such that it captures the divergence can have detrimental consequences: As a divergence of these potentials is generated in a semilocal fashion, small, normally insignificant changes of the density in the asymptotic region

close to a nodal surface can cause tremendous feedback on these potentials. Hence, in an iterative KS calculation, a positive feedback loop for irregularities and numerical instabilities can arise, impeding a self-consistent solution of the KS equations. We find this to be very much the case for our own attempts at converging AK13 results for systems with nodal surfaces, and also other authors have reported numerical problems with self-consistent calculations [78]. Furthermore, unusual oscillations in the AK13 potential have also been observed in the interstitial region of Si crystals [35], and these might be another consequence of the features that we discussed here for finite systems. Quite generally, one might speculate that similar issues could have influenced the convergence of some of the many published values obtained with B88- and BJ-based potential functionals.

VII. SUMMARY AND CONCLUSIONS

We have introduced and used a minimal model of general utility to examine exchange potentials along nodal surfaces of the highest occupied orbital. The model was used to investigate the corresponding potentials from the exchange-energy functionals AK13 and B88, as well as the BJ and LB94 model exchange potentials. We commented on several other functionals that are expected to have nodal surface properties in close similarity to these four paradigm cases. None of these potentials is well-behaved in the vicinity of a nodal surface, but rather they diverge exponentially. The AK13 functional has the most strongly divergent potential, which appears to prevent numerical convergence in practical calculations on molecular systems with nodal surfaces. The present work gives results and tools that should be useful for the investigation of other functional constructs, and for creating future expressions that avoid nodal surface anomalies. In particular, we derived a condition that is sufficient for avoiding nodal surface problems, and we pointed out that, e.g., LDA, B86a, and PBE fulfill this condition. Our results are relevant for the developers of density functionals, and also for users of DFT: Divergent potentials pose a challenge for the numerical convergence of solutions to the KS equations. Our work serves to caution that great care has to be taken in calculations with functionals that show special features close to nodal surfaces.

ACKNOWLEDGMENTS

S.K. and T.A. acknowledge financial support by the German-Israeli Foundation for Scientific Research and Development. T.A. acknowledges support by the University of Bayreuth Graduate School. R.A. acknowledges financial support from the Swedish Research Council (VR), Grant No. 2016-04810 and the Swedish e-Science Research Centre (SeRC). S.K. acknowledges a discussion with W. Kohn about the question of an “exact exchange perpetuum mobile.”

APPENDIX A: ASYMPTOTICS OF GGA POTENTIALS EXACTLY ALONG THE NODAL PLANE OF THE MINIMAL MODEL

Here we provide a detailed derivation of Eq. (36), i.e., rate of divergence for GGA potentials exactly along a nodal plane

of the minimal model: As we have demonstrated in Sec. III, the Laplacian of the density is the only ingredient of the GGA potential of Eq. (18) whose p contribution does not vanish exactly on the nodal plane and therefore dominates,

$$(\nabla^2 n)(r, z = 0) \sim (\nabla^2 n_p)(r, z = 0) \propto \exp(-\alpha_p r) \quad (\text{A1})$$

in the limit $r \rightarrow \infty$. On the contrary, the p contribution to n , ∇n , and $\nabla|\nabla n|$ vanishes at $z = 0$, thus their dominant behavior as $r \rightarrow \infty$ is determined by the exponential decay of the s orbital,

$$\begin{aligned} n(r, z = 0) &\propto (\nabla n)(r, z = 0) \propto (\nabla|\nabla n|)(r, z = 0) \\ &\propto n_s(r, z = 0) \propto \exp(-\alpha_s r). \end{aligned} \quad (\text{A2})$$

Because the exponential divergence of GGA potentials along nodal planes stems from the occurrence of these different decay lengths, it is given by Eq. (21),

$$v_x^{\text{GGA}}(r, z = 0) \sim -A_x n^{1/3} \frac{t}{s^2} s \partial_s F(s), \quad (\text{A3})$$

where we have to consider $F(s)$ in the limit $s \rightarrow \infty$, as this limit is approached for $r \rightarrow \infty$ on the nodal plane (just as in the spherically symmetric case for $|\mathbf{r}| \rightarrow \infty$). Now, we consider a general asymptotic enhancement factor in this limit,

$$F(s) \sim C s^d \ln^c(s), \quad (\text{A4})$$

where C , d , and c are arbitrary constants. Therefore,

$$v_x^{\text{GGA}}(r, z = 0) \sim -A_x C d n^{1/3} \frac{t}{s^2} s^d \ln^c(s). \quad (\text{A5})$$

Concerning the exponential divergence, we can neglect the prefactor and the logarithm as $\ln^c(s)$ is only polynomial in r . Inserting the definitions of s and t [cf. Eq. (3)] and using relations (A1) and (A2) gives the final result,

$$\begin{aligned} v_x^{\text{GGA}}(r, z = 0) &\propto n^{1/3} t s^{d-2} \\ &\propto n^{1/3-5/3-(d-2)4/3} (\nabla^2 n) |\nabla n|^{d-2} \\ &\propto n_s^{-(d+2)/3} n_p \propto \exp \left[\left(\frac{2+d}{3} \alpha_s - \alpha_p \right) r \right], \end{aligned} \quad (\text{A6})$$

which was presented in Eq. (36) and discussed thereupon.

APPENDIX B: INCOMPATIBILITY OF ASYMPTOTIC SEMILOCAL DESIGN CRITERIA WITH NODAL SURFACES

Under the assumption of a regularly decaying density in the sense of Eq. (5), one can connect a given asymptotic behavior of the corresponding potential, e.g., a nonvanishing asymptotic constant or the correct Coulombic $-1/|\mathbf{r}|$ asymptotic, to the asymptotic enhancement factor $F(s)$ of an exchange-only GGA. The connection is based on an asymptotic differential equation, which was derived in the supplemental material of Ref. [36] and determines $F(s)$ as $s \rightarrow \infty$ for a given asymptotic behavior of the corresponding potential,

$$F(s) - s \left(1 - \frac{1}{2 \ln(s)} \right) F'(s) + \frac{1}{4} s^2 F''(s) = v(s). \quad (\text{B1})$$

The source term on the right-hand side of this equation is uniquely determined by the asymptotic behavior of the

potential,

$$v(s) \sim \frac{3}{4A_x} \frac{v_x^{\text{GGA}}[n,s]}{n^{1/3}}, \quad (\text{B2})$$

as $s \rightarrow \infty$ via $|\mathbf{r}| \rightarrow \infty$. Therefore, a nonvanishing asymptotic constant corresponds to $v(s) \propto s$, and the correct Coulomb asymptotics corresponds to

$$v(s) = -\frac{\gamma}{2A_x} \frac{s}{\ln(s)}. \quad (\text{B3})$$

Thus, up to a linear combination of the two homogeneous solutions $h_1(s)$ and $h_2(s)$ of this differential equation, $F(s)$ is asymptotically uniquely determined by the behavior of the potential. To leading order, the homogeneous solutions are characterized by the relations

$$h_1(s) \sim s \ln^{2/3}(s) \quad (\text{B4})$$

and

$$h_2(s) \sim \frac{s^4}{\ln^{8/3}(s)} \quad (\text{B5})$$

as $s \rightarrow \infty$, i.e., in terms of Eq. (35) by $d = 1$ and 4. Therefore, both homogeneous solutions represent enhancement factors

that lead to irregular behavior in the vicinity of nodal surfaces. Consequently, if for a given potential asymptotic the particular solution [79] for $F(s)$ also exhibits nodal surfaces issues, then this specific potential asymptotic is (in the GGA exchange form) incompatible with a potential that behaves regularly in the vicinity of nodal surfaces. This is the case for the criteria of a nonvanishing asymptotic constant and of the correct Coulombic $-1/|\mathbf{r}|$ asymptotic of the potential, where the asymptotics of the particular solutions are $F(s) \sim B_1 s \ln(s)$ and $F(s) \sim -(\gamma/A_x)s$ as $s \rightarrow \infty$, correspondingly. The latter asymptotic is, e.g., used in a recent GGA of Carmona-Espíndola *et al.* [27].

Moreover, the correct asymptotic behavior of the exchange-energy density, $e_x(\mathbf{r}) \sim -n(\mathbf{r})/2|\mathbf{r}|$, is in the GGA form only realizable by the asymptotic enhancement factor

$$F(s) \sim -\frac{\gamma}{3A_x} \frac{s}{\ln(s)}, \quad (\text{B6})$$

as implemented in the B88-GGA. Therefore, we conclude based on Sec. IV C that this asymptotic-design criterion is also incompatible with regular behavior close to nodal surfaces.

-
- [1] P. Hohenberg and W. Kohn, *Phys. Rev.* **136**, B864 (1964).
 [2] W. Kohn and L. J. Sham, *Phys. Rev.* **140**, A1133 (1965).
 [3] J. P. Perdew, R. G. Parr, M. Levy, and J. L. Balduz, *Phys. Rev. Lett.* **49**, 1691 (1982).
 [4] M. Mundt and S. Kümmel, *Phys. Rev. Lett.* **95**, 203004 (2005).
 [5] M. Lein and S. Kümmel, *Phys. Rev. Lett.* **94**, 143003 (2005).
 [6] M. Hellgren and E. K. U. Gross, *Phys. Rev. A* **85**, 022514 (2012).
 [7] P. Elliott, J. I. Fuks, A. Rubio, and N. T. Maitra, *Phys. Rev. Lett.* **109**, 266404 (2012).
 [8] M. J. P. Hodgson, J. D. Ramsden, and R. W. Godby, *Phys. Rev. B* **93**, 155146 (2016).
 [9] T. Dimitrov, H. Appel, J. I. Fuks, and A. Rubio, *New J. Phys.* **18**, 083004 (2016).
 [10] D. J. Tozer, *J. Chem. Phys.* **119**, 12697 (2003).
 [11] S. Kümmel, L. Kronik, and J. P. Perdew, *Phys. Rev. Lett.* **93**, 213002 (2004).
 [12] D. Hofmann and S. Kümmel, *Phys. Rev. B* **86**, 201109 (2012).
 [13] F. Wilken and D. Bauer, *Phys. Rev. Lett.* **97**, 203001 (2006).
 [14] M. Thiele, E. K. U. Gross, and S. Kümmel, *Phys. Rev. Lett.* **100**, 153004 (2008).
 [15] S. R. Whittleton, X. A. S. Vazquez, C. M. Isborn, and E. R. Johnson, *J. Chem. Phys.* **142**, 184106 (2015).
 [16] N. L. Nguyen, G. Borghi, A. Ferretti, I. Dabo, and N. Marzari, *Phys. Rev. Lett.* **114**, 166405 (2015).
 [17] R. van Leeuwen and E. J. Baerends, *Phys. Rev. A* **49**, 2421 (1994).
 [18] A. D. Becke and M. R. Roussel, *Phys. Rev. A* **39**, 3761 (1989).
 [19] P. Jemmer and P. J. Knowles, *Phys. Rev. A* **51**, 3571 (1995).
 [20] E. Engel and S. H. Vosko, *Phys. Rev. B* **47**, 13164 (1993).
 [21] V. N. Staroverov, *J. Chem. Phys.* **129**, 134103 (2008).
 [22] R. Armiento, S. Kümmel, and T. Körzdörfer, *Phys. Rev. B* **77**, 165106 (2008).
 [23] A. P. Gaiduk and V. N. Staroverov, *J. Chem. Phys.* **128**, 204101 (2008).
 [24] A. Karolewski, R. Armiento, and S. Kümmel, *Phys. Rev. A* **88**, 052519 (2013).
 [25] F. Tran, P. Blaha, and K. Schwarz, *J. Chem. Theory Comput.* **11**, 4717 (2015).
 [26] F. Tran, P. Blaha, M. Betzinger, and S. Blügel, *Phys. Rev. B* **94**, 165149 (2016).
 [27] J. Carmona-Espíndola, J. L. Gázquez, A. Vela, and S. B. Trickey, *J. Chem. Phys.* **142**, 054105 (2015).
 [28] A. D. Becke and E. R. Johnson, *J. Chem. Phys.* **124**, 221101 (2006).
 [29] F. Tran and P. Blaha, *Phys. Rev. Lett.* **102**, 226401 (2009).
 [30] E. Räsänen, S. Pittalis, and C. R. Proetto, *J. Chem. Phys.* **132**, 044112 (2010).
 [31] D. Koller, F. Tran, and P. Blaha, *Phys. Rev. B* **85**, 155109 (2012).
 [32] F. Tran, P. Blaha, and K. Schwarz, *J. Phys.: Condens. Matter* **19**, 196208 (2007).
 [33] D. J. Singh, *Phys. Rev. B* **82**, 205102 (2010).
 [34] D. Koller, F. Tran, and P. Blaha, *Phys. Rev. B* **83**, 195134 (2011).
 [35] F. Tran, P. Blaha, M. Betzinger, and S. Blügel, *Phys. Rev. B* **91**, 165121 (2015).
 [36] R. Armiento and S. Kümmel, *Phys. Rev. Lett.* **111**, 036402 (2013).
 [37] T. Aschebrock, R. Armiento, and S. Kümmel (unpublished).
 [38] F. Della Sala and A. Görling, *J. Chem. Phys.* **116**, 5374 (2002).
 [39] F. Della Sala and A. Görling, *Phys. Rev. Lett.* **89**, 033003 (2002).
 [40] S. Kümmel and J. P. Perdew, *Phys. Rev. Lett.* **90**, 043004 (2003).
 [41] S. Kümmel and J. P. Perdew, *Phys. Rev. B* **68**, 035103 (2003).
 [42] M. Mundt, S. Kümmel, B. Huber, and M. Moseler, *Phys. Rev. B* **73**, 205407 (2006).
 [43] L. Kronik, A. Makmal, M. L. Tiago, M. M. G. Alemany, M. Jain, X. Huang, Y. Saad, and J. R. Chelikowsky, *Phys. Status Solidi B* **243**, 1063 (2006).
 [44] A. Makmal, S. Kümmel, and L. Kronik, *J. Chem. Theory Comput.* **5**, 1731 (2009).

- [45] A. Makmal, S. Kümmel, and L. Kronik, *J. Chem. Theory Comput.* **7**, 2665 (2011).
- [46] S. Kümmel and L. Kronik, *Rev. Mod. Phys.* **80**, 3 (2008).
- [47] Q. Wu, P. W. Ayers, and W. Yang, *J. Chem. Phys.* **119**, 2978 (2003).
- [48] P. Gori-Giorgi, T. Gál, and E. J. Baerends, *Mol. Phys.* **114**, 1086 (2016).
- [49] T. Schmidt, E. Kraisler, L. Kronik, and S. Kümmel, *Phys. Chem. Chem. Phys.* **16**, 14357 (2014).
- [50] One can argue that Ref. [58] shows that the ground-state density of a fermionic many-electron system can be mapped to the ground state of a bosonic system if one assumes that the effective potential of Ref. [58] is regular and does not introduce nodes. Under this condition, one can conclude that fermionic ground-state densities are nodeless due to fact that the ground-state wave function of any bosonic system is nodeless [80].
- [51] A. D. Becke, *Phys. Rev. A* **38**, 3098 (1988).
- [52] A. D. Becke, *J. Chem. Phys.* **98**, 5648 (1993).
- [53] F. J. Devlin, J. W. Finley, P. J. Stephens, and M. J. Frisch, *J. Phys. Chem.* **99**, 16883 (1995).
- [54] W. E. Pickett, *Comput. Phys. Rep.* **9**, 115 (1989).
- [55] J. R. Chelikowsky and M. L. Cohen, *Handbook on Semiconductors* (Elsevier, Amsterdam, 1992), p. 59.
- [56] J. B. Krieger, Y. Li, and G. J. Iafrate, *Phys. Rev. A* **46**, 5453 (1992).
- [57] Wolfram Research, Inc., MATHEMATICA 8.0 (2010).
- [58] M. Levy, J. P. Perdew, and V. Sahni, *Phys. Rev. A* **30**, 2745 (1984).
- [59] J. Jaramillo, G. E. Scuseria, and M. Ernzerhof, *J. Chem. Phys.* **118**, 1068 (2003).
- [60] J. C. Slater, *Phys. Rev.* **81**, 385 (1951).
- [61] A. P. Gaiduk and V. N. Staroverov, *J. Chem. Phys.* **131**, 044107 (2009).
- [62] A. Karolewski, R. Armiento, and S. Kümmel, *J. Chem. Theory Comput.* **5**, 712 (2009).
- [63] M. Mundt, S. Kümmel, R. van Leeuwen, and P.-G. Reinhard, *Phys. Rev. A* **75**, 050501(R) (2007).
- [64] S. L. Li and D. G. Truhlar, *J. Chem. Theory Comput.* **11**, 3123 (2015).
- [65] E. Engel, J. A. Chevary, L. D. Macdonald, and S. H. Vosko, *Z. Phys. D* **23**, 7 (1992).
- [66] R. Armiento and A. E. Mattsson, *Phys. Rev. B* **72**, 085108 (2005).
- [67] A. P. Gaiduk and V. N. Staroverov, *J. Chem. Phys.* **136**, 064116 (2012).
- [68] A. Lembarki, F. Rogemond, and H. Chermette, *Phys. Rev. A* **52**, 3704 (1995).
- [69] J. P. Perdew and Y. Wang, *Phys. Rev. B* **33**, 8800(R) (1986).
- [70] A. D. Becke, *J. Chem. Phys.* **85**, 7184 (1986).
- [71] L. Vitos, B. Johansson, J. Kollár, and H. L. Skriver, *Phys. Rev. B* **62**, 10046 (2000).
- [72] M. Levy, *Phys. Rev. A* **43**, 4637 (1991).
- [73] L. Pollack and J. P. Perdew, *J. Phys.: Condens. Matter* **12**, 1239 (2000).
- [74] J. P. Perdew, A. Ruzsinszky, J. Sun, and K. Burke, *J. Chem. Phys.* **140**, 18A533 (2014).
- [75] A. D. Becke, *J. Chem. Phys.* **84**, 4524 (1986).
- [76] J. P. Perdew, K. Burke, and M. Ernzerhof, *Phys. Rev. Lett.* **77**, 3865 (1996).
- [77] M. Filatov and W. Thiel, *Phys. Rev. A* **57**, 189 (1998).
- [78] T. F. T. Cerqueira, M. J. T. Oliveira, and M. A. L. Marques, *J. Chem. Theory Comput.* **10**, 5625 (2014).
- [79] Our reasoning here is that we are always looking at such particular solutions that are not asymptotically equivalent to either h_1 or h_2 . This can always be achieved because due to the linearity of the differential equation, homogenous contributions can be subtracted.
- [80] R. P. Feynman, *Statistical Mechanics: A Set of Lectures* (Addison-Wesley, New York, 1972), pp. 321–323.

Publication 2

Challenges for semilocal density functionals with asymptotically nonvanishing potentials

Physical Review B **96**, 075140 (2017)

Thilo Aschebrock,¹ Rickard Armineto,² and Stephan Kümmel¹

¹Theoretical Physics IV, University of Bayreuth, 95440 Bayreuth, Germany

²Department of Physics, Chemistry and Biology (IFM), Linköping University, 58183 Linköping, Sweden

Publ. 2

My contribution

I put forward all presented challenges, performed all analytical and numerical calculations, implemented the relevant routines in DARSEC and PARSEC, prepared all figures, and wrote the first draft of the paper. I began to gather these insights during my master's thesis [[Asc14](#)].

Publ.2

Challenges for semilocal density functionals with asymptotically nonvanishing potentialsThilo Aschebrock,¹ Rickard Armiento,² and Stephan Kümmel^{1,*}¹*Theoretical Physics IV, University of Bayreuth, D-95440 Bayreuth, Germany*²*Department of Physics, Chemistry and Biology (IFM), Linköping University, SE-58183 Linköping, Sweden*

(Received 22 June 2017; published 21 August 2017)

The Becke-Johnson model potential [A. D. Becke and E. R. Johnson, *J. Chem. Phys.* **124**, 221101 (2006)] and the potential of the AK13 functional [R. Armiento and S. Kümmel, *Phys. Rev. Lett.* **111**, 036402 (2013)] have been shown to mimic features of the exact Kohn-Sham exchange potential, such as step structures that are associated with shell closings and particle-number changes. A key element in the construction of these functionals is that the potential has a limiting value far outside a finite system that is a system-dependent constant rather than zero. We discuss a set of anomalous features in these functionals that are closely connected to the nonvanishing asymptotic potential. The findings constitute a formidable challenge for the future development of semilocal functionals based on the concept of a nonvanishing asymptotic constant.

DOI: [10.1103/PhysRevB.96.075140](https://doi.org/10.1103/PhysRevB.96.075140)**I. INTRODUCTION**

The paramount decision to be made when using Kohn-Sham (KS) density functional theory (DFT) [1,2] for physical, chemical, or biological applications is the choice of the approximation used for the universal exchange-correlation (xc) functional $E_{xc}[n]$. A variety of approximations is available, sometimes classified according to Jacob's ladder [3,4] of DFT, reaching from the basic local functionals to constructs of increasing sophistication. The high-rung functionals nowadays achieve an accuracy that rivals the one of higher-order wavefunction-based methods [5]. However, many questions of practical relevance require functionals of the lower rungs for reasons of computational cost. These semilocal density functionals, which only depend on the electron density $n(\mathbf{r})$ and its spatial derivatives, e.g., $|\nabla n(\mathbf{r})|$, can provide an overall reasonable accuracy for E_{xc} . Yet their functional derivatives, i.e., the corresponding xc potentials, typically completely miss important features of the exact xc potential [6–15]. Among them are, e.g., the particle-number discontinuity [16,17] and step structures or steepening effects [8,18–23] that enforce [24], e.g., the principle of integer preference. Particle-number discontinuities and potential step structures and steepenings are mathematically different properties, but they are closely related to each other [8,17]. Also the asymptotic features of the exact exchange [25–28] and xc [6,29] potential are not reproduced at all by standard semilocal approximations.

It became clear that these omitted features play a decisive role, e.g., in the description of charge transfer [20,30,31] and ionization [8,17,18,32,33]. Attempts have been made to model such features directly into semilocal xc potentials [34–45], partially also with an additional (nonlocal) eigenvalue dependence, e.g., as done by Gritsenko et al. (GLLB) [46] and Kuisma et al. [47].

In past years, the Becke-Johnson (BJ) model potential [36] and various modifications thereof [41,48,49] have sparked interest in this respect by showing improved atomic-shell structure, polarizabilities, atomic and molecular properties, and band gaps closer to experimental values [36,39,48,50].

Two of the present authors have discussed that one of its key features is to effectively mimic “nonlocal” exchange features in the asymptotic behavior of the potential caused by the particle-number discontinuity by means of having a nonzero limiting value far away from a finite system [39].

However, model potentials are only of limited usefulness. Since they lack a corresponding xc energy, they cannot be used in applications that require energies, and not being functional derivatives [51,52] also renders them useless for propagating the time-dependent Kohn-Sham equations [53,54]. Furthermore, they are problematic from a formal perspective: directly modeling the xc potential sidesteps the original derivation of the KS equations as variational equations over the energy, and thus forgoes much of the formal framework of KS DFT. This limitation was resolved by the derivation of a semilocal energy functional, AK13 [55], designed to yield as its functional derivative a potential that shares the key features with the BJ model, in particular the asymptotically nonvanishing potential with a system-dependent limiting value.

The overall appeal of BJ, AK13, and derived methods is clear: including features in the exact xc potential missing from other functionals bears the promise of computational results closer to higher-order methods at the low computational expense of a semilocal functional. To some degree, the various modifications of the BJ approach and AK13 have delivered on this promise [39,48,50]. Thus, it may seem pertinent to ask why these methods are not more widely used. In applying AK13 and BJ to broader sets of systems, and in our attempts at improving the properties of AK13, we have identified a set of anomalies, most of which are more or less directly connected to the key property of the asymptotically nonvanishing potential. These anomalies pose a clear problem to broader adoption of functionals of this kind and present a serious challenge to their further development. The purpose of the present paper is to bring these issues to light, both as a warning against a too indiscriminating use of the present realizations of this type of methods and with the hope to inspire further development to resolve these issues.

The paper is organized as follows. First, in Sec. II, we review the AK13 and BJ functionals and their key features. In Sec. III, we discuss issues that appear when AK13 is applied to noninteger particle-number systems in the context

*stephan.kuettel@uni-bayreuth.de

of ensemble DFT. Sections IV and VI summarize findings presented elsewhere on energies and energetics of AK13 and the issue of divergent potentials along nodal surfaces. In Sec. VII, we discuss the behavior of AK13 and the BJ model in external electrical fields. Section VIII focuses on difficulties that can arise when evaluating these potentials, stemming from the numerical representation of the KS orbitals. Finally, Sec. IX gives our summary and conclusions. Hartree atomic units are used throughout this paper.

II. AK13 AND BJ MODEL REVIEW

The AK13 functional [55] is of the standard generalized-gradient approximation (GGA) form for exchange (x) functionals, [56] i.e.,

$$E_x^{\text{GGA}} = A_x \int n^{4/3} F(s) d^3r, \quad (1)$$

parametrized by the reduced density gradient,

$$s = \frac{|\nabla n|}{2\gamma n^{4/3}}, \quad (2)$$

where $A_x = -3/4(3/\pi)^{1/3}$ and $\gamma = (3\pi^2)^{1/3}$. Nevertheless, it is uniquely different from other GGAs. Its foremost feature is that its potential, as usually given by the functional derivative

$$v_x^{\text{GGA}} = A_x \frac{4}{3} n^{1/3} \left[F(s) - s \partial_s F(s) + \frac{3}{4} \left(\frac{u}{s^3} - \frac{t}{s^2} \right) s \partial_s F(s) + \left(1 - \frac{3}{4} \frac{u}{s^3} \right) s^2 \partial_s^2 F(s) \right], \quad (3)$$

with the semilocal quantities

$$t = \frac{\nabla^2 n}{4\gamma^2 n^{5/3}} \quad \text{and} \quad u = \frac{\nabla n \cdot \nabla |\nabla n|}{8\gamma^3 n^3}, \quad (4)$$

typically approaches a positive system-dependent constant outside a finite system. This is achieved by a divergence of the enhancement factor $F(s) \propto s \ln(s)$ as $s \rightarrow \infty$, which typically marks the threshold between a vanishing and a diverging asymptotic GGA potential. The AK13 functional implements this and additional requirements with the choice

$$F^{\text{AK13}}(s) = 1 + B_1 s \ln(1 + s) + B_2 s \ln[1 + \ln(1 + s)], \quad (5)$$

where the constants $B_1 = 2/27 + 8\pi/15$ and $B_2 = 4/81 - 8\pi/15$ have been determined in a nonempirical fashion. This asymptotic behavior has been adopted from the model potential of Becke and Johnson (BJ) [36], which proposes a semilocal correction to the Slater potential [57] utilizing the positively defined kinetic-energy density,

$$\tau = \frac{1}{2} \sum_i f_i |\nabla \varphi_i|^2, \quad (6)$$

to mimic missing exchange features,

$$v_x^{\text{BJ}} = v_x^{\text{Slater}} + C_{\Delta v} \sqrt{\frac{2\tau}{n}}, \quad (7)$$

where $C_{\Delta v} = \sqrt{5/12}/\pi$, and the occupation numbers f_i .

Concerning their limiting value, both potentials rely semilocally on the fact that far outside the system, the density as well as τ are governed by the highest occupied orbital. Under the assumption of spherical symmetry, this leads to the asymptotic relation [58]

$$n(\mathbf{r}) \sim n_0 |\mathbf{r}|^q \exp(-\alpha |\mathbf{r}|) \quad \text{as} \quad |\mathbf{r}| \rightarrow \infty, \quad (8)$$

where n_0 and q are system-dependent constants. The decay parameter

$$\alpha = 2\sqrt{-2(\varepsilon_{\text{ho}} - v_x^\infty)} \quad (9)$$

is determined by the highest occupied eigenvalue ε_{ho} relative to the limiting value of the potential $v_x^\infty = \lim_{|\mathbf{r}| \rightarrow \infty} v_x(\mathbf{r})$. Additional asymptotic relations involving the spatial derivatives of the density follow hereby:

$$\frac{u}{s^3} \sim 1, \quad \frac{t}{s^2} \sim 1 - \frac{2}{3} \frac{1}{\ln(s)}, \quad (10)$$

$$2\gamma n^{1/3} s \sim \alpha, \quad \frac{\tau}{n} \sim \frac{\alpha^2}{8},$$

as $|\mathbf{r}| \rightarrow \infty$. Utilizing these, one can calculate the limits

$$v_x^{\text{AK13},\infty} = -\frac{A_x B_1 \alpha}{6\gamma}, \quad v_x^{\text{BJ},\infty} = \frac{C_{\Delta v} \alpha}{2}, \quad (11)$$

to show the asymptotic similarities of both potentials. Thus, the limit of the AK13 potential approximately equates to 68% of the limit of the BJ potential. For further discussions, we note that the limit of the AK13 potential relies on the cancellation of the first-order terms $\propto s \ln(s)$, while the limit of the BJ potential is determined by a single first-order term.

Solving Eqs. (9) and (11) for a self-consistent value of v_x^∞ gives

$$v_x^\infty = Q(1 + \sqrt{1 - 2\varepsilon_{\text{ho}}/Q}) \quad (12)$$

with, respectively, $Q = (A_x B_1 / 6\gamma)^2$ in the case of AK13 and $Q = (C_{\Delta v} / 2)^2$ in the case of BJ. Hence, the limiting values of both semilocal potentials depend on the value of the highest occupied eigenvalue and therefore change discontinuously if, e.g., an additional fraction of an electron is added to the system.

As the limiting value of the exact exchange-correlation potential equals zero [59], it is tempting [39,55] to apply a constant shift v_x^{DD} to both semilocal potentials,

$$v_x^0(\mathbf{r}) = v_x^{\text{SL}}(\mathbf{r}) + v_x^{\text{DD}}, \quad (13)$$

where $v_x^{\text{DD}} = -\lim_{|\mathbf{r}| \rightarrow \infty} v_x^{\text{SL}}(\mathbf{r}) = -v_x^\infty$. Due to this realignment, the semilocal limiting value v_x^∞ gives rise to a nonlocal discontinuity of the potential triggered by a change in the value of the highest occupied eigenvalue. Thus, both realigned versions of the AK13 and the BJ potential mimic a feature associated with the derivative discontinuity (DD) [16] of the exact exchange (EXX) functional. Moreover, both models for exchange share additional attractive properties such as a step structure in the potential for well-separated subsystems and an improved shell structure in the potential for atoms [36,55]; in bulk systems, they show band gaps, band structures, and optical dielectric constants closer to EXX results [50,55,60]—and are thus typically in better agreement with experiments. Hence, AK13 and BJ functionals implement several promising features. In terms of qualitative results, they are quite similar

with the decisive advantage that the AK13 potential is an actual functional derivative while the BJ potential is not [37,52,54].

However, as explained in Sec. I, we have now identified a number of anomalies and general difficulties caused by the construction scheme summarized above. Some stem from specific choices made in the construction of AK13 and could thus potentially be circumvented by improved design criteria. However, others appear more intimately coupled to the key feature of an asymptotically nonvanishing potential.

III. AK13 FOR SYSTEMS WITH FRACTIONAL PARTICLE NUMBERS

In this section, we will point out some features that AK13 shows when particle-number variations are explicitly considered. The shift v_x^{DD} must be carefully examined in this context. For a system with fixed integer electron number, the constant shift of the potential by v_x^{DD} serves two purposes: On the one hand, this shift realigns the zero of the eigenvalues, $\{\varepsilon_i^0 = \varepsilon_i + v_x^{\text{DD}}\}$, onto the limiting value of the potential. This is a natural choice, as it separates bound from unbound states. On the other hand, the realignment of the potential introduces a nonlocal mechanism akin to the discontinuity of the exchange optimized effective potential (OEP) [61], a feature that is associated with the DD of the corresponding energy functional.

Such a shift is fully in line with the Hohenberg-Kohn theorem [1], as the effective potential is only determined up to an arbitrary constant. One may further argue that strictly speaking such a shift does not affect observables: It does not change the density, but only affects the Kohn-Sham eigenvalues, which are auxiliary quantities. A subtlety in this argument is related to the highest occupied eigenvalue, which equals minus the first ionization potential in exact DFT [59,62] and therefore can be equated to an observable. One may thus wonder whether in a functional such as AK13 the shifted or the unshifted highest occupied eigenvalue should be used as an approximation to the first ionization potential. As the self-consistent density from such a functional decays according to Eq. (8), i.e., the asymptotic decay is governed by the shifted highest occupied eigenvalue, $\varepsilon_{\text{ho}} - v_x^{\infty}$, whereas the decay of the exact density is likewise determined by the ionization potential, it seems reasonable to use the negative-shifted eigenvalue as an approximation to the ionization potential. In practice, the shifted AK13 eigenvalues generally are in better [55] agreement with the ionization potential from EXX (and thus also experimental values) than the highest occupied eigenvalues of other, commonly used, semilocal functionals [63].

However, the idea of shifting the eigenvalues can also be seen more critically when one adopts a different perspective. Consider the behavior of AK13 within the ensemble extension of DFT by Perdew et al. [16], i.e., the generalization to fractional particle numbers. In this framework, the absolute offset of the exchange-correlation potential is fixed and the exchange-correlation potential, $v_{\text{xc}} = \delta E_{\text{xc}}/\delta n$, is defined uniquely for a given energy functional E_{xc} . This can be understood directly from Janak's theorem [65],

$$\frac{\partial E}{\partial N} = \varepsilon_{\text{ho}}(N), \quad (14)$$

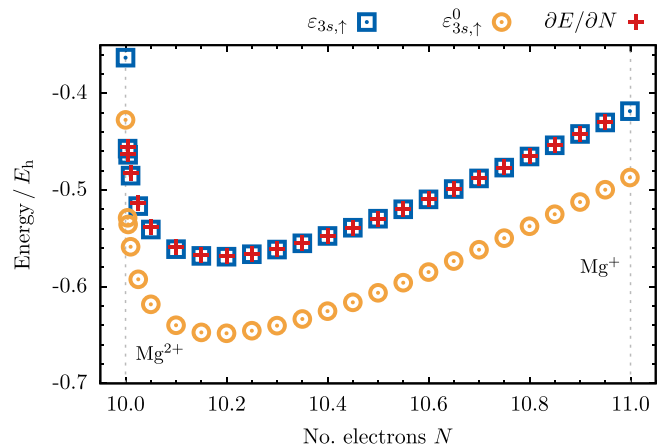


FIG. 1. Highest occupied orbital energy $\varepsilon_{3s,\uparrow}$ corresponding to the semilocal AK13 potential [see Eq. (3)] $\varepsilon_{3s,\uparrow}^0 = \varepsilon_{3s,\uparrow} + v_x^{\text{DD}}$ corresponding to its realigned version [see Eq. (13)] and the total-energy derivative $\partial E/\partial N$ as a function of the number of electrons N for ionized atomic magnesium. $\partial E/\partial N$ is calculated using central nonuniform first-order finite differences and the values of $E(N)$ at the shown points. The data points are based on self-consistent calculations with a code for atoms originating from Ref. [64].

which establishes a direct link between the particle-number dependence of the energy functional and the absolute offset of the eigenvalue energies in the KS system. Hence, one is not allowed to shift the energy scale of the KS system (which would shift the potential and eigenvalues) without also modifying the energy functional.

Janak's theorem can also be used to numerically verify the correct absolute offset. We demonstrate this in the following for AK13 (and in Fig. 6 of Appendix A for EXX). Figure 1 confirms that in a straightforward extension of AK13 to ensemble DFT [66], the appropriate exchange potential is not the zero-aligned one v_x^0 , but the unshifted, semilocal potential v_x^{SL} . This should not be surprising since v_x^{SL} is the unmodified expression given by a straightforward functional derivative of the AK13 energy functional of Eq. (1).

A major conclusion from Janak's theorem is that the straightforward application of the AK13 energy functional in ensemble DFT gives a functional derivative that does not explicitly exhibit a discontinuity, i.e., a discontinuous shift of the potential at integer particle number. We illustrate the difference between the AK13 potential and the EXX potential with respect to the discontinuity in Appendix A using Mg^{2+} as an example. Despite lacking this absolute overall shift, fractional particle AK13 reproduces the step structure in its asymptotic behavior that is associated with the shift. For example, for a single ion, when the fractional occupancy goes through an integer, the asymptotic potential incorporates a step related to the atomic-shell structure that moves inwards as the fractional particle number increases, qualitatively mimicking a behavior seen in the EXX potential [55,67].

The discussion above may suggest the idea of adding a term to the AK13 energy functional with the sole responsibility of generating a discontinuous shift. We have explored this idea, and in Appendix B we discuss why such an energy correction term is not straightforward to construct.

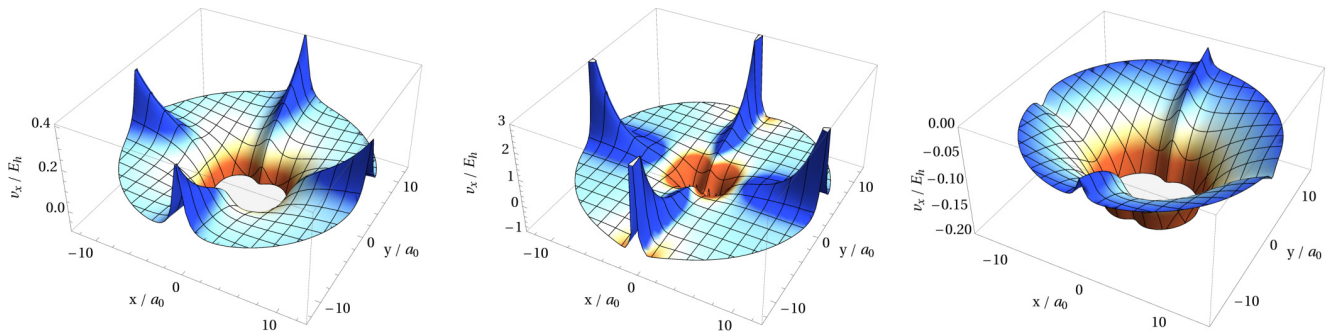


FIG. 2. Contour plot of the BJ, AK13, and EXX (OEP) potential landscapes of O_2 for the majority spin channel in the plane containing the bond axis (x axis). The figure demonstrates that both semilocal potentials diverge exponentially along the nodal surfaces of the highest occupied orbital. Note that the scale of the potential axis as well as the coloring visualizing the height of the potentials differ. Due to serious numerical difficulties, which are intensified by the nodal surfaces [68], the BJ and AK13 potentials could not be calculated self-consistently and were instead evaluated on tightly converged self-consistent local spin density approximation (LSDA) orbitals. The calculations were performed with the all-electron code DARSEC [69], which is specialized on diatomic molecules and operates on a real-space grid of prolate-spheroidal coordinates.

Looking once more at the graph of Fig. 1 with the focus on the region close to $N \rightarrow 10^+$ reveals that the AK13 energy response to a change in the fractional particle number deviates significantly from the exact behavior. Due to the critical behavior of $F^{\text{AK13}}(s)$ in the limit $s \rightarrow \infty$ [see Eq. (5)], the exchange-energy density of AK13 is highly sensitive to small changes of the electron density which alter its exponential decay. Addition of a fraction of an electron to the system by fractionally occupying a new orbital is such a change. The result is a short interval with high curvature of the $E(N)$ curve which deviates from the desired piecewise-linear behavior [16]. Thus, whereas the exact DD goes along with piecewise linearity, its semilocal imitation here is acting contrarily.

Finally, it is worthwhile to return to the discussion of whether it is more appropriate to use the shifted or the unshifted highest occupied eigenvalue to approximate the negative first ionization potential. At the beginning of this section, we had presented arguments for using the shifted eigenvalue. However, Janak's theorem shows that the highest occupied eigenvalue equals the total-energy difference between the $N - 1$ and N particle system for functionals that sufficiently fulfill the piecewise-linearity condition [16] (which AK13 does not). This applies regardless of whether or not the functional has a nonvanishing asymptotic potential. Therefore, from the perspective of Janak's theorem, one comes to the conclusion that from a formal standpoint, it is appropriate to identify the unshifted highest occupied eigenvalue with the negative-ionization potential. Although this seems like a contradiction to the arguments given above, there is no formal mistake. These two different perspectives are possible due to the approximative nature of the functionals under consideration—the exact functional does not exhibit a nonvanishing asymptotic constant and is piecewise linear. From a pragmatic point of view, it makes sense to adopt the perspective which gives better results in practice, i.e., for AK13 to use the shifted eigenvalue.

IV. ENERGIES AND ENERGETICS

AK13 can be seen as an improvement over the BJ model especially because it *has* an energy functional. However, as

discussed in past works that go back to the original AK13 paper, the accuracy of total energies from this functional is not as good [40,45,55,70] as from established GGAs, e.g., the one of Perdew, Burke, and Ernzerhof (PBE) [71]. Instead, one finds that the energetics displayed upon structural relaxation are distorted beyond what seems reasonable even for an exchange-only functional (see Ref. [72] and the Supplemental Material of Ref. [55]). This was the topic of a recent work [72], with a typical example of a bad structural relaxation being AlAs, which deviates from the experimental lattice constant by 16%. Another similar indication of something missing from the AK13 total energies is the self-consistent field (SCF) results for atomic ionization; AK13 SCF energies deviate more from exact-exchange results than those of the local density approximation (LDA) [55].

V. DIVERGENT POTENTIAL ALONG NODAL SURFACES

In many finite systems, the highest occupied ground-state KS orbital has a nodal surface extending to infinity. The asymptotic density is normally governed by the highest occupied orbital; however, this is not necessarily the case for all its asymptotic properties in the vicinity of nodal surfaces. We recently pointed out that this region is troublesome for many semilocal exchange functionals [68]. In summary, the behavior of EXX on nodal surfaces is a protruding ridge along such regions [25–28]. Ordinary semilocal potentials such as the LDA potential decay rapidly in the asymptotic region in a way that mostly does not distinguish nodal surfaces. Energy functionals with divergent enhancement factors can display a range of different behaviors, but, if the divergence is strong enough, the potential will diverge exponentially along the nodal surface. Examples of such functionals are the BJ potential, the Becke 1988 exchange functional [73], and AK13. Of these, AK13 displays the strongest divergence; it is twice as strongly diverging as the BJ model. A demonstration of this issue is presented in Fig. 2, which features the divergent BJ and AK13 potentials in comparison with the EXX (OEP) potential evaluated for O_2 , a system with nodal surfaces of the highest occupied KS orbital. As previously discussed

[68], these divergences are not only theoretically worrisome but also lead to major numerical difficulties when trying to converge calculations for finite systems with nodal surfaces. The O_2 molecule that we show here presents a situation that somewhat differs from the common cases discussed previously in Ref. [68], as here the doubly degenerate highest occupied orbitals of the majority spin channel form a nodal line along the bond axis in addition to a nodal plane between the two oxygen nuclei, and also the two degenerate orbitals below the highest occupied ones exhibit this nodal line along the bond axis. As a consequence of this unusual electronic structure, the density of the majority spin channel along the bond axis is asymptotically dominated by the fifth-highest occupied orbital [74] and produces a rare feature in the asymptotic exact exchange potential as well: In addition to a ridge that results from a positive limiting value along the nodal plane, a furrow related to an uncommon negative limiting value shows up in the potential along the nodal line of the bond axis, as can be seen in Fig. 2(c).

VI. SECOND-ORDER ASYMPTOTICS

Next we discuss an unintended behavior of the AK13 construct that relates to its asymptotic second-order term, $\sim B_2 s \ln[\ln(s)]$ as $s \rightarrow \infty$, in the enhancement factor $F^{\text{AK13}}(s)$; cf. Eq. (5). The original motivation [55] of the $s \ln[\ln(s)]$ term was to mimic the leading asymptotic behavior $v_x \sim -c/z$ outside the surface of a half-infinite bulk system with c a system-dependent prefactor and z the distance to the surface. However, in leading asymptotic order, a term $\sim s \ln[\ln(s)]$ results in a system-independent contribution to the potential $\propto 1/z$. Nonetheless, this term is important as it balances the divergence of the enhancement factor in the limit $s \rightarrow \infty$ having the opposite sign of the leading term, $\sim B_1 s \ln(s)$. This balance is needed to provide reasonable energies as well as to improve numerical evaluability of the potential in the asymptotic region of finite systems.

The drawback of this B_2 term becomes evident when evaluating the asymptotics of the AK13 potential in detail,

$$v_x^{\text{AK13}}(r) \sim -\frac{A_x B_1}{6\gamma} \alpha + \frac{A_x B_2 \ln(\alpha r/3)}{\gamma r} + \frac{A_x}{\gamma} \left[\left(B_1 - \frac{3}{2} B_2 \right) - B_1 \ln(2\gamma n_0^{1/3}/\alpha) \right] \frac{1}{r}, \quad (15)$$

as $r = |\mathbf{r}| \rightarrow \infty$ and given the asymptotic density of Eq. (8) with $q = 0$ for simplicity. The first term of Eq. (15) represents the positive system-dependent asymptotic constant of AK13, whereas the second and third terms describe how the potential approaches this nonvanishing asymptotic constant. The system-independent contribution to the third term gives by construction the desired $-1/r$ behavior. However, this term is asymptotically dominated by the second term $\propto \ln(r)/r$, which has a positive sign. Therefore, the asymptotic constant of the AK13 potential is ultimately approached from above and the potential has a local maximum in the asymptotic region. The latter is approached too fast for the potential to be able to bind additional electrons [70].

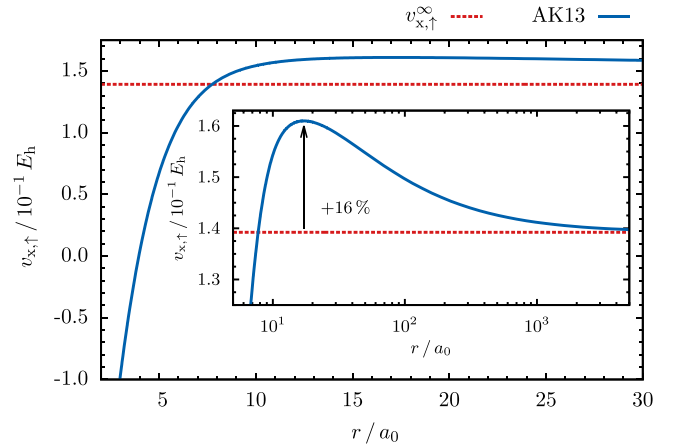


FIG. 3. AK13 potential evaluated for the exact hydrogen ground-state density. Looking at the outer graph, i.e., a typical computational length scale, the potential seems to approach a positive constant unequal to v_x^∞ given by Eq. (11). The inset shows the same potential on a logarithmic scale.

A second consequence is exemplified by Fig. 3. It shows the AK13 potential for the exact hydrogen ground-state density. Within the typical length scale of a numerical electronic structure calculation of less than 30 Bohr radii, the AK13 potential seemingly approaches an asymptotic constant which is 16% higher than the actual limiting value given by Eq. (11). The true limiting value is approached only within a length scale of several-thousand Bohr radii. This is a consequence of $\ln(r)/r$ decaying only marginally more slowly than $1/r$. This undesirable behavior can be noticed in numerical calculations of other systems as well. The theoretical limiting value of the potential is therefore of only limited significance in typical calculations.

This drawback could be corrected by modifying the construction of AK13. In such a revised construction of AK13, one could, e.g., replace the $B_2 s \ln[1 + \ln(1 + s)]$ term by a term that exhibits an asymptotic behavior $\propto s$ as $s \rightarrow \infty$ and maintains reasonable balance with the original B_1 term.

VII. EXTERNAL ELECTRICAL FIELDS

The hope for improved charge-transfer characteristics spurred some of the investigations of the BJ potential [39,41,52], and corresponding hopes may have been associated with AK13. Mimicking the field-counteracting behavior of exact exchange [31,75] with the semilocal BJ potential, however, turned out to be difficult. In order to clarify the situation for AK13, here we look at a standard test case. We study external electrical fields that are weak and linear, i.e., their contribution to the Hamiltonian is $\mathcal{F}z$ with some small field amplitude \mathcal{F} and the z axis chosen in the direction of the field. Such “infinitely large, weak fields” are, e.g., used to calculate the electrical response of molecules [76], in particular of molecular chains, within DFT. In the following, we study a frequently used [31,75–87] model molecular system: the hydrogen chains.

Given the asymptotic similarities of the AK13 and BJ potential pointed out in Sec. II, it does not come as a surprise

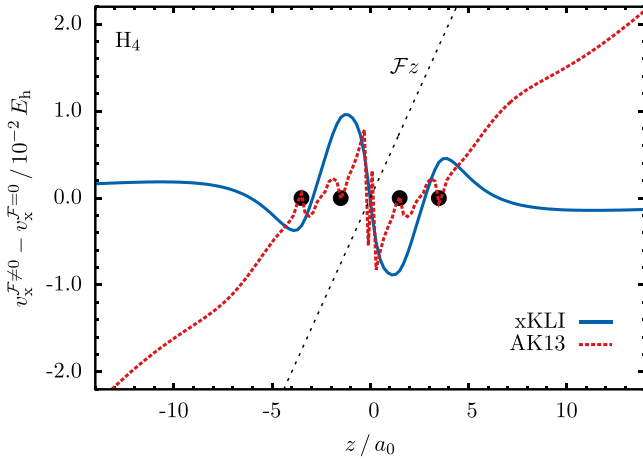


FIG. 4. Difference between the exchange potential of calculations with and without an external electric field of strength $\mathcal{F} = 5 \times 10^{-3} E_h/a_0$ for a H_4 chain (atom positions are indicated by circles). The solid blue line shows the desired field-counteracting behavior of EXX within the Krieger-Li-Iafrate (KLI) approximation (xKLI). AK13 (dashed red line) is tilted in the direction of the field, similarly to BJ (see Fig. 5 of Ref. [39]). The AK13 potentials are not calculated self-consistently due to the discussed numerical difficulties, but evaluated on self-consistent xKLI KS orbitals in PARSEC [88] with Giannozzi pseudopotentials [89], ellipsoidal boundaries with semiaxis of $10a_0$ perpendicular to and $30a_0$ along the chain, and a grid spacing of $0.2a_0$.

that in the presence of an external electric field, AK13 shows the same surprising unphysical behavior as BJ [39], i.e., the potential is asymptotically tilted in the direction of the external field and does not go to zero. Figure 4 demonstrates this by showing the difference between the exchange potential of a chain of four hydrogen atoms in a weak electric field and the potential with no external field, $v_x^{F \neq 0} - v_x^{F = 0}$. The approximately linear tilt of the AK13 potential in the asymptotic region arises solely in the presence of the external field. It can be understood as a consequence of the deviation of the asymptotic density from Eq. (8) in response to the electric field. Terms of the AK13 potential that contribute to an asymptotic constant when Eq. (8) holds, i.e., terms that arise from $F(s) \sim B_1 s \ln(s)$ as $s \rightarrow \infty$, now yield (in first order) a linearly diverging contribution to the potential.

The leading asymptotic behavior in the presence of a linear electric field can be retraced by utilizing the one-dimensional Airy gas model in the spirit of the analogous calculation for the BJ potential of Ref. [39]. While the result of the corresponding AK13 calculation for this one-dimensional model is in full analogy to the BJ result [90], it is not quantitatively transferable to the three-dimensional case, as the asymptotics of the AK13 potential show a direct dependence on the spatial dimension [55] (which BJ does not show). The one-dimensional result and Fig. 4 suggest that

$$v_x^{\text{AK13}}(\rho = 0, z) \sim v_x^{\text{AK13}, \infty} + C \frac{\mathcal{F}z}{\sqrt{-2\epsilon_{\text{ho}}}} \quad (16)$$

in the asymptotic region while $|z| \ll |\mathcal{F}/\epsilon_{\text{ho}}|$ with some constant $C > 0$ and $\rho = \sqrt{x^2 + y^2}$.

In Ref. [39], the relation that is the analog of Eq. (16) for BJ was used to justify a linear, field-dependent correction to the BJ potential. Since this correction is applied globally, it fixes the unphysical tilt in the asymptotic region, but more importantly leads to a slope counteracting the external field in the inner region, thus mimicking response physics that could previously not be captured by semilocal constructions. The resulting total BJ potential response to the electrical field is remarkably close to exact-exchange calculations and yields vastly improved polarizabilities [39,52]. Consequently, an analogue correction to AK13 suggests itself. However, the one important benefit of AK13 over BJ is the fact that its potential is an actual functional derivative of a well-defined energy expression. Thus, to maintain a correspondence between energy and potential, the field-dependent correction to AK13 has to originate from an energy correction. Given that this energy correction cannot explicitly depend on the external electrical field in order to yield consistent polarizabilities from energy and potential [76], there is no clear way to create such a term.

VIII. INFLUENCE OF THE NUMERICAL REPRESENTATION

Next we will discuss how strongly the chosen numerical representation (basis set) of the KS orbitals influences calculations of finite systems for functionals with asymptotically nonvanishing potentials. This can hardly be referenced as anomalies in the functionals themselves, but is still an issue of high relevance for their application. For usual (semi)local functionals, the accuracy of the numerical representation of the far asymptotic density is typically of little concern because the energy and potential of such functionals are not sensitive to these regions of space. The AK13 energy and the AK13 and BJ potentials, however, are by construction highly sensitive to the precise decay of the density, which is measured by ratios such as $|\nabla n|/n$. When this ratio is numerically evaluated, a representation of the asymptotic density that is not highly accurate can cause serious numerical problems, e.g., instabilities. Small numerical errors might, for example, prevent the required cancellation of the leading-order terms $\propto s \ln(s)$ in the AK13 potential, and therefore cause a linearly growing error in the potential in the asymptotic region. This then can amplify the numerical error in the next step of a KS iteration.

In the following, we discuss three common approaches to represent KS orbitals, and their implications for the asymptotic potential: real-space grids [69,88,91–94], Slater-type orbitals (STOs) [95], and Gaussian-type orbitals (GTOs) [96,97].

The representation of orbitals on real-space grids is the most flexible, yet the computationally most expensive one of these three. The relative numerical accuracy of this representation is typically decaying in the far asymptotic region, especially when looking at spatial derivatives represented via finite differences. The restriction to a necessarily finite grid also introduces boundary effects. As a consequence, the above-discussed problems of evaluating the AK13 potential in the asymptotic region are strongly noticeable and make three-dimensional, grid-based AK13 calculations extremely hard.

The usage of either STOs or GTOs circumvents some of these problems. The reason is that, on the one hand,

critical ingredients to the semilocal potential, i.e., the density derivatives $|\nabla n|$ and $\nabla^2 n$, are analytically accessible and are thereby numerically arbitrarily accurate, even in the asymptotic region. On the other hand, both representations require only a relative small basis-set size, as these sets are highly tailored and specific to each atom. Therefore, the degrees of freedom and, consequently, the susceptibility to instabilities are considerably reduced compared to real-space methods. Yet, there is a non-negligible price to pay for this “convenience”: It is the qualitatively wrong behavior of the density in the asymptotic region that occurs for both STOs and GTOs. It in turn has the following conceptual implications: In the case of STOs, the issue is that the exponential decay of the KS orbitals is predefined by the basis set. This means that when using semilocal density functionals with an asymptotically nonvanishing potential, the nonzero limiting value of the potential, v_x^∞ , is not determined by the system within the self-consistent calculation, but rather is given by the basis set and thus already fixed prior to the actual calculation. Therefore, in the case of STOs, neither Eq. (9) nor Eq. (12) hold strictly. Yet, they can hold approximately when a reasonable basis set of STOs is chosen.

The issue with GTOs is similar, but even more apparent. GTOs sacrifice the correct orbital asymptotic that is achieved with STOs. Thus, in the case of GTOs, the asymptotic relation $n(r) \propto \exp(-\beta r^2)$ as $r \rightarrow \infty$ replaces Eq. (8), which results in a qualitatively different behavior of semilocally nonvanishing potentials: Instead of approaching a system-dependent asymptotic constant outside of a finite system, the AK13 and BJ potentials spuriously diverge linearly to positive infinity, e.g.,

$$v_x^{\text{AK13}}(r) \sim -\frac{2A_x B_1}{3\gamma} \beta r, \quad (17)$$

as $r \rightarrow \infty$. Additionally, the asymptotic slope of these potentials is akin to the asymptotic constant in the case of STOs, predefined by the basis set via the value of β .

Hence, one should be aware that semilocal density functionals with an asymptotically nonvanishing potential show significantly higher demands on the numerical representation of the KS orbitals, especially in the asymptotic region. To summarize, real-space methods provide, in principle, the qualitatively most accurate representation in this region, but are susceptible to instabilities, whereas STOs or GTOs provide higher stability, but imply a qualitatively wrong asymptotic density and potential.

IX. SUMMARY AND CONCLUSIONS

In this paper, we have investigated a set of anomalous features of semilocal functionals with nonvanishing asymptotic exchange potentials, with a particular focus on AK13 and its predecessor BJ. We also commented on the numerical difficulties that appear when evaluating such functionals in standard electronic structure codes. In particular, we have discussed misfeatures seen in the direct application of AK13 in ensemble DFT for systems with fractional particle numbers, inaccurate energies and energetics, divergent potentials along nodal surfaces, nonphysical response to an external electric dipole field, and practical difficulties due to the numerical

orbital representation used. The issues we have identified and discussed in this work provide a formidable challenge for the future development of functionals with nonvanishing potentials.

There are different approaches one can try to overcome these difficulties and move forward with the aim to incorporate important exact-exchange features into functionals with modest computational cost. One option is to continue the development of semilocal density functionals with asymptotically nonvanishing potentials. Extending the AK13 construction idea, one can try to explicitly tackle each deficit that we have pointed out here. This is a major challenge, but when carried out successfully such a strategy should lead to a formally satisfying consistent energy-potential pair. A second option is to follow the idea of GLLB [46,47] and construct model potentials that incorporate some of the desired exact-exchange features via an explicit orbital and eigenvalue dependence. This type of scheme can provide numerically robust potentials that do not suffer from the issues that are related to the semilocal realization of a nonvanishing asymptotic constant. A downside of this approach is that such constructions are not functional derivatives of a corresponding energy functional. This implies serious drawbacks that we have already discussed briefly in Sec. I, such as instabilities in time-dependent DFT and no possibility for geometry optimization. A third option is meta-generalized-gradient approximations (meta-GGAs), i.e., energy functionals that are semilocal not in the density but in the orbitals and make use of, e.g., the kinetic-energy density τ . As discussed previously by Eich and Hellgren [98], meta-GGAs used in the Kohn-Sham scheme in general have a derivative discontinuity due the nonlocal character of their multiplicative potential. However, as commonly used meta-GGAs to date largely underestimate the exchange derivative discontinuity and related properties, it remains to be seen whether the desired potential features can be captured on the meta-GGA level to an extent that is useful in practice.

ACKNOWLEDGMENTS

S.K. and T.A. acknowledge financial support by the German-Israeli Foundation for Scientific Research and Development. T.A. acknowledges support by the University of Bayreuth Graduate School. R.A. acknowledges financial support from the Swedish Research Council (V.R.), Grant No. 2016-04810, and the Swedish e-Science Research Centre (SeRC).

APPENDIX A: COMPARISON OF AK13 AND EXX POTENTIALS FOR FRACTIONAL PARTICLES NUMBERS

Section III discussed the straightforward extension of AK13 to ensemble DFT using fractional particle numbers. We argued on general grounds, and explicitly demonstrated for ionized atomic magnesium in Fig. 1, that the AK13 (ensemble) potential does not exhibit a global discontinuous shift at integer particle number. Yet, the AK13 potential reproduces a step in the asymptotic region that is typically associated with such a discontinuous shift. In order to further discuss and illustrate the relation between the step structure and the shift, we compare the functional derivative with respect to the density of the EXX

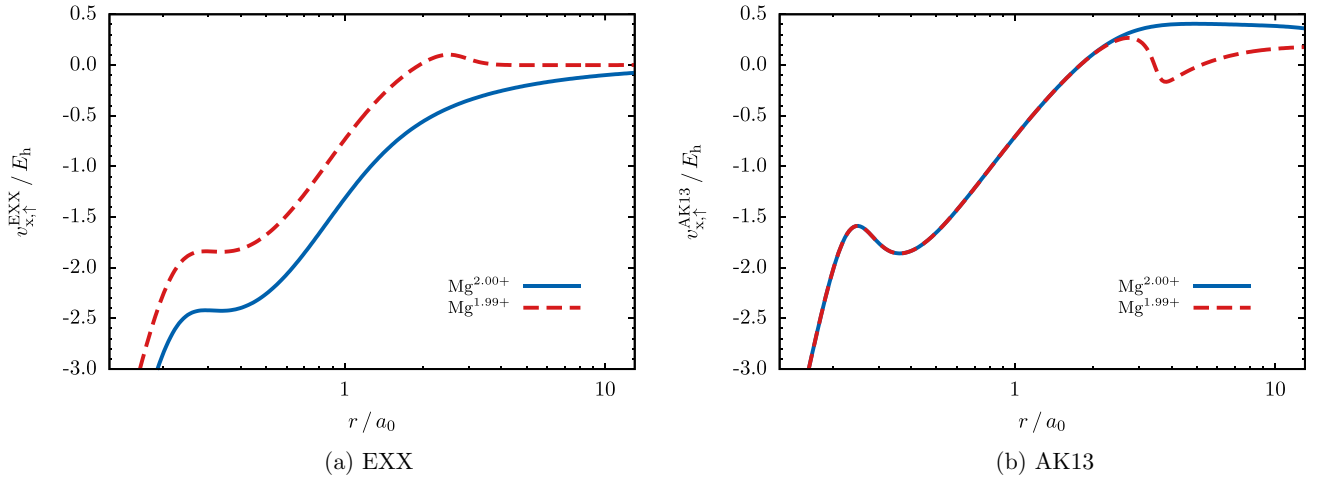


FIG. 5. Change of the EXX (in the KLI approximation) and the (unshifted) AK13 spin-up potentials upon addition of a fraction of an electron to double-ionized atomic magnesium. The potentials are based on self-consistent calculations with a code for atoms operating on a logarithmic grid and originating from Ref. [64]. While the EXX potential jumps globally and discontinuously at integer particle numbers, solely the asymptotic limiting value of the AK13 potentials jumps. Similar plots were shown for BJ in Fig. 2 of Ref. [39] and for AK13 in Fig. 4 of Ref. [55].

energy, on the one hand, to the unshifted functional derivative of the AK13 energy functional for Mg^{2+} , on the other hand, as we add a small fraction of an electron to the system. The functional derivatives are shown in Fig. 5 for a fractional occupation of one percent, i.e., $N = 10 + \epsilon$ with $\epsilon = 0.01$. By virtue of the spin-scaling relation for exchange [99], it is to be expected that only the exchange potential of the spin channel in which the particle number changes is substantially affected and can show a discontinuity or step. This is also reflected in the AK13 functional and becomes manifest in the fact that the asymptotic constant of the AK13 potential is spin dependent and may differ between spin channels. Therefore, we deliberately focus our discussion only on this spin channel, which is here chosen to be the up-spin channel.

Upon addition of a fraction of an electron, the functional derivative of the EXX energy jumps up in the interior region, $r \lesssim 2a_0$, by approximately a constant, Δ_x^{EXX} , whereas in the asymptotic region the EXX potential maintains the same limiting value as the EXX potential at integer number of electrons,

$$\lim_{r \rightarrow \infty} v_{x,\uparrow}^{\text{EXX},N=10+\epsilon}(r) = \lim_{r \rightarrow \infty} v_{x,\uparrow}^{\text{EXX},N=10}(r) = 0. \quad (\text{A1})$$

As $\epsilon \rightarrow 0^+$, the step between these two regions moves outwards and the discontinuous shift of the potential at integer particle number becomes apparent; the potentials at any point r at a finite distance differ by just a constant shift in this case,

$$\lim_{\epsilon \rightarrow 0^+} v_{x,\uparrow}^{\text{EXX},N=10+\epsilon}(r) - v_{x,\uparrow}^{\text{EXX},N=10}(r) = \Delta_x^{\text{EXX}}. \quad (\text{A2})$$

In the case of the unshifted AK13 functional derivative, the situation is different: In the interior region, the potentials with and without fractional particle number overlap perfectly due to their semilocal nature. However, by construction, the limiting value of the AK13 potential decreases discontinuously upon addition of a fraction of an electron [cf. Eq. (12)], thus

$$\lim_{r \rightarrow \infty} [v_{x,\uparrow}^{\text{AK13},N=10+\epsilon}(r) - v_{x,\uparrow}^{\text{AK13},N=10}(r)] = \Delta_x^{\text{AK13}}. \quad (\text{A3})$$

The result is a step downward in the fractional AK13 potential between the interior and the asymptotic region. Similar to the step that is present in the EXX potential, the step between these two regions moves outwards as $\epsilon \rightarrow 0^+$. However, as the AK13 potentials with different particle numbers differ in the asymptotic region and not in the interior region, there remains no global discontinuous shift of the potential,

$$\lim_{\epsilon \rightarrow 0^+} v_{x,\uparrow}^{\text{AK13},N=10+\epsilon}(r) - v_{x,\uparrow}^{\text{AK13},N=10}(r) = 0, \quad (\text{A4})$$

in contrast to EXX.

This contrast can also be summarized in the following order of limits relation, which in the case of the EXX potential (as well as the exact xc potential) reads

$$\lim_{\epsilon \rightarrow 0^+} \lim_{|\mathbf{r}| \rightarrow \infty} [v_x^{N_0+\epsilon}(\mathbf{r}) - v_x^{N_0-\epsilon}(\mathbf{r})] = 0, \quad (\text{A5})$$

$$\lim_{|\mathbf{r}| \rightarrow \infty} \lim_{\epsilon \rightarrow 0^+} [v_x^{N_0+\epsilon}(\mathbf{r}) - v_x^{N_0-\epsilon}(\mathbf{r})] = \Delta_x, \quad (\text{A6})$$

whereas the relation is reversed for AK13,

$$\lim_{\epsilon \rightarrow 0^+} \lim_{|\mathbf{r}| \rightarrow \infty} [v_x^{N_0+\epsilon}(\mathbf{r}) - v_x^{N_0-\epsilon}(\mathbf{r})] = \Delta_x^{\text{AK13}}, \quad (\text{A7})$$

$$\lim_{|\mathbf{r}| \rightarrow \infty} \lim_{\epsilon \rightarrow 0^+} [v_x^{N_0+\epsilon}(\mathbf{r}) - v_x^{N_0-\epsilon}(\mathbf{r})] = 0. \quad (\text{A8})$$

In the left-hand sides of these equations, we dropped the superscripts EXX and AK13 for brevity of notation. Thus, the qualitative difference between AK13 and EXX essentially comes down to a missing global shift of the AK13 functional derivative. This missing shift is precisely the one proposed to be added in relation to Eq. (13) and discussed in Sec. III as being in line with the Hohenberg-Kohn theorem for integer particle systems but inadmissible in ensemble DFT.

If one is familiar with the OEP (or KLI) construction in detail, one may wonder why we chose to align the EXX potential for $N = 10 + \epsilon$ such that it goes to zero at infinity—after all, one has to make a deliberate choice for the asymptotic constant in the OEP construction [61,67]. So if we chose to

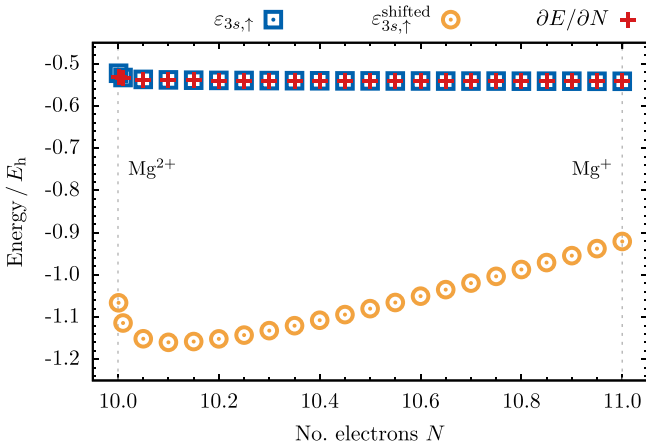


FIG. 6. Highest occupied orbital energy $\epsilon_{3s,\uparrow}$ corresponding to the EXX (KLI) potential aligned to zero at infinity, $\epsilon_{3s,\uparrow}^{\text{shifted}}$ corresponding to the EXX (KLI) potential aligned in the interior region with the potential at integer number of electrons (Mg^{2+}), and the total-energy derivative $\partial E / \partial N$ as a function of the number of electrons N for ionized atomic magnesium. $\partial E / \partial N$ is calculated using central nonuniform first-order finite differences and the values of $E(N)$ at the shown points. The data points are based on self-consistent calculations with the all-electron code DARSEC [69].

not align the AK13 potential at zero, why did we choose to align the EXX potential? The answer to this question is that as mentioned previously, we have no liberty in choosing the constant in ensemble DFT but have to accept the constant that comes out of the functional derivative. Figure 6 demonstrates via Janak's theorem that the EXX potential aligned to zero at infinity corresponds to the functional derivative of the EXX energy, whereas Fig. 1 shows that the unaligned AK13 potential is the functional derivative of the AK13 energy. Therefore, Fig. 5 depicts the proper functional derivatives. We note in passing that for model potentials such as BJ or GLLB, the question of “properly aligning” is irrelevant, as these potentials are not functional derivatives to begin with.

APPENDIX B: NONEXISTENCE OF A STRAIGHTFORWARD ENERGY CORRECTION

As discussed in Sec. III, one might wonder if there exists a straightforward energy correction to the semilocal AK13 functional that realigns the potential and introduces a discontinuous shift of the potential in ensemble DFT. If such a correction could be devised, the corrected AK13 functional would take the form

$$E_x^{\text{AK13},0}[n] = E_x^{\text{AK13}}[n] + E_x^{\text{DD}}[n], \quad (\text{B1})$$

where the functional derivative equals the realigned AK13 potential, as given by Eq. (13). We will in the following prove that the behaviors under uniform density coordinate scaling of Eqs. (13) and (B1) are in contradiction. This disproves the existence of a “straightforward” energy correction whose action is only a simple system-independent realignment of the potential to zero by a constant homogeneous shift in the whole system. We specifically note that therefore the following proof

is valid only for shifts that are rigorously constant everywhere, i.e., including the boundary of the space that is considered.

Assume the functional $E_x^{\text{DD}}[n]$ exists. On addition to $E_x^{\text{AK13}}[n]$, the combined exchange potential then is

$$\frac{\delta E_x^{\text{AK13}}[n]}{\delta n(\mathbf{r})} + \frac{\delta E_x^{\text{DD}}[n]}{\delta n(\mathbf{r})} = v_x^{\text{AK13}}([n]; \mathbf{r}) + v_x^{\text{DD}}[n], \quad (\text{B2})$$

where $v_x^{\text{DD}}[n] = -\lim_{|\mathbf{r}| \rightarrow \infty} v_x^{\text{AK13}}(\mathbf{r})$ by assumption. Now, consider some well-behaved spherical-symmetric density $n(\mathbf{r})$ of a finite system, which satisfies the asymptotic relation of Eq. (8). Hence, by virtue of Eq. (9),

$$v_x^{\text{DD}}[n] = -\lim_{|\mathbf{r}| \rightarrow \infty} v_x^{\text{AK13}}([n]; \mathbf{r}) = -\frac{A_x B_1 \alpha}{6\gamma}. \quad (\text{B3})$$

Given this density, we define the uniform density path,

$$n_\lambda(\mathbf{r}) = \lambda^3 n(\lambda \mathbf{r}) \quad \text{for } \lambda \in (0; 1], \quad (\text{B4})$$

and investigate the derivative of $E_x^{\text{DD}}[n]$ with respect to λ along this path,

$$\frac{dE_x^{\text{DD}}[n_\lambda]}{d\lambda} = \int \frac{\delta E_x^{\text{DD}}[n_\lambda]}{\delta n_\lambda(\mathbf{r})} \frac{dn_\lambda(\mathbf{r})}{d\lambda} d^3r, \quad (\text{B5})$$

where $\delta E_x^{\text{DD}}[n_\lambda] / \delta n_\lambda(\mathbf{r}) = v_x^{\text{DD}}([n_\lambda]; \mathbf{r})$ and

$$\frac{dn_\lambda(\mathbf{r})}{d\lambda} = 3\lambda^2 n(\lambda \mathbf{r}) + \lambda^3 \mathbf{r} \cdot \frac{\partial n(\lambda \mathbf{r})}{\partial (\lambda \mathbf{r})}. \quad (\text{B6})$$

As by construction $v_x^{\text{DD}}[n]$ has to system independently cancel the nonzero asymptotic value of the AK13 potential, one can show

$$v_x^{\text{DD}}[n_\lambda] = -\frac{A_x B_1 \alpha \lambda}{6\gamma} = \lambda v_x^{\text{DD}}[n] \quad (\text{B7})$$

by evaluating $v_x^{\text{AK13}}([n_\lambda]; \mathbf{r})$ along the density path of Eq. (B4) and by applying Eq. (B3), respectively. Inserting this result together with Eq. (B6) into Eq. (B5) while applying the substitution $\lambda \mathbf{r} \rightarrow \mathbf{r}$ gives

$$\begin{aligned} \frac{dE_x^{\text{DD}}[n_\lambda]}{d\lambda} &= \int v_x^{\text{DD}}[n][3n(\mathbf{r}) + \mathbf{r} \cdot \nabla n(\mathbf{r})] d^3r \\ &= v_x^{\text{DD}}[n] \int \nabla \cdot [\mathbf{r}n(\mathbf{r})] d^3r = 0, \end{aligned} \quad (\text{B8})$$

where we have utilized the divergence theorem in the final step with no boundary contribution due to $n(\mathbf{r})$ satisfying Eq. (8). Thus, the energy correction $E_x^{\text{DD}}[n]$ is invariant under uniform density scaling for a density that satisfies the asymptotics relations of Eq. (8),

$$E_x^{\text{DD}}[n_\lambda] = E_x^{\text{DD}}[n]. \quad (\text{B9})$$

Taking the functional derivative of Eq. (B9) with respect to $n(\mathbf{r})$ and applying the chain rule on the left-hand side then yields

$$v_x^{\text{DD}}([n_\lambda]; \mathbf{r}) = v_x^{\text{DD}}([n]; \lambda \mathbf{r}), \quad (\text{B10})$$

which is a contradiction to Eq. (B7).

We specifically note in passing that the correction of Cerqueira et al. [70],

$$E_x^{\text{AK13},0} = E_x^{\text{AK13}} + v_x^{\text{DD}} \int n(\mathbf{r}) d^3r, \quad (\text{B11})$$

is not the energy functional corresponding to the realigned potential of Eq. (13) (as one can show using Janak's theorem

in the spirit of Fig. 1) and would imply a discontinuity of the total energy $E(N)$ rather than of its derivative $\partial E/\partial N$.

-
- [1] P. Hohenberg and W. Kohn, *Phys. Rev.* **136**, B864 (1964).
 [2] W. Kohn and L. J. Sham, *Phys. Rev.* **140**, A1133 (1965).
 [3] J. P. Perdew and K. Schmidt, *AIP Conf. Proc.* **577**, 1 (2001).
 [4] J. P. Perdew, A. Ruzsinszky, J. Tao, V. N. Staroverov, G. E. Scuseria, and G. I. Csonka, *J. Chem. Phys.* **123**, 062201 (2005).
 [5] P. Bleiziffer, A. Heßelmann, and A. Görling, *J. Chem. Phys.* **139**, 084113 (2013).
 [6] C. J. Umrigar and X. Gonze, *Phys. Rev. A* **50**, 3827 (1994).
 [7] M. J. Allen and D. Tozer, *Mol. Phys.* **100**, 433 (2002).
 [8] M. Lein and S. Kümmel, *Phys. Rev. Lett.* **94**, 143003 (2005).
 [9] R. Cuevas-Saavedra and V. N. Staroverov, *Mol. Phys.* **114**, 1050 (2016).
 [10] J. D. Ramsden and R. W. Godby, *Phys. Rev. Lett.* **109**, 036402 (2012).
 [11] S. V. Kohut, I. G. Ryabinkin, and V. N. Staroverov, *J. Chem. Phys.* **140**, 18A535 (2014).
 [12] I. Grabowski, E. Fabiano, A. M. Teale, S. Smiga, A. Buksztel, and F. D. Sala, *J. Chem. Phys.* **141**, 024113 (2014).
 [13] P. Verma and R. J. Bartlett, *J. Chem. Phys.* **140**, 18A534 (2014).
 [14] O. V. Gritsenko, L. M. Mentel, and E. J. Baerends, *J. Chem. Phys.* **144**, 204114 (2016).
 [15] S. Smiga, F. Della Sala, A. Buksztel, I. Grabowski, and E. Fabiano, *J. Comput. Chem.* **37**, 2081 (2016).
 [16] J. P. Perdew, R. G. Parr, M. Levy, and J. L. Balduz, *Phys. Rev. Lett.* **49**, 1691 (1982).
 [17] M. Mundt and S. Kümmel, *Phys. Rev. Lett.* **95**, 203004 (2005).
 [18] M. Thiele, E. K. U. Gross, and S. Kümmel, *Phys. Rev. Lett.* **100**, 153004 (2008).
 [19] M. Hellgren and E. K. U. Gross, *Phys. Rev. A* **85**, 022514 (2012).
 [20] P. Elliott, J. I. Fuks, A. Rubio, and N. T. Maitra, *Phys. Rev. Lett.* **109**, 266404 (2012).
 [21] T. Dimitrov, H. Appel, J. I. Fuks, and A. Rubio, *New J. Phys.* **18**, 083004 (2016).
 [22] S. V. Kohut, A. M. Polgar, and V. N. Staroverov, *Phys. Chem. Chem. Phys.* **18**, 20938 (2016).
 [23] N. Maitra, *J. Chem. Phys.* **144**, 220901 (2016).
 [24] D. Hofmann and S. Kümmel, *Phys. Rev. B* **86**, 201109 (2012).
 [25] F. Della Sala and A. Görling, *Phys. Rev. Lett.* **89**, 033003 (2002).
 [26] F. Della Sala and A. Görling, *J. Chem. Phys.* **116**, 5374 (2002).
 [27] S. Kümmel and J. P. Perdew, *Phys. Rev. Lett.* **90**, 043004 (2003).
 [28] S. Kümmel and J. P. Perdew, *Phys. Rev. B* **68**, 035103 (2003).
 [29] P. Gori-Giorgi, T. Gál, and E. J. Baerends, *Mol. Phys.* **114**, 1086 (2016).
 [30] D. J. Tozer, *J. Chem. Phys.* **119**, 12697 (2003).
 [31] S. Kümmel, L. Kronik, and J. P. Perdew, *Phys. Rev. Lett.* **93**, 213002 (2004).
 [32] F. Wilken and D. Bauer, *Phys. Rev. Lett.* **97**, 203001 (2006).
 [33] S. R. Whittleton, X. A. S. Vazquez, C. M. Isborn, and E. R. Johnson, *J. Chem. Phys.* **142**, 184106 (2015).
 [34] A. D. Becke and M. R. Roussel, *Phys. Rev. A* **39**, 3761 (1989).
 [35] R. van Leeuwen and E. J. Baerends, *Phys. Rev. A* **49**, 2421 (1994).
 [36] A. D. Becke and E. R. Johnson, *J. Chem. Phys.* **124**, 221101 (2006).
 [37] A. P. Gaiduk and V. N. Staroverov, *J. Chem. Phys.* **128**, 204101 (2008).
 [38] V. N. Staroverov, *J. Chem. Phys.* **129**, 134103 (2008).
 [39] R. Armiento, S. Kümmel, and T. Körzdörfer, *Phys. Rev. B* **77**, 165106 (2008).
 [40] F. Tran, P. Blaha, M. Betzinger, and S. Blügel, *Phys. Rev. B* **91**, 165121 (2015).
 [41] E. Räsänen, S. Pittalis, and C. R. Proetto, *J. Chem. Phys.* **132**, 044112 (2010).
 [42] F. Tran, P. Blaha, and K. Schwarz, *J. Chem. Theory Comput.* **11**, 4717 (2015).
 [43] J. D. Gledhill and D. J. Tozer, *J. Chem. Phys.* **143**, 024104 (2015).
 [44] J. Carmona-Espindola, J. L. Gázquez, A. Vela, and S. B. Trickey, *J. Chem. Phys.* **142**, 054105 (2015).
 [45] F. Tran, P. Blaha, M. Betzinger, and S. Blügel, *Phys. Rev. B* **94**, 165149 (2016).
 [46] O. Gritsenko, R. van Leeuwen, E. van Lenthe, and E. J. Baerends, *Phys. Rev. A* **51**, 1944 (1995).
 [47] M. Kuisma, J. Ojanen, J. Enkovaara, and T. T. Rantala, *Phys. Rev. B* **82**, 115106 (2010).
 [48] F. Tran and P. Blaha, *Phys. Rev. Lett.* **102**, 226401 (2009).
 [49] D. Koller, F. Tran, and P. Blaha, *Phys. Rev. B* **85**, 155109 (2012).
 [50] F. Tran, P. Blaha, and K. Schwarz, *J. Phys.: Condens. Matter* **19**, 196208 (2007).
 [51] A. P. Gaiduk and V. N. Staroverov, *J. Chem. Phys.* **131**, 044107 (2009).
 [52] A. Karolewski, R. Armiento, and S. Kümmel, *J. Chem. Theory Comput.* **5**, 712 (2009).
 [53] M. Mundt, S. Kümmel, R. van Leeuwen, and P.-G. Reinhard, *Phys. Rev. A* **75**, 050501(R) (2007).
 [54] A. Karolewski, R. Armiento, and S. Kümmel, *Phys. Rev. A* **88**, 052519 (2013).
 [55] R. Armiento and S. Kümmel, *Phys. Rev. Lett.* **111**, 036402 (2013).
 [56] J. P. Perdew and Y. Wang, *Phys. Rev. B* **33**, 8800 (1986).
 [57] J. C. Slater, *Phys. Rev.* **81**, 385 (1951).
 [58] T. Kreibich, S. Kurth, T. Grabo, and E. K. U. Gross, *Adv. Quantum Chem.* **33**, 31 (1998).
 [59] M. Levy, J. P. Perdew, and V. Sahni, *Phys. Rev. A* **30**, 2745 (1984).
 [60] V. Vlček, G. Steinle-Neumann, L. Leppert, R. Armiento, and S. Kümmel, *Phys. Rev. B* **91**, 035107 (2015).
 [61] S. Kümmel and L. Kronik, *Rev. Mod. Phys.* **80**, 3 (2008).
 [62] C.-O. Almbladh and U. von Barth, *Phys. Rev. B* **31**, 3231 (1985).
 [63] G. Zhang and C. B. Musgrave, *J. Phys. Chem. A* **111**, 1554 (2007).

- [64] J. D. Talman and W. F. Shadwick, *Phys. Rev. A* **14**, 36 (1976).
- [65] J. F. Janak, *Phys. Rev. B* **18**, 7165 (1978).
- [66] References [100,101] discuss that when going from integer to fractional particle numbers, there are different options for how to generalize a given functional to the ensemble case. Here we use the common definition and insert the density that integrates a fractional electron number into the regular functional expression.
- [67] J. B. Krieger, Y. Li, and G. J. Iafrate, *Phys. Rev. A* **46**, 5453 (1992).
- [68] T. Aschebroek, R. Armiento, and S. Kümmel, *Phys. Rev. B* **95**, 245118 (2017).
- [69] A. Makmal, S. Kümmel, and L. Kronik, *J. Chem. Theory Comput.* **5**, 1731 (2009).
- [70] T. F. T. Cerqueira, M. J. T. Oliveira, and M. A. L. Marques, *J. Chem. Theory Comput.* **10**, 5625 (2014).
- [71] J. P. Perdew, K. Burke, and M. Ernzerhof, *Phys. Rev. Lett.* **77**, 3865 (1996).
- [72] A. Lindmaa and R. Armiento, *Phys. Rev. B* **94**, 155143 (2016).
- [73] A. D. Becke, *Phys. Rev. A* **38**, 3098 (1988).
- [74] While this is the case for LDA and EXX in the KLI approximation, for EXX (OEP) the orbital in question moves up in the energetic order from fifth- to third-highest occupied orbital.
- [75] S. J. A. van Gisbergen, P. R. T. Schipper, O. V. Gritsenko, E. J. Baerends, J. G. Snijders, B. Champagne, and B. Kirtman, *Phys. Rev. Lett.* **83**, 694 (1999).
- [76] S. Kümmel and L. Kronik, *Comput. Mater. Sci.* **35**, 321 (2006).
- [77] B. Champagne, D. H. Mosley, M. Vračko, and J.-M. André, *Phys. Rev. A* **52**, 178 (1995).
- [78] M. Gruning, O. V. Gritsenko, and E. J. Baerends, *J. Chem. Phys.* **116**, 6435 (2002).
- [79] M. van Faassen, P. L. de Boeij, R. van Leeuwen, J. A. Berger, and J. G. Snijders, *Phys. Rev. Lett.* **88**, 186401 (2002).
- [80] P. Mori-Sánchez, Q. Wu, and W. Yang, *J. Chem. Phys.* **119**, 11001 (2003).
- [81] P. Umari, A. J. Williamson, G. Galli, and N. Marzari, *Phys. Rev. Lett.* **95**, 207602 (2005).
- [82] N. T. Maitra and M. van Faassen, *J. Chem. Phys.* **126**, 191106 (2007).
- [83] T. Körzdörfer, M. Mundt, and S. Kümmel, *Phys. Rev. Lett.* **100**, 133004 (2008).
- [84] A. Ruzsinszky, J. P. Perdew, G. I. Csonka, G. E. Scuseria, and O. A. Vydrov, *Phys. Rev. A* **77**, 060502(R) (2008).
- [85] C. D. Pemmaraju, S. Sanvito, and K. Burke, *Phys. Rev. B* **77**, 121204(R) (2008).
- [86] B. Champagne and B. Kirtman, *Int. J. Quantum Chem.* **109**, 3103 (2009).
- [87] T. Körzdörfer and S. Kümmel, in *Theoretical and Computational Developments in Modern Density Functional Theory*, edited by A. K. Roy (Nova Science, New York, 2012), pp. 211–222.
- [88] L. Kronik, A. Makmal, M. L. Tiago, M. M. G. Alemany, M. Jain, X. Huang, Y. Saad, and J. R. Chelikowsky, *Phys. Status Solidi B* **243**, 1063 (2006).
- [89] F. Gygi, *Phys. Rev. B* **48**, 11692 (1993).
- [90] F. Hofmann (unpublished).
- [91] J. R. Chelikowsky, N. Troullier, and Y. Saad, *Phys. Rev. Lett.* **72**, 1240 (1994).
- [92] F. Calvayrac, P.-G. Reinhard, E. Suraud, and C. A. Ullrich, *Phys. Rep.* **337**, 493 (2000).
- [93] M. A. L. Marques, A. Castro, G. F. Bertsch, and A. Rubio, *Comput. Phys. Commun.* **151**, 60 (2003).
- [94] S. Kümmel, *J. Comput. Phys.* **201**, 333 (2004).
- [95] J. C. Slater, *Phys. Rev.* **36**, 57 (1930).
- [96] S. F. Boys, *Proc. R. Soc. London A* **200**, 542 (1950).
- [97] R. McWeeny, *Nature (London)* **166**, 21 (1950).
- [98] F. G. Eich and M. Hellgren, *J. Chem. Phys.* **141**, 224107 (2014).
- [99] G. L. Oliver and J. P. Perdew, *Phys. Rev. A* **20**, 397 (1979).
- [100] E. Kraisler and L. Kronik, *Phys. Rev. Lett.* **110**, 126403 (2013).
- [101] A. Görling, *Phys. Rev. B* **91**, 245120 (2015).

Publication 3

Ultranonlocality and accurate band gaps from a meta-generalized gradient approximation

Physical Review Research **1**, 033082 (2019)

Thilo Aschebrock and Stephan Kümmel

Theoretical Physics IV, University of Bayreuth, 95440 Bayreuth, Germany

Publ. 3

My contribution

I developed both density functionals presented in this manuscript. I implemented relevant routines in BAND, BTDFD, DARSEC, and PARSEC. I performed all calculations, prepared all figures, and wrote a first draft of the manuscript and of the supplemental material.

Publ.3

Ultranonlocality and accurate band gaps from a meta-generalized gradient approximation

Thilo Aschebrock  and Stephan Kümmel ^{*}

Theoretical Physics IV, University of Bayreuth, 95440 Bayreuth, Germany



(Received 12 April 2019; revised manuscript received 1 July 2019; published 6 November 2019)

The proper description of step structures in the exchange correlation potential, of charge localization, and a reasonable prediction of band gaps have been long-standing, serious challenges for semilocal density functionals. In practice, obtaining all of these properties from the functional derivative of an energy functional was possible only at the price of incorporating exact exchange. We here show that they can be achieved at significantly lower, semilocal computational expense by using kinetic-energy density-dependent functionals. The key to obtaining these features is a functional construction strategy that focuses on the derivative discontinuity and the density response.

DOI: [10.1103/PhysRevResearch.1.033082](https://doi.org/10.1103/PhysRevResearch.1.033082)

I. INTRODUCTION

The success of density functional theory (DFT) is based on its favorable ratio of accuracy to computational cost. Semilocal functionals such as generalized gradient approximations (GGAs) [1–5] are to this day popular in solid-state physics and material science because of their moderate computational cost. They also continue to play a role, especially for large-scale applications, in the molecular sciences, where hybrid functionals [6] have become the standard functionals for systems of small to moderate size. However, DFT based on semilocal functionals has also faced notorious problems, with prime examples known since the early days of DFT. In solid-state physics, the prediction of the fundamental (band) gap is an intrinsic limitation of explicit density-dependent semilocal functionals [7,8]. In material science, the proper description of charge localization and charge distributions between subsystems is a major challenge [9,10] that affects many problems, e.g., surface adsorption [11,12]. In molecular physics and chemistry, missing field-counteracting terms have serious, detrimental consequences for the calculation of polarizabilities, hyperpolarizabilities, and charge transfer [13–15]. These problems originate from several fundamental shortcomings that are closely interconnected: a missing derivative discontinuity [16–18], a lack of step structures in the exchange correlation (xc) potential [19–22], and the delocalization error [23,24]. Density-driven errors [25,26] characterize many of these problems.

The standard approach to overcome the limitations is turning to functionals that are nonlocal. Self-interaction corrections can restore nonlocality [27–31], but the dominant

and highly successful strategy of incorporating nonlocality has been the use of exact (Fock) exchange. By exploiting the adiabatic connection, yet higher accuracy can be reached [32], with DFT starting to rival wave-function-based methods in accuracy. However, the accuracy comes at a steep increase in computational cost. A standard hybrid functional is computationally already much more demanding than a GGA. Therefore, calculations incorporating Fock exchange are restricted to much smaller systems than semilocal calculations. This restriction can have serious consequences because often the interesting features of real-world systems, especially in the realm of nanomolecular and supramolecular science, stem from an intrinsic complexity that requires the explicit treatment of a large number of particles. Understanding light-harvesting systems [33–35] is a paradigm example: it requires calculating energy and charge transfer through arrays of dozens of chromophores, where each chromophore typically has hundreds of electrons. The chromophores in turn are typically embedded in a protein matrix, at least parts of which should also be taken into account explicitly [33,35–37]. However, semilocal functionals are currently at their limits for such systems due to their inability to properly describe charge transfer [38–40]. Therefore, there is a serious need for functionals that do not suffer from the large, qualitative errors that traditional semilocal functionals plague, yet come at a comparable computational price.

Here we demonstrate that one can achieve this with functionals that depend on the noninteracting kinetic energy density

$$\tau(\mathbf{r}) = \frac{\hbar^2}{2m} \sum_{i=1}^N |\nabla \varphi_i(\mathbf{r})|^2. \quad (1)$$

These so-called meta-GGAs are well established and their development has become an impressive success story [41–56]. They are the natural candidates for curing the above-mentioned deficiencies because the explicit use of the (occupied) orbitals creates nonlocality since each $\varphi_i(\mathbf{r})$ depends on the density $n(\mathbf{r}')$ at all points \mathbf{r}' . Yet, their computational cost is manifestly semilocal. In the following, we show how

^{*}Corresponding author: stephan.kuettel@uni-bayreuth.de;
<http://www.tp4.uni-bayreuth.de/en>

Published by the American Physical Society under the terms of the Creative Commons Attribution 4.0 International license. Further distribution of this work must maintain attribution to the author(s) and the published article's title, journal citation, and DOI.

meta-GGA nonlocality can be led to unfold by focusing on the potential response and derivative discontinuity features.

Focusing the xc functional development less on the energy and also on the density or potential has already been advocated in principle [57–59] in the past, but in practice relied on expensive functionals [58,60,61]. The development of model potentials [62–66] has demonstrated that beneficial properties can be achieved semilocally. However, model potentials lack a corresponding energy functional and are not functional derivatives [63,67–69]. Furthermore, many of these constructions, as well as the attempt to restore the functional derivative property within the GGA form [70], lead to divergences [71–73]. Moreover, such purely multiplicative potentials are formally inappropriate to yield the fundamental gap [74].

The meta-GGA form allows to bring these earlier approaches to a unifying success. To this end, we write the exchange energy in the form

$$E_x^{\text{mGGA}}[n] = A_x \int n^{4/3} F_x(s, \alpha) d^3r, \quad (2)$$

where as usual $A_x = -(3e^2/4)(3/\pi)^{1/3}$, thereby satisfying the correct uniform coordinate density-scaling behavior [75]. Here the enhancement factor $F_x(s, \alpha)$ is parametrized by the dimensionless variables

$$s = \frac{|\nabla n|}{2(3\pi^2)^{1/3} n^{4/3}} \quad (3)$$

and [51–54,76,77]

$$\alpha = (\tau - \tau^W)/\tau^{\text{unif}}, \quad (4)$$

where the von Weizsäcker kinetic energy density

$$\tau^W = \frac{\hbar^2}{8m} \frac{|\nabla n|^2}{n} \quad (5)$$

is the single-orbital limit of τ and $\tau^{\text{unif}} = A_s n^{5/3}$ with $A_s = (3\hbar^2/10m)(3\pi^2)^{2/3}$ its uniform-density limit. Spin polarization can be accounted for via the spin-scaling relation for exchange [78].

II. ORIGIN OF ULTRANONLOCALITY

In order to demonstrate that crucial (ultra)nonlocal features of exact exchange (EXX) can be captured by a meta-GGA, we recall that the EXX Kohn-Sham (KS) potential for a spin-saturated N -electron system

$$\begin{aligned} v_x^{\text{EXX}}(\mathbf{r}) &= e^2 \int \frac{n_x^{\text{EXX}}(\mathbf{r}, \mathbf{r}')}{|\mathbf{r} - \mathbf{r}'|} d^3r' \\ &+ \frac{1}{n(\mathbf{r})} \sum_{i=1}^{N/2} \left\{ |\varphi_i(\mathbf{r})|^2 (\bar{v}_{xi}^{\text{EXX}} - \bar{u}_{xi}^{\text{EXX}}) \right. \\ &\left. - \frac{\hbar^2}{m} \nabla \cdot [\psi_i^*(\mathbf{r}) \nabla \varphi_i(\mathbf{r})] \right\} + \text{c.c.} \end{aligned} \quad (6)$$

can be decomposed [79] into the smooth Coulomb potential of the EXX hole n_x^{EXX} (first term) and the response potential (second term). Here, a short overscore with index i denotes

taking the expectation value with the i th orbital. Furthermore,

$$u_{xi}^{\text{EXX}}(\mathbf{r}) = \frac{1}{\varphi_i^*(\mathbf{r})} \frac{\delta E_x^{\text{EXX}}[n]}{\delta \varphi_i(\mathbf{r})} \quad (7)$$

is the associated orbital-specific potential and $\psi_i(\mathbf{r})$ denotes the usual orbital shift of optimized effective potential (OEP) theory [80,81]. Hallmark nonlocal features of EXX result from the response potential [13,15,79,82,83], in particular from the orbital-average terms on the right of Eq. (6). Note that the KS potential retains the very same mathematical structure [84] when the EXX energy is replaced by another orbital-dependent energy functional, e.g., a meta-GGA. The only difference is that EXX quantities are replaced by the corresponding meta-GGA quantities, e.g.,

$$u_{xi}^{\text{mGGA}}(\mathbf{r}) = \frac{1}{\varphi_i^*(\mathbf{r})} \frac{\delta E_x^{\text{mGGA}}[n]}{\delta \varphi_i(\mathbf{r})}. \quad (8)$$

Thus, it is clear that, in principle, a meta-GGA can incorporate ultranonlocal features because the ultranonlocality of the potential stems from the orbital-average terms. For EXX, this nonlocality is enhanced by the Fock integrals. As meta-GGAs lack such integrals, one has to take special care to embed the nonlocality in the $\bar{v}_{xi}^{\text{mGGA}} - \bar{u}_{xi}^{\text{mGGA}}$ terms with proper magnitude and sign.

Guidance on how this can be achieved can be found by recalling that the ultranonlocality in the KS potential is closely connected [15,85] to the derivative discontinuity

$$\Delta_x = v_x(\mathbf{r})|_+ - v_x(\mathbf{r})|_- = \left. \frac{\delta E_x[n]}{\delta n(\mathbf{r})} \right|_+ - \left. \frac{\delta E_x[n]}{\delta n(\mathbf{r})} \right|_-, \quad (9)$$

where the positive and negative signs denote evaluation of the functional derivative approaching the integer particle number from above and below, respectively. All experience to date is in line with $\Delta_x \geq 0$ [7,86,87]. When evaluating the functional derivative of a meta-GGA,

$$\begin{aligned} \frac{\delta E_x^{\text{mGGA}}[n]}{\delta n(\mathbf{r})} &= \frac{\delta}{\delta n(\mathbf{r})} \int e_x(n, \nabla n, \tau) d^3r' \\ &= \frac{\partial e_x}{\partial n}(\mathbf{r}) - \nabla \cdot \left[\frac{\partial e_x}{\partial \nabla n}(\mathbf{r}) \right] \\ &+ \int \frac{\partial e_x}{\partial \tau}(\mathbf{r}') \frac{\delta \tau(\mathbf{r}')}{\delta n(\mathbf{r})} d^3r', \end{aligned} \quad (10)$$

only the τ dependence contributes to the derivative discontinuity as the first two terms correspond to the ones found in a usual GGA potential and originate from the explicit density dependence [85]. Therefore, and since $n(\mathbf{r}) = n(\mathbf{r})|_- = n(\mathbf{r})|_+$ as well as $\tau(\mathbf{r}) = \tau(\mathbf{r})|_- = \tau(\mathbf{r})|_+$,

$$\Delta_x^{\text{mGGA}} = \int \frac{\partial e_x}{\partial \tau}(\mathbf{r}') \left[\left. \frac{\delta \tau(\mathbf{r}')}{\delta n(\mathbf{r})} \right|_+ - \left. \frac{\delta \tau(\mathbf{r}')}{\delta n(\mathbf{r})} \right|_- \right] d^3r'. \quad (11)$$

In order to simplify this into a transparent expression, we assume (similar to previous work [88]) that the first factor can be approximated by its average over the energetically relevant region of space. Thus,

$$\Delta_x^{\text{mGGA}} \approx \overline{\frac{\partial e_x}{\partial \tau}} \left[\left. \frac{\delta T_s[n]}{\delta n(\mathbf{r})} \right|_+ - \left. \frac{\delta T_s[n]}{\delta n(\mathbf{r})} \right|_- \right] = \overline{\frac{\partial e_x}{\partial \tau}} \Delta_s, \quad (12)$$

where $T_s[n]$ is the usual noninteracting kinetic energy functional and Δ_s the corresponding non-negative KS gap. Equation (12) thus establishes a link between the magnitude and sign of $\partial e_x/\partial\tau$ and Δ_x^{mGGA} .¹

A meta-GGA with a sizable discontinuity of proper sign can therefore be constructed by requesting

$$\partial e_x/\partial\tau > 0, \quad (13)$$

as this ensures

$$\overline{\partial e_x/\partial\tau} > 0 \quad (14)$$

for any system. For a parametrization in s and α [cf. Eq. (2)],

$$\frac{\partial e_x}{\partial\tau} = \frac{A_x}{A_s} \frac{1}{n^{1/3}} \frac{\partial F_x}{\partial\alpha}. \quad (15)$$

With A_s and n positive and $A_x < 0$, a positive Δ_x^{mGGA} follows from

$$\partial F_x/\partial\alpha < 0, \quad (16)$$

and a larger negative slope in the energetically relevant regions of space can be expected to lead to a larger Δ_x^{mGGA} . We further note that the sign in Eq. (16) goes well along with the conjectured strongly tightened bound

$$F_x(s, \alpha) \leq F_x(s, \alpha = 0) \leq 1.174 \quad (17)$$

for all α [89]. It is also in line with the observations of ultranonlocality for the polarization dependence of solids [90] in the meta-GGA kernel [88] (see the detailed discussion in Appendix C). Furthermore, as α is a well-established measure of electron localization [51,91,92], Eq. (16) can be interpreted as a condition to energetically favor electron localization via the exchange energy, as EXX does.

III. PROOF OF CONCEPT

In order to demonstrate how these findings can be used in actual meta-GGA construction, we proceed in two steps. First, as a proof of concept (PoC) we discuss the simple, conceptual enhancement factor

$$F_x^{\text{PoC}}(\alpha) = c_H - c_1\alpha/(1 + c_2\alpha) \quad (18)$$

which uses only α and three parameters. This will not yield a generally useful functional, but allows to clearly demonstrate the connection between Eq. (16) and practically important manifestations of meta-GGA (ultra)nonlocality. We chose

$$c_H = \frac{40}{81} \left(\frac{4\pi^2}{3} \right)^{1/3} \quad (19)$$

to obtain the correct hydrogen atom energy (cf. Appendix B for a derivation). The parameters c_1 and c_2 determine the slope and the curvature of $F_x^{\text{PoC}}(\alpha)$ and will be discussed in the following.

¹Note that the above arguments do not exclude the possibility that $\Delta_x^{\text{mGGA}} \neq 0$ for $\Delta_s = 0$; the former is in principle possible when ones go beyond the averaging approximation of Eq. (12). Further note that the argument formulated here for Δ_x can readily be extended to Δ_{xc} .

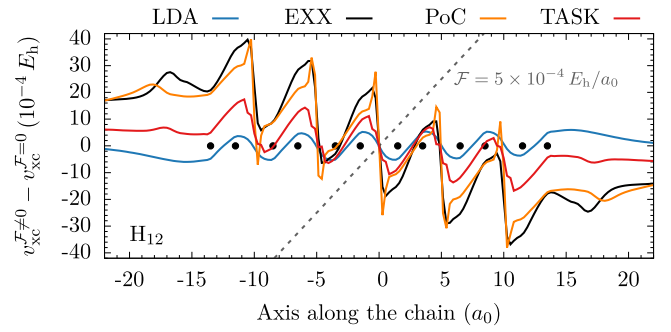


FIG. 1. Difference between the $x(c)$ potentials (OEP) with and without a homogeneous external electric field for a chain of 12 hydrogen atoms at alternating distances of $2a_0$ and $3a_0$ (cf. Appendix D for computational details).

As a challenging, paradigm test of nonlocality we analyze the response potential of hydrogen chains [13,30,97–103]. Figure 1 shows the potential response obtained from LDA and EXX for a H_{12} chain in a static electric field, demonstrating the well-known field-counteracting term of EXX [13] and its absence in LDA. The striking observation in Fig. 1 is that F_x^{PoC} can achieve a potential response that is very close to the one of EXX with a suitable choice of parameters, namely, $c_1 = 27/40$ and $c_2 = c_1/(3 + c_H)$. Table I shows that the polarizabilities for hydrogen chains obtained with this F_x^{PoC} are close to the coupled-cluster (CCSDT) reference values for all chain lengths. Hence, this meta-GGA exhibits the correct trend with increasing chain length that so far has not been accessible with any semilocal functional due to the lack of the field-counteracting term. This is a proof of concept that even a simple meta-GGA can yield strong ultranonlocality.

Furthermore, this simple meta-GGA allows to transparently and explicitly demonstrate the relation between the derivative $\partial F_x/\partial\alpha$ and the field-counteracting term in the KS potential. By choosing different values for the parameters c_1 and c_2 , different slopes in α can easily be realized. For a first alternative (1st alt.) PoC meta-GGA we opt for the opposite slope at $\alpha = 0$ compared to the original (orig.) PoC

TABLE I. Polarizability calculated from the dipole moment in a_0^{-3} for hydrogen chains of different length and $x(c)$ energy functionals. CCSD(T) values from Ref. [94]. DFT calculations were performed self-consistently in a locally modified version of PARSEC [95,96], orbital-dependent functionals treated in full OEP unless noted otherwise (cf. Appendix D).

| | H ₄ | H ₆ | H ₈ | H ₁₂ | H ₁₈ |
|------------------------|----------------|----------------|----------------|-----------------|-----------------|
| LDA (xc) [93] | 37.6 | 72.8 | 115.0 | 211.4 | 369 |
| PKZB (xc) [45] | 35.5 | 65.8 | 105.1 | 189.1 | 323 |
| τ -HCTH (xc) [46] | 35.7 | 68.6 | 96.9 | 194.3 | 335 |
| MVS (x) [54] | 34.0 | 63.6 | 102.3 | 181.5 | 308 |
| SCAN (xc) [52] | 35.4 | 67.8 | 106.6 | 192.3 | 329 |
| TASK (x) | 34.0 | 62.9 | 96.2 | 169.8 | 286 |
| PoC (x) | 30.3 | 51.6 | 74.4 | 121.7 | 194 |
| EXX (x) | 32.1 | 56.5 | 83.0 | 138.7 | 225 |
| CCSD(T) | 28.8 | 50.5 | 74.1 | 123.6 | 200 |

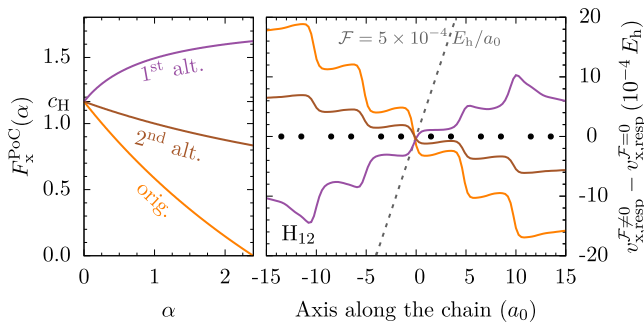


FIG. 2. Explicit demonstration of the relation between $\partial F_x/\partial\alpha$ and the field-counteracting term in $v_x(\mathbf{r})$. Left: original and alternative PoC enhancement factors. Right: difference between the exchange response potentials (KLI) with and without a homogeneous external electric field of strength $\mathcal{F} = 5 \times 10^{-4} E_h/a_0$ for the H_{12} chain evaluated with the respective enhancement factors.

and use the Lieb-Oxford bound [104] as a natural limiting value for $\alpha \rightarrow \infty$ and thus as the upper bound. This leads to $c_1 = -27/40$ and $c_2 = -c_1/(1.804 - c_H)$. The left panel of Fig. 2 shows the resulting 1st alt. PoC enhancement factor as a function of α . It has a strictly positive slope, contrary to the strictly negative one of the orig. PoC meta-GGA. The right panel of Fig. 2 displays the difference between the exchange response potential [in Krieger-Li-Iafrate (KLI) approximation [82]] [cf. decomposition in hole and response potential as in Eq. (6), with and without a homogeneous external electric field for the H_{12} chain]. While the orig. PoC meta-GGA exhibits a pronounced field-counteracting behavior, the 1st alt. PoC meta-GGA also displays substantial ultranonicity in the potential, but with the opposite sign and thus unphysically enhances the external field. This clearly demonstrates the link between $\partial F_x/\partial\alpha < 0$ and the field-counteracting term in the KS potential. In similar fashion one can transparently alter the slope $\partial F_x/\partial\alpha$ in the PoC meta-GGA form to show that the amplitude of $\partial F_x/\partial\alpha$ is directly correlated to the amplitude of the field-counteracting term in the KS potential. To this end, we construct a second alternative (2nd alt.) PoC meta-GGA with $c_1 = c_H(c_H - 1)$ and $c_2 = c_H - 1$, where these parameters are determined by the homogeneous electron gas limit, $F_x(\alpha = 1) = 1$, and by the negativity of exchange energy density, i.e., $\lim_{\alpha \rightarrow \infty} F_x(\alpha) = 0$. Figure 2 shows that the restricted slope of $F_x(\alpha)$ of this 2nd alt. PoC meta-GGA also limits the amplitude of the field-counteracting term in the KS potential.

Another stringent test of discontinuity features that probes the delocalization problem is defined by the H_8 - H_8 system of Ref. [9]. To the best of our knowledge, no semilocal functional to date has passed this test and even regular and local hybrids fail it [9,105]. Two aligned, but well-separated hydrogen chains are exposed to a constant external electric field of increasing strength in a series of ground-state calculations. As the field strength increases, charge eventually transfers from one chain to the other. Due to their large separation of 8 \AA , integer preference [106] must be preserved, i.e., charge transfer should only occur via integer electron jumps at specific field strengths. However, as shown in the upper panel of Fig. 3, the local density approximation (LDA) leads to a gradual transfer of fractional charges, and usual semilocal

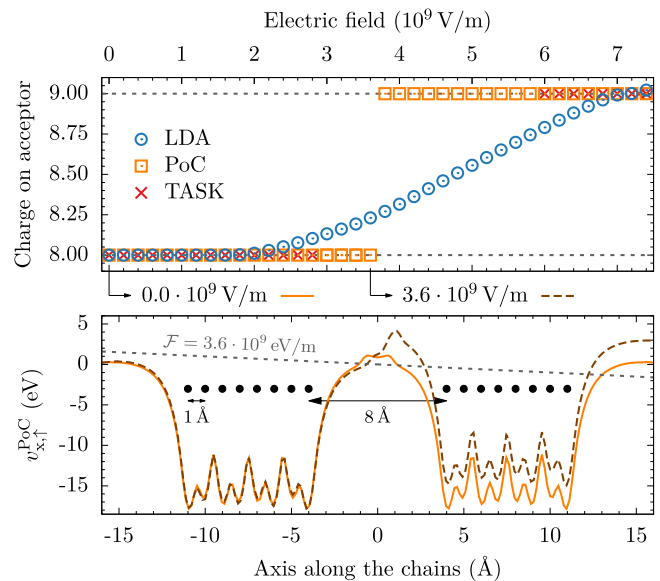


FIG. 3. Top: integrated (unsigned) charge on the H_8 acceptor as a function of the external field for LDA, as well as the PoC and TASK meta-GGAs. Bottom: plots of the exchange potential revealing the step structure in the PoC meta-GGA, by which the principle of integer preference is enforced. See Appendix E for computational details.

functionals and hybrids show similar behavior [9]. The upper panel of Fig. 3 shows that F_x^{PoC} (with the same choice of parameters that lead to good hydrogen chain polarizabilities) also correctly restores integer preference. If a step function would be used as an external field and the chains would be infinitely far apart, the critical step size associated with an integer electron transfer would be given directly [17] by the fundamental gap

$$I - A = \Delta_s + \Delta_{xc} \quad (20)$$

of a single H_8 chain. The situation considered here is more complex due to the finite distance as well as the linear field that induces a considerable polarization of both chains. Nevertheless, the Δ_{xc} contribution remains pivotal for a correct description of this charge transfer within KS theory. It manifests itself in the KS potential [21] as depicted in the lower panel of Fig. 3, which demonstrates that F_x^{PoC} leads to the right properties for the right reason: At $\mathcal{F} = 3.6 \times 10^9 \text{ eV/m}$, which would lead to a fractional charge transfer for any conventional semilocal functional, a pronounced step structure that counteracts the charge transfer is observed. Similarly, after the jump a potential step with opposite sign stabilizes the charge transfer. This is exactly the behavior that EXX exhibits and by which a nonlocal self-interaction correction cures the charge-transfer problem [21].

IV. TASK: A GENERAL PURPOSE META-GGA

After this proof of concept as to how nonlocality can be achieved in meta-GGA construction, we take a second step and devise a more generally useful meta-GGA for exchange that features nonlocality. The outer framework of this functional, named TASK for the initials of the authors, is adopted

from the exchange part of the SCAN meta-GGA [52] and reads as

$$F_x^{\text{TASK}}(s, \alpha) = h_x^0 g_x(s) + [1 - f_x(\alpha)] [h_x^1(s) - h_x^0] [g_x(s)]^d. \quad (21)$$

We likewise choose

$$F_x \leq h_x^0 = 1.174 \quad (22)$$

as an upper bound, thereby obeying the rigorous strongly tightened bound [89] for $\alpha = 0$, as well as the more strict conjectured bound given by Eq. (17). By implying $f_x(\alpha = 0) = 1$ this meta-GGA is identical to SCAN for one-orbital systems ($\alpha = 0$), with

$$g_x(s) = 1 - \exp(-cs^{-1/2}), \quad (23)$$

where $c = 4.9479$ was obtained to recover the exact hydrogen atom energy. Moreover, $g_x(s)$ governs $F_x(s, \alpha)$ for $s \rightarrow \infty$ and vanishes like $s^{-1/2}$ [89], making the exchange energy per particle scale correctly to a negative constant under nonuniform coordinate scaling to the true two-dimensional limit [107,108].

We chose $h_x^1(s)$ to only depend on s . In this way, we can readily satisfy the construction principle of a negative slope in α of sizable magnitude [cf. Eq. (16)] to preserve the desired field-counteracting properties. Furthermore, we determine $f_x(\alpha)$ and $h_x^1(s)$ by recovering the fourth-order gradient expansion (GE4) for exchange [109], valid for slowly varying densities with small s and $\alpha \approx 1$. We do this in a way, however, that deviates decisively from SCAN, where the GE4 is solely recovered by h_x^1 and without a leading-order contribution of α , as $f_x(\alpha)$ is chosen to be flat, i.e., to vanish in any power of ∇n . Our aim, however, is to fulfill Eq. (16) with an appreciable slope, and therefore we require nonvanishing GE4 contributions of $f_x(\alpha)$ and thus α to all relevant orders. To this end, we start from the general expression for the gradient expansion around $s = 0$ and $\alpha = 1$,

$$F_x^{\text{GE4}}(s, \alpha) \sim 1 + \mu_s s^2 + \mu_\alpha (\alpha - 1) + C_s s^4 + C_{s\alpha} s^2 (\alpha - 1) + C_\alpha (\alpha - 1)^2 + \mathcal{O}(\nabla^6), \quad (24)$$

and then make use of the GE4 of τ [110,111] as detailed in Appendix A. Comparison with the usual GE4 for exchange then leads to the coefficients

$$\mu_s = \frac{10 + 60\mu_\alpha}{81}, \quad C_s = -\frac{1606 - 50\mu_\alpha}{18225}, \quad (25)$$

$$C_{s\alpha} = -\frac{511 - 50\mu_\alpha}{13500}, \quad C_\alpha = \frac{73 - 50\mu_\alpha}{5000} \quad (26)$$

and one degree of freedom, the choice of μ_α . However, due to the separation of variables with respect to s and α in our ansatz for the enhancement factor of Eq. (21), the mixed fourth-order term in the GE4 of Eq. (24) is generated by multiplication and is thereby not independent of the second-order terms. Therefore, in our construction, the corresponding mixed coefficient $C_{s\alpha}$ is directly linked to the second-order coefficients via

$$\mu_s \mu_\alpha = (1 - h_x^0) C_{s\alpha}, \quad (27)$$

which implies two possible values for μ_α :

$$\mu_\alpha^\pm = -\frac{97 + 3h_x^0 \pm \sqrt{9(h_x^0)^2 + 74166h_x^0 - 64175}}{1200}. \quad (28)$$

To obtain a sizable derivative discontinuity we choose the more negative solution

$$\mu_\alpha = \mu_\alpha^+ \approx -0.209897, \quad (29)$$

and, thus, a pronounced negative slope in α in accordance with Eq. (16).

To satisfy the listed constraints while obtaining a smooth $F_x(s, \alpha)$, we choose the following ansatz:

$$h_x^1(s) = \sum_{\nu=0}^2 a_\nu R_\nu(s^2), \quad f_x(\alpha) = \sum_{\nu=0}^4 b_\nu R_\nu(\alpha), \quad (30)$$

which is based on Chebyshev rational functions [112,113] $R_\nu(x)$ of degree ν . The eight coefficients are determined by

$$h_x^1(0) = 1, \quad f_x(0) = 1, \quad f_x(1) = 0 \quad (31)$$

as well as the values of

$$\left. \frac{\partial^2 h_x^1}{\partial s^2} \right|_{s=0}, \quad \left. \frac{\partial^4 h_x^1}{\partial s^4} \right|_{s=0}, \quad \left. \frac{\partial f_x}{\partial \alpha} \right|_{\alpha=1}, \quad \left. \frac{\partial^2 f_x}{\partial \alpha^2} \right|_{\alpha=1} \quad (32)$$

that follow from imposing the GE4 as given by Eq. (24). The final condition to determine the coefficients can be formulated as choosing the limiting value of $f_x(\alpha)$ as $\alpha \rightarrow \infty$. In order to ensure $\partial F_x / \partial \alpha < 0$ everywhere as well as negativity of the exchange energy density, $f_x(\alpha \rightarrow \infty)$ has to be limited to the interval] -4.4, -2.5[approximately. We here choose

$$f_x(\alpha \rightarrow \infty) = -3 \quad (33)$$

as a good balance between a pronounced negative slope for small values of α and minimizing undesired curvature in α . We find $a_0 = 0.938719$, $a_1 = -0.076371$, $a_2 = -0.0150899$, $b_0 = -0.628591$, $b_1 = -2.10315$, $b_2 = -0.5$, $b_3 = 0.103153$, $b_4 = 0.128591$.

Remarkably, the central premise of Eq. (16) follows naturally from the ansatz (21) when one opts for recovering the GE4 with a nonvanishing leading-order α contribution. Finally, we choose $d = 10$ to bundle $F(s, \alpha)$ quickly for $s \rightarrow \infty$, thereby restricting numerical issues that may arise as $\mathbf{r} \rightarrow \infty$ in the asymptotic region of finite systems, as well as to enforce negativity of the exchange energy density. In summary, our TASK functional fulfills all of the exact constraints for exchange that were imposed on SCAN (yet only the hydrogen atom norm), and in addition achieves a more pronounced negative slope in Eq. (16) that is crucial for field-counteracting properties. The resulting enhancement factor of TASK is depicted in Fig. 4. The constraints force the TASK functional toward a field-counteracting term that is somewhat less pronounced than the one of F_x^{PoC} and EXX, as seen in Fig. 1. However, as seen in Table I the polarizabilities are still substantially improved compared to LDA and SCAN. Also, the upper panel of Fig. 3 depicts a clear improvement over LDA for the H₈-H₈ charge-transfer system.

The potential that we obtain is relatively smooth and we did not experience difficulties in the numerical representation. By fulfilling Eq. (16), one guarantees that as functions of

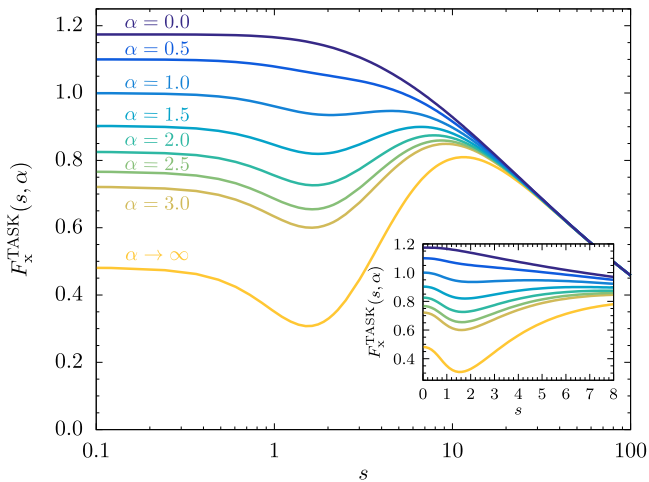


FIG. 4. TASK exchange enhancement factor $F_x^{\text{TASK}}(s, \alpha)$ as a function of s for fixed values of α .

s curves for different α do not cross, a condition that has been associated with numerical stability [52]. Several meta-GGAs that have previously been constructed have numerical features that require special attention in their computational evaluation, and the underlying reasons have been studied with a new iso-orbital indicator [114].

We here deliberately focused on the exchange functional because exchange is decisive for curing charge-transfer errors. A recent study [118] furthermore demonstrated that correlation contributes to the field-counteracting term in a similar fashion as exchange. Therefore, it is not unreasonable to cover the field-counteracting terms by meta-GGA exchange. Ground-state energetics, on the other hand, usually benefit from a correlation functional which is especially tailored toward the corresponding semilocal exchange. However, constructing such a correlation functional is a task in itself, to be addressed in future work. Therefore, we presently combine the TASK exchange with PW92-LDA correlation [93], as LDA is universal and not tied to a specific exchange functional.

We calculated atomization energies for a set of diatomic molecules. The set is small, but comprises single, double, and triple bonds and thus gives a first impression of binding properties. The mean absolute error for the atomization energy are reported in Table II. Without further context, TASK+PW92 accuracy for atomization energies is not impressive. However, one can here see a parallel between meta-GGAs and hybrid functionals: Hybrids with a small (ca. 20%) fraction of Fock exchange are good for atomization energies. A reliable description of charge transfer and charge localization, however, requires much larger (up to 75%) fractions [125] and correspondingly leads to a considerably poorer description of atomization energies [126]. Therefore, we see it as a sign of hope that TASK+PW92 atomization energies are at least significantly better than LDA while at the same time successfully tackling the charge-transfer errors. Furthermore, as the TASK functional is constructed in purely nonempirical fashion, it can be expected to be reliable over a wide range of systems and situations.

TABLE II. Atomization energies in kcal/mol of diatomic molecules based on self-consistent KS calculations at experimental bond lengths and mean absolute error (MAE) across the test set. The calculations were performed on a real-space prolate spheroidal grid with DARSEC [115], an all-electron code for single atoms or diatomic molecules. SCAN, EXX, and TASK (here in combination with PW92-LDA correlation) potentials were evaluated in the KLI approximation [82]. The experimental values (with zero point vibration removed) and the experimental bond lengths are taken from Ref. [116] (cf. the Supplemental Material of Ref. [117] for computational details).

| Molecule | EXX | LDA | PBE | SCAN | TASK | Expt. |
|-----------------|-------|-------|-------|-------|-------|-------|
| H ₂ | 83.8 | 112.9 | 104.6 | 107.7 | 117.0 | 109.5 |
| LiH | 34.1 | 60.8 | 53.5 | 55.6 | 58.9 | 58.0 |
| Li ₂ | 3.6 | 23.8 | 19.9 | 18.1 | 11.6 | 24.7 |
| LiF | 90.5 | 156.3 | 139.0 | 138.1 | 130.2 | 138.3 |
| CO | 172.3 | 299.2 | 269.1 | 255.2 | 248.2 | 259.5 |
| N ₂ | 112.4 | 268.0 | 243.9 | 220.9 | 174.9 | 228.5 |
| NO | 47.6 | 199.4 | 170.9 | 146.5 | 122.9 | 152.5 |
| OH | 65.4 | 123.2 | 105.0 | 94.9 | 97.6 | 106.4 |
| O ₂ | 30.0 | 175.1 | 144.1 | 126.8 | 131.0 | 120.5 |
| FH | 96.6 | 162.0 | 142.0 | 140.4 | 139.2 | 141.1 |
| F ₂ | -41.7 | 78.0 | 52.8 | 37.4 | 23.4 | 38.4 |
| MAE | 62.1 | 25.7 | 9.1 | 4.6 | 14.6 | |

Further evidence that the TASK functional indeed incorporates correct physics and yields a sizable Δ_x^{mGGA} is seen when calculating band gaps. For the study of gaps, we resorted to general KS (gKS) theory [127], as it gives direct access to the

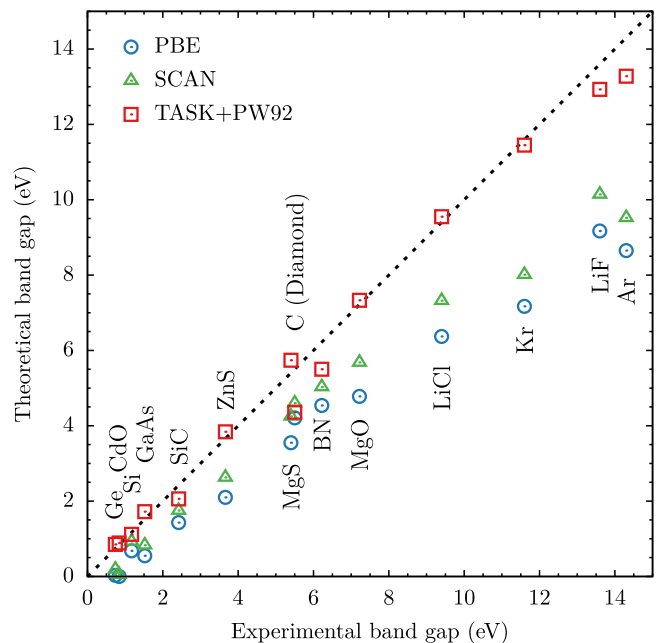


FIG. 5. Experimental band gaps compared to band gaps computed by PBE [4], SCAN (gKS) [52], and TASK+PW92 (gKS). See Table III for values and further details.

TABLE III. Structure, experimental geometrical parameters, and fundamental band gaps of the solids considered in this work. All band gaps are obtained from band structures that are sampled with a step size of $0.02a_0^{-1}$.

| Solid | Structure | Lattice parameter (\AA) | Fundamental band gaps (eV) | | | |
|-------|-------------|------------------------------------|----------------------------|-------|-----------|------------|
| | | | PBE | SCAN | TASK+PW92 | Expt. |
| Ge | Diamond | 5.652 [119] | 0.03 | 0.19 | 0.85 | 0.74 [120] |
| CdO | Rock salt | 4.704 [121] | 0.00 | 0.05 | 0.89 | 0.84 [122] |
| Si | Diamond | 5.430 [119] | 0.68 | 0.93 | 1.12 | 1.17 [120] |
| GaAs | Zinc blende | 5.648 [119] | 0.55 | 0.83 | 1.72 | 1.52 [120] |
| SiC | Zinc blende | 4.358 [119] | 1.43 | 1.75 | 2.06 | 2.42 [120] |
| ZnS | Zinc blende | 5.409 [120] | 2.10 | 2.63 | 3.84 | 3.66 [120] |
| MgS | Zinc blende | 5.622 [120] | 3.55 | 4.25 | 5.74 | 5.4 [120] |
| C | Diamond | 3.567 [119] | 4.21 | 4.60 | 4.36 | 5.48 [120] |
| BN | Zinc blende | 3.603 [120] | 4.54 | 5.03 | 5.50 | 6.22 [120] |
| MgO | Rock salt | 4.207 [119] | 4.78 | 5.68 | 7.33 | 7.22 [120] |
| LiCl | Rock salt | 5.106 [119] | 6.37 | 7.32 | 9.55 | 9.4 [123] |
| Kr | fcc | 6.130 [123] | 7.17 | 8.01 | 11.45 | 11.6 [123] |
| LiF | Rock salt | 4.010 [123] | 9.17 | 10.14 | 12.93 | 13.6 [124] |
| Ar | fcc | 5.310 [123] | 8.65 | 9.52 | 13.28 | 14.3 [124] |

fundamental gap [74,124,128,129], i.e.,

$$\Delta_s^{\text{gKS}} \approx \Delta_s + \Delta_{\text{xc}}. \quad (34)$$

All calculations were performed at the experimental geometry with a modified version of the periodic all-electron code BAND [130], a $9 \times 9 \times 9$ Monkhorst-Pack \mathbf{k} grid [131], and the TZ2P [132] basis set (except for Ar and Kr, for which QZ4P is used). The scalar relativistic effects are included by the ZORAMethod [133]. Figure 5 shows that gaps calculated with TASK in combination with PW92-LDA correlation are uniformly and significantly improved compared to usual semilocal results, here represented by PBE [4], for systems ranging from traditional semiconductors to wide-gap insulators (see Table III for detailed numbers). For most systems studied, TASK also performs significantly better than SCAN, which was reported [124] to already yield considerably more

realistic band gaps. It is noticeable that TASK band gaps are remarkably close to experiment for a wide range of materials, reaching from the semiconductors Ge, CdO, Si, and GaAs to minerals such as MgO and LiCl. The functional also gives significantly improved values for the large-gap insulators Kr, LiF, and Ar. Most notably, TASK opens the band gap with a magnitude close to the experimental value for Ge and CdO, whereas PBE and SCAN incorrectly predict both systems to be metallic (see Figs. 6 and 7 for the corresponding band structures).

V. SUMMARY AND CONCLUSIONS

In summary, we laid out an exchange-correlation functional construction strategy that takes into account properties of the KS potential such as the derivative discontinuity and

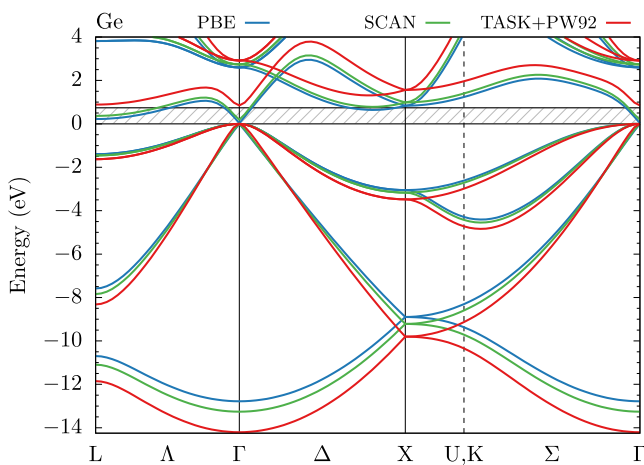


FIG. 6. Band structure of Ge calculated with PBE [4] (blue), SCAN [52] (green), and TASK+PW92 (red) at the experimental geometry (meta-GGAs calculated in gKS scheme). The top of the valance band is the zero of the energy scale. The experimental fundamental band gap is visually indicated by the hatched region.

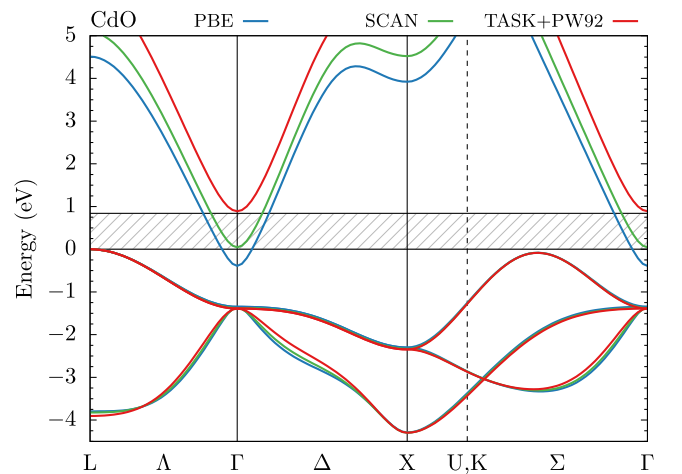


FIG. 7. Band structure of CdO calculated with PBE [4] (blue), SCAN [52] (green), and TASK+PW92 (red) at the experimental geometry (meta-GGAs calculated in gKS scheme). The top of the valance band is the zero of the energy scale. The experimental fundamental band gap is visually indicated by the hatched region.

the density response in addition to the ground-state energy. We derived a transparent general criterion for obtaining a sizable derivative discontinuity from a meta-GGA. In a proof-of-concept construction we demonstrated that this criterion directly governs the response potential and the ultranonlocality of a meta-GGA. Taking into account known exact constraints, we further developed a nonempirical, general-purpose meta-GGA for exchange that yields improved response properties and band gaps. This suggests that the ground-state energy need not be the only focus of meta-GGA construction, but construction strategies can also target the density and the potential. Our work shows that meta-GGAs can live up to the orbital functional promise of yielding ultranonlocal features without requiring costly exchange integrals. The meta-GGA form thus continues to hold great promise for future functional development.

ACKNOWLEDGMENTS

We acknowledge discussion with A. Kaiser and F. Hofmann. Financial support from the Elite Study Program

“Biological Physics” of the Elite Network of Bavaria, from the German-Israeli Foundation for Scientific Research and Development, from the Bavarian State Ministry of Science, Research, and the Arts for the Collaborative Research Network “Solar Technologies go Hybrid,” and from the Bavarian Polymer Institute in terms of computing resources, is gratefully acknowledged.

APPENDIX A: FOURTH-ORDER GRADIENT EXPANSION FOR EXCHANGE IN s AND α

We here describe in detail how $F_x(s, \alpha)$ is able to recover the GE4 for exchange [47,109] with one degree of freedom. Typically, the GE4 is written in s^2 and

$$q = \frac{\nabla^2 n}{4(3\pi^2)^{2/3} n^{5/3}} \quad (\text{A1})$$

as

$$F_x^{\text{GE4}}(s, q) \sim 1 + \frac{10}{81} s^2 + \frac{146}{2025} q^2 - \frac{73}{405} s^2 q + 0 \cdot s^4 + \mathcal{O}(\nabla^6) \quad \text{as } s, q \rightarrow 0 \quad (\text{A2})$$

assuming a vanishing s^4 coefficient as the best numerical estimate. As $\alpha \rightarrow 1$ in the homogeneous electron gas limit, the GE4 for exchange in s and α has the general form of Eq. (24) with its five coefficients $\mu_s, \mu_\alpha, C_s, C_{s\alpha}$, and C_α to be determined as follows: First, $\alpha = \tau/\tau^{\text{unif}} - 5s^2/3$ is expanded by utilizing the GE4 of τ [110,111] to obtain

$$\alpha \sim 1 - \frac{40}{27} s^2 + \frac{20}{9} q + \frac{1}{81} \left[-14q^2 + \frac{140}{3} s^2 q - 48s^2 + 12 \frac{\nabla^2(\nabla^2 n)}{2^4(3\pi^2)^{4/3} n^{7/3}} - 30 \frac{\nabla n \cdot \nabla(\nabla^2 n)}{2^4(3\pi^2)^{4/3} n^{10/3}} - 7 \frac{\nabla^2 |\nabla n|^2}{2^4(3\pi^2)^{4/3} n^{10/3}} + \frac{92}{3} \frac{\nabla n \cdot \nabla |\nabla n|^2}{2^4(3\pi^2)^{4/3} n^{13/3}} \right] + \mathcal{O}(\nabla^6). \quad (\text{A3})$$

Inserting this expansion into Eq. (24) gives

$$F_x^{\text{GE4}}(s, \alpha) \sim 1 + \left(\mu_s - \frac{40}{27} \mu_\alpha \right) s^2 + \left(\frac{20}{9} \mu_\alpha \right) q + \left(-\frac{14}{81} \mu_\alpha + \frac{400}{81} C_\alpha \right) q^2 + \left(\frac{140}{243} \mu_\alpha + \frac{20}{9} C_{s\alpha} - \frac{1600}{243} C_\alpha \right) s^2 q + \left(-\frac{48}{81} \mu_\alpha + C_s - \frac{40}{27} C_{s\alpha} + \frac{1600}{729} C_\alpha \right) s^4 + \mu_\alpha \left[\frac{4}{27} \frac{\nabla^2(\nabla^2 n)}{2^4(3\pi^2)^{4/3} n^{7/3}} - \frac{10}{27} \frac{\nabla n \cdot \nabla(\nabla^2 n)}{2^4(3\pi^2)^{4/3} n^{10/3}} - \frac{7}{81} \frac{\nabla^2 |\nabla n|^2}{2^4(3\pi^2)^{4/3} n^{10/3}} + \frac{92}{243} \frac{\nabla n \cdot \nabla |\nabla n|^2}{2^4(3\pi^2)^{4/3} n^{13/3}} \right] + \mathcal{O}(\nabla^6). \quad (\text{A4})$$

Note that, under integration by parts,

$$\int n^{4/3} s^2 d^3 r = 3 \int n^{4/3} q d^3 r. \quad (\text{A5})$$

Therefore, and as we only consider $F_x^{\text{GE4}}(s, \alpha)$ under the exchange energy integral $E_x = A_x \int n^{4/3} F_x^{\text{GE4}}(s, \alpha) d^3 r$, the separate occurrences of q in Eq. (A4) can be recast to $s^2/3$. Moreover, one can transform the remaining fourth-order terms to the variables s and q in similar fashion via integration by parts:

$$\int n^{4/3} \frac{\nabla^2(\nabla^2 n)}{2^4(3\pi^2)^{4/3} n^{7/3}} d^3 r = \int n^{4/3} (2s^2 q - q^2) d^3 r, \quad (\text{A6a})$$

$$\int n^{4/3} \frac{\nabla n \cdot \nabla(\nabla^2 n)}{2^4(3\pi^2)^{4/3} n^{10/3}} d^3 r = \int n^{4/3} (2s^2 q - q^2) d^3 r, \quad (\text{A6b})$$

$$\int n^{4/3} \frac{\nabla^2 |\nabla n|^2}{2^4(3\pi^2)^{4/3} n^{10/3}} d^3 r = \int n^{4/3} (-2s^2 q + 6s^4) d^3 r, \quad (\text{A6c})$$

$$\int n^{4/3} \frac{\nabla n \cdot \nabla |\nabla n|^2}{2^4(3\pi^2)^{4/3} n^{13/3}} d^3 r = \int n^{4/3} (-s^2 q + 3s^4) d^3 r. \quad (\text{A6d})$$

This allows us to write Eq. (A4) as

$$F_x^{\text{GE4}}(s, \alpha) \sim 1 + \left(\mu_s - \frac{20}{27} \mu_\alpha \right) s^2 + \left(\frac{4}{81} \mu_\alpha + \frac{400}{81} C_\alpha \right) q^2 + \left(-\frac{2}{27} \mu_\alpha + \frac{20}{9} C_{s\alpha} - \frac{1600}{243} C_\alpha \right) s^2 q + \left(\frac{2}{81} \mu_\alpha + C_s - \frac{40}{27} C_{s\alpha} + \frac{1600}{729} C_\alpha \right) s^4 + \mathcal{O}(\nabla^6). \quad (\text{A7})$$

Finally, comparison with the GE4 of Eq. (24) yields the values for the coefficients already given by Eqs. (25) and (26) with one degree of freedom, the choice of μ_α . When choosing $\mu_\alpha = 0$ the resulting GE4 is identical to the one given in the Supplemental Material of Ref. [52].

APPENDIX B: HYDROGEN ATOM NORM

A meta-GGA for exchange defined by an enhancement factor $F_x(\alpha)$ that only depends on α reduces for any single-orbital system to a multiple of LDA,

$$E_x^{\text{mGGA}}[n] = A_x \int F_x(\alpha(\mathbf{r})) n^{4/3}(\mathbf{r}) d^3r = F_x(0) A_x \int n^{4/3}(\mathbf{r}) d^3r = F_x(0) E_x^{\text{LDA}}[n] \quad (\text{B1})$$

since $\alpha(\mathbf{r}) \equiv 0$ in the single-orbital limit. Given the completely spin-polarized exact hydrogen ground-state density

$$n_{\text{H}}(\mathbf{r}) = \frac{1}{\pi a_0^3} \exp(-2r/a_0), \quad (\text{B2})$$

the associated exchange energy of the meta-GGA is obtained by virtue of the spin-scaling relation for exchange [78] to be

$$E_x^{\text{mGGA}}[n_{\text{H}}, 0] = F_x(0) E_x^{\text{LDA}}[2n_{\text{H}}]/2 = -F_x(0) \frac{81 e^2}{128 a_0} \left(\frac{3}{4\pi^2} \right)^{1/3}. \quad (\text{B3})$$

Consequently, the exchange energy of the meta-GGA matches the exact value at the hydrogen ground-state density

$$E_x[n_{\text{H}}, 0] = -E_{\text{H}}[n_{\text{H}}] = -\frac{e^2}{2} \iint \frac{n_{\text{H}}(\mathbf{r}) n_{\text{H}}(\mathbf{r}')}{|\mathbf{r} - \mathbf{r}'|} d^3r d^3r' = -\frac{5 e^2}{16 a_0}, \quad (\text{B4})$$

if one chooses

$$F_x(0) = c_{\text{H}} := \frac{40}{81} \left(\frac{4\pi^2}{3} \right)^{1/3} \approx 1.16588 \quad (\text{B5})$$

[cf. Eq. (19)].

APPENDIX C: ULTRANONLOCALITY IN RECIPROCAL SPACE

Having explicitly demonstrated that and how a meta-GGA can achieve ultranonlocality associated with the derivative discontinuity in real space and for finite systems, a comparison with previous work on ultranonlocality in reciprocal space and extended systems is worthwhile. Nazarov and Vignale [88] showed via a reciprocal space analysis that the xc kernel f_{xc} of a meta-GGA is capable of long-rangedness, which also is an aspect of ultranonlocality. When thinking about f_{xc} ,

different aspects of ultranonlocality are associated [90,134] with a singularity of the type

$$f_{\text{xc},00}(\mathbf{q}) \sim \frac{\beta}{q^2} \quad (\text{C1})$$

in the optical limit $\mathbf{q} \rightarrow 0$. Using an averaging approximation similar to the one that we use in Eq. (12) to demonstrate the relation between Δ_x and $\partial e_{\text{xc}}/\partial \tau$, they extract the singularity to be

$$f_{\text{xc},\text{GG}'}(\mathbf{q}) \approx -\frac{\partial e_{\text{xc}}}{\partial \tau} \chi_{\text{s},\text{GG}'}^{-1}(\mathbf{q}), \quad (\text{C2})$$

where χ_{s}^{-1} is the inverse of the noninteracting KS response function. Using this expression as an approximation to the full kernel, they calculate the excitation spectra of semiconductors with a special focus on the excitonic peak. These spectra and comparison with the work of Reining *et al.* [134] then suggest $\beta < 0$, and hence $\partial e_{\text{xc}}/\partial \tau < 0$ in order to capture the electron-hole interaction. Their analysis thus leads to the opposite sign of $\partial e_{\text{xc}}/\partial \tau$ that we reach based on the functional derivative of Eq. (10) and the fact that Δ_x is determined by its last term.

To resolve this seemingly contradiction, we first note that Ref. [88] focuses on a different physical problem than we do. Nazarov and Vignale [88] study the binding of excitons. As argued in Ref. [134], this merely requires a static long-range contribution to the kernel,

$$\Delta f_{\text{xc}}(\mathbf{r}, \mathbf{r}') = \frac{\beta}{4\pi |\mathbf{r} - \mathbf{r}'|} \quad (\text{C3})$$

with $\beta < 0$. We further note that obtaining properties of f_{xc} and v_{xc} that are long range in real space correctly with semilocal approximations is only possible within narrow conditions and typically leads to divergences of the KS potential for many finite systems [71,72].

In our work here, we focus on the ultranonlocality that is associated with potential step structures and the derivative discontinuity. Our tests were done for finite systems, but Ghosez *et al.* [90] demonstrated that this type of ultranonlocality is also present in solids. When calculating the polarization dependence of solids, which is in close analogy to the ultranonlocality effects in the electrical response of molecular chains, this ultranonlocality is connected to a positive ($\beta > 0$) singularity of the form of Eq. (C1) (see, e.g., Fig. 1 of Ref. [90]). Within the approximation of Eq. (C2) this singularity can in turn be associated with $\partial e_{\text{xc}}/\partial \tau > 0$. Therefore, the analysis of Ghosez *et al.* [90] is in line with our arguments.

Finally, we note that also Ref. [134] finds a positive contribution to the singularity in f_{xc} that stems from the energy shift between KS and quasiparticle eigenvalues. Within KS

TABLE IV. Dimensions of ellipsoidal boundaries used for the hydrogen chain polarizability calculation in PARSEC in a_0 .

| Semiaxis | H ₄ | H ₆ | H ₈ | H ₁₂ | H ₁₈ |
|----------|----------------|----------------|----------------|-----------------|-----------------|
| Parallel | 15.0 | 17.5 | 20.0 | 25.0 | 32.5 |
| Perp. | 10.0 | 10.0 | 10.0 | 10.0 | 13.0 |

theory this energy shift is accounted for by the derivative discontinuity Δ_{xc} . In the calculations of Ref. [134], however, it is absorbed into an energy shift of the starting χ_s .

APPENDIX D: HYDROGEN CHAIN POLARIZABILITY CALCULATION DETAILS

The polarizabilities of hydrogen chains were calculated with a locally modified version of the publicly available electronic structure program PARSEC [95] on a real-space grid with a grid spacing of $0.27a_0$. The linear chains with alternating H–H distances of $2a_0$ and $3a_0$ are centered in an ellipsoid with dimensions as listed in Table IV. All calculations were performed self-consistently with a functional independent pseudopotential [135], an energy convergence criterion for the KS iterations of $5 \times 10^{-7} E_h$, and a field strength of $5 \times 10^{-5} E_h/a_0$. To obtain the KS potential based on the OEP scheme via S -Iterations [81], S was converged to at least $3 \times 10^{-7} E_h$. The implementation of all meta-GGAs with the exception of PoC, TASK, and SCAN is built on an interface to LIBXC version 4.3.4 [136]. We found that for several of the meta-GGAs that are available in LIBXC [136], e.g., TPSS [47], revTPSS [50], TM [55], and the Minnesota meta-GGAs [49], the grid-based calculations are difficult to converge as their potentials show rapidly varying features. This type of observation is in line with the arguments of, e.g., Ref. [114]. Therefore, the results reported here are restricted to numerically benevolent meta-GGAs. For the calculations with the MVS functional we found that the OEP calculations converged very slowly for the longer hydrogen chains.

Therefore, for the MVS functional [54], Table I reports OEP polarizabilities for H₄ and H₆, but the values reported for H₈, H₁₂, and H₁₈ are based on the KLI approximation [82]. All other values are OEP based.

APPENDIX E: H₈–H₈ CHARGE-TRANSFER CALCULATION DETAILS

All calculations for the H₈–H₈ charge-transfer system were performed spin polarized, self-consistently on a real-space grid with BTDF [40] using Troullier-Martins LDA pseudopotentials [137], ellipsoidal boundaries with semiaxis of $20a_0$ perpendicular to and $32a_0$ along the chains, and a grid spacing of $0.3a_0$. For the KS iterations, an energy convergence criterion of $5 \times 10^{-6} E_h$ was used. The two hydrogen chains, each containing eight hydrogen atoms separated by 1 \AA , are centered in the ellipsoid with a mutual distance of 8 \AA . Due to the nature of the situation with nearly degenerate ground-state solutions, the calculations are numerically very challenging (cf. Refs. [9,105]). The LDA calculations were performed with occupation numbers following from a Fermi-Dirac distribution with a temperature of 800 K, as zero-temperature calculations cannot be converged once the external field strength leads to (a fractional) transfer of charge. The meta-GGA calculations in the KLI approximation [82] were performed at 0 K. For the PoC meta-GGA, convergence was possible for any considered field strength. We can carefully converge two nearly degenerate ground states with an integer charge of 8 and 9 electrons, respectively, even for field strengths below and above the critical field strength of $3.7 \times 10^9 \text{ V/m}$, at which an integer electron transfer occurs. Consequently, the associated Fig. 3 only shows the solution of lower total energy at each field strength and the critical field strength is given by the energy crossing point of both solutions. While the TASK functional does not allow for a numerical stable solution from field strengths of $3.0 \times 10^9 \text{ V/m}$ to $5.8 \times 10^9 \text{ V/m}$, it still improves considerably over LDA as it allows to counteract the charge transfer up to $2.8 \times 10^9 \text{ V/m}$ and yields a broad integer electron plateau starting at $6.0 \times 10^9 \text{ V/m}$.

- [1] J. P. Perdew and Y. Wang, Accurate and simple density functional for the electronic exchange energy: Generalized gradient approximation, *Phys. Rev. B* **33**, 8800 (1986).
- [2] A. D. Becke, Density-functional exchange-energy approximation with correct asymptotic behavior, *Phys. Rev. A* **38**, 3098 (1988).
- [3] C. Lee, W. Yang, and R. G. Parr, Development of the Colle-Salvetti correlation-energy formula into a functional of the electron density, *Phys. Rev. B* **37**, 785 (1988).
- [4] J. P. Perdew, K. Burke, and M. Ernzerhof, Generalized Gradient Approximation Made Simple, *Phys. Rev. Lett.* **77**, 3865 (1996).
- [5] R. Armiento and A. E. Mattsson, Functional designed to include surface effects in self-consistent density functional theory, *Phys. Rev. B* **72**, 085108 (2005).
- [6] A. D. Becke, Density-functional thermochemistry. III. The role of exact exchange, *J. Chem. Phys.* **98**, 5648 (1993).
- [7] J. P. Perdew and M. Levy, Physical Content of the Exact Kohn-Sham Orbital Energies: Band Gaps and Derivative Discontinuities, *Phys. Rev. Lett.* **51**, 1884 (1983).
- [8] R. W. Godby, M. Schlüter, and L. J. Sham, Accurate Exchange-Correlation Potential for Silicon and Its Discontinuity on Addition of an Electron, *Phys. Rev. Lett.* **56**, 2415 (1986).
- [9] S.-H. Ke, H. U. Baranger, and W. Yang, Role of the exchange-correlation potential in ab initio electron transport calculations, *J. Chem. Phys.* **126**, 201102 (2007).
- [10] A. J. Cohen, P. Mori-Sánchez, and W. Yang, Challenges for density functional theory, *Chem. Rev.* **112**, 289 (2012).
- [11] G. Kresse, A. Gil, and P. Sautet, Significance of single-electron energies for the description of CO on Pt(111), *Phys. Rev. B* **68**, 073401 (2003).
- [12] S. Luo, Y. Zhao, and D. G. Truhlar, Improved CO adsorption energies, site preferences, and surface formation energies

- from a meta-generalized gradient approximation exchange–correlation functional, M06-L, *J. Phys. Chem. Lett.* **3**, 2975 (2012).
- [13] S. J. A. van Gisbergen, P. R. T. Schipper, O. V. Gritsenko, E. J. Baerends, J. G. Snijders, B. Champagne, and B. Kirtman, Electric Field Dependence of the Exchange–Correlation Potential in Molecular Chains, *Phys. Rev. Lett.* **83**, 694 (1999).
- [14] P. Mori-Sánchez, Q. Wu, and W. Yang, Accurate polymer polarizabilities with exact exchange density-functional theory, *J. Chem. Phys.* **119**, 11001 (2003).
- [15] S. Kümmel, L. Kronik, and J. P. Perdew, Electrical Response of Molecular Chains from Density Functional Theory, *Phys. Rev. Lett.* **93**, 213002 (2004).
- [16] J. P. Perdew, R. G. Parr, M. Levy, and J. L. Balduz, Jr., Density-Functional Theory for Fractional Particle Number: Derivative Discontinuities of the Energy, *Phys. Rev. Lett.* **49**, 1691 (1982).
- [17] D. Tozer, Relationship between long-range charge-transfer excitation energy error and integer discontinuity in Kohn–Sham theory, *J. Chem. Phys.* **119**, 12697 (2003).
- [18] M. Mundt and S. Kümmel, Derivative Discontinuities in Time-Dependent Density-Functional Theory, *Phys. Rev. Lett.* **95**, 203004 (2005).
- [19] M. van Faassen and N. Maitra, Improved exchange–correlation potential for polarizability and dissociation in density functional theory, *J. Chem. Phys.* **126**, 191106 (2007).
- [20] P. Elliott, J. I. Fuks, A. Rubio, and N. T. Maitra, Universal Dynamical Steps in the Exact Time-Dependent Exchange–Correlation Potential, *Phys. Rev. Lett.* **109**, 266404 (2012).
- [21] D. Hofmann and S. Kümmel, Integer particle preference during charge transfer in Kohn–Sham theory, *Phys. Rev. B* **86**, 201109(R) (2012).
- [22] M. J. P. Hodgson, E. Kraisler, A. Schild, and E. K. U. Gross, How interatomic steps in the exact Kohn–Sham potential relate to derivative discontinuities of the energy, *Phys. Chem. Lett.* **8**, 5974 (2017).
- [23] A. J. Cohen, P. Mori-Sánchez, and W. Yang, Insights into current limitations of density functional theory, *Science* **321**, 792 (2008).
- [24] P. Mori-Sánchez, A. J. Cohen, and W. Yang, Localization and Delocalization Errors in Density Functional Theory and Implications for Band-Gap Prediction, *Phys. Rev. Lett.* **100**, 146401 (2008).
- [25] B. G. Janesko, Reducing density-driven error without exact exchange, *Phys. Chem. Chem. Phys.* **19**, 4793 (2017).
- [26] A. Wasserman, J. Nafziger, K. Jiang, M.-C. Kim, E. Sim, and K. Burke, The importance of being inconsistent, *Annu. Rev. Phys. Chem.* **68**, 555 (2017).
- [27] J. P. Perdew and A. Zunger, Self-interaction correction to density-functional approximations for many-electron systems, *Phys. Rev. B* **23**, 5048 (1981).
- [28] W. M. Temmerman, H. Winter, Z. Szotek, and A. Svane, Cu Valency Change Induced by O Doping in YBCO, *Phys. Rev. Lett.* **86**, 2435 (2001).
- [29] O. A. Vydrov, G. E. Scuseria, and J. P. Perdew, Tests of functionals for systems with fractional electron number, *J. Chem. Phys.* **126**, 154109 (2007).
- [30] T. Körzdörfer, M. Mundt, and S. Kümmel, Electrical Response of Molecular Systems: The Power of Self-Interaction Corrected Kohn–Sham Theory, *Phys. Rev. Lett.* **100**, 133004 (2008).
- [31] G. Borghi, A. Ferretti, N. L. Nguyen, I. Dabo, and N. Marzari, Koopmans-compliant functionals and their performance against reference molecular data, *Phys. Rev. B* **90**, 075135 (2014).
- [32] J. Erhard, P. Bleiziffer, and A. Görling, Power Series Approximation for the Correlation Kernel Leading to Kohn–Sham Methods Combining Accuracy, Computational Efficiency, and General Applicability, *Phys. Rev. Lett.* **117**, 143002 (2016).
- [33] J. Jorner-Somoza, J. Alberdi-Rodriguez, B. F. Milne, X. Andrade, M. A. L. Marques, F. Nogueira, M. J. T. Oliveira, J. J. P. Stewart, and A. Rubio, Insights into color-tuning of chlorophyll optical response in green plants, *Phys. Chem. Chem. Phys.* **17**, 26599 (2015).
- [34] C. Curutchet and B. Mennucci, Quantum chemical studies of light harvesting, *Chem. Rev.* **117**, 294 (2017).
- [35] I. Schelter, J. M. Foerster, A. T. Gardiner, A. W. Roszak, R. J. Cogdell, G. M. Ullmann, T. B. de Queiroz, and S. Kümmel, Assessing density functional theory in real-time and real-space as a tool for studying bacteriochlorophylls and the light-harvesting complex 2, *J. Chem. Phys.* **151**, 134114 (2019).
- [36] L. Cupellini, S. Jurinovich, M. Campetella, S. Caprasecca, C. A. Guido, S. M. Kelly, A. T. Gardiner, R. Cogdell, and B. Mennucci, An *ab initio* description of the excitonic properties of LH2 and their temperature dependence, *J. Phys. Chem. B* **120**, 11348 (2016).
- [37] A. Anda, L. De Vico, and T. Hansen, Intermolecular modes between LH2 bacteriochlorophylls and protein residues: The effect on the excitation energies, *J. Phys. Chem. B* **121**, 5499 (2017).
- [38] D. Sundholm, A density-functional-theory study of bacteriochlorophyll b, *Phys. Chem. Chem. Phys.* **5**, 4265 (2003).
- [39] A. Dreuw and M. Head-Gordon, Failure of time-dependent density functional theory for long-range charge-transfer excited states: The zincbacteriochlorin–bacteriochlorin and bacteriochlorophyll–spheroidene complexes, *J. Am. Chem. Soc.* **126**, 4007 (2004).
- [40] I. Schelter and S. Kümmel, Accurate evaluation of real-time density functional theory providing access to challenging electron dynamics, *J. Chem. Theory Comput.* **14**, 1910 (2018).
- [41] A. D. Becke, Local exchange–correlation approximations and first-row molecular dissociation energies, *Int. J. Quantum Chem.* **27**, 585 (1985).
- [42] A. D. Becke, Density-functional thermochemistry. IV. A new dynamical correlation functional and implications for exact-exchange mixing, *J. Chem. Phys.* **104**, 1040 (1996).
- [43] A. D. Becke, A new inhomogeneity parameter in density-functional theory, *J. Chem. Phys.* **109**, 2092 (1998).
- [44] T. V. Voorhis and G. E. Scuseria, A novel form for the exchange–correlation energy functional, *J. Chem. Phys.* **109**, 400 (1998).
- [45] J. P. Perdew, S. Kurth, A. Zupan, and P. Blaha, Accurate Density Functional with Correct Formal Properties: A Step Beyond the Generalized Gradient Approximation, *Phys. Rev. Lett.* **82**, 2544 (1999).

- [46] A. D. Boese and N. C. Handy, New exchange-correlation density functionals: The role of the kinetic-energy density, *J. Chem. Phys.* **116**, 9559 (2002).
- [47] J. Tao, J. P. Perdew, V. N. Staroverov, and G. E. Scuseria, Climbing the Density Functional Ladder: Nonempirical Meta-Generalized Gradient Approximation Designed for Molecules and Solids, *Phys. Rev. Lett.* **91**, 146401 (2003).
- [48] K. Pernal, R. Podeszwa, K. Patkowski, and K. Szalewicz, Dispersionless Density Functional Theory, *Phys. Rev. Lett.* **103**, 263201 (2009).
- [49] Y. Zhao and D. G. Truhlar, A new local density functional for main-group thermochemistry, transition metal bonding, thermochemical kinetics, and noncovalent interactions, *J. Chem. Phys.* **125**, 194101 (2006); R. Peverati and D. G. Truhlar, An improved and broadly accurate local approximation to the exchange–correlation density functional: The MN12-L functional for electronic structure calculations in chemistry and physics, *Phys. Chem. Chem. Phys.* **14**, 13171 (2012); H. S. Yu, X. He, and D. G. Truhlar, MN15-L: A new local exchange–correlation functional for Kohn–Sham density functional theory with broad accuracy for atoms, molecules, and solids, *J. Chem. Theory Comput.* **12**, 1280 (2016).
- [50] J. P. Perdew, A. Ruzsinszky, G. I. Csonka, L. A. Constantin, and J. Sun, Workhorse Semilocal Density Functional for Condensed Matter Physics and Quantum Chemistry, *Phys. Rev. Lett.* **103**, 026403 (2009).
- [51] J. Sun, B. Xiao, Y. Fang, R. Haunschuld, P. Hao, A. Ruzsinszky, G. I. Csonka, G. E. Scuseria, and J. P. Perdew, Density Functionals that Recognize Covalent, Metallic, and Weak Bonds, *Phys. Rev. Lett.* **111**, 106401 (2013).
- [52] J. Sun, A. Ruzsinszky, and J. P. Perdew, Strongly Constrained and Appropriately Normed Semilocal Density Functional, *Phys. Rev. Lett.* **115**, 036402 (2015).
- [53] J. Sun, B. Xiao, and A. Ruzsinszky, Communication: Effect of the orbital-overlap dependence in the meta generalized gradient approximation, *J. Chem. Phys.* **137**, 051101 (2012); J. Sun, R. Haunschuld, B. Xiao, I. W. Bulik, G. E. Scuseria, and J. P. Perdew, Semilocal and hybrid meta-generalized gradient approximations based on the understanding of the kinetic-energy-density dependence, *ibid.* **138**, 044113 (2013).
- [54] J. Sun, J. P. Perdew, and A. Ruzsinszky, Semilocal density functional obeying a strongly tightened bound for exchange, *Proc. Natl. Acad. Sci. USA* **112**, 685 (2015).
- [55] J. Tao and Y. Mo, Accurate Semilocal Density Functional for Condensed-Matter Physics and Quantum Chemistry, *Phys. Rev. Lett.* **117**, 073001 (2016).
- [56] F. Della Sala, E. Fabiano, and L. A. Constantin, Kinetic-energy-density dependent semilocal exchange–correlation functionals, *Int. J. Quantum Chem.* **116**, 1641 (2016).
- [57] M. G. Medvedev, I. S. Bushmarinov, J. Sun, J. P. Perdew, and K. A. Lyssenko, Density functional theory is straying from the path toward the exact functional, *Science* **355**, 49 (2017).
- [58] T. Schmidt, E. Kraisler, A. Makmal, L. Kronik, and S. Kümmel, A self-interaction-free local hybrid functional: Accurate binding energies vis-à-vis accurate ionization potentials from Kohn-Sham eigenvalues, *J. Chem. Phys.* **140**, 18A510 (2014).
- [59] V. Polo, E. Kraka, and D. Cremer, Electron correlation and the self-interaction error of density functional theory, *Mol. Phys.* **100**, 1771 (2002).
- [60] P. Verma and R. J. Bartlett, Increasing the applicability of density functional theory. III. Do consistent Kohn-Sham density functional methods exist? *J. Chem. Phys.* **137**, 134102 (2012).
- [61] E. Trushin, M. Betzinger, S. Blügel, and A. Görling, Band gaps, ionization potentials, and electron affinities of periodic electron systems via the adiabatic-connection fluctuation-dissipation theorem, *Phys. Rev. B* **94**, 075123 (2016).
- [62] A. D. Becke and E. R. Johnson, A simple effective potential for exchange, *J. Chem. Phys.* **124**, 221101 (2006).
- [63] R. Armiento, S. Kümmel, and T. Körzdörfer, Electrical response of molecular chains in density functional theory: Ultranonlocal response from a semilocal functional, *Phys. Rev. B* **77**, 165106 (2008).
- [64] F. Tran and P. Blaha, Accurate Band Gaps of Semiconductors and Insulators with a Semilocal Exchange–Correlation Potential, *Phys. Rev. Lett.* **102**, 226401 (2009).
- [65] E. Räsänen, S. Pittalis, and C. R. Proetto, Universal correction for the Becke–Johnson exchange potential, *J. Chem. Phys.* **132**, 044112 (2010).
- [66] F. Tran, P. Blaha, M. Betzinger, and S. Blügel, Comparison between exact and semilocal exchange potentials: An all-electron study for solids, *Phys. Rev. B* **91**, 165121 (2015).
- [67] A. P. Gaiduk, S. K. Chulkov, and V. N. Staroverov, Reconstruction of density functionals from Kohn–Sham potentials by integration along density scaling paths, *J. Chem. Theory Comput.* **5**, 699 (2009).
- [68] A. Karolewski, R. Armiento, and S. Kümmel, Polarizabilities of polyacetylene from a field-counteracting semilocal functional, *J. Chem. Theory Comput.* **5**, 712 (2009).
- [69] A. Karolewski, R. Armiento, and S. Kümmel, Electronic excitations and the Becke–Johnson potential: The need for and the problem of transforming model potentials to functional derivatives, *Phys. Rev. A* **88**, 052519 (2013).
- [70] R. Armiento and S. Kümmel, Orbital Localization, Charge Transfer, and Band Gaps in Semilocal Density-Functional Theory, *Phys. Rev. Lett.* **111**, 036402 (2013).
- [71] T. Aschebrock, R. Armiento, and S. Kümmel, Orbital nodal surfaces: Topological challenges for density functionals, *Phys. Rev. B* **95**, 245118 (2017).
- [72] T. Aschebrock, R. Armiento, and S. Kümmel, Challenges for semilocal density functionals with asymptotically nonvanishing potentials, *Phys. Rev. B* **96**, 075140 (2017).
- [73] J. Garhammer, F. Hofmann, R. Armiento, and S. Kümmel, On the challenge to improve the density response with unusual gradient approximations, *Eur. Phys. J. B* **91**, 159 (2018).
- [74] F. Tran, J. Doumont, L. Kalantari, A. W. Huran, M. A. L. Marques, and P. Blaha, Semilocal exchange–correlation potentials for solid-state calculations: Current status and future directions, *J. Appl. Phys.* **126**, 110902 (2019).
- [75] M. Levy and J. P. Perdew, Hellmann–Feynman, virial, and scaling requisites for the exact universal density functionals. Shape of the correlation potential and diamagnetic susceptibility for atoms, *Phys. Rev. A* **32**, 2010 (1985).
- [76] A. Ruzsinszky, J. Sun, B. Xiao, and G. I. Csonka, A meta-GGA made free of the order of limits anomaly, *J. Chem. Theory Comput.* **8**, 2078 (2012).
- [77] F. Della Sala, E. Fabiano, and L. A. Constantin, Kohn-Sham kinetic energy density in the nuclear and asymptotic regions: Deviations from the von Weizsäcker behavior and

- applications to density functionals, *Phys. Rev. B* **91**, 035126 (2015).
- [78] G. L. Oliver and J. P. Perdew, Spin-density gradient expansion for the kinetic energy, *Phys. Rev. A* **20**, 397 (1979).
- [79] O. V. Gritsenko, R. van Leeuwen, E. van Lenthe, and E. J. Baerends, Self-consistent approximation to the Kohn-Sham exchange potential, *Phys. Rev. A* **51**, 1944 (1995).
- [80] T. Grabo, T. Kriebich, S. Kurth, and E. K. U. Gross, in *Strong Coulomb Correlation in Electronic Structure: Beyond the Local Density Approximation*, edited by V. Anisimov (Gordon & Breach, Tokyo, 2000), pp. 203–311.
- [81] S. Kümmel and J. P. Perdew, Simple Iterative Construction of the Optimized Effective Potential for Orbital Functionals, Including Exact Exchange, *Phys. Rev. Lett.* **90**, 043004 (2003).
- [82] J. B. Krieger, Y. Li, and G. J. Iafrate, Construction and application of an accurate local spin-polarized Kohn-Sham potential with integer discontinuity: Exchange-only theory, *Phys. Rev. A* **45**, 101 (1992).
- [83] M. Grüning, O. V. Gritsenko, and E. J. Baerends, Exchange potential from the common energy denominator approximation for the Kohn-Sham Green's function: Application to (hyper)polarizabilities of molecular chains, *J. Chem. Phys.* **116**, 6435 (2002).
- [84] S. Kümmel and L. Kronik, Orbital-dependent density functionals: Theory and applications, *Rev. Mod. Phys.* **80**, 3 (2008).
- [85] F. G. Eich and M. Hellgren, Derivative discontinuity and exchange-correlation potential of meta-GGAs in density-functional theory, *J. Chem. Phys.* **141**, 224107 (2014).
- [86] G. K.-L. Chan, A fresh look at ensembles: Derivative discontinuities in density functional theory, *J. Chem. Phys.* **110**, 4710 (1999).
- [87] E. Sagvolden and J. P. Perdew, Discontinuity of the exchange-correlation potential: Support for assumptions used to find it, *Phys. Rev. A* **77**, 012517 (2008).
- [88] V. U. Nazarov and G. Vignale, Optics of Semiconductors from Meta-Generalized-Gradient-Approximation-Based Time-Dependent Density-Functional Theory, *Phys. Rev. Lett.* **107**, 216402 (2011).
- [89] J. P. Perdew, A. Ruzsinszky, J. Sun, and K. Burke, Gedanken densities and exact constraints in density functional theory, *J. Chem. Phys.* **140**, 18A533 (2014).
- [90] P. Ghosez, X. Gonze, and R. W. Godby, Long-wavelength behavior of the exchange-correlation kernel in the Kohn-Sham theory of periodic systems, *Phys. Rev. B* **56**, 12811 (1997).
- [91] A. D. Becke and K. E. Edgecombe, A simple measure of electron localization in atomic and molecular systems, *J. Chem. Phys.* **92**, 5397 (1990).
- [92] A. Savin, O. Jepsen, J. Flad, O. K. Andersen, H. Preuss, and H. G. von Schnering, Electron localization in solid-state structures of the elements: the diamond structure, *Angew. Chem., Int. Ed. Engl.* **31**, 187 (1992); B. Silvi and A. Savin, Classification of chemical bonds based on topological, *Nature (London)* **371**, 683 (1994); A. Savin, R. Nesper, S. Wengert, and T. F. Fässler, ELF: The electron localization function, *Angew. Chem., Int. Ed. Engl.* **36**, 1808 (1997).
- [93] J. P. Perdew and Y. Wang, Accurate and simple analytic representation of the electron-gas correlation energy, *Phys. Rev. B* **45**, 13244 (1992).
- [94] B. Champagne, D. H. Mosley, M. Vračko, and J.-M. André, Electron-correlation effects on the static longitudinal polarizability of polymeric chains, *Phys. Rev. A* **52**, 178 (1995).
- [95] L. Kronik, A. Makmal, M. L. Tiago, M. M. G. Alemany, M. Jain, X. Huang, Y. Saad, and J. R. Chelikowsky, PARSEC — the pseudopotential algorithm for real-space electronic structure calculations: recent advances and novel applications to nano-structures, *Phys. Status Solidi B* **243**, 1063 (2006).
- [96] M. Mundt, S. Kümmel, B. Huber, and M. Moseler, Photoelectron spectra of sodium clusters: The problem of interpreting Kohn-Sham eigenvalues, *Phys. Rev. B* **73**, 205407 (2006).
- [97] M. van Faassen, P. L. de Boeij, R. van Leeuwen, J. A. Berger, and J. G. Snijders, Ultranonlocality in Time-Dependent Current-Density-Functional Theory: Application to Conjugated Polymers, *Phys. Rev. Lett.* **88**, 186401 (2002).
- [98] P. Umari, A. J. Williamson, G. Galli, and N. Marzari, Dielectric Response of Periodic Systems from Quantum Monte Carlo Calculations, *Phys. Rev. Lett.* **95**, 207602 (2005).
- [99] H. Sekino, Y. Maeda, M. Kamiya, and K. Hirao, Polarizability and second hyperpolarizability evaluation of long molecules by the density functional theory with long-range correction, *J. Chem. Phys.* **126**, 014107 (2007).
- [100] A. Ruzsinszky, J. P. Perdew, G. I. Csonka, G. E. Scuseria, and O. A. Vydrov, Understanding and correcting the self-interaction error in the electrical response of hydrogen chains, *Phys. Rev. A* **77**, 060502(R) (2008).
- [101] A. Ruzsinszky, J. P. Perdew, and G. I. Csonka, Simple charge-transfer model to explain the electrical response of hydrogen chains, *Phys. Rev. A* **78**, 022513 (2008).
- [102] C. D. Pemmaraju, S. Sanvito, and K. Burke, Polarizability of molecular chains: A self-interaction correction approach, *Phys. Rev. B* **77**, 121204(R) (2008).
- [103] B. Champagne and B. Kirtman, Polarizabilities and second hyperpolarizabilities of hydrogen chains using the spin-component-scaled Møller–Plesset second-order method, *Int. J. Quantum Chem.* **109**, 3103 (2009).
- [104] E. H. Lieb and S. Oxford, Improved lower bound on the indirect Coulomb energy, *Int. J. Quantum Chem.* **19**, 427 (1981).
- [105] T. Schmidt and S. Kümmel, One- and many-electron self-interaction error in local and global hybrid functionals, *Phys. Rev. B* **93**, 165120 (2016).
- [106] J. P. Perdew, Size-consistency, self-interaction correction, and derivative discontinuity in density functional theory, *Adv. Quantum Chem.* **21**, 113 (1990).
- [107] M. Levy, Density-functional exchange correlation through coordinate scaling in adiabatic connection and correlation hole, *Phys. Rev. A* **43**, 4637 (1991).
- [108] L. Pollack and J. P. Perdew, Evaluating density functional performance for the quasi-two-dimensional electron gas, *J. Phys.: Condens. Matter* **12**, 1239 (2000).
- [109] P. S. Svendsen and U. von Barth, Gradient expansion of the exchange energy from second-order density response theory, *Phys. Rev. B* **54**, 17402 (1996).
- [110] M. Brack, B. Jennings, and Y. Chu, On the extended Thomas-Fermi approximation to the kinetic energy density, *Phys. Lett. B* **65**, 1 (1976).
- [111] J. P. Perdew, V. Sahni, M. K. Harbola, and R. K. Pathak, Fourth-order gradient expansion of the fermion kinetic energy:

- Extra terms for nonanalytic densities, *Phys. Rev. B* **34**, 686 (1986).
- [112] J. P. Boyd, Orthogonal rational functions on a semi-infinite interval, *J. Comput. Phys.* **70**, 63 (1987).
- [113] W. H. Press, S. A. Teukolsky, W. T. Vetterling, and B. P. Flannery, *Numerical Recipes* (Cambridge University Press, Cambridge, New York, 1992).
- [114] J. W. Furness and J. Sun, Enhancing the efficiency of density functionals with an improved iso-orbital indicator, *Phys. Rev. B* **99**, 041119(R) (2019).
- [115] A. Makmal, S. Kümmel, and L. Kronik, Fully numerical all-electron solutions of the optimized effective potential equation for diatomic molecules, *J. Chem. Theory Comput.* **5**, 1731 (2009).
- [116] *CRC Handbook of Chemistry and Physics*, 98th ed., edited by J. Rumble (CRC Press, Boca Raton, FL, 2017).
- [117] T. Aschebrock and S. Kümmel, Exploring local range separation: The role of spin scaling and one-electron self-interaction, *J. Chem. Phys.* **151**, 154108 (2019).
- [118] A. Kaiser and S. Kümmel, Revealing the field-counteracting term in the exact Kohn-Sham correlation potential, *Phys. Rev. A* **98**, 052505 (2018).
- [119] V. N. Staroverov, G. E. Scuseria, J. Tao, and J. P. Perdew, Tests of a ladder of density functionals for bulk solids and surfaces, *Phys. Rev. B* **69**, 075102 (2004).
- [120] J. Heyd, J. E. Peralta, G. E. Scuseria, and R. L. Martin, Energy band gaps and lattice parameters evaluated with the Heyd-Scuseria-Ernzerhof screened hybrid functional, *J. Chem. Phys.* **123**, 174101 (2005).
- [121] R. J. Guerrero-Moreno and N. Takeuchi, First principles calculations of the ground-state properties and structural phase transformation in CdO, *Phys. Rev. B* **66**, 205205 (2002).
- [122] F. P. Koffyberg, Thermoreflectance spectra of CdO: Band gaps and band-population effects, *Phys. Rev. B* **13**, 4470 (1976).
- [123] F. Tran, P. Blaha, and K. Schwarz, Band gap calculations with Becke-Johnson exchange potential, *J. Phys.: Condens. Matter* **19**, 196208 (2007).
- [124] Z. H. Yang, H. Peng, J. Sun, and J. P. Perdew, More realistic band gaps from meta-generalized gradient approximations: Only in a generalized Kohn-Sham scheme, *Phys. Rev. B* **93**, 205205 (2016).
- [125] N. Sai, P. F. Barbara, and K. Leung, Hole Localization in Molecular Crystals from Hybrid Density Functional Theory, *Phys. Rev. Lett.* **106**, 226403 (2011).
- [126] C. Adamo and V. Barone, Toward reliable density functional methods without adjustable parameters: The PBE0 model, *J. Chem. Phys.* **110**, 6158 (1999).
- [127] A. Seidl, A. Görling, P. Vogl, J. A. Majewski, and M. Levy, Generalized Kohn-Sham schemes and the band-gap problem, *Phys. Rev. B* **53**, 3764 (1996).
- [128] J. P. Perdew, W. Yang, K. Burke, Z. Yang, E. K. U. Gross, M. Scheffler, G. E. Scuseria, T. M. Henderson, I. Y. Zhang, A. Ruzsinszky, H. Peng, J. Sun, E. Trushin, and A. Görling, Understanding band gaps of solids in generalized Kohn-Sham theory, *Proc. Natl. Acad. Sci. USA* **114**, 2801 (2017).
- [129] L. Kronik, T. Stein, S. Refaely-Abramson, and R. Baer, Excitation gaps of finite-sized systems from optimally tuned range-separated hybrid functionals, *J. Chem. Theory Comput.* **8**, 1515 (2012).
- [130] G. te Velde and E. J. Baerends, Precise density-functional method for periodic structures, *Phys. Rev. B* **44**, 7888 (1991); G. Wiesenekker and E. J. Baerends, Quadratic integration over the three-dimensional Brillouin zone, *J. Phys.: Condens. Matter* **3**, 6721 (1991); M. Franchini, P. H. T. Philipsen, and L. Visscher, The Becke fuzzy cells integration scheme in the Amsterdam density functional program suite, *J. Comput. Chem.* **34**, 1819 (2013); M. Franchini, P. H. T. Philipsen, E. van Lenthe, and L. Visscher, Accurate Coulomb potentials for periodic and molecular systems through density fitting, *J. Chem. Theory Comput.* **10**, 1994 (2014); BAND2017, SCM, Theoretical Chemistry, Vrije Universiteit, Amsterdam, The Netherlands, <https://www.scm.com>.
- [131] H. J. Monkhorst and J. D. Pack, Special points for Brillouin-zone integrations, *Phys. Rev. B* **13**, 5188 (1976).
- [132] E. Van Lenthe and E. J. Baerends, Optimized Slater-type basis sets for the elements 1-118, *J. Comput. Chem.* **24**, 1142 (2003).
- [133] P. H. T. Philipsen, E. van Lenthe, J. G. Snijders, and E. J. Baerends, Relativistic calculations on the adsorption of CO on the (111) surfaces of Ni, Pd, and Pt within the zeroth-order regular approximation, *Phys. Rev. B* **56**, 13556 (1997).
- [134] L. Reining, V. Olevano, A. Rubio, and G. Onida, Excitonic Effects in Solids Described by Time-Dependent Density-Functional Theory, *Phys. Rev. Lett.* **88**, 066404 (2002).
- [135] F. Gygi, Electronic-structure calculations in adaptive coordinates, *Phys. Rev. B* **48**, 11692 (1993).
- [136] S. Lehtola, C. Steigemann, M. J. Oliveira, and M. A. Marques, Recent developments in libxc — A comprehensive library of functionals for density functional theory, *SoftwareX* **7**, 1 (2018).
- [137] N. Troullier and J. L. Martins, Efficient pseudopotentials for plane-wave calculations, *Phys. Rev. B* **43**, 1993 (1991).

Publication 4

Exploring local range separation: The role of spin scaling and one-electron self-interaction

Journal of Chemical Physics **151**, 154108 (2019)

Thilo Aschebrock and Stephan Kümmel

Theoretical Physics IV, University of Bayreuth, 95440 Bayreuth, Germany

Publ. 4

My contribution

I developed the local range-separation parameters presented in this manuscript, performed all analytical derivations and numerical calculations. The Slater-type basis set code for closed shell atoms used in some of the numerical calculations was written by myself. I implemented relevant routines in DARSEC, prepared all figures, and wrote a first draft of the manuscript and of the supplementary material.

Publ.4

Exploring local range separation: The role of spin scaling and one-electron self-interaction

Cite as: J. Chem. Phys. 151, 154108 (2019); doi: 10.1063/1.5121731

Submitted: 27 July 2019 • Accepted: 30 September 2019 •

Published Online: 17 October 2019



View Online



Export Citation



CrossMark

Thilo Aschebrock  and Stephan Kümmel^{a)} 

AFFILIATIONS

Theoretical Physics IV, University of Bayreuth, 95440 Bayreuth, Germany

^{a)}stephan.kuemmel@uni-bayreuth.de

ABSTRACT

Range-separated hybrid functionals with a fitted or tuned global range-separation parameter are frequently used in density functional theory. We here explore the concept of local range separation, i.e., of turning the range-separation parameter into an explicit semilocal density functional. We impose three simple constraints on the local range-separation parameter that are frequently used in density functional construction: uniform density scaling, the homogeneous electron gas limit, and freedom from one-electron self-interaction. We further discuss different ways of how to model the spin dependence in combination with local range separation. We evaluate our local range-separation energy functionals exactly for closed-shell atoms using the previously suggested hypergeneralized gradient approximation for molecules and assess the quality of this approximation. We find a local range-separated hybrid functional that yields accurate binding energies for a set of small molecules.

Published under license by AIP Publishing. <https://doi.org/10.1063/1.5121731>

I. INTRODUCTION

Exchange-correlation (xc) functionals in which exact Fock exchange is combined with semilocal functional components in a range-separation approach^{1,2} have been very successful, in particular, for describing processes that depend sensitively on charge-rearrangement, such as long-range (LR) charge-transfer.^{3,4} Yet, commonly used range-separation functionals have at least two drawbacks. First, they are not one-electron self-interaction^{3–7} free. This is a formal deficiency as the functional is not correct in the important limiting case of one-electron systems. It is a practical limitation in problems that depend on one-electron properties, such as electronic binding in certain systems, stretched hydrogen bonds, and ionization energies. Second, there is no universal choice for the range-separation parameter.⁸ The latter plays a decisive role in these functionals. When it is determined empirically^{9–12} to optimize binding energies, then one is led to relatively low fractions of Fock exchange in the functional that do not yield a reliable description of charge-transfer characteristics. If one chooses the parameter such that ionization potentials or charge-transfer characteristics are well reproduced, then one finds binding energies that are of limited accuracy. Additionally, neither of these

or any other method for determining a global but system-specific range-separation parameter conform¹³ with the formal concept of size-consistency.¹⁴

In the present work, we take a step to tackle these problems. The central idea of our approach is to solve the first problem, i.e., design a range-separated hybrid in such a way that it is one-electron self-interaction free, in the hope that this will also alleviate the second problem. To do so, we follow up on the work of Krukau *et al.*¹⁵ that probed the concept of a local range-separation parameter as well as a hyper-GGA (generalized gradient approximation) approximation to range-separated hybrids. Our findings indicate, though, that the formal property of being correct for one-electron systems does not necessarily translate into an improved description of electronic binding. On the other hand, we note that the way in which spin-polarization is treated in the range-separated hybrid construction is important for the description of binding—especially when realizing one-electron self-interaction freedom. We also test the reliability and robustness of the hyper-GGA approximation that has been introduced to facilitate the evaluation of local range-separated hybrids. We show that it can have significant consequences and, therefore, should rather be seen as an alternative definition of range-separation functionals.

This paper is organized as follows: Section II starts by summarizing the concept and formulas for the usual range-separation approach based on a *global* range-separation parameter. We then discuss the merits and limitation of a *local* range-separation parameter and how it can be utilized to eliminate the one-electron self-interaction error in Sec. II B. We continue in Sec. II C by suggesting new avenues to make use of spin-polarization which are opened up by a local range-separation parameter. Next, the hyper-GGA approximation for range-separation hybrids is recapped and its reliability and robustness is assessed in Sec. III. Finally, in Sec. IV, we present and analyze the results obtained with several local range-separation parameters that we developed.

II. THEORY OF RANGE-SEPARATED HYBRIDS

The primary idea of the range-separation approach is to split^{1,2} the Coulomb interaction into short-range (SR) and long-range (LR) components,

$$\frac{1}{|\mathbf{r}-\mathbf{r}'|} = \underbrace{\frac{\operatorname{erfc}(\omega|\mathbf{r}-\mathbf{r}'|)}{|\mathbf{r}-\mathbf{r}'|}}_{\text{SR}} + \underbrace{\frac{\operatorname{erf}(\omega|\mathbf{r}-\mathbf{r}'|)}{|\mathbf{r}-\mathbf{r}'|}}_{\text{LR}}, \quad (1)$$

where $\operatorname{erfc}(\cdot) = 1 - \operatorname{erf}(\cdot)$ and the screening ω determines an inverse length for the associated range separation. This range separation is then utilized to split the exchange energy $E_x[n]$ based on its representation^{16,17} via the exchange hole $h_x(\mathbf{r}, \mathbf{r}')$,

$$E_x[n] = \frac{1}{2} \iint \frac{n(\mathbf{r})h_x(\mathbf{r}, \mathbf{r}')}{|\mathbf{r}-\mathbf{r}'|} d^3r' d^3r, \quad (2)$$

into SR and LR components of the exchange hole as well as of the corresponding exchange energy. When focusing on finite systems, one typically treats the LR component exactly,

$$E_x^{\text{ex,LR}}[n, \omega] = -\frac{1}{2} \sum_{\sigma=\uparrow, \downarrow} \sum_{ij=1}^{N_\sigma} \iint \frac{\varphi_{i\sigma}^*(\mathbf{r})\varphi_{j\sigma}^*(\mathbf{r}')\varphi_{j\sigma}(\mathbf{r})\varphi_{i\sigma}(\mathbf{r}')}{|\mathbf{r}-\mathbf{r}'|} \times \operatorname{erf}(\omega|\mathbf{r}-\mathbf{r}'|) d^3r' d^3r, \quad (3)$$

whereas the SR component is modeled by a semilocal approximation for the exchange hole,

$$E_x^{\text{sl,SR}}[n, \omega] = \frac{1}{2} \iint \frac{n(\mathbf{r})h_x^{\text{sl}}(\mathbf{r}, \mathbf{r}')}{|\mathbf{r}-\mathbf{r}'|} \times \operatorname{erfc}(\omega|\mathbf{r}-\mathbf{r}'|) d^3r' d^3r. \quad (4)$$

Most semilocal exchange hole models only depend on quantities at the reference point \mathbf{r} and are customarily angle averaged with respect to that point, i.e.,

$$h_x^{\text{sl}}(\mathbf{r}, \mathbf{r}') = \bar{h}_x^{\text{sl}}(n(\mathbf{r}), |\nabla n(\mathbf{r})|, \dots, |\mathbf{r}-\mathbf{r}'|). \quad (5)$$

Thus, one can perform the integration over \mathbf{r}' analytically. This simplifies the expression considerably. For example, when using the exchange hole of the local density approximation (LDA), one arrives at^{18,19}

$$E_x^{\text{LDA,SR}}[n, \omega] = A_x \int n^{4/3}(\mathbf{r}) F_{\text{SR}}(\omega/k_F(\mathbf{r})) d^3r \quad (6)$$

with $A_x = -(3/4)(3/\pi)^{1/3}$, the Fermi wavevector $k_F(\mathbf{r}) = [3\pi^2 n(\mathbf{r})]^{1/3}$, and an associated function

$$F_{\text{SR}}(x) = 1 - \frac{2x}{3} [2\sqrt{\pi} \operatorname{erf}(x^{-1}) - 3x + x^3 + (2x - x^3) \exp(-x^{-2})]. \quad (7)$$

The combination of two different exchange holes for SR and LR then effectively models not only exchange but to some extent also correlation.

The remaining correlation part is typically approximated by an ordinary semilocal correlation—in this work, we use, unless otherwise specified, LDA correlation $E_c^{\text{LDA}}[n]$ in the parameterization of Perdew and Wang.²⁰ A complete range-separated hybrid (here based on LDA) is thus given by^{21,22}

$$E_{xc}^{\text{LC-}\omega\text{LDA}}[n, \omega] = E_x^{\text{ex,LR}}[n, \omega] + E_x^{\text{LDA,SR}}[n, \omega] + E_c^{\text{LDA}}[n]. \quad (8)$$

We note that in the past successful functionals have also been constructed by further including a SR component of Fock exchange.^{9,23,24} Such more general forms have proven particularly useful when extended, solid-state systems are of interest. However, for the sake of transparency, we here restrict ourselves to the general functional form of Eq. (8), to which we refer as LR corrected (LC) LDA in the following. The fact that the local range-separation approach is effectively modeling correlation with the help of SR exchange can be emphasized by bringing the range-separated hybrid to the form

$$E_{xc}^{\text{LC-}\omega\text{LDA}}[n, \omega] = E_x^{\text{ex}}[n] + E_c^{\text{LC-}\omega\text{LDA}}[n, \omega] \quad (9)$$

with

$$E_c^{\text{LC-}\omega\text{LDA}}[n, \omega] = E_x^{\text{LDA,SR}}[n, \omega] - E_x^{\text{ex,SR}}[n, \omega] + E_c^{\text{LDA}}[n]. \quad (10)$$

Depending on the choice of the range-separation parameter, the properties of a range-separated hybrid can vary drastically.²² It can range from treating all of the Coulomb interactions as LR for $\omega \rightarrow \infty$ to treating all of them as SR for $\omega \rightarrow 0$. Many implementations of range separation use a universal, i.e., system-independent range-separation parameter. However, it has been shown that the scheme can unfold considerable further power when the parameter is tuned for each system separately.^{3,25} Among the important successes of the tuning scheme are the prediction of charge-transfer excitations,²⁶ fundamental gaps,^{27,28} and optical gaps.^{29,30}

Tuning is partially motivated by the already mentioned observation that there is no truly universal parameter that, e.g., accurately describes binding energies and ionization potentials simultaneously. However, the tuning procedure also has drawbacks. A practical disadvantage is that it requires many more computational steps than a usual one-way self-consistent calculation. However, there are also conceptual questions. Most notably, a nonuniversal system-dependent range-separation parameter violates size-consistency.^{11,13} Tuning for a system with a complicated intrinsic electronic structure is thus conceptually and practically challenging. Furthermore, if one interprets tuning as a way to turn the range-separation parameter into an (implicit) density functional, then one would have to take the density dependence into account when taking the

functional derivative that leads to the potential.¹³ This, however, is and cannot be done as the density dependence is not explicitly known. Also, tuning for extended, solid-state systems faces special challenges.³¹

A. From a global to a local range-separation parameter

In order to satisfy size-consistency, ω cannot just be a global density functional, i.e., it must have an explicit spatial dependence. Therefore, an (at least) local range-separation parameter, i.e., $\omega([n]; \mathbf{r})$, is inevitable. A functional of this type was proposed and explored by Krukau *et al.*¹⁵ The more general case, where $\omega([n]; \mathbf{r}, \mathbf{r}')$ is even a two point function, is deliberately not considered in this work, as already a single spatial dependence proves to be challenging—both in the construction and implementation of such functionals. This will become clear in the course of this paper.

The important advantage of $\omega([n]; \mathbf{r})$ only depending on the reference point \mathbf{r} is that the integration over \mathbf{r}' can be performed analytically for any spherically symmetric exchange hole model that only depends on semilocal ingredients at the reference point [cf. Eq. (5)]. Therefore, the associated local range-separated hybrid of a given $\omega([n]; \mathbf{r})$ can be obtained by simply replacing ω with $\omega([n]; \mathbf{r})$ in Eqs. (3) and (6). One might be led to believe that the corresponding total xc energy, in particular, when written in the form of Eq. (4), is not symmetric with respect to interchange of electrons ($\mathbf{r} \leftrightarrow \mathbf{r}'$), given that ω only depends on \mathbf{r} . However, as demonstrated in Ref. 15, this is purely of computational convenience since the xc energy can formally always be symmetrized.

A so far promising ansatz by Krukau *et al.*¹⁵ for a local range-separation parameter is

$$\omega^K([n]; \mathbf{r}) = \eta \frac{|\nabla n(\mathbf{r})|}{n(\mathbf{r})} \quad (11)$$

with $\eta = 0.135$ optimized for enthalpies of formation. As detailed in Ref. 15, this functional form and the magnitude of the value of the parameter η can be motivated based on previous work.^{32–34} In the following, we will investigate alternative expressions for $\omega([n]; \mathbf{r})$ based on formal constraints, in particular, to eliminate the one-electron self-interaction error.

B. Formal constraints

In the realm of semilocal density functionals, the concept of a constraint-guided construction has become a tremendous success story.^{35–38} Given that we seek a semilocal expression for $\omega([n]; \mathbf{r})$, it might be worthwhile to also explore exact constraints on $\omega([n]; \mathbf{r})$.

First, we consider the uniform density scaling³⁹ to the high-density limit,

$$n(\mathbf{r}) \rightarrow n_\lambda(\mathbf{r}) = \lambda^3 n(\lambda\mathbf{r}) \quad \text{as } \lambda \rightarrow \infty. \quad (12)$$

In this limit, the exact exchange energy should dominate,⁴⁰

$$\lim_{\lambda \rightarrow \infty} \frac{E_{xc}[n_\lambda]}{E_x^\lambda[n_\lambda]} = 1. \quad (13)$$

In the context of range-separation, this implies that LR should prevail, and consequently, the local range-separation parameter needs to scale up faster than linearly,¹⁵

$$\omega([n_\lambda]; \mathbf{r}) \gg \lambda \omega([n]; \lambda\mathbf{r}) \quad \text{as } \lambda \rightarrow \infty. \quad (14)$$

Second, we seek to reproduce the homogeneous electron gas limit. Therefore, it is natural to require $\omega([n]; \mathbf{r}) \rightarrow 0$ in the limit of a slowly varying density, thereby the local range-separated hybrid of Eq. (8) reduces to LDA exactly.

A third reasonable constraint that can be imposed on ω is freedom from one-electron self-interaction, i.e.,

$$E_H[n_{i\sigma}] + E_{xc}[n_{i\sigma}, 0] = 0 \quad (15)$$

for any one-spin-orbital density $n_{i\sigma} = |\varphi_{i\sigma}(\mathbf{r})|^2$, where

$$E_H[n] = \frac{1}{2} \iint \frac{n(\mathbf{r})n(\mathbf{r}')}{|\mathbf{r} - \mathbf{r}'|} d^3r' d^3r \quad (16)$$

is the usual (classical) Hartree energy. A common technique to eliminate (or reduce) the self-interaction error is the use of a semilocal iso-orbital indicator or even of a one-spin-orbital-region indicator.^{41–45} Both indicators are typically based on the noninteracting kinetic energy density

$$\tau(\mathbf{r}) = \frac{1}{2} \sum_{\sigma=\uparrow, \downarrow} \sum_{i=1}^{N_\sigma} |\nabla \varphi_{i\sigma}(\mathbf{r})|^2 \quad (17)$$

and its single-orbital limit

$$\tau^W(\mathbf{r}) = \frac{|\nabla n(\mathbf{r})|^2}{8n(\mathbf{r})}, \quad (18)$$

the von Weizsäcker kinetic energy density. Their dimensionless ratio

$$z(\mathbf{r}) = \frac{\tau^W(\mathbf{r})}{\tau(\mathbf{r})}, \quad (19)$$

a common meta-GGA ingredient, is bound between its homogeneous electron gas limit, 0, and its single-orbital limit, 1. As the LR part is by definition one-electron self-interaction free and the SR part is not, we deduce that $\omega \rightarrow \infty$ in the one-spin-orbital limit. Thus, freedom from one-electron self-interaction for a local range-separated hybrid can be formulated as

$$\omega([n]; \mathbf{r}) \rightarrow \infty \quad (20)$$

as $z \rightarrow 1$ in the one-orbital limit or more strictly as additionally the spin-polarization

$$\zeta(\mathbf{r}) = \frac{n_\uparrow(\mathbf{r}) - n_\downarrow(\mathbf{r})}{n_\uparrow(\mathbf{r}) + n_\downarrow(\mathbf{r})} \rightarrow \pm 1 \quad (21)$$

in the one-spin-orbital limit—provided that one uses a one-electron self-interaction free density functional to model the semilocal correlation. To this end, we employ a simple, one-electron self-interaction corrected LDA correlation variant,

$$E_c^{\text{sic-LDA}}[n] = \int [1 - z(\mathbf{r})\zeta^2(\mathbf{r})] e_c^{\text{LDA}}(\mathbf{r}) d^3r, \quad (22)$$

in Eq. (8) instead of $E_c^{\text{LDA}}[n]$, where $e_c^{\text{LDA}}(\mathbf{r})$ is the usual LDA correlation energy density per unit volume. This expression has been used previously in a local hybrid functional.⁴⁵ Alternatively, one could replace $E_c^{\text{LDA}}[n]$ with one of the many established meta-GGAs for correlation with more sophisticated one-electron self-interaction freedom built in.^{36,37,42}

We note in passing that it is difficult to precisely define single-electron regions in many-electron systems and that this difficulty can be reflected in mathematical properties, such as an order-of-limits problem.^{46,47} In a similar vein, it has been shown that the formal property of being one-electron self-interaction free does not necessarily lead to a reduction of the many-electron self-interaction error.^{48–50}

The three constraints on the construction of a local range-separation parameter with the addition of the trivial requirement of positivity, i.e., $\omega([n]; \mathbf{r}) \geq 0$, can be combined as follows:

First, for one-electron self-interaction freedom, we have to generate a singularity in $\omega([n]; \mathbf{r})$ as $z \rightarrow 1$. A straightforward pole for this purpose is

$$\Theta(z) = \frac{1}{1-z}, \quad (23)$$

with the property $\Theta(z) \geq 1$, where the equality is approached in the homogeneous electron gas limit. Moreover, z and therefore $\Theta(z)$ are invariant under uniform density scaling,

$$\Theta([n_\lambda]; \mathbf{r}) = \Theta([n]; \lambda \mathbf{r}). \quad (24)$$

Thus, one can multiply any local range-separation parameter that already satisfies the two other constraints with this pole to add one-electron self-interaction freedom to the list. We have also tested generalizations of this pole, e.g.,

$$\Theta_n(z) = \frac{1}{1-z} - \sum_{k=0}^n z^k, \quad (25)$$

as well as stronger logarithmic singularities,

$$\Theta_n^{\text{ln}}(z) = 1 - \ln(1-z) - \sum_{k=0}^n \frac{z^k}{k}, \quad (26)$$

with $n \in \mathbb{N}_0$ for both expressions, but find that the straightforward pole of Eq. (23) gives ultimately the best results.

Second, we seek a simple ansatz for a positive local range-separation parameter that (i) vanishes in the homogeneous electron gas limit, (ii) scales faster than linearly in the high-density limit, and hence, when multiplied with $\Theta(z)$ fulfills all proposed exact constraints. The work of Krukau *et al.*¹⁵ suggests—and we have independently confirmed this in a search for an alternative—that ω^K of Eq. (11) is almost optimal for this purpose. Only “almost” because it only scales linearly under uniform density scaling to the high-density limit,

$$\omega^K([n_\lambda]; \mathbf{r}) = \lambda \omega^K([n]; \lambda \mathbf{r}). \quad (27)$$

This deficit can, however, be fixed in a minimally invasive fashion by adding a logarithmic contribution to the high-density limit,

$$\omega([n]; \mathbf{r}) = c_1 \omega^K[1 + \ln(1 + c_2 \omega^K)], \quad (28)$$

and consequently,

$$\omega([n_\lambda]; \mathbf{r}) \sim \lambda \ln(\lambda) \omega([n]; \lambda \mathbf{r}) \gg \lambda \omega([n]; \lambda \mathbf{r}) \quad (29)$$

as $\lambda \rightarrow \infty$. Therefore, we propose

$$\omega = c_1 \omega^K[1 + \ln(1 + c_2 \omega^K)] \Theta(z) \quad (30)$$

as a local range-separation parameter that satisfies all herein imposed exact constraints. The two positive parameters c_1 and c_2 , however, cannot be determined from the imposed constraints. This demonstrates that there is a need for additional constraints to guide the construction of local range-separation parameters further. In Sec. IV, we try to circumvent this issue in a similar manner as Ref. 15 by testing the proposed local range-separation parameter functional with parameters c_1 and c_2 that are optimized for binding energies. Looking at other observables, e.g., reaction barriers, may lead to other optimal parameters. The fitting to energies, however, gives us a first estimate for the values of the parameters.

C. Spin-polarization revisited

When using a global range-separation parameter, the extension of a range-separate hybrid in the form of Eq. (8) to the spin-polarized case is straightforward, given the standard generalization for the semilocal correlation energy, $E_c^{\text{sl}}[n_\uparrow, n_\downarrow]$, and the spin-scaling relationship for the exchange energy,⁵¹

$$E_x[n_\uparrow, n_\downarrow] = \frac{1}{2} (E_x[2n_\uparrow, 2\tau_\uparrow] + E_x[2n_\downarrow, 2\tau_\downarrow]), \quad (31)$$

as well as the relationship for the exchange hole,⁵²

$$h_x([n_\uparrow, n_\downarrow]; \mathbf{r}, \mathbf{r}') = \sum_{\sigma=\uparrow, \downarrow} \frac{n_\sigma(\mathbf{r})}{n(\mathbf{r})} h_x([2n_\sigma, 2\tau_\sigma]; \mathbf{r}, \mathbf{r}'), \quad (32)$$

where we have notated the kinetic energy dependence explicitly on the right-hand side for convenience of the reader.

As the local range-separation approach is essentially a mixing of two different exchange energies, more specifically exchange holes, it appears to be obvious¹⁵ to apply this spin-scaling relation to the local range-separation parameter as well. The result is a different range-separation parameter for each spin channel,

$$\omega_\sigma([n_\sigma, \tau_\sigma]; \mathbf{r}) = \omega([2n_\sigma, 2\tau_\sigma]; \mathbf{r}), \quad (33)$$

which only depends on the quantities of the respective spin channel.

However, when we remind ourselves that the mixing of the exact and the semilocally approximated exchange holes within a range-separated hybrid is essentially modeling correlation, it stands to reason that the spin scaling for exchange is not mandatory for a local range-separation parameter. Similar reasoning and approaches have been proven successful in the related field of local hybrid functionals.⁴⁵ The idea is particularly appealing here because this allows us to make use of the spin-polarization $\zeta(\mathbf{r})$ explicitly and, thus, to employ a one-spin-orbital indicator instead of an iso-orbital indicator. Therefore, we explore using the same local range-separation parameter

$$\omega_{\sigma}([n_{\uparrow}, n_{\downarrow}, \tau_{\uparrow}, \tau_{\downarrow}]; \mathbf{r}) = \omega([n, \tau, \zeta]; \mathbf{r}) \quad (34)$$

for both spin channels, but with an explicit dependence on the spin-polarization.

This can readily be done by replacing $\Theta(z)$ with $\Theta(z\zeta^2)$. We will also consider an intermediate path with independent range-separation parameters for each spin channel that depend on ζ in addition to the quantities of the respective spin channel, i.e.,

$$\omega_{\sigma}([n_{\uparrow}, n_{\downarrow}, \tau_{\sigma}]; \mathbf{r}) = \omega([2n_{\sigma}, 2\tau_{\sigma}, \zeta]; \mathbf{r}). \quad (35)$$

For this purpose, $z_{\sigma}\zeta^2$ is used as the parameter of the pole function, e.g.,

$$\omega_{\sigma} = c_1 \omega_{\sigma}^{\text{K}} [1 + \ln(1 + c_2 \omega_{\sigma}^{\text{K}})] \Theta(z_{\sigma}\zeta^2), \quad (36)$$

where we keep the original definition

$$\omega_{\sigma}^{\text{K}} = \omega^{\text{K}}([2n_{\sigma}]; \mathbf{r}) = 0.135 |\nabla n_{\sigma}| / n_{\sigma} \quad (37)$$

to ease comparisons. The results that we find with these different functionals are discussed in Sec. IV.

III. HYPER-GGA APPROXIMATION

A. Merits and limitation of the hyper-GGA approximation

One of the biggest obstacles that arises when going from a global to a local range-separation parameter is a steep increase in the computational cost for evaluating the energy—not even considering the evaluation of the severely more complex corresponding functional derivative that would be needed for a self-consistent (generalized) Kohn-Sham calculation. While a standard range-separated hybrid is computationally already much more demanding than any semilocal density functional, there exist various numerical techniques, e.g., analytic integration^{18,19} of electrostatic integrals in a Gaussian basis set or using a resolution of identity approximation.⁵³ Unfortunately, neither technique can be applied to full extent once the range-separation parameter is an arbitrary spatial function.¹⁵

With this in mind, Krukau *et al.*¹⁵ proposed a hyper-GGA approximation for the LR component,

$$\begin{aligned} E_{\text{x}}^{\text{ex,LR}}[n, \omega] &\approx E_{\text{x}}^{\text{hyper-GGA,LR}}[n, \omega] \\ &= \frac{1}{2} \iint \frac{n(\mathbf{r}) \tilde{h}_{\text{x}}^{\text{sl}}(n(\mathbf{r}), |\nabla n(\mathbf{r})|, \tau(\mathbf{r}), e_{\text{x}}^{\text{ex}}(\mathbf{r}), |\mathbf{r} - \mathbf{r}'|)}{|\mathbf{r} - \mathbf{r}'|} \\ &\quad \times \text{erf}(\omega([n]; \mathbf{r})|\mathbf{r} - \mathbf{r}'|) d^3 r' d^3 r. \end{aligned} \quad (38)$$

At each point in space \mathbf{r} , the exact exchange hole associated with this reference point, $h_{\text{x}}^{\text{ex}}(\mathbf{r}, \mathbf{r}')$, represented via the exact exchange energy density

$$\begin{aligned} e_{\text{x}}^{\text{ex}}(\mathbf{r}) &= \frac{1}{2} \int \frac{n(\mathbf{r}) h_{\text{x}}^{\text{ex}}(\mathbf{r}, \mathbf{r}')}{|\mathbf{r} - \mathbf{r}'|} d^3 r' \\ &= -\frac{1}{2} \sum_{\sigma=\uparrow, \downarrow} \sum_{ij=1}^{N_{\sigma}} \int \frac{\varphi_{i\sigma}^*(\mathbf{r}) \varphi_{j\sigma}^*(\mathbf{r}') \varphi_{j\sigma}(\mathbf{r}) \varphi_{i\sigma}(\mathbf{r}')}{|\mathbf{r} - \mathbf{r}'|} d^3 r', \end{aligned} \quad (39)$$

is approximated by the corresponding spherically averaged semilocal exchange hole model. This is a common technique that has

proven successful, e.g., for modeling non-dynamical correlation.^{54–57} In the context of a (local) range-separated hybrid, this approximation then again allows for an analytic \mathbf{r}' -integration of the LR component. Thereby, the LR energy component is reduced to the hyper-GGA form, i.e.,

$$\begin{aligned} E_{\text{x}}^{\text{hyper-GGA,LR}}[n, \omega] &= A_{\text{x}} \int n^{4/3}(\mathbf{r}) F(n(\mathbf{r}), |\nabla n(\mathbf{r})|, \nabla^2 n(\mathbf{r}), \\ &\quad \times \tau(\mathbf{r}), e_{\text{x}}^{\text{ex}}(\mathbf{r}), \omega(\mathbf{r})) d^3 r, \end{aligned} \quad (40)$$

where the exact exchange energy density is used as an additional ingredient alongside semilocal ingredients. The resulting computational expense is thus, at least in principle, reduced to the level of, e.g., a local hybrid. Due to the fact that the unscreened semilocal exchange hole is designed to yield the exact exchange energy density, this approximation is also exact in the limit $\omega \rightarrow \infty$, in addition to the $\omega \rightarrow 0$ limit, where exactness is given trivially as the LR component vanishes.

The quality of the hyper-GGA approximation to a range-separated hybrid is by construction closely linked to the choice of the semilocal exchange hole model because different hole models are constructed to satisfy different exact constraints. So far, only the original Tao, Perdew, Staroverov, Scuseria (TPSS) exchange hole,⁵⁸ adopted to reproduce the exact exchange energy density, has been used.¹⁵ In order to explore new avenues and thereby test the robustness of the hyper-GGA approximation, we here choose to employ a revised TPSS (TPSSrev) exchange hole model that has been recently proposed⁵⁹ as well as a generalized version^{54,57} of the Becke-Roussel (BR) exchange hole model.⁶⁰ The three free parameters of the spherical-averaged BR hole are determined by the on-top value condition,

$$\tilde{h}_{\text{x}}(\mathbf{r}, \mathbf{r}') \Big|_{\mathbf{r}'=\mathbf{r}} = -\frac{1}{2} n(\mathbf{r}), \quad (41)$$

the requirement that the exchange hole model must have the same curvature^{60–62} as the exact exchange hole,

$$\left. \frac{\partial^2 \tilde{h}_{\text{x}}(\mathbf{r}, u)}{\partial u^2} \right|_{u=0} = -Q(\mathbf{r}) \quad (42)$$

with

$$Q(\mathbf{r}) = \frac{1}{6} \{ \nabla^2 n(\mathbf{r}) - 4[\tau(\mathbf{r}) - \tau^{\text{W}}(\mathbf{r})] \} \quad (43)$$

and the inter-electron separation $u = |\mathbf{r} - \mathbf{r}'|$, and the reproduction of the exact exchange energy density,

$$e_{\text{x}}^{\text{ex}}(\mathbf{r}) = 2\pi n(\mathbf{r}) \int_0^{\infty} \tilde{h}_{\text{x}}(\mathbf{r}, u) u du. \quad (44)$$

This, however, implies that the corresponding hole is not properly normalized to -1 . It has been argued that employing a non-normalized hole can be advantageous in cases where the exact exchange hole is delocalized.^{54,57}

A detailed overview of the TPSS, the TPSSrev, and BR hole models as well as their analytically integrated screened representations that are used in this work is given in the [supplementary material](#).

The reliability of the hyper-GGA approximation to a range-separated hybrid has so far only been assessed¹⁵ for a global range-separated hybrid, LC- ω LDA, but not for an actual local range-separation parameter. Aside from indirectly analyzing this approximation by using different semilocal models for the exchange hole, we investigate a special case where a direct comparison is possible as the computational expense can be reduced to a feasible level, namely, spherically symmetric systems, e.g., closed-shell atoms. As we demonstrate in detail in the [supplementary material](#), once the system has spherical symmetry, both angular integrations corresponding to \mathbf{r} and \mathbf{r}' can be performed analytically. Thereupon, the costly LR energy component reduces to a single two dimensional integral

$$E_x^{\text{ex,LR}}[n, \omega] = - \int_0^\infty \int_0^\infty \sum_{l=0}^\infty \sum_{l_1, l_2=0}^{l_{\max}} (2l_1 + 1)(2l_2 + 1) \begin{pmatrix} l_1 & l_2 & l \\ 0 & 0 & 0 \end{pmatrix}^2 \times c_l(\omega(r), r, r') \sum_{n_1=1}^{N_{l_1}} \sum_{n_2=1}^{N_{l_2}} R_{n_1}^{l_1}(r) R_{n_2}^{l_2}(r') \times R_{n_2}^{l_2}(r) R_{n_1}^{l_1}(r') r^2 r'^2 dr' dr, \quad (45)$$

which is readily integrated numerically on a radial grid. Here, the first sum runs over all angular quantum numbers l (but only a finite number of terms is nonvanishing), the second double sum runs over all occupied angular quantum numbers l_1 , l_2 , and the third and fourth sums run over all occupied principal quantum numbers n_i of the associated angular momentum l_i , and

$$\begin{pmatrix} l_1 & l_2 & l \\ 0 & 0 & 0 \end{pmatrix} \quad (46)$$

are the (mostly vanishing) Wigner 3-j symbols. Furthermore, $\{R_n^l(r)\}$ are the radial orbitals of angular momentum l , and the $c_l(\omega(r), r, r')$ are the coefficients of the Legendre expansion of the LR kernel,⁶⁴

$$\frac{\text{erf}[\omega(r)|\mathbf{r} - \mathbf{r}'|]}{|\mathbf{r} - \mathbf{r}'|} = \sum_{l=0}^\infty c_l(\omega(r), r, r') P_l(\cos \delta) \quad (47)$$

with the intermediate angle δ between \mathbf{r} and \mathbf{r}' , and the usual Legendre polynomial $P_l(x)$ of degree l . The first three coefficients of this expansion that are required for a calculation up to the p -shell, i.e., up to calcium, are given in the [supplementary material](#).

B. Reliability of the hyper-GGA approximation

We have implemented the analytic LR angular integration, i.e., Eq. (45), as well as the hyper-GGA approximation of Eq. (40) based on the TPSS, on the TPSSrev, and on the BR hole in our own code for closed-shell atoms. While the angular components described by spherical harmonics are handled analytically, the radial functions are represented by an even-tempered Slater-type QZ basis set,⁶⁵ and the numerical integration is performed on a logarithmic radial grid of 500 points reaching from 0.001 a_0 to 25 a_0 . The local range-separated hybrids are evaluated on self-consistent LDA orbitals.

Table I presents the total energies of a global ($\omega = 0.6 a_0^{-1}$) and a local range-separated hybrid, i.e., $\omega^{\text{K}}(\mathbf{r})$ of Eq. (11), for all closed-shell atoms up to Ca in comparison with the energies from the corresponding hyper-GGA approximation based on the three semilocal exchange hole models. We chose $\omega = 0.6 a_0^{-1}$ as the reference value for the closed-shell atom calculations with a fixed range-separation parameter because this allows for direct comparison with the work of Krukau *et al.*¹⁵ There, this value was shown to minimize standard enthalpies of formation of the AE6 test when the hyper-GGA approximation is not employed.

On the face of it, the quality of the three hyper-GGA approximations seems comparable. They yield energies reasonably close to the exact (local) range-separated hybrid energies. Most notably, however, is that the error of the hyper-GGA approximation doubles when going from the global to the local range-separation

TABLE I. Total non-relativistic energies in Hartree of closed-shell atoms in the hyper-GGA approximations based on the TPSS, BR, and TPSSrev hole models in comparison with the exact (EXX) local range-separated hybrid energies and with the exact energies for a constant range-separation parameter (LC- ω -LDA) with $\omega = 0.6 a_0^{-1}$ and for a local range-separation parameter (LRS- ω^{K} -LDA) of Eq. (11). All energies are evaluated on self-consistent LDA orbitals.

| Atom\hole | LC- ω -LDA | | | | LRS- ω^{K} -LDA | | | | Exact ^a |
|--------------------------------|-------------------|----------|----------|----------|-------------------------------|----------|----------|----------|--------------------|
| | EXX | TPSS | BR | TPSSrev | EXX | TPSS | BR | TPSSrev | |
| He | -2.925 | -2.940 | -2.919 | -2.940 | -2.899 | -2.909 | -2.893 | -2.909 | -2.904 |
| Be | -14.560 | -14.578 | -14.559 | -14.572 | -14.590 | -14.621 | -14.589 | -14.616 | -14.667 |
| Ne | -128.511 | -128.506 | -128.525 | -128.526 | -128.582 | -128.669 | -128.621 | -128.689 | -128.938 |
| Mg | -199.421 | -199.410 | -199.454 | -199.429 | -199.569 | -199.659 | -199.633 | -199.691 | -200.053 |
| Ar | -526.323 | -526.270 | -526.406 | -526.317 | -526.635 | -526.702 | -526.817 | -526.800 | -527.540 |
| Ca | -676.026 | -675.948 | -676.120 | -676.002 | -676.429 | -676.477 | -676.653 | -676.600 | -676.908 |
| MA(E/ \bar{e}) ^b | | 0.0034 | 0.0027 | 0.0023 | | 0.0059 | 0.0056 | 0.0084 | |
| MA(E/ \bar{e}) ^c | 0.041 | 0.043 | 0.038 | 0.041 | 0.029 | 0.024 | 0.024 | 0.021 | |

^aReference 63.

^bMean absolute error per electron relative to the corresponding (local) range-separated hybrid based on the exact exchange (EXX) hole.

^cMean absolute error per electron relative to exact nonrelativistic total energy.

parameter. The hyper-GGA approximation error is thus comparable to the energy difference between different local range-separation parameters. Therefore, we argue to take an alternative point of view on the hyper-GGA approximation to a local range separation hybrid: One should rather consider it a range-separated hybrid motivated definition of a different functional, i.e., of a hyper-GGA, than an approximation to a local range separation hybrid.

A closer look at Table I reveals that for atoms of smaller nuclear charge the hyper-GGA approximation based on the BR hole performs considerably better than the TPSS based approximations, whereas the TPSS hole approximation performs notably better for atoms of larger nuclear charge. To investigate this further, we compare the LR exchange energy densities,

$$e_x^{\text{LR}}(\mathbf{r}) = 2\pi n(\mathbf{r}) \int_0^\infty \bar{h}_x(\mathbf{r}, u) u \operatorname{erf}(\omega(\mathbf{r})u) du, \quad (48)$$

as well as the screened spherical-averaged exchange holes of these approximations for the Be and Ca atoms in the top panels of Fig. 1. Figure 1 demonstrates that the good performance of the hyper-GGA approximation with respect to total energies is not based on error cancellation, as the LR exchange energy density is also pointwise well approximated by both hole models. This picture changes, however, when looking directly at the (LR-screened) spherical-averaged exchange holes in comparison with the exact spherical-averaged exchange hole,

$$\bar{h}_x^{\text{ex}}(\mathbf{r}, u) = - \sum_{\sigma=\uparrow, \downarrow} \sum_{ij=1}^{N_\sigma} \frac{\varphi_{i\sigma}^*(\mathbf{r})\varphi_{j\sigma}(\mathbf{r})}{n(\mathbf{r})} \oint \varphi_{j\sigma}^*(\mathbf{r}+\mathbf{u})\varphi_{i\sigma}(\mathbf{r}+\mathbf{u}) d\Omega_u. \quad (49)$$

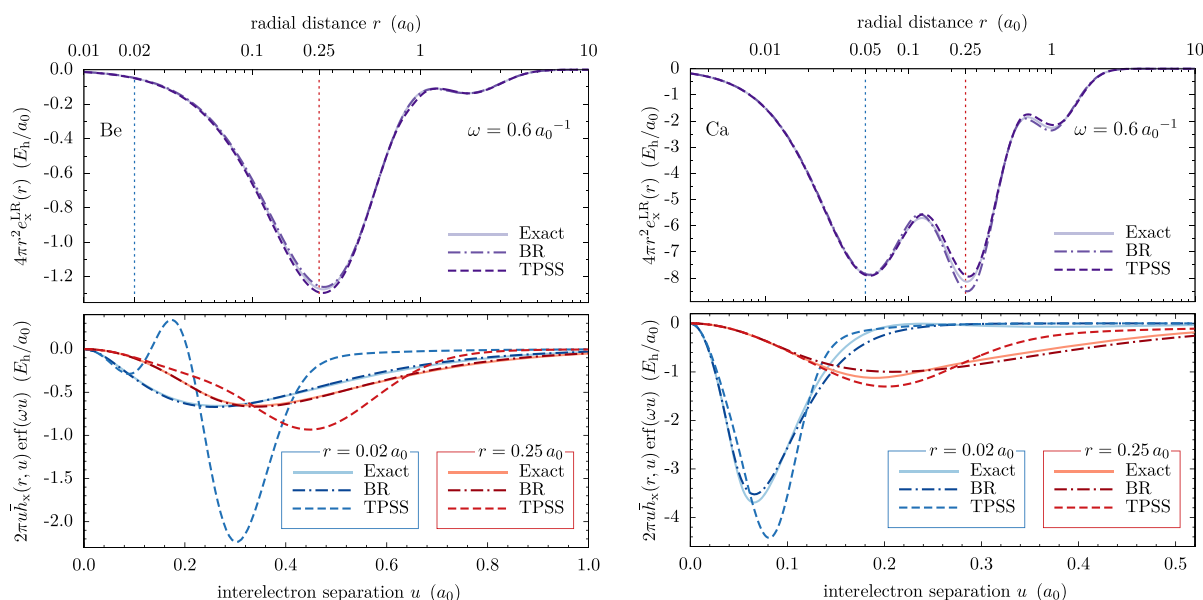


FIG. 1. LR exchange energy densities $e_x^{\text{LR}}(r)$ (top) and LR-screened spherical-averaged exchange holes $\bar{h}_x(r, u)$ (bottom) of the Be (left) and Ca (right) atoms for the hyper-GGA approximations based on the BR (dashed-dotted lines) and TPSS (dashed lines) hole models in comparison with the exact (solid lines) densities and holes. The two reference points r of holes (blue and red) are each indicated by vertically colored lines in the upper plots. The constant range-separation parameter $\omega = 0.6 a_0^{-1}$ is used throughout. All quantities are evaluated on self-consistent LDA orbitals.

averaging cannot take place. The TPSSrev hole, which is not shown in Fig. 1, improves only slightly on the original TPSS hole with respect to these shortcomings.

The error of the BR hole model for large nuclear charges may also be understood in terms of the hole norm: As already discussed in Sec. III A, the generalized BR hole model that we use in this work is not normalized to -1 . While this can be advantageous in some situations, this is not the case for atoms, where the exchange hole exhibits only one center. At each reference point, the local BR hole norm is given by^{54,57}

$$N_x^{\text{BR}}(\mathbf{r}) = -\frac{8\gamma(\mathbf{r})}{3\pi\alpha^3(\mathbf{r})}. \quad (50)$$

Aside of the asymptotic region of low energetic significance, we find that the local BR norm is reasonably close to -1 with deviations of less than 10%. Close to the nucleus, the local norm is greater than -1 for atoms with lower nuclear charge and tends to the proper norm when the nuclear charge is increased. However, in the outer shell regions, the local norm develops local minima that coincide with the regions where LR exchange densities deviate the most. For Ca (cf. Fig. 1), these minima are close to $r = 0.25 a_0$ with a norm of -1.05 and close to $r = 0.8 a_0$ with a local norm of -1.10 . Therefore, we conclude that the proper hole norm is vital to the quality of the hyper-GGA approximation to a local range-separated hybrid. However, when taking the alternative point of view that we have advocated, i.e., when considering the local range-separated hybrid and BR motivated hyper-GGA by itself, we have to note that the error of the hyper-GGA approximation due to the hole norm deviation for atoms of larger nuclear charge actually improves the total energy relative to the exact total energy (cf. Table I).

IV. RESULTS AND DISCUSSION

In the following, we turn to a test set for atomization energies of dimers for which we can perform very accurate grid-based all-electron Kohn-Sham calculations with DARSEC.⁶⁸ The set is small (H_2 , LiH , LiF , CO , N_2 , NO , OH , O_2 , FH , F_2 , CO , NO , and FH), but comprises different bond types (single, double, and triple) and, therefore (cf. Refs. 45 and 69), gives an impression of binding properties. The computational details including the experimental bond lengths and all numerical parameters can be found in the supplementary material. All results presented in the following are post-LDA, i.e., the energies are evaluated on self-consistent LDA orbitals—cf. supplementary material for an assessment of the influence of the reference orbitals.

Before discussing new local range-separation parameters, we use this test set to once more assess the robustness of the hyper-GGA approximation. In Fig. 2, we plot mean absolute errors (MAEs) in atomization energies for this test set as a function of the ω -prefactor η for the local range-separated hybrid based on ω^{K} of Eq. (11), LRS- ω^{K} -LDA, in the hyper-GGA approximations build on the TPSS, BR, and TPSSrev hole models. We first note that we obtain the minimal MAE for the TPSS-based hyper-GGA approximation at $\eta = 0.135$, the exact same value that was found by Krukau *et al.*¹⁵ to give the optimal MAE for standard enthalpies of formation in the AE6 set⁷⁰—a test set that has been designed to reproduce the errors of the much larger G3 test set.⁷¹ This confirms the quality of our

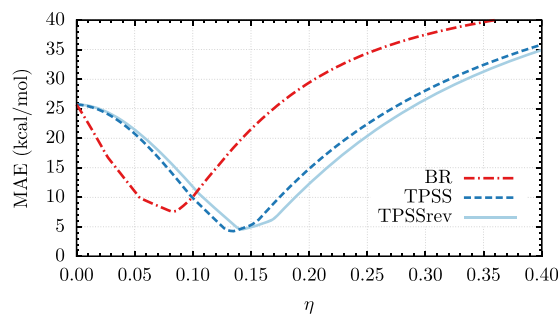


FIG. 2. MAEs in atomization energies for the dimer test set as a function of the prefactor η for the local range-separated hybrid based on ω^{K} of Eq. (11), LRS- ω^{K} -LDA, in the hyper-GGA approximations build on the TPSS, BR, and TPSSrev hole models. For $\eta \rightarrow 0$, all models reduce to LDA and its MAE of 25.7 kcal/mol.

test set as well as of the AE6 test set. While the TPSS and TPSSrev based hyper-GGA approximations perform very similar with MAE minima of 4.3 kcal/mol at $\eta = 0.135$ for TPSS and of 4.6 kcal/mol at $\eta = 0.140$ for TPSSrev, the BR based hyper-GGA minimizes at $\eta = 0.084$ with 7.6 kcal/mol. This again demonstrates that a local range-separated hybrid within the hyper-GGA approximation defines a distinct functional for each hole model. While the different functionals are likely to behave similar on a qualitative level, they likely differ quantitatively in thermochemistry.

We now turn to discuss the effect of eliminating the one-electron self-interaction error and the treatment of spin for a local range-separated hybrid. In Sec. II B, we have advocated from a theoretical point of view for a pole in $\omega([n]; \mathbf{r})$ to cure the one-electron self-interaction error. The practical implication of such a pole, which we find to be strongly interconnected with the treatment of spin, will be assessed in the following with help of the dimer test set that was introduced in the previous paragraph. Table II lists the atomization energies across the dimer test set and their MAE for various local range-separation parameters. The tabulated results are all based on the hyper-GGA approximation using the TPSS hole because the previous results indicate that the TPSS hole performs best with respect to energetics. Moreover, we have optimized and listed the parameters (in the following referred to as c_1 and c_2) that give the best MAE for each $\omega([n]; \mathbf{r})$.

We first stick to the spin scaling of exchange given by Eq. (33) and change ω^{K} of Eq. (11) by multiplication with the self-interaction pole $\Theta(z)$ of Eq. (23), i.e.,

$$\omega_\sigma(\mathbf{r}) = c_1 \omega_\sigma^{\text{K}}(\mathbf{r}) \Theta(z_\sigma), \quad (51)$$

where $\omega_\sigma^{\text{K}}(\mathbf{r})$ is given by Eq. (37). Although having combined the resulting local range-separation hybrid with the one-electron self-interaction free $E_c^{\text{sic-LDA}}[n]$ of Eq. (22) for semilocal correlation, the resulting MAE of 14.4 kcal/mol is considerably larger than the 4.3 kcal/mol MAE of ω^{K} without the self-interaction pole. If $E_c^{\text{LDA}}[n]$ was used instead, the optimal MAE would double to 25.6 kcal/mol. It is, therefore, important to remove the one-electron self-interaction error in both parts of the functional simultaneously.

As the introduction of the self-interaction pole to $\omega([n]; \mathbf{r})$ in combination with the spin scaling of exchange is not satisfying, we

TABLE II. Atomization energies in kcal/mol of diatomic molecules at experimental bond lengths and mean absolute error (MAE) across the test set. LRS energies are evaluated post-LDA in the hyper-GGA approximation based on the original TPSS hole. Each ω_σ is shown with its optimized parameters as listed. LRS- ω -sic-LDA uses the one-electron self-interaction free $E_c^{\text{sic-LDA}}[n]$ of Eq. (22) for semilocal correlation instead of $E_c^{\text{LDA}}[n]$ that is used in LRS- ω -LDA. Experimental atomization energies (with zero point vibration removed) are taken from Ref. 67.

| Molecule | LRS- ω -LDA | | | LRS- ω -sic-LDA | | | Expt. |
|-----------------|--------------------|-------------------|---|----------------------------------|---|---|-------|
| | LDA | ω_σ^K | $1.08 \omega_\sigma^K \Theta(z_\sigma)$ | $1.26 \omega^K \Theta(z\zeta^2)$ | $1.00 \omega_\sigma^K \Theta(z_\sigma \zeta^2)$ | $0.68 \omega_\sigma^K [1 + \ln(1 + 0.90 a_0 \omega_\sigma^K)] \Theta(z_\sigma \zeta^2)$ | |
| H ₂ | 112.9 | 115.4 | 143.6 | 126.0 | 117.4 | 111.4 | 109.5 |
| LiH | 60.8 | 62.0 | 64.0 | 72.7 | 65.6 | 60.0 | 58.0 |
| Li ₂ | 23.8 | 21.3 | 8.9 | 31.7 | 26.5 | 23.0 | 24.7 |
| LiF | 156.3 | 138.6 | 129.1 | 143.3 | 141.6 | 136.6 | 138.3 |
| CO | 299.2 | 256.5 | 255.3 | 260.0 | 259.9 | 259.6 | 259.5 |
| N ₂ | 268.0 | 228.3 | 212.6 | 239.4 | 230.9 | 229.8 | 228.3 |
| NO | 199.4 | 150.2 | 152.7 | 150.9 | 151.5 | 152.4 | 152.5 |
| OH | 123.2 | 95.9 | 95.3 | 96.2 | 96.3 | 94.6 | 107.1 |
| O ₂ | 175.1 | 129.6 | 139.8 | 126.3 | 128.7 | 129.6 | 120.5 |
| FH | 162.0 | 143.3 | 147.5 | 146.6 | 144.8 | 141.1 | 141.1 |
| F ₂ | 78.0 | 43.7 | 73.4 | 40.6 | 44.6 | 45.6 | 38.4 |
| MAE | 25.7 | 4.3 | 14.4 | 7.4 | 4.9 | 3.4 | |

now explore the alternatives to handle the spin that we proposed in Sec. II C. The first alternative to be considered is to use the same local range-separation parameter based on ω^K for both spin channels but weaken the self-interaction pole by using the one-spin-orbital indicator $z\zeta^2$ instead of the iso-orbital indicator z , i.e.,

$$\omega_\sigma(\mathbf{r}) = c_1 \omega^K(\mathbf{r}) \Theta(z\zeta^2). \quad (52)$$

As detailed in Table II, this alternative treatment of spin halves the (optimal) MAE to 7.4 kcal/mol—a decent value, but still double the MAE of the original local range-separation parameter ω^K . We note that once more the combination of this particular local range-separation parameter with the self-interaction corrected LDA correlation in place of the standard LDA correlation gives an improved MAE. This, however, is not necessarily so for this treatment of spin. This becomes evident when considering a local range-separation parameter with a different self-interaction pole: when using the damped pole $\Theta_2(z\zeta^2)$, an optimal MAE of 7.0 kcal/mol can be achieved in combination with the standard LDA correlation, whereas the combination of this pole with self-interaction corrected LDA correlation only yields 12.9 kcal/mol.

The second alternative treatment of spin to be considered is to again use different range-separation parameters for each spin channel that only depend on the quantities of the respective spin channel as implied by the spin scaling for exchange, but with the sole exception of the spin-polarization ζ . The spin-polarization, in turn, is used, once more, to limit the self-interaction pole to one-spin-orbital regions, i.e.,

$$\omega_\sigma(\mathbf{r}) = c_1 \omega_\sigma^K(\mathbf{r}) \Theta(z_\sigma \zeta^2). \quad (53)$$

This compromise between the two former proposals gives an optimal MAE of 4.9 kcal/mol, which is not far from the original

ω^K —interestingly even the optimal prefactors coincide. We, thus, conclude that when the spin is treated in the right way, one can achieve good energetics in conjunction with the formal requirement of one-electron self-interaction freedom.

Last but not least, we seek to incorporate the correct scaling to the high-density limit. As proposed in Eq. (30), this can be achieved via a logarithmic contribution, i.e., we use

$$\omega_\sigma = c_1 \omega_\sigma^K [1 + \ln(1 + c_2 \omega_\sigma^K)] \Theta(z_\sigma \zeta^2). \quad (54)$$

We note that in the absence of a self-interaction pole, this modification is not able to decrease the MAE significantly with respect to the MAE of ω^K . In the presence of this particular pole, however, the logarithmic contribution yields a significant improvement, as we obtain an optimal MAE of only 3.4 kcal/mol for $c_1 = 0.68$ and $c_2 = 0.90 a_0$ (cf. Table II). As visualized in Fig. 3, we find a set of parameter tuples for c_1 and c_2 that yield a comparable result with respect to the test set with an MAE close to or below 3.5 kcal/mol. This new-found freedom might be exploited to optimize the local range-separation parameter simultaneously for other observables, e.g., reaction barriers. The remaining error in atomization energies is essentially given by OH and F₂. This variant is thus more accurate for atomization energies than the original ω^K . We reach this accuracy with the local range-separation parameter of Eq. (54) that satisfies two additional exact constraints—freedom from one-electron self-interaction as defined by Eq. (15) and the correct scaling to the high-density limit in the sense of Eq. (13). This low MAE can only be achieved in combination with a one-electron self-interaction free semilocal correlation energy—here, $E_c^{\text{sic-LDA}}[n]$ of Eq. (22). For completeness, we note that this result is again specifically tied to the TPSS hole used for the hyper-GGA approximation: The optimal MAE for the TPSSrev hole is 3.7 kcal/mol ($c_1 = 0.47$, $c_2 = 4.22 a_0$) and only 7.4 kcal/mol for the BR hole ($c_1 = 0.67$, $c_2 = 0.15 a_0$)—heat

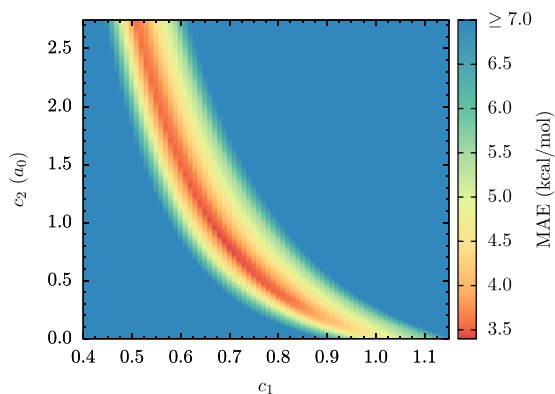


FIG. 3. Heat map of the mean absolute error (MAE) across the test set for atomization energies of the local range-separation parameter $\omega_\sigma(\mathbf{r})$ of Eq. (54) as a function of its two parameters c_1 and c_2 . The (red) band of low MAE is characterized by $\omega_\sigma(\mathbf{r})$ reducing to $\omega_\sigma^K(\mathbf{r})\Theta(z_\sigma\zeta^2)$ near points of space where $\omega_\sigma^K(\mathbf{r})$ is close to $0.7 a_0^{-1}$.

maps for these hole models in analogy to Fig. 3 are presented in the [supplementary material](#).

To illustrate our local range-separation parameter, we present in Figs. 4 and 5 plots of $\omega(\mathbf{r})$ of Eq. (54), labeled $\omega^{\text{sic}}(\mathbf{r})$, in comparison with the original $\omega^K(\mathbf{r})$ for the CO molecule and the Li atom, respectively. For the spin-saturated CO-molecule, $\omega^{\text{sic}}(\mathbf{r})$ does not change much compared to $\omega^K(\mathbf{r})$. This is because the pole function $\Theta(z_\sigma\zeta^2)$ evaluates uniformly to a value of one as no spin-polarization is present ($\zeta \equiv 0$). While close to the nuclei, our new local range-separation parameters tend to have higher maxima, these approach a slightly lower value in the asymptotic regions, where both screening functions approach a system dependent constant governed by the asymptotic decay of the density (cf. Ref. 15). A different situation is found in the case of the lithium atom, as shown in Fig. 5. Due to the spin-polarization, the self-interaction pole $\Theta(z_\sigma\zeta^2)$ comes in effect in both spin-channels and leads to a divergent screening function in the asymptotic region, i.e., to no screening and bare exchange.

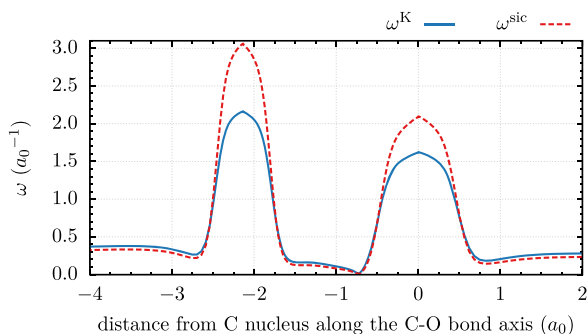


FIG. 4. Local range-separation parameters $\omega^K(\mathbf{r})$ of Eq. (11) and $\omega^{\text{sic}}(\mathbf{r})$ of Eq. (54) along the bond axis of the CO molecule.

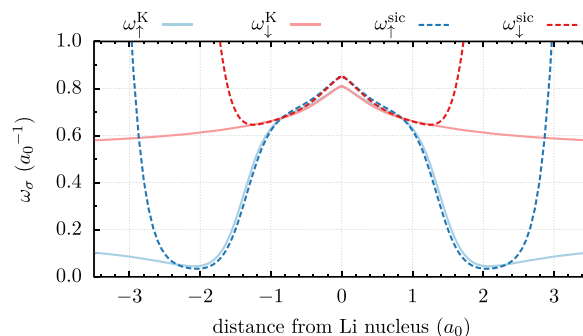


FIG. 5. Local range-separation parameters $\omega^K(\mathbf{r})$ of Eq. (11) and $\omega^{\text{sic}}(\mathbf{r})$ of Eq. (54) for both spin channels (\uparrow : majority-spin, \downarrow : minority-spin) for the lithium atom.

V. SUMMARY AND CONCLUSION

We have explored the concept of a local range-separation parameter in the hyper-GGA approximation, extending earlier work by Krukau *et al.*¹⁵ For computational reasons, the hyper-GGA approximation is presently inevitable once a local range-separation parameter is used. With the help of an analytical solid-angle integration for closed-shell atoms, we were able to assess the quality and implications of the hyper-GGA approximation. We found that the robustness of the approximation is closely tied to the semilocal exchange hole model that it uses. Based on these findings, we advocate to look at the hyper-GGA approximation not as an approximation for evaluating a local range-separated hybrid, but instead as a way to motivate, construct, and define a hyper-GGA whose functional form is motivated by a range-separated hybrid. Additionally, we formulated and applied an additional exact constraint in the construction of local range-separation parameters. Freedom from self-interaction suggested to abandon the straightforward use of the exchange spin-scaling and explore the explicit inclusion of spin-polarization. We demonstrated that a one-electron self-interaction free local range-separation parameter with a correct high-density scaling limit can give accurate atomization energies. Other properties related to the self-interaction error, e.g., the physical interpretability of eigenvalues, are expected to benefit as well. However, testing this would require self-consistent calculations with local range separation. This is a major task in itself to be addressed in future work.

SUPPLEMENTARY MATERIAL

See the [supplementary material](#) for the analytic solid-angle integration for closed-shell atoms and a detailed overview of the TPSS, the TPSSrev, and BR hole models as well as their analytically integrated screened representations.^{23,72,73,75} Furthermore, we report computational details of the atomization energies calculations with DARSEC,⁶⁸ show heat maps in analogy to Fig. 3 for the TPSSrev and BR hole models, and assess the influence of the use of different orbitals in the non-self-consistent calculations.⁷⁴

ACKNOWLEDGMENTS

We gratefully acknowledge financial support from the German-Israeli Foundation for Scientific Research and Development, from

the Bavarian State Ministry of Science, Research, and the Arts for the Collaborative Research Network “Solar Technologies go Hybrid”, and from the Bavarian Polymer Institute in terms of computing resources.

REFERENCES

- ¹A. Savin and H.-J. Flad, *Int. J. Quantum Chem.* **56**, 327 (1995).
- ²J. Toulouse, F. Colonna, and A. Savin, *Phys. Rev. A* **70**, 062505 (2004).
- ³L. Kronik, T. Stein, S. Refaely-Abramson, and R. Baer, *J. Chem. Theory Comput.* **8**, 1515 (2012).
- ⁴S. Kümmel, *Adv. Energy Mater.* **7**, 1700440 (2017).
- ⁵J. Perdew, *Chem. Phys. Lett.* **64**, 127 (1979).
- ⁶J. P. Perdew and A. Zunger, *Phys. Rev. B* **23**, 5048 (1981).
- ⁷Y. Zhang and W. Yang, *J. Chem. Phys.* **109**, 2604 (1998).
- ⁸M. A. Rohrdanz and J. M. Herbert, *J. Chem. Phys.* **129**, 034107 (2008).
- ⁹T. Yanai, D. P. Tew, and N. C. Handy, *Chem. Phys. Lett.* **393**, 51 (2004).
- ¹⁰J.-W. Song, T. Hirokawa, T. Tsuneda, and K. Hirao, *J. Chem. Phys.* **126**, 154105 (2007).
- ¹¹E. Livshits and R. Baer, *Phys. Chem. Chem. Phys.* **9**, 2932 (2007).
- ¹²J.-D. Chai and M. Head-Gordon, *J. Chem. Phys.* **128**, 084106 (2008).
- ¹³A. Karolewski, L. Kronik, and S. Kümmel, *J. Chem. Phys.* **138**, 204115 (2013).
- ¹⁴A. Savin, *Chem. Phys.* **356**, 91 (2009).
- ¹⁵A. V. Krukau, G. E. Scuseria, J. P. Perdew, and A. Savin, *J. Chem. Phys.* **129**, 124103 (2008).
- ¹⁶D. Langreth and J. Perdew, *Solid State Commun.* **17**, 1425 (1975).
- ¹⁷O. Gunnarsson and B. I. Lundqvist, *Phys. Rev. B* **13**, 4274 (1976); **15**, 6006 (1977).
- ¹⁸P. M. W. Gill, R. D. Adamson, and J. A. Pople, *Mol. Phys.* **88**, 1005 (1996).
- ¹⁹A. Savin, in *Recent Developments and Applications of Modern Density Functional Theory*, Theoretical and Computational Chemistry Vol. 4, edited by J. Seminario (Elsevier, 1996), p. 327.
- ²⁰J. P. Perdew and Y. Wang, *Phys. Rev. B* **45**, 13244 (1992).
- ²¹I. C. Gerber and J. G. Ángyán, *Chem. Phys. Lett.* **415**, 100 (2005).
- ²²O. A. Vydrov, J. Heyd, A. V. Krukau, and G. E. Scuseria, *J. Chem. Phys.* **125**, 074106 (2006).
- ²³J. Heyd, G. E. Scuseria, and M. Ernzerhof, *J. Chem. Phys.* **118**, 8207 (2003).
- ²⁴S. Refaely-Abramson, M. Jain, S. Sharifzadeh, J. B. Neaton, and L. Kronik, *Phys. Rev. B* **92**, 081204(R) (2015).
- ²⁵J. Autschbach and M. Srebro, *Acc. Chem. Res.* **47**, 2592 (2014).
- ²⁶T. Stein, L. Kronik, and R. Baer, *J. Am. Chem. Soc.* **131**, 2818 (2009).
- ²⁷T. Stein, H. Eisenberg, L. Kronik, and R. Baer, *Phys. Rev. Lett.* **105**, 266802 (2010).
- ²⁸S. Refaely-Abramson, R. Baer, and L. Kronik, *Phys. Rev. B* **84**, 075144 (2011).
- ²⁹T. B. de Queiroz and S. Kümmel, *J. Chem. Phys.* **141**, 084303 (2014).
- ³⁰T. B. de Queiroz and S. Kümmel, *J. Chem. Phys.* **143**, 034101 (2015).
- ³¹V. Vlček, H. R. Eisenberg, G. Steinle-Neumann, L. Kronik, and R. Baer, *J. Chem. Phys.* **142**, 034107 (2015).
- ³²J. Toulouse, F. Colonna, and A. Savin, *J. Chem. Phys.* **122**, 014110 (2005).
- ³³J. Krieger, J. Chen, G. Iafate, and A. Savin, in *Electron Correlations and Materials Properties*, edited by A. Gonis, N. Kioussis, and M. Cifan (Plenum, New York, 1999).
- ³⁴D. C. Langreth and M. J. Mehl, *Phys. Rev. Lett.* **47**, 446 (1981).
- ³⁵J. P. Perdew, K. Burke, and M. Ernzerhof, *Phys. Rev. Lett.* **77**, 3865 (1996).
- ³⁶J. Tao, J. P. Perdew, V. N. Staroverov, and G. E. Scuseria, *Phys. Rev. Lett.* **91**, 146401 (2003).
- ³⁷J. Sun, A. Ruzsinszky, and J. P. Perdew, *Phys. Rev. Lett.* **115**, 036402 (2015).
- ³⁸J. Tao and Y. Mo, *Phys. Rev. Lett.* **117**, 073001 (2016).
- ³⁹M. Levy and J. P. Perdew, *Phys. Rev. A* **32**, 2010 (1985).
- ⁴⁰M. Levy, *Phys. Rev. A* **43**, 4637 (1991).
- ⁴¹A. D. Becke, *J. Chem. Phys.* **109**, 2092 (1998).
- ⁴²J. P. Perdew, S. Kurth, A. Zupan, and P. Blaha, *Phys. Rev. Lett.* **82**, 2544 (1999).
- ⁴³J. Jaramillo, G. E. Scuseria, and M. Ernzerhof, *J. Chem. Phys.* **118**, 1068 (2003).
- ⁴⁴S. Kümmel and J. P. Perdew, *Mol. Phys.* **101**, 1363 (2003).
- ⁴⁵T. Schmidt, E. Kraisler, A. Makmal, L. Kronik, and S. Kümmel, *J. Chem. Phys.* **140**, 18A510 (2014).
- ⁴⁶J. P. Perdew, J. Tao, V. N. Staroverov, and G. E. Scuseria, *J. Chem. Phys.* **120**, 6898 (2004).
- ⁴⁷T. Schmidt, E. Kraisler, L. Kronik, and S. Kümmel, *Phys. Chem. Chem. Phys.* **16**, 14357 (2014).
- ⁴⁸P. Mori-Sánchez, A. J. Cohen, and W. Yang, *J. Chem. Phys.* **125**, 201102 (2006).
- ⁴⁹A. Ruzsinszky, J. P. Perdew, G. I. Csonka, O. A. Vydrov, and G. E. Scuseria, *J. Chem. Phys.* **126**, 104102 (2007).
- ⁵⁰T. Schmidt and S. Kümmel, *Phys. Rev. B* **93**, 165120 (2016).
- ⁵¹G. L. Oliver and J. P. Perdew, *Phys. Rev. A* **20**, 397 (1979).
- ⁵²J. P. Perdew, K. Burke, and Y. Wang, *Phys. Rev. B* **54**, 16533 (1996); **57**, 14999 (1998).
- ⁵³F. Della Sala and A. Görling, *J. Chem. Phys.* **115**, 5718 (2001).
- ⁵⁴A. D. Becke, *J. Chem. Phys.* **119**, 2972 (2003).
- ⁵⁵H. Antaya, Y. Zhou, and M. Ernzerhof, *Phys. Rev. A* **90**, 032513 (2014).
- ⁵⁶J. Přecechtělová, H. Bahmann, M. Kaupp, and M. Ernzerhof, *J. Chem. Phys.* **141**, 111102 (2014).
- ⁵⁷J. Pavlíková Přecechtělová, H. Bahmann, M. Kaupp, and M. Ernzerhof, *J. Chem. Phys.* **143**, 144102 (2015).
- ⁵⁸L. A. Constantin, J. P. Perdew, and J. Tao, *Phys. Rev. B* **73**, 205104 (2006).
- ⁵⁹J. Tao, I. W. Bulik, and G. E. Scuseria, *Phys. Rev. B* **95**, 125115 (2017).
- ⁶⁰A. D. Becke and M. R. Roussel, *Phys. Rev. A* **39**, 3761 (1989).
- ⁶¹A. D. Becke, *Int. J. Quantum Chem.* **23**, 1915 (1983).
- ⁶²R. Wang, Y. Zhou, and M. Ernzerhof, *Phys. Rev. A* **96**, 022502 (2017).
- ⁶³S. J. Chakravorty, S. R. Gwaltney, E. R. Davidson, F. A. Parpia, and C. F. Fischer, *Phys. Rev. A* **47**, 3649 (1993).
- ⁶⁴See Ref. 75 for a similar spherical harmonic expansion of the SR Coulomb interaction and further insight.
- ⁶⁵E. Van Lenthe and E. J. Baerends, *J. Comput. Chem.* **24**, 1142 (2003).
- ⁶⁶J. Tao, V. N. Staroverov, G. E. Scuseria, and J. P. Perdew, *Phys. Rev. A* **77**, 012509 (2008).
- ⁶⁷*CRC Handbook of Chemistry and Physics*, 98th ed., edited by J. Rumble (CRC Press, 2017).
- ⁶⁸A. Makmal, S. Kümmel, and L. Kronik, *J. Chem. Theory Comput.* **5**, 1731 (2009).
- ⁶⁹T. Aschebrock and S. Kümmel, “Ultranonlocality and accurate band gaps from a Meta-Generalized Gradient Approximation” (to be published).
- ⁷⁰B. J. Lynch and D. G. Truhlar, *J. Phys. Chem. A* **107**, 8996 (2003).
- ⁷¹L. A. Curtiss, K. Raghavachari, P. C. Redfern, and J. A. Pople, *J. Chem. Phys.* **112**, 7374 (2000).
- ⁷²T. M. Henderson, B. G. Janesko, and G. E. Scuseria, *J. Chem. Phys.* **128**, 194105 (2008).
- ⁷³W. H. Press, S. A. Teukolsky, W. T. Vetterling, and B. P. Flannery, *Numerical Recipes* (Cambridge University Press, Cambridge, New York, 1992).
- ⁷⁴J. B. Krieger, Y. Li, and G. J. Iafate, *Phys. Rev. A* **46**, 5453 (1992).
- ⁷⁵J. G. Ángyán, I. Gerber, and M. Marsman, *J. Phys. A: Math. Gen.* **39**, 8613 (2006).

Supplementary material for “Exploring local range separation: The role of spin scaling and one-electron self-interaction”

Thilo Aschebrock and Stephan Kümmel
Theoretical Physics IV, University of Bayreuth, 95440 Bayreuth, Germany

I. SCREENED EXCHANGE HOLE MODELS IN DETAIL

A. Screened TPSS model

The spherically symmetric TPSS exchange hole model¹ at reference point \mathbf{r} is defined via

$$h_x^{\text{TPSS}}(n, s, z, e_x, u) = n J_x^{\text{TPSS}}(n, s, z, e_x^{\text{ex}}, y) \quad (\text{S.1})$$

by the associated dimensionless hole J_x^{TPSS} as a function of the dimensionless inter-electron separation $y = k_{\text{F}}u$ with $u = |\mathbf{r} - \mathbf{r}'|$. The hole is parametrized by $s = |\nabla n| / [2(3\pi^2)^{1/3}n^{4/3}]$ and $z = \tau^{\text{W}}/\tau$ alongside the density n and the exact exchange energy density e_x^{ex} – all evaluated at the reference point:

$$J_x^{\text{TPSS}}(n, s, z, e_x, y) = \left(-\frac{\mathcal{A}}{y^2} \frac{1}{1 + (4/9)\mathcal{A}y^2} + \left\{ \frac{\mathcal{A}}{y^2} + \mathcal{B} + \mathcal{C} [1 + \mathcal{F}(s, z)] y^2 \right. \right. \\ \left. \left. + \mathcal{E} [1 + G(n, s, z, e_x)] y^4 + \mathcal{K}(n, s, z, e_x) y^6 \right\} e^{-\mathcal{D}y^2} \right) \exp[-s^2 \mathcal{H}(s, z) y^2] \quad (\text{S.2})$$

with $\mathcal{A} = 1.016\,114\,4$, $\mathcal{B} = -0.371\,708\,36$, $\mathcal{C} = -0.077\,215\,461$, $\mathcal{D} = 0.577\,863\,48$, and $\mathcal{E} = -0.051\,955\,731$. Moreover, the functions \mathcal{F} , \mathcal{G} , \mathcal{K} , and \mathcal{H} are defined as follows:

$$\mathcal{H}(s, z) = z^5 \frac{c_1 + c_2 s^2 + c_3 s^4}{1 + c_4 s^4 + c_5 s^5 + c_6 s^6}, \quad (\text{S.3})$$

with $c_1 = 0.122\,499$, $c_2 = 0.121\,785$, $c_3 = 0.066\,065$, $c_4 = 0.187\,440$, $c_5 = 0.001\,208\,24$, $c_6 = 0.034\,718\,8$;

$$\mathcal{F}(s, z) = \frac{1}{2\mathcal{C}} \left[L(s) \left(\frac{1}{z} + 1 \right) - \frac{1}{5} - s^2 \mathcal{H} \right] \quad (\text{S.4})$$

with

$$L(s) = \frac{1}{3} \frac{s^2}{(1 + cs^6)^{1/3}} \quad (\text{S.5})$$

and $c = 0.000\,12$;

$$\mathcal{K}(n, s, z, e_x) = \left[-\frac{9}{8} \left(\frac{e_x}{A_x n^{4/3}} \right) - d_2 + \left(\frac{3\pi}{4} + a \right) \frac{1}{bd_1^3} - d_3 \right] \frac{d_1^4}{3} \left(1 - \frac{d_1 d_4}{3b} \right)^{-1} \quad (\text{S.6})$$

with

$$d_1(s, z) = \mathcal{D} + \mathcal{H}s^2, \quad (\text{S.7})$$

$$d_2(s, z) = [\mathcal{C}\mathcal{D} + \mathcal{B}\mathcal{D}^2 + 2\mathcal{E} + \mathcal{C}\mathcal{D}\mathcal{F} + \mathcal{C}\mathcal{H}s^2 + 2\mathcal{B}\mathcal{D}\mathcal{H}s^2 + \mathcal{C}\mathcal{F}\mathcal{H}s^2 + \mathcal{B}\mathcal{H}^2s^4] / (2d_1^3), \quad (\text{S.8})$$

$$d_3(s, z) = \frac{\mathcal{A}}{2} \left[\ln \left(\frac{\mathcal{H}s^2}{d_1} \right) - \exp \left(\frac{9\mathcal{H}s^2}{4\mathcal{A}} \right) \text{Ei} \left(-\frac{9\mathcal{H}s^2}{4\mathcal{A}} \right) \right], \quad d_4(s, z) = \frac{105}{32} \frac{1}{d_1^4} \sqrt{\frac{\pi}{d_1}}, \quad (\text{S.9})$$

$$a(s, z) = \sqrt{\pi} [15\mathcal{E} + 6\mathcal{C}(1 + \mathcal{F})d_1 + 4\mathcal{B}d_1^2 + 8\mathcal{A}d_1^3] / (16d_1^{7/2}) - \frac{3\pi\sqrt{\mathcal{A}}}{4} \exp \left(\frac{9\mathcal{H}s^2}{4\mathcal{A}} \right) \left[1 - \text{erf} \left(\frac{3s}{2} \sqrt{\frac{\mathcal{H}}{\mathcal{A}}} \right) \right], \quad (\text{S.10})$$

and

$$b(s, z) = \frac{15\sqrt{\pi}}{16d_1^{7/2}}; \quad (\text{S.11})$$

$$\mathcal{G}(s, z, e_x) = \frac{1}{\mathcal{E}b} \left\{ -\frac{3\pi}{4} - a - \mathcal{K}d_4 \right\}. \quad (\text{S.12})$$

To calculate the screened interaction, one has to evaluate the integral

$$I^{\text{TPSS}}(n, s, z, e_x, \omega) = \int_0^\infty y J_x^{\text{TPSS}}(n, s, z, e_x, y) \operatorname{erf}\left(\frac{\omega}{k_F} y\right) dy. \quad (\text{S.13})$$

In order to give an analytic expression for this integral, it is necessary to approximate

$$-\frac{\mathcal{A}}{y} \frac{1}{1 + (4/9)\mathcal{A}y^2} + \frac{\mathcal{A}}{y} \exp(-\mathcal{D}y^2), \quad (\text{S.14})$$

as proposed in Ref. 2, with

$$\text{fit}(y) = a_1 y e^{-b_1 y^2} + a_2 y e^{-b_2 y^2} + a_3 y^2 e^{-b_3 y^2} + a_4 y^2 e^{-b_4 y^2} + a_5 y^3 e^{-b_5 y^2} \quad (\text{S.15})$$

where $a_1 = -0.000\,205\,484$, $b_1 = 0.006\,601\,306$, $a_2 = -0.109\,465\,240$, $b_2 = 0.259\,931\,140$, $a_3 = -0.064\,078\,780$, $b_3 = 0.520\,352\,224$, $a_4 = -0.008\,181\,735$, $b_4 = 0.118\,551\,043$, $a_5 = -0.000\,110\,666$, $b_5 = 0.046\,003\,777$. Moreover, we note the following integrals

$$I_1(a, k) = \int_0^\infty y \exp(-ay^2) \operatorname{erf}(ky) dy = \frac{k}{2a\sqrt{a+k^2}}, \quad (\text{S.16})$$

$$I_2(a, k) = \int_0^\infty y^2 \exp(-ay^2) \operatorname{erf}(ky) dy = \frac{1}{2a\sqrt{\pi}} \left[\frac{k}{a+k^2} + \frac{\arctan(k/\sqrt{a})}{\sqrt{a}} \right], \quad (\text{S.17})$$

$$I_3(a, k) = \int_0^\infty y^3 \exp(-ay^2) \operatorname{erf}(ky) dy = \frac{3ak + 2k^3}{4a^2(a+k^2)^{3/2}}, \quad (\text{S.18})$$

$$I_5(a, k) = \int_0^\infty y^5 \exp(-ay^2) \operatorname{erf}(ky) dy = \frac{15a^2k + 20ak^3 + 8k^5}{8a^3(a+k^2)^{5/2}}, \quad (\text{S.19})$$

$$I_7(a, k) = \int_0^\infty y^7 \exp(-ay^2) \operatorname{erf}(ky) dy = \frac{3(35a^3k + 70a^2k^3 + 56ak^5 + 16k^7)}{16a^4(a+k^2)^{7/2}}, \quad (\text{S.20})$$

and therefore

$$\begin{aligned} I^{\text{TPSS}}(n, s, z, e_x, \omega) &= \mathcal{B} I_1(\mathcal{D} + s^2\mathcal{H}, \omega/k_F) + \mathcal{C}(1 + \mathcal{F}) I_3(\mathcal{D} + s^2\mathcal{H}, \omega/k_F) + \mathcal{E}(1 + \mathcal{G}) I_5(\mathcal{D} + s^2\mathcal{H}, \omega/k_F) \\ &\quad + \mathcal{K} I_7(\mathcal{D} + s^2\mathcal{H}, \omega/k_F) + a_1 I_1(b_1 + s^2\mathcal{H}, \omega/k_F) + a_2 I_1(b_2 + s^2\mathcal{H}, \omega/k_F) \\ &\quad + a_3 I_2(b_3 + s^2\mathcal{H}, \omega/k_F) + a_4 I_2(b_4 + s^2\mathcal{H}, \omega/k_F) + a_5 I_3(b_5 + s^2\mathcal{H}, \omega/k_F). \end{aligned} \quad (\text{S.21})$$

Consequently, we obtain

$$\begin{aligned} E_x^{\text{hyper-GGA,TPSS,LR}}[n, \omega] &= 4\pi \int \frac{n^2}{k_F^2} \int_0^\infty J_x^{\text{TPSS}}(n, s, z, e_x, y) \operatorname{erf}\left(\frac{\omega}{k_F} y\right) y dy d^3r \\ &= A_x \int n^{4/3} \left[-\frac{8}{9} I^{\text{TPSS}}(n, s, z, e_x, \omega) \right] d^3r \end{aligned} \quad (\text{S.22})$$

and therefore the hyper-GGA enhancement function F of Eq. (40) is given by

$$F^{\text{TPSS}}(n, s, z, e_x, \omega) = -\frac{8}{9} I^{\text{TPSS}}(n, s, z, e_x, \omega) \quad (\text{S.23})$$

for the TPSS exchange hole model.

B. Screened TPSSrev model

A revised TPSS based spherical-averaged exchange hole model³ is given by

$$h_x^{\text{TPSSrev}}(n, s, z, e_x, u) = n J_x^{\text{TPSSrev}}(n, s, z, e_x^{\text{ex}}, y) \quad (\text{S.24})$$

where again $y = k_F u$ and the shape function is defined by

$$J_x^{\text{TPSSrev}}(n, s, z, e_x, y) = \left\{ -\frac{9}{4y^4} [1 - \exp(-\mathcal{A}y^2)] + \left[\frac{9\mathcal{A}}{4y^2} + \mathcal{B} + \mathcal{C}(s, z)y^2 + \mathcal{G}(n, s, z, e_x)y^4 + \mathcal{K}(n, s, z, e_x)y^6 \right] e^{-\mathcal{D}y^2} \right\} \exp[-\mathcal{H}(s, z)y^2] \quad (\text{S.25})$$

with $\mathcal{A} = 0.757211$, $\mathcal{B} = -0.106364$, and $\mathcal{D} = 0.609650$. Moreover,

$$\mathcal{C}(s, z) = \frac{1}{8} (4L + 3\mathcal{A}^3 + 9\mathcal{A}^2\mathcal{H} - 9\mathcal{A}\mathcal{D}^2 - 18\mathcal{A}\mathcal{D}\mathcal{H} + 8\mathcal{B}\lambda), \quad (\text{S.26})$$

$$\begin{aligned} \mathcal{G}(n, s, z, e_x) = & -\frac{63}{8}\lambda^3 \left[\left(\frac{e_x}{A_x n^{4/3}} \right) + \mathcal{A} \ln\left(\frac{\beta}{\lambda}\right) + \mathcal{H} \ln\left(\frac{\beta}{\mathcal{H}}\right) \right] \\ & - \frac{24}{5}\lambda^{7/2} \left(\frac{3\mathcal{A}}{\sqrt{\mathcal{H}} + \sqrt{\beta}} - \sqrt{\pi} \right) + \frac{603}{40}\mathcal{A}\lambda^3 - \frac{19}{10}\mathcal{B}\lambda^2 - \frac{11}{10}\mathcal{C}\lambda, \end{aligned} \quad (\text{S.27})$$

$$\mathcal{K}(n, s, z, e_x) = \frac{8}{35}\lambda^{9/2} \left(\frac{3\mathcal{A}}{\sqrt{\mathcal{H}} + \sqrt{\beta}} - \sqrt{\pi} \right) - \frac{12}{35}\mathcal{A}\lambda^4 - \frac{8}{105}\mathcal{B}\lambda^3 - \frac{4}{35}\mathcal{C}\lambda^2 - \frac{2}{7}\mathcal{G}\lambda, \quad (\text{S.28})$$

with $\lambda = D + \mathcal{H}$, $\beta = \mathcal{A} + \mathcal{H}$,

$$L(s, z) = \frac{1}{2} \operatorname{erfc}\left(\frac{s^2 - s_0^2}{s_0}\right) \left[-\frac{1}{3} \left(\frac{1}{2} \frac{s^2}{z} - \frac{9}{10} + \frac{5}{6} s^2 \right) \right] + \left[1 - \frac{1}{2} \operatorname{erfc}\left(\frac{s^2 - s_0^2}{s_0}\right) \right] \left(\frac{1}{5} - \frac{2}{27} s^2 \right), \quad (\text{S.29})$$

and

$$\mathcal{H}(s, z) = z^3 \frac{1}{2} \operatorname{erfc}\left(\frac{s^2 - s_0^2}{s_0}\right) \frac{h_0 + h_1 s^2 + h_2 s^4 + h_3 s^6}{d_0 + d_1 s^2 + d_2 s^4 + d_3 s^6} + \left[1 - \frac{1}{2} \operatorname{erfc}\left(\frac{s^2 - s_0^2}{s_0}\right) \right] \frac{p_1 s^2 + p_2 s^4 + p_3 s^6}{1 + p_4 s^2 + p_5 s^4 + p_6 s^6} \quad (\text{S.30})$$

with $s_0 = 6$ and $h_0 = 0.0060$, $h_1 = 2.8916$, $h_2 = 0.7768$, $h_3 = 2.0876$, $d_0 = 13.696$, $d_1 = -0.2219$, $d_2 = 4.9917$, $d_3 = 0.7972$, $p_1 = 0.0302$, $p_2 = -0.1035$, $p_3 = 0.1272$, $p_4 = 0.1203$, $p_5 = 0.4859$, $p_6 = 0.1008$.

Unlike for the original TPSS hole, the screening integral of the revised TPSS hole can be calculated analytically⁴ as

$$\begin{aligned} I_0(\mathcal{H}, \lambda, \beta, k) &= \int_0^\infty y \left\{ -\frac{9}{4y^4} [1 - \exp(-\mathcal{A}y^2)] + \frac{9\mathcal{A}}{4y^2} e^{-\mathcal{D}y^2} \right\} \exp(-\mathcal{H}y^2) \operatorname{erf}(ky) dy \\ &= \frac{9}{4} \left[k \left(\sqrt{\mathcal{H} + k^2} - \sqrt{\beta + k^2} \right) + \mathcal{H} \ln\left(\frac{k + \sqrt{\mathcal{H} + k^2}}{k + \sqrt{\lambda + k^2}}\right) - \beta \ln\left(\frac{k + \sqrt{\beta + k^2}}{k + \sqrt{\lambda + k^2}}\right) - \frac{\mathcal{H}}{2} \ln\left(\frac{\mathcal{H}}{\lambda}\right) + \frac{\beta}{2} \ln\left(\frac{\beta}{\lambda}\right) \right] \end{aligned} \quad (\text{S.31})$$

and hence

$$I^{\text{TPSSrev}}(n, s, z, e_x, \omega) = I_0(\mathcal{H}, \lambda, \beta, \omega/k_F) + \mathcal{B} I_1(\lambda, \omega/k_F) + \mathcal{C} I_3(\lambda, \omega/k_F) + \mathcal{G} I_5(\lambda, \omega/k_F) + \mathcal{K} I_7(\lambda, \omega/k_F) \quad (\text{S.32})$$

with I_1 , I_3 , I_5 , and I_7 as defined in the previous section. Thus, the hyper-GGA enhancement function F of Eq. (40) is given by

$$F^{\text{TPSSrev}}(n, s, z, e_x, \omega) = -\frac{8}{9} I^{\text{TPSSrev}}(n, s, z, e_x, \omega) \quad (\text{S.33})$$

for the TPSSrev exchange hole model.

C. Screened BR model

An alternative spherical-averaged exchange hole model is given by the generalized^{5,6} Becke-Roussel hole model⁷

$$h_x^{\text{BR}}(n, \alpha, \beta, \gamma, u) = n J_x^{\text{BR}}(\alpha, \beta, \gamma, y) \quad (\text{S.34})$$

as a function of the dimensionless inter-electron separation $y = k_F u$ and the associated dimensionless hole,

$$J_x^{\text{BR}}(\alpha, \beta, \gamma, y) = -\frac{\gamma}{2\alpha^2\beta y} [(\alpha|\beta - y| + 1) \exp(-\alpha|\beta - y|) - (\alpha|\beta + y| + 1) \exp(-\alpha|\beta + y|)]. \quad (\text{S.35})$$

The BR hole is a generalized version of the exact hydrogen exchange hole that is reparametrized by $\alpha(\mathbf{r})$, $\beta(\mathbf{r})$ and $\gamma(\mathbf{r})$. At each reference point \mathbf{r} these parameters are determined such that exact conditions of Eqs. (41)-(43) are met. With the help of a new variable

$$x = \alpha\beta, \quad (\text{S.36})$$

which is uniquely but implicitly defined by

$$\frac{x-2}{x^2} \left[\exp(x) - 1 - \frac{x}{2} \right] = -\frac{3}{\pi} \frac{Q}{n^3} e_x^{\text{ex}} =: u_x, \quad (\text{S.37})$$

it follows

$$\gamma = \frac{1}{2} \exp(x), \quad (\text{S.38})$$

$$\alpha^2 = \frac{6Q}{k_F^2 n} \frac{x}{x-2}, \quad (\text{S.39})$$

and $\beta = x/\alpha$. Equation (S.37) is typically solved numerically for x by bisection.⁸ For $u_x < 0$ an initial bisection interval $]x_l, x_r[$ is given by $x_l = 0$ and $x_r = 2$, whereas x can be found within $x_l = 2 + \ln(1 + u_x/2)$ and $x_r = 2 + \ln(1 + u_x) + \ln[1 + \ln(1 + u_x)]$ for $u_x > 0$.

To calculate the screened interaction given by this model, the following integral is required:

$$\begin{aligned} I_x^{\text{BR}} &= \int_0^\infty y J_x^{\text{BR}} \operatorname{erf}(\eta y) dy = -\frac{\gamma}{4\alpha^3\beta\eta^2} \left\{ 8\eta^2 \operatorname{erf}(\beta\eta) + \exp\left(\frac{\alpha^2}{4\eta^2}\right) \right. \\ &\quad \times \left. \left[(\alpha^2 - 4\eta^2 - 2\alpha\beta\eta^2) \operatorname{erfc}\left(\frac{\alpha}{2\eta} - \beta\eta\right) \exp(-\alpha\beta) - (\alpha^2 - 4\eta^2 + 2\alpha\beta\eta^2) \operatorname{erfc}\left(\frac{\alpha}{2\eta} + \beta\eta\right) \exp(\alpha\beta) \right] \right\} \\ &= -\frac{\gamma}{\alpha^2} \frac{1}{xz^2} \left\{ 2z^2 \operatorname{erf}(z/2) + e^{(x/z)^2} \left[(x^2 - z^2 - xz^2/2) \operatorname{erfc}\left(\frac{x}{z} - z/2\right) e^{-x} - (x^2 - z^2 + xz^2/2) \operatorname{erfc}\left(\frac{x}{z} + z/2\right) e^x \right] \right\} \\ &= -\frac{\gamma}{\alpha^2} \frac{1}{xz^2} \left\{ 2z^2 \operatorname{erf}(z/2) + e^{-z^2/4} \left[(x^2 - z^2 - xz^2/2) \mathcal{E}\left(\frac{x}{z} - \frac{z}{2}\right) - (x^2 - z^2 + xz^2/2) \mathcal{E}\left(\frac{x}{z} + \frac{z}{2}\right) \right] \right\} \quad (\text{S.40}) \end{aligned}$$

with $\eta = \omega/k_F$, $x = \alpha\beta$, $z = 2\beta\eta$, and the shortcut

$$\mathcal{E}(x) = \operatorname{erfc}(x)e^{x^2}, \quad (\text{S.41})$$

which has the property $\mathcal{E}(-x) = 2e^{x^2} - \mathcal{E}(x)$. Thus,

$$\mathcal{E}\left(\frac{x}{z} \pm \frac{z}{2}\right) e^{-z^2/4} = \operatorname{erfc}\left(\frac{x}{z} \pm z/2\right) \exp\left[\left(\frac{x}{z}\right)^2 \pm x\right]. \quad (\text{S.42})$$

As for obvious reasons the numerical implementation via the right-hand side of this expression is highly problematic, we recommend to use the following approximation⁸ for $x/z \pm z/2 > 0$:

$$\mathcal{E}(x) \approx t(x) \exp\left\{ \sum_{n=0}^9 a_n [t(x)]^n \right\} \quad (\text{S.43})$$

with

$$t(x) = \frac{2}{2 + |x|} \quad (\text{S.44})$$

and $a_0 = -1.26551223$, $a_1 = 1.00002368$, $a_2 = 0.37409196$, $a_3 = 0.09678418$, $a_4 = -0.18628806$, $a_5 = 0.27886807$, $a_6 = -1.13520398$, $a_7 = 1.48851587$, $a_8 = -0.82215223$, $a_9 = 0.17087277$. For $x/z - z/2 < 0$, on the other hand, we use the relation

$$\mathcal{E}\left(\frac{x}{z} - \frac{z}{2}\right) e^{-z^2/4} = 2 \exp\left[\left(\frac{x}{z} - \frac{z}{2}\right)^2 - \frac{z^2}{4}\right] - \mathcal{E}\left(-\frac{x}{z} + \frac{z}{2}\right) e^{-z^2/4} = 2 \exp\left[\left(\frac{x}{z}\right)^2 - x\right] - \mathcal{E}\left(-\frac{x}{z} + \frac{z}{2}\right) e^{-z^2/4} \quad (\text{S.45})$$

and afterwards evaluate \mathcal{E} on the right-hand side via Eq. (S.43), while the first term is mathematically benign as by assumption the the argument of the exponential function is negative.

Consequently, we obtain

$$\begin{aligned} E_x^{\text{hyper-GGA,BR,LR}}[n, \omega] &= 4\pi \int \frac{n^2}{k_F^2} \int_0^\infty J_x^{\text{BR}}(n, s, z, e_x, y) \operatorname{erf}\left(\frac{\omega}{k_F} y\right) y \, dy \, d^3r \\ &= A_x \int n^{4/3} \left[-\frac{8}{9} I^{\text{BR}}(n, s, \nabla^2 n, \tau, e_x, \omega)\right] d^3r \quad (\text{S.46}) \end{aligned}$$

and the hyper-GGA enhancement function F of Eq. (40) is given by

$$F^{\text{BR}}(n, s, \nabla^2 n, \tau, e_x, \omega) = -\frac{8}{9} I^{\text{BR}}(n, s, \nabla^2 n, \tau, e_x, \omega) \quad (\text{S.47})$$

for the BR exchange hole model.

II. ANALYTIC SOLID-ANGLE INTEGRATION

We look to simplify $E_x^{\text{ex,LR}}[n]$ of Eq. (3) in case of a spin-saturated, closed-shell system by performing both solid-angle integrations analytically. Due to the closed shells the sum over all occupied orbitals can be written as

$$\sum_{i=1}^N \varphi_i(\mathbf{r}) = \sum_{l=0}^{l_{\max}} \sum_{n=1}^{N_l} R_n^l(r) \sum_{m=-l}^l Y_{lm}(\theta, \phi), \quad (\text{S.48})$$

where N is the number of occupied orbitals per spin channel, i.e., half of the number of electrons, l_{\max} is the highest occupied angular quantum number l , N_l is the number of occupied states with quantum number l , $R_n^l(r)$ is the radial function associated with the n -th state for quantum number l (i.e., n is the principle quantum number), m is the magnetic quantum number, and $Y_{lm}(\theta, \phi)$ notates the spherical harmonic of degree l and order m . This relation in conjunction with the spherical harmonic addition theorem

$$\sum_{m=-l}^l Y_{lm}^*(\theta', \phi') Y_{lm}(\theta, \phi) = \frac{2l+1}{4\pi} P_l(\cos \delta), \quad (\text{S.49})$$

where δ is the intermediate angle between \mathbf{r} and \mathbf{r}' , and $P_l(x)$ is the Legendre polynomial of degree l , allows us to simplify Eq. (3):

$$\begin{aligned} E_x^{\text{ex,LR}}[n] &= - \sum_{i,j=1}^N \iint \frac{\varphi_i^*(\mathbf{r}) \varphi_j^*(\mathbf{r}') \varphi_j(\mathbf{r}) \varphi_i(\mathbf{r}')}{|\mathbf{r} - \mathbf{r}'|} \operatorname{erf}[\omega(r)|\mathbf{r} - \mathbf{r}'|] \, d^3r' \, d^3r \\ &= - \sum_{l_1, l_2=0}^{l_{\max}} \sum_{n_1=1}^{N_{l_1}} \sum_{n_2=1}^{N_{l_2}} \sum_{m_1=-l_1}^{l_1} \sum_{m_2=-l_2}^{l_2} \iint \frac{R_{n_1}^{l_1}(r) R_{n_2}^{l_2}(r') R_{n_2}^{l_2}(r) R_{n_1}^{l_1}(r')}{|\mathbf{r} - \mathbf{r}'|} \\ &\quad \times \operatorname{erf}[\omega(r)|\mathbf{r} - \mathbf{r}'|] Y_{l_1 m_1}^*(\theta, \phi) Y_{l_2 m_2}^*(\theta', \phi') Y_{l_2 m_2}(\theta, \phi) Y_{l_1 m_1}(\theta', \phi') \, d^3r' \, d^3r \\ &= - \sum_{l_1, l_2=0}^{l_{\max}} \sum_{n_1=1}^{N_{l_1}} \sum_{n_2=1}^{N_{l_2}} \frac{(2l_1+1)(2l_2+1)}{(4\pi)^2} \iint \frac{R_{n_1}^{l_1}(r) R_{n_2}^{l_2}(r') R_{n_2}^{l_2}(r) R_{n_1}^{l_1}(r')}{|\mathbf{r} - \mathbf{r}'|} \\ &\quad \times \operatorname{erf}[\omega(r)|\mathbf{r} - \mathbf{r}'|] P_{l_1}(\cos \delta) P_{l_2}(\cos \delta) \, d^3r' \, d^3r. \quad (\text{S.50}) \end{aligned}$$

In order to perform the angular integration in spherical coordinates the screened Coulomb kernel has to be represented by its Legendre expansion,

$$\frac{\text{erf}[\omega(r)|\mathbf{r}-\mathbf{r}'|]}{|\mathbf{r}-\mathbf{r}'|} = \sum_{l=0}^{\infty} c_l(\omega(r), r, r') P_l(\cos \delta), \quad (\text{S.51})$$

in analogy to the well known relation for bare kernel,⁹

$$\frac{1}{|\mathbf{r}-\mathbf{r}'|} = \frac{1}{\sqrt{r^2 + r'^2 - 2rr' \cos \delta}} = \sum_{l=0}^{\infty} \frac{r_{<}^l}{r_{>}^{l+1}} P_l(\cos \delta), \quad (\text{S.52})$$

where $r_{>} = \max(r, r')$ and $r_{<} = \min(r, r')$. Next, for each \mathbf{r} in the integral in the last line of Eq. (S.50) the spherical coordinate system used for the \mathbf{r}' -integration can always be chosen such that z' -axis points along the \mathbf{r} -direction due to symmetry and, therefore, δ becomes the polar angle of \mathbf{r}' -integration. Subsequently, this integration can be performed with the help of the relation

$$\int_{-1}^1 P_k(x) P_l(x) P_m(x) dx = 2 \begin{pmatrix} k & l & m \\ 0 & 0 & 0 \end{pmatrix}^2. \quad (\text{S.53})$$

When considering only atoms up to the p -shell, all of the Wigner 3- j symbols on the right-hand side of this relation vanish with the exception of

$$\begin{pmatrix} 0 & 0 & 0 \\ 0 & 0 & 0 \end{pmatrix}^2 = 1, \quad \begin{pmatrix} 0 & 1 & 1 \\ 0 & 0 & 0 \end{pmatrix}^2 = \frac{1}{3}, \quad \begin{pmatrix} 1 & 1 & 2 \\ 0 & 0 & 0 \end{pmatrix}^2 = \frac{2}{15} \quad (\text{S.54})$$

and their cyclic permutations, which yield the same squared value. Consequently, we have calculated the Legendre expansion coefficients,

$$c_l(\omega(r), r, r') = \frac{2l+1}{2} \times \int_{-1}^1 P_l(x) \frac{\text{erf}[\omega(r)\sqrt{r^2 + r'^2 - 2rr'x}]}{\sqrt{r^2 + r'^2 - 2rr'x}} dx \quad (\text{S.55})$$

only up to $l = 2$, as this is sufficient for this work. These coefficients have the form

$$c_l(\omega, r, r') = \frac{[h_l(\omega r_{>}, \omega r_{<}) - h_l(\omega r_{>}, -\omega r_{<})]}{(2r_{>}r_{<})^{l+1} \omega^{2l+1}} \quad (\text{S.56})$$

with

$$h_0(x_{>}, x_{<}) = \frac{e^{-x_+^2}}{\sqrt{\pi}} + x_+ \text{erf}(x_+), \quad (\text{S.57})$$

$$h_1(x_{>}, x_{<}) = [2(x_{>}^2 - x_{>}x_{<} + x_{<}^2) - 1] \frac{e^{-x_+^2}}{\sqrt{\pi}} + 2(x_{>}^3 + x_{<}^3) \text{erf}(x_+), \quad (\text{S.58})$$

and

$$h_2(x_{>}, x_{<}) = 4(x_{>}^5 - x_{<}^5) \text{erf}(x_+) + \left[4(x_{>}^4 - x_{>}^3x_{<} + x_{>}^2x_{<}^2 - x_{>}x_{<}^3 + x_{<}^4) - 2(x_{>}^2 - 3x_{>}x_{<} + x_{<}^2) + 3 \right] \frac{e^{-x_+^2}}{\sqrt{\pi}}, \quad (\text{S.59})$$

where $x_+ = x_{>} + x_{<}$. It is straightforward to show that this expansion recovers the correct limits: (i) $c_l \rightarrow 0$ and thus LR vanishes as $\omega \rightarrow 0$; (ii) $c_l \rightarrow r_{<}^l/r_{>}^{l+1}$ and thus LR reduces to exact exchange as $\omega \rightarrow \infty$, cf. Eq. (S.52).

Insertion of the Legendre expansion of Eq. (S.51) into Eq. (S.50) and the application of relation (S.53) as well as the remaining trivial angle integrations then yield the final result already presented in Eq. (45) of the article. In case of a calculation up to the p -shell, this result can be evaluated further to

$$E_x^{\text{ex,LR}}[n, \omega] = \Gamma_{0,0,0} + \Gamma_{1,0,1} + \Gamma_{0,1,1} + 3\Gamma_{1,1,0} + \frac{6}{5}\Gamma_{1,1,2}. \quad (\text{S.60})$$

with

$$\Gamma_{l_1, l_2, l} = - \sum_{n_1=1}^{N_{l_1}} \sum_{n_2=1}^{N_{l_2}} \iint R_{n_1}^{l_1}(r) R_{n_2}^{l_2}(r') R_{n_2}^{l_2}(r) R_{n_1}^{l_1}(r') c_l(\omega(r), r, r') r^2 r'^2 dr' dr. \quad (\text{S.61})$$

III. ATOMIZATION ENERGIES OF DIATOMIC MOLECULES

Supplementary material to the atomization energies of Tab. II. The calculations were performed on a real-space prolate spheroidal grid with DARSEC¹⁰, an all-electron code for single atoms or diatomic molecules with occupation numbers following from a Fermi-Dirac distribution with a temperature of 1 K.

| LRS- ω -LDA | | | | | Numerical parameters | | | | |
|--------------------|------------------------|------------------------|------------------------|-------|----------------------|--------------------|---------|---------|----------------------|
| Molecule | ω_σ^K @LDA | ω_σ^K @PBE | ω_σ^K @EXX | Expt. | System | R_{AB} (a_0) | N_μ | N_ν | R_{\max} (a_0) |
| H ₂ | 115.4 | 115.4 | 115.4 | 109.5 | H ₂ | 1.4011 | 79 | 103 | 19.49 |
| LiH | 62.0 | 62.1 | 62.0 | 58.0 | LiH | 3.0139 | 79 | 103 | 19.59 |
| Li ₂ | 21.3 | 21.3 | 21.7 | 24.7 | Li ₂ | 5.0518 | 79 | 103 | 19.65 |
| LiF | 138.6 | 138.8 | 137.1 | 138.3 | LiF | 2.9553 | 79 | 103 | 19.57 |
| CO | 256.5 | 256.9 | 256.5 | 259.5 | CO | 2.1322 | 79 | 103 | 19.55 |
| N ₂ | 228.3 | 228.9 | 229.0 | 228.5 | N ₂ | 2.0744 | 103 | 133 | 19.65 |
| NO | 150.2 | 150.6 | 150.3 | 152.5 | NO | 2.1743 | 79 | 103 | 19.55 |
| OH | 95.9 | 96.0 | 91.0 | 106.4 | OH | 1.8324 | 79 | 103 | 19.53 |
| O ₂ | 129.6 | 130.0 | 128.3 | 120.5 | O ₂ | 2.2817 | 73 | 103 | 19.56 |
| FH | 143.3 | 143.2 | 142.4 | 141.1 | FH | 1.7327 | 79 | 91 | 19.52 |
| F ₂ | 43.7 | 43.7 | 45.4 | 38.4 | F ₂ | 2.6681 | 73 | 91 | 19.57 |
| MAE | 4.3 | 4.3 | 4.8 | | H | | 79 | 91 | 19.54 |
| | | | | | Li | | 79 | 91 | 19.54 |
| | | | | | C | | 73 | 91 | 19.54 |
| | | | | | N | | 73 | 109 | 14.65 |
| | | | | | O | | 73 | 103 | 19.50 |
| | | | | | F | | 73 | 91 | 19.50 |

(a) Assessment of the influence of the reference orbitals.

(b) Numerical parameters

TABLE S.I. (a) Assessment of the influence of the input non-self consistent orbitals for LRS- ω -LDA with ω_σ^K of Eq. (11) in the hyper-GGA approximation based on the original TPSS hole, cf. column 3 of Tab. II. The notation @LDA indicates that LDA orbitals were used, @PBE indicates that PBE orbitals were used, etc. The exact exchange (EXX) reference orbitals were generated from EXX potentials evaluated in the KLI-approximation¹¹. (b) Numerical parameters as listed: R_{AB} interatomic distance; N_μ , N_ν , number of grid points along the μ , ν directions respectively; R_{\max} length of the semi-major axis. All single atoms were calculated with $R_{AB} = 2.0 a_0$.

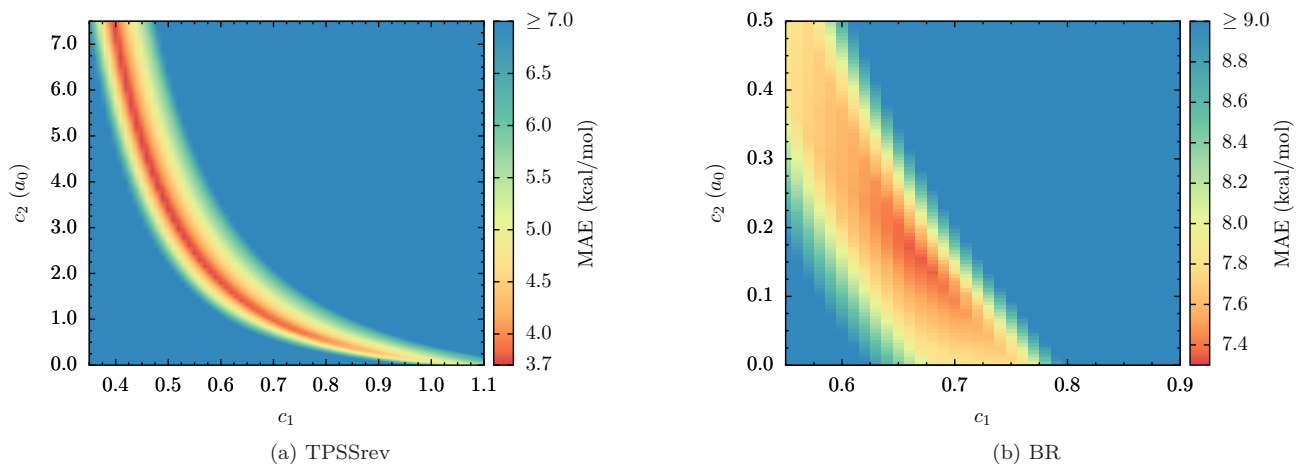


FIG. S.1. Heat map of the mean absolute error (MAE) across the test set for atomization energies of the local range-separation parameter $\omega_\sigma(\mathbf{r})$ of Eq. (54) as a function of its two parameters c_1 and c_2 in analogy to Fig. 3 of the article but the hyperGGA-approximation evaluated with the (a) TPSSrev and (b) BR hole model respectively.

Acknowledgments

I owe my deepest gratitude to numerous people that accompanied me during the process of creating this thesis. In particular, I wish to thank:

- **Stephan Kümmel** for being the best supervisor I can imagine, both from a scientific and human point of view. I am deeply grateful for his unwavering confidence in me and my work, especially at times when I was rather skeptical myself, and for providing me extensive freedom to choose the direction of this thesis along the way.
- **Rickard Armiento** for countless insightful scientific debates both in person and via email.
- **Monika Birkelbach, Markus Hilt, and Ingo Schelter** for their administrative and technical assistance.
- **Stan van Gisbergen** for the opportunity to implement and test my functionals in BAND and **Pier Philipsen** for the technical assistance therewith.
- **All former and current members of the Theoretical Physics IV group** for the superb atmosphere and the unconditional mutual helpfulness. In particular, I would like to thank **Fabian Hofmann, Ingo Schelter, Julian Garhammer, Alexander Kaiser, Sabrina Kroll, Johannes Förster, and Juliana Kehrer** for carefully proofreading the manuscript of this dissertation and for their support during my preparation for the defense of this thesis. Moreover, it has been a pleasure to share an office with both **Philipp Schaffhauser** and **Alexander Kaiser**.
- My parents **Heike** and **Berndt** as well as my sister **Marit Aschebrock** for always supporting me in every possible way.

I further acknowledge financial support from the German-Israeli Foundation for Scientific Research and Development, from the Bavarian State Ministry of Science, Research, and the Arts for the Collaborative Research Network “Solar Technologies go Hybrid”, and from the University of Bayreuth Graduate School.

Eidesstattliche Versicherung

Hiermit versichere ich an Eides statt, dass ich die vorliegende Arbeit selbstständig verfasst und keine anderen als die von mir angegebenen Quellen und Hilfsmittel verwendet habe.

Weiterhin erkläre ich, dass ich die Hilfe von gewerblichen Promotionsberatern bzw. -vermittlern oder ähnlichen Dienstleistern weder bisher in Anspruch genommen habe, noch künftig in Anspruch nehmen werde.

Zusätzlich erkläre ich hiermit, dass ich keinerlei frühere Promotionsversuche unternommen habe.

Bayreuth, den 30.07.2019

Thilo Aschebrock